IMMUNOMETABOLIC REQUIREMENTS OF T CELL ACTIVATION AND EXHAUSTION

by

Nicole Elizabeth Scharping

Bachelor of Science, University of Washington, 2011

Submitted to the Graduate Faculty of

the School of Medicine in partial fulfillment

of the requirements for the degree of

Doctor of Philosophy

University of Pittsburgh

2019

UNIVERSITY OF PITTSBURGH

SCHOOL OF MEDICINE

This dissertation was presented

by

Nicole Elizabeth Scharping

It was defended on

April 12, 2019

and approved by

Robert L. Ferris, Director, UPMC Hillman Cancer Center, Hillman Professor of Oncology, Professor of Otolaryngology, Immunology, and Radiation Oncology

Lawrence P. Kane, Vice Chair for Education, Professor Immunology

Bennett Van Houten, Richard M. Cyert Professor of Molecular Oncology, Professor Pharmacology and Chemical Biology

Dario A. A. Vignali, Frank Dixon Chair in Cancer Immunology, Vice Chair and Professor, Immunology

Dissertation Director: Greg M. Delgoffe, Assistant Professor, Immunology

Immunometabolic requirements of T cell activation and exhaustion

Nicole Elizabeth Scharping, PhD

University of Pittsburgh, 2019

The metabolic requirements of T cells depend on activation, differentiation state, and functionality. These metabolic requirements are integral to T cell function in an acute activation setting, but can become a barrier to function in chronic disease. In acute activation, when CD8+ effector T cells become activated, they immediately switch to prioritizing glycolysis via PDHK1. This allows effector T cells to release cytokine mRNA from glycolytic enzyme regulation, allowing immediate protein synthesis and T cell effector function. In the setting of disease, effector T cells that infiltrate a tumor experience the immunologic and metabolically suppressive tumor microenvironment (TME), which in combination with chronic T cell activation inherent to the environment, causes effector T cells to differentiate into dysfunctional, exhausted T cells. The exhausted T cells also lose mitochondrial mass and function, creating a metabolic disadvantage for the T cell that contributes to their dysfunctional state. This loss of mitochondria is due to repression of mitochondrial biogenesis, mediated by PGC1α. T cell functionality can be restored in the TME with enforced PGC1α expression, which leads to decreased tumor burden and increased survival in mouse melanoma. We also

have shown exhausted T cells suffer from additional metabolic disadvantages – decreased fatty acid oxidation. This causes the exhausted T cells to store lipids rather than burn them as fuel. This phenomenon is due to chronic T cell activation under hypoxic conditions, causing dysfunctional mitochondrial to produce excessive mitochondrial reactive oxygen species (ROS). By enforcing fatty acid oxidation by overexpressing PPARγ, we can improve T cell functionality in the TME. Finally, targeting the metabolically suppressive TME is another avenue for bolstering T cell function. By using mitochondrial complex I inhibitor metformin in mouse melanoma, we can dramatically decrease tumor hypoxia, reoxygenating the TME, and in combination with immunotherapeutic checkpoint blockade, decrease tumor burden and increase mouse survival. Together, this thesis elucidates many immunometabolic requirements of T cell activation and exhaustion, allowing us to better understand how biology and metabolism intersect in T cell function, and informs upon designing therapies that better target T cell or TME metabolism to improve cancer immunotherapy.

TABLE OF CONTENTS

LIST OF FIGURES

PREFACE

I would like to take this opportunity to acknowledge everyone who contributed their time, effort, patience, and skills to training me during my graduate school career. My number one thanks goes to my mentor Greg Delgoffe, who deserves a document just as long as this thesis filled with my gratitude for his endless support, training, and enthusiasm these past five years. You not only directly trained me with the technical skills I would need to study cancer immunometabolism, but with all the other tools I needed to be successful in science. You taught me how to effectively communicate with my audience, conveying not only our awesome science, but my passion so that I would inspire others. You taught me how teach, how to collaborate, how to navigate the politics of academia, how to fail, and how to overcome failure. You never shot down my ideas, even when they were bad, which gave me the confidence to chase down my ideas when I finally had some good ones. Thank you for letting me argue with you when I thought I was right, and not making me feel bad when I was wrong. I am inspired daily by your boundless enthusiasm and curiosity, and hope to one day run a lab half as successful as yours.

I must also thank all the Delgoffe lab members, past and present, who I have worked with over the years. Specifically, I am grateful to have known and worked with Dayana Rivadeneira, Mac Watson, Yiyang (Steve) Wang, Ronal Peralta, Kristin

DePeaux, Paolo Vignali, Xue (Lucy) Zeng, and Becca Moreci. But most of all, I must thank my labmate Ashley Menk. We have been working together since (almost) the beginning and have collaborated on innumerable projects. Through good times and tough, Ashley has been the best labmate I could ask for.

A special thanks to all our collaborators and coauthors in our work, but especially, I would like to thank Amanda Poholek and Natalie Rittenhouse. They have been excellent collaborators to work with, and I look forward to seeing what we continue to discover about exhausted T cell epigenetics together.

Many thanks to my committee members Bob Ferris, Larry Kane, Ben Van Houten, and Dario Vignali for all your advice and support over the years – I could not have made it to this point without your help!

Many thanks to my funding (both the Cancer Immunology T32 Training Program and the Predoctoral to Postdoctoral Fellow F99/K00 Transition Award), to the Program in Immunology and Microbiology, the department of Immunology at the University of Pittsburgh, UPMC Hillman Cancer Center, the Tumor Microenvironment Center, the Center for Biological Imaging, the Flow Cytometry Core at Hillman, and the Animal Facilities at Hillman. None of this would be possible without your support!

Finally, I would like to thank my family and friends, both near and far. My PMI classmates and friends Helen Rich, Adolfo Frias, and Hiroshi Yano, as well as my besties Audra Linsenmayer, Courtney Holmes, and Katie Hoffman. All my love to my family – my mom Connie, my dad Bob, my brother Paul, my niece Willow, my aunt and uncle Victoria and John Ryan, and my grandparents Wilma Dalby, Bob Dalby, and

Gretchen Alexander. Your unwavering support of my career has always inspired me to live up to your expectations. Thank you!

1.0 INTRODUCTION

1.1 FOREWORD

This chapter was adapted from a previously published review in *Vaccines*: **Nicole E. Scharping** and Greg M. Delgoffe. “Tumor Microenvironment Metabolism: A New Checkpoint for Anti-Tumor Immunity.” *Vaccines*, 2016. DOI: 10.3390/vaccines4040046.

1.2 T CELL IN THE TUMOR MICROENVIRONMENT

Most of the hallmarks of cancer cells can be attributed to the inability to respond to environmental cues to slow proliferation or induce cell death[1]. These environmental insensitivities are generally due to DNA mutations, usually occurring during an individual’s lifetime and in response to a variety of exogenous genetic insults and endogenous modulatory factors[1]. While the initial neoplastic event is due to these uncorrected DNA mutations, it is widely believed that the progression from neoplasia to malignancy is due in part to a failure of immunosurveillance[2–4]. The immune system excels at identifying and eliminating mutated cells, but cancer can evade recognition through a process called “immunoediting”. The immune system puts selective pressure on the tumor cell population, making it advantageous for tumor cells to mutate or alter

the production of antigens that might be recognized as foreign by the immune system. Tumor cells also downregulate antigen processing and presentation machinery, rendering them invisible to the immune system. Thus, if cancerous cells keep mutating, they can keep evading immune recognition[5].

Concomitant with cancer cells escaping immune recognition and elimination, cancer cells may begin to utilize additional mechanisms to create an immunosuppressive environment. This can be induced by the recruitment of immunosuppressive cells (myeloid-derived suppressor cells (MDSCs) and regulatory T cells) to create a “wound healing” environment and the generation of tolerogenic signals, such as interleukin-10 (IL-10), transforming growth factor-beta (TGFβ) and extracellular adenosine[6]. Tumor cells can induce T cell dysfunction through direct receptor-ligand interactions, expressing co-inhibitory ligands, such as programmed death-ligand 1 (PD-L1) to inhibit CD8+ tumor-infiltrating lymphocytes’ (TIL) function through programmed death-1 (PD-1), a process further enhanced through contact with the immune system[7]. T cell function can also be inhibited by other co-inhibitory “checkpoint” molecules, such as cytotoxic T lymphocyte-associated protein-4 (CTLA-4), T cell immunoglobulin and mucin domain containing-3 (Tim-3), lymphocyte activating gene 3 (Lag3) and T cell immunoreceptor with Ig and ITIM domains (TIGIT), which are upregulated on the surface of T cells after activation and remain highly expressed on T cells in the tumor microenvironment (TME) due to persistent activation signals. Ligation of these co-inhibitory checkpoint molecules results in downregulation of T effector function.

One of the most promising new immunotherapies, generally termed “checkpoint blockade”, utilizes monoclonal antibodies specific to either the co-inhibitory ligand or receptor to block their interaction[8]. Anti-CTLA-4 and anti-PD1/PD-L1 were among the first in clinical trials, showing promising objective clinical responses[9,10]. However, these therapies are only effective in a subset of patients, and the biomarkers of responsiveness to these immunotherapies remain elusive[11]. This likely indicates that immunosuppression from these “immunologic” sources does not account for the whole suppressive microenvironment. In this introduction, we postulate that tumor cells are also immunosuppressive due to a suppressive metabolic microenvironment characterized by a lack of crucial carbon sources and intermediates needed for T cell function.

1.3 METABOLISM IN THE TUMOR MICROENVIRONMENT

The driving force behind the malignancy and morbidity of cancer is its ability to proliferate unrestrained. While individual cancer cells may be insensitive to growth inhibition, it is not without cost for these cells. Their unrestrained growth requires the cancer cells to utilize aerobic glycolysis (also called the “Warburg effect”, after Otto von Warburg who initially described it) over oxidative metabolism[12,13]. This occurs when cells convert glucose-derived pyruvate into lactic acid, rather than acetyl-CoA to fuel oxidative phosphorylation (OXPHOS). While this glucose fermentation occurs in all cells when oxygen is limiting, most tumors cells acquire a metabolic adaptation to perform glycolysis even in the presence of oxygen[14].

Why glycolysis occurs in cancer cells has been a matter of debate since its discovery[12]. It was originally hypothesized that aerobic glycolysis may occur in cancer cells due to mitochondrial damage, but it is now clear that cancer cells still utilize their mitochondria for oxidative metabolism[15]. Thus, it may seem perplexing why a tumor cell might choose this bioenergetically unfavorable pathway, as biochemical studies show that glycolysis generates eighteen times less ATP per mole of glucose than OXPHOS[16,17]. However, there are other important considerations for the cellular metabolism of tumor cells. First, while glycolysis generates less ATP per mole of glucose compared to OXPHOS, the kinetics of this reaction are considerably different: glycolysis generates ATP nearly a hundred times faster than OXPHOS, such that if a tumor cell could compete for glucose, it could meet its metabolic demands[16,17]. Second, by utilizing aerobic glycolysis, the cancer cell can regenerate the reductive molecule NAD+, which is utilized in the initial steps of glycolysis, as well as in other essential metabolic pathways in the cell. Third and most importantly, aerobic glycolysis serves to free a portion of mitochondrial function to perform anabolic metabolism: producing the lipids, amino acids and nucleotides needed to generate daughter cells[14,18]. Due to the high metabolic demands of these highly proliferative cells, cancer cells utilize aerobic glycolysis and consume essential metabolites in the surrounding environment, secreting lactic acid as metabolic waste of the glycolytic pathway[14]. As a result, the tumor microenvironment has low glucose, low oxygen and a low pH[17,19–21]. These crucial metabolites, especially oxygen, are replenished poorly due to dysregulated angiogenesis caused by the tumor[22]. Low oxygen levels also help induce a glycolytic

program by increasing HIF-1α expression[23]. HIF-1α turns on gene expression programs that directly inhibit OXPHOS, further enforcing tumor cell aerobic glycolysis[24].

The altered metabolism of tumor cells was posited by Warburg to be not only a characteristic of malignancy, but even causative of the malignant phenotype[12]. While the last several decades have explored exactly why and how developing cancer undergoes this type of metabolic transformation, it is clear that this emerging hallmark of cancer does not only impact the cancer cells themselves[1]. This hunger in cancer cells for available nutrients to fuel their unrestrained proliferation creates a bioenergetic sink for any cell that enters the tumor microenvironment. It is now understood that a lack of metabolites and oxygen, as well as high intratumoral acidity, act as additional immunosuppressive mechanisms the tumor exploits to prevent infiltrating T cells from functioning efficiently (Figure 1).

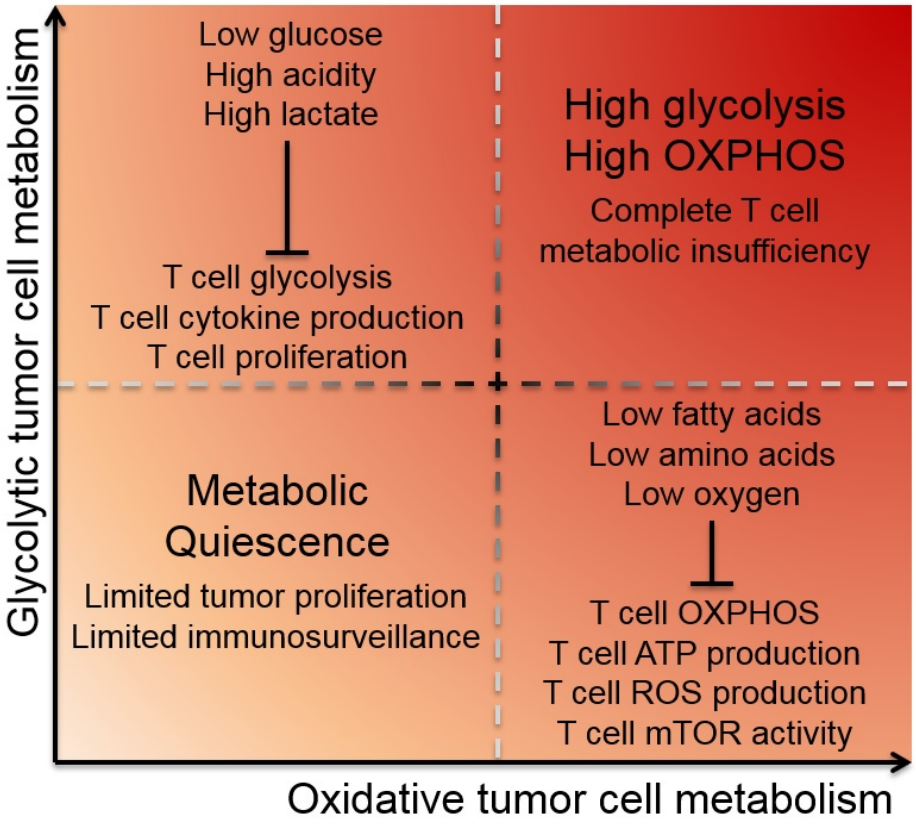

Figure 1. Tumor cell energetics dictate the metabolic landscape of the TME.

Tumor cells utilize glycolysis and oxidative phosphorylation metabolism, causing depletion of particular environmental metabolites and inhibiting TIL in different ways. Glycolytic tumors primarily utilize glycolysis for energy, creating a TME that has low glucose and high acidity and lactate. This inhibits T cell function by limiting fuel for T cell glycolysis, as well as inhibiting T cell cytokine production and proliferation. Oxidative tumors primarily utilize OXPHOS and their mitochondria for energy, creating a TME that has low oxygen, low fatty acids and low amino acids. This inhibits T cell function by limiting oxygen for T cell OXPHOS, as well as inhibiting T cell mitochondria from producing ATP and ROS. Low ATP production has the downstream consequence of inhibiting mTOR activity. Tumor cells that are both glycolytic and oxidative inflict complete metabolic insufficiency on T cells, while quiescent tumors with minimal metabolic demands can better hide from immunosurveillance via reduced proliferation. Abbreviations: tumor microenvironment (TME), tumor-infiltrating lymphocyte (TIL), oxidative phosphorylation (OXPHOS), reactive oxygen species (ROS), and mechanistic target of rapamycin (mTOR).

1.4 METABOLIC REGULATION OF T CELLS

Recent studies have demonstrated the essential role of metabolism for immune cells, beyond simply growth or death decisions. The link between fuel source and metabolic program and how these impact immune cell phenotype and function are an active area of research[25]. One of the first contributions to the immunometabolism field was looking at the relative contributions of glycolysis and OXPHOS during lymphocyte activation[26]. It was noted that when lymphocytes were activated via receptor crosslinking with phytohemagglutinin, the lymphocytes (like tumor cells) also underwent aerobic glycolysis. Later studies revealed that T cells use both glycolysis and OXPHOS to generate ATP, and both pathways are required for in vitro proliferation[27]. As T cells also undergo aerobic glycolysis upon activation, they have high energy demands from their environment in order to proliferate and function. To better understand the basics of T cell metabolism, the following section will review when T cells change their metabolic demands, as well as how environmental nutrient sensing can change the fate of T cells. With this understanding, we will then see how energy sensing and utilization becomes dysfunctional in the TME when T cells need to compete with tumor cells for glucose and other nutrients.

1.4.1 T Cells Change Their Metabolic Demands upon Activation

Of all immune cells, T cells in particular have become a research focus, as the progression through activation comes with distinct metabolic changes[28]. Naive T cells, which are required to be quiescent for a lifetime, have low metabolic demands. The

maintenance of this quiescent state requires minimal OXPHOS, dividing only to maintain the clonal repertoire throughout life. The pro-survival cytokine interleukin-7 (IL-7) is necessary for the maintenance of these quiescent cells[29]. IL-7 is important for the uptake of glucose through glucose transporter 1 (Glut1) for the maintenance of ATP levels[30]. Thus, these quiescent T cells have minimal metabolic demands until activated, preserving fuel in the environment for those T cells that have entered their effector phase.

When a T cell encounters an antigen, it first begins cellular growth and prepares for cell division. Since antigen-specific naive T cells are have such a low precursor frequency, it is important for the cell to proliferate quickly to generate sufficient numbers of effector cells. However, this proliferation has high metabolic demands. Thus, like highly proliferative tumor cells, activated T cells utilize glucose as a primary fuel source[31]. Glut1 is upregulated upon T cell activation, through T cell receptor (TCR) and CD28-induced serine/threonine kinase Akt activation, allowing activated T cells to increase their glucose uptake eighteen-fold higher than naive T cells[32]. This allows cells to use aerobic glycolysis for anabolic cell growth[30]. Failure to upregulate metabolic pathways upon T cell activation leads to a hyporesponsive phenotype much like clonal anergy, a state in which even a full antigenic stimulation cannot induce a T cell response[33]. Similar to an anergic T cell, T cells that have been activated in nutrient-poor conditions will become unresponsive to future stimulation. This finding highlights the important link between metabolism and T cell function: starving a T cell can have lasting effects on its ability to perform in the future, even in nutrient-rich conditions.

While adopting aerobic glycolysis allows cells to keep up with ATP demands, regenerate NAD+ and promote anabolic pathways for mitochondrially-derived substrates, recent studies have also revealed that glycolysis may directly contribute to effector functions. It has long been known that glycolytic enzymes can “moonlight” as RNA-binding proteins when not performing enzymatic reactions[34]. Indeed, T cell-derived glyceraldehyde 3-phosphate dehydrogenase (GAPDH) was shown to bind interferon gamma (Ifng) mRNA in resting, non-glycolytic T cells, suggesting that glycolysis promotes cytokine secretion, in part, by relieving post-transcriptional repression of cytokine messages[27].

Chapter 2 of this thesis further explores the metabolic demands and functional consequences of T cell activation, work that has also been published[35]. Using real-time metabolic flux analysis, we found that TCR engagement is sufficient to rapidly induce aerobic glycolysis, independent of CD28 and Akt. We identified pyruvate dehydrogenase kinase 1 (PDHK1), which acts on pyruvate dehydrogenase to inhibit pyruvate import into the mitochondria, as a key node in this glycolytic switch. Using pharmacologic and genetic inhibition, we found that PDHK1 is required for initiation of aerobic glycolysis and interacts with proximal TCR signaling machinery. Intriguingly, we found that PDHK1 supports differential T cell effector functions: while PDHK1 is required for cytokine production, it is dispensable for cytolytic activity and proliferation. Downstream analysis revealed PDHK1 is necessary for post-transcriptional synthesis of cytokines. Specifically, we found the glycolytic enzyme lactate dehydrogenase also functions as an inhibitory RNA-binding protein for cytokine transcripts, releasing them from regulation when aerobic glycolysis is engaged. Our data support a model which

places aerobic glycolysis as an immediate consequence of TCR ligation, critical for cytokine synthesis.

T cells continue to utilize aerobic glycolysis during the effector phase of their activation, but switch back to primarily utilizing OXPHOS as they become memory cells[36]. The formation of memory T cells leads to a larger mitochondrial reserve than naive T cells, termed spare respiratory capacity[36]. The gamma-chain cytokine interleukin-15 (IL-15), important for forming long-lasting memory T cells, also increases mitochondrial biogenesis and the expression of the mitochondrial enzyme carnitine palmitoyltransferase 1a (CPT1a), a rate-limiting enzyme in fatty acid oxidation[37]. As such, it is thought that the increase in memory T cell mitochondria primes the cells for a quick recall response with a bioenergetic advantage over naive T cells. In a recall response, memory T cells can also switch to glycolysis in an Akt-dependent manner, but have higher glycolytic flux and increased upregulation of glycolytic enzymes, such as GAPDH, than do naive T cells[38]. However, antigen-experienced T cells also have additional metabolic demands, as evidenced by the fact that memory T cells also rely on fatty acid oxidation. For instance, CD8+ T cells lacking TNF receptor associated factor 6 (TRAF6), a signaling molecule downstream of the tumor necrosis factor (TNF) cytokine receptor superfamily, they are unable to form memory after immunization[39]. TRAF6-deficient T cells show repression of fatty acid metabolism genes, leading to defective lipid oxidation. Thus, memory T cells may require a variety of metabolites to fuel their increased mitochondria to carry out their recall responses more effectively.

The metabolism of T cells is tied directly to proliferation, cytokine production and cytolytic function: essential functions of an effector T cell. While many of these studies

have utilized inhibitors or genetic targeting to determine the contributions of various metabolic pathways to T cell function, a pair of recent studies has revealed that these pathways are dynamically regulated even during the generation of a “typical” T cell response[40,41]. One model for the generation of memory hypothesizes that T cells have both short-lived effector and memory potential. However, upon contact with antigen-presenting cell (APC)-bound peptide-major histocompatibility complex (MHC), the T cell will grow and then divide in an asymmetric manner. The proximal cell to the APC receives the majority of signaling molecules and activation signals and becomes fated to be a short-lived, effector cell, while the distal cell is less proliferative in subsequent divisions and inherits more memory potential[42]. Interestingly, the metabolic demands of a T cell can also be asymmetrically inherited upon activation[40,41]. Proximal daughter cells have more Myc and mechanistic target of rapamycin (mTOR) activity, resulting in part due to asymmetric partitioning of lysosomes and amino acid transporters. As both Myc and mTOR are important factors for cell proliferation, differentiation and metabolism, differences in these metabolic programs lead to distinct cell fates for the dividing daughter cells.

1.4.2 T Cells Utilize Nutrient Sensing to Dictate Their Differentiation

It is clear that metabolite availability and changes in metabolic pathways can have major effects on T cell function, but this is largely unsurprising since energy is required to perform any complex cellular task. However, unlike other renewable cell types present in the body, clonal diversity must be preserved in T cells. This creates a need for reliance upon nutrient sensing. It would not be favorable for a T cell to engage an

effector response if it could not metabolically support the expansion; subsequent cell death might eliminate that clone. T cells thus have conscripted the nutrient-sensing machinery to make more complex fate determinations, rather than growth-or-death decisions.

mTOR is a key molecule in the nutrient sensing machinery. mTOR integrates environmental signals, such as amino acid and oxygen availability, intracellular ATP concentration, extracellular growth/survival signals, and cellular activation status. These signals then induce changes in cell size, proliferation, metabolism and survival to respond to extracellular signals and environmental status[43]. The importance of mTOR in T cells was discovered by its inhibition by rapamycin, a macrolide antibiotic that is a potent immunosuppressant[44]. Rapamycin was first found to induce anergy in T cells[45]. Once rapamycin was determined to inhibit mTOR, the role of this signaling molecule in T cell activation and differentiation was investigated.

mTOR was shown to be the signaling molecule responsible for “full” T cell activation upon TCR engagement in T cell clones. Further activated and anergic T cells could be distinguished by mTOR-induced metabolic machinery, which provided evidence for a critical role of metabolism in T cell functionality[46]. Further exploration of the role of mTOR found that it is essential for T cell lineage commitment[47]. CD4+ T cells lacking mTOR preferentially differentiate into regulatory T cells over Type 1 T helper (Th1), Th2 or Th17 cells. It is interesting to note the lack of mTOR favors regulatory T cells, since it could be interpreted as the lack of metabolic cues from a T cell’s environment that defaults to a regulatory phenotype and that T cell anergy and regulation are very similar from a metabolic standpoint. CD8+ T cells are also

dependent on mTOR signaling; low-dose mTOR inhibition increases memory T cell precursors and accelerates memory T cell differentiation, somewhat paradoxically as mTOR is used clinically as an immunosuppressant[48]. As CD8+ memory relies more on OXPHOS than glycolysis and mTOR activation is associated with glycolysis and AKT activation, low-level mTOR signaling in CD8 T cells may bias their metabolism towards that which supports a memory phenotype.

mTOR does not signal by itself; rather, it exists as a larger signaling complex with other molecules. Specific T cell-conditional deletion of mTOR complex 1 (mTORC1) and mTORC2 revealed that these complexes play distinct roles in directing T cell fate. When mTORC1-dependent Ras homolog enriched in brain (Rheb) was deleted from CD4+ T cells, they failed to differentiate into Th1 or Th17 T cells, but Th2 differentiation was intact[49]. Conversely, when mTORC2 signaling was deleted, CD4+ T cells failed to differentiate into Th2 T cells, but Th1 and Th17 differentiation was intact. The opposing roles of mTORC1 and 2 in T cell fate determination highlight the ability of T cells to make widely different fate decisions based on subtle metabolic environmental differences. This allows for greater T cell plasticity and an ability to respond to a wide range of environmental changes. mTORC1 and 2 were also found to have specific roles in generating effector and memory CD8+ T cell subsets. Constitutively active mTORC1 generates glycolytic effector T cells unable to enter the memory phase, while mTORC1-deficient effector T cells failed to activate an effector response, but maintained memory T cell characteristics[50]. The control of T cell fate by mTORC1 and mTORC2 supports the idea that the T cells have cell-intrinsic potential to be either effector *or* memory upon activation, rather than all effector T cells having the ability to differentiate to memory as

activation progresses. The ability of mTOR to sense the environmental state thus impacts T cell activation and differentiation; nutrient availability can have a long-term impact on T cell fate.

In addition to mTOR, T cells use other metabolic signaling molecules to sense and respond to their environment, namely Myc and AMP-activated protein kinase (AMPK). Myc is essential for glycolytic reprogramming, with deletion of Myc inhibiting activation-induced glycolysis and glutaminolysis[51]. AMPK senses nutrient deprivation and can limit mTOR activity in low glucose environments[52]. AMPK also impacts T cell differentiation; AMPK 1 knockout T cells are unable to form memory and display defects in CD4+ Th1 and Th17 differentiation[52,53].

Additional transcription factors can also play a role in how T cells respond to environmental metabolic cues promoting cellular proliferation, differentiation, or homeostasis. Sterol regulatory-element binding proteins (SREBPs) are a family of transcription factors that control cholesterol synthesis and uptake. SREBP family members are upregulated upon T cell activation and are required for the increased lipid membrane synthesis needed to generate daughter cells[54]. Peroxisome proliferator-activated receptors (PPARs), the family of nuclear receptor transcription factors also involved in lipid metabolism, have also been shown to play a role in T cell immunoregulation[55]. PPAR has specifically been shown to be a negative regulator of T cell activation, regulating interleukin-2 (IL-2) production in activated T cells, and the loss of PPAR in T cells contributes to autoimmunity[56,57]. Transcription factor EB (TFEB), a regulator of lysosomal biogenesis, has been shown to be negatively regulated by mTORC1[58]. When intracellular metabolites are high, TFEB is retained in the cytosol, but

when nutrients are needed, TFEB disassociates from mTORC1 and translocates to the nucleus to increase lysosome biogenesis. Lysosomes are important for mTORC1 activation and further downstream signaling, but the effects of the loss of TFEB in T cells are still unknown. However, transcription factor A mitochondrial (TFAM) has also been shown to play a role in T cell lysosomal function[59]. Deletion of TFAM in T cells impairs lysosomal function and promotes proinflammatory T cell differentiation, linking T cell homeostasis with differentiation. For mitochondrial function, Yin Yang 1 (YY1) acts as a mediator between mTOR and mitochondrial biogenesis; mTOR activates YY1 to promote mitochondrial biogenesis via transcriptional coactivator PPAR gamma coactivator 1 alpha (PGC1α)[60]. These families of transcription factors allow T cells to integrate environmental metabolite signals, initiating fine-tuned gene programs associated with cell proliferation, differentiation, and homeostasis.

As described above, T cells rely on metabolism to both become activated and make complex fate determinations. However, these decisions are often carried out in environments where T cells have adequate metabolites to carry out these functions. When the microenvironment cannot metabolically support T cell expansion, the signals to grow and differentiate can be misinterpreted, resulting in T cell dysfunction.

1.5 METABOLISM OF T CELLS IN THE TUMOR MICROEVNIORNMENT

When T cells infiltrate the TME, they are subjected to immunosuppressive signals and low metabolites. These signals impact T cell function in the form of immunologic and

metabolic checkpoints (Figure 2). In this section, we will discuss immunologic and metabolic checkpoints and how they overlap to suppress effector function in the TME.

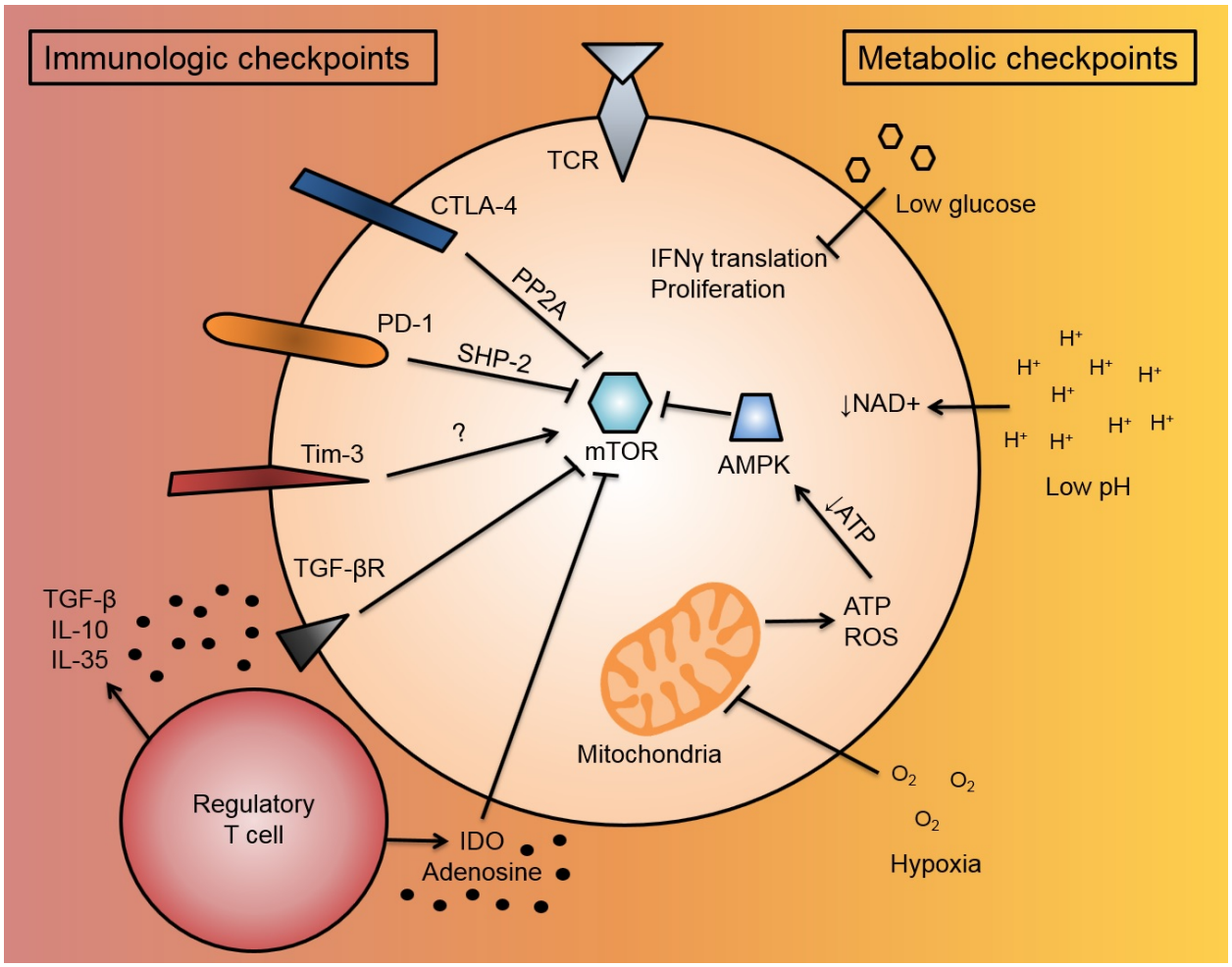

Figure 2. T cell immunologic and metabolic checkpoints in the tumor microenvironment

When a T cell enters the TME, it is subjected to a variety of immunosuppressive and metabolic signals, termed “immunologic and metabolic checkpoints”, which have overlapping functionalities to suppress T cell function. When a T cell becomes activated, it upregulates co-inhibitory molecules, such as CTLA-4 and PD-1, to inhibit further activation. These cell-intrinsic co-inhibitory molecules inhibit mTOR function through PP2A or SHP-2 signaling, respectively. Tim-3, another co-inhibitory molecule, can activate mTOR through unknown mechanisms. For cell-extrinsic immunologic checkpoints, immunosuppressive cells in the TME, such as regulatory T cells and MDSCs, can secrete or convert soluble factors, such as TGF-β, IL-10, IL-35, IDO, or adenosine, which suppress T cell activity. TGF-β can suppress T cell activity by suppressing mTOR through TGF-βR signaling. IDO also can suppress mTOR. For metabolic checkpoints, low glucose has been shown to inhibit IFNγ cytokine translation and T cell proliferation. The low pH of the TME prevents the regeneration of NAD+, important as a reducing equivalent to drive the mitochondrial

TCA cycle forward to generate ATP. TME hypoxia can also inhibit the mitochondria by limiting electron acceptors of ATP synthase. This can decrease T cell ROS, as well as decrease cellular ATP levels. Low cellular ATP activates AMPK, which can further inhibit mTOR activity. Abbreviations include tumor microenvironment (TME), cytotoxic T lymphocyte-associated protein-4 (CTLA-4), programmed death-1 (PD-1), mechanistic target of rapamycin (mTOR), protein phosphatase 2A (PP2A), SH2-domain containing tyrosine phosphatase 2 (SHP-2), T cell immunoglobulin and mucin domain containing-3 (Tim-3), myeloid-derived suppressor cells (MDSCs), transforming growth factor-beta (TGF-β), interleukin-10 (IL-10), interleukin-35 (IL-35), indoleamine 2,3-dioxygenase (IDO), interferon gamma (IFNγ), tricarboxylic acid (TCA), reactive oxygen species (ROS), and 5′ AMP-activated protein kinase (AMPK).

1.5.1 T Cell Co-Inhibitory Signaling and Metabolism

Classical immunosuppressive mechanisms in the TME can overlap with the more recently elucidated metabolic checkpoints. T cell co-inhibitory molecules, found on CD8+ T cells that enter the TME, have signaling pathways that intersect with metabolic signaling. The co-inhibitory molecule CTLA-4, which is upregulated upon T cell activation and competes with CD28 for B7 ligands, can intersect with mTOR via protein phosphatase 2A (PP2A)[61]. PP2A, a regulatory phosphatase involved with cell cycle regulation, is recruited to the cytoplasmic tail of CTLA-4 and can inhibit mTOR activity by dephosphorylating and inactivating upstream Akt[61–63]. The co-inhibitory molecule PD-1 can also inhibit mTOR via SH2-domain containing tyrosine phosphatase 2 (SHP-2) signaling[64–66]. SHP-2 is recruited to the immunoreceptor tyrosine-based switch motif (ITSM) sequence in the PD-1 cytoplasmic tail, and SHP-2 has been shown to inhibit phosphoinositide 3-kinase (PI3K) activity, thereby inhibiting downstream Akt and mTOR

activity. Forkhead box protein o1 (Foxo1), a transcription factor downstream of Akt and mTOR signaling, also intersects with co-inhibitory signaling[67]. Impaired Akt and mTOR signaling due to chronic viral infection enhances Foxo1 activity, thereby increasing the expression of PD-1 on T cells. Additionally, Tim-3, which is found upregulated on exhausted T cells, has been implicated in upregulating ribosomal protein S6, downstream of the PI3K/Akt/mTOR pathway[68]. Rather than inhibiting mTOR, Tim-3 could be promoting it, increasing glycolysis and other metabolic functions.

T cells upregulate co-inhibitory molecules to prevent further activation of already activated cells[8]. This prevents the pathological effects of unrestrained activation and potential autoimmune or autoinflammatory tissue damage. It makes sense that these co-inhibitory molecules (CTLA-4 and PD-1) evolved to also inhibit the metabolic phenotype of activation. However, the ligand used to signal through Tim-3 in the tumor microenvironment and the consequent downstream signaling pathways are still unclear. However, the idea that Tim-3 might increase mTOR function may help to discover the true function of Tim-3 on activated T cells.

1.5.2 Low Glucose and T Cell Function

The importance of glucose for T cell function was first determined with *in vitro* assays. When T cells have limited access to glucose, they decrease their glycolytic flux through a decrease in Akt activity and can activate proapoptotic B cell lymphoma-2 (Bcl-2) family members to induce apoptosis[69–71]. Recent work has begun to explore in-depth how the metabolite-deficient TME impacts the effector function of T cells. Several recent studies in tumor-T cell immunometabolism have focused on understanding how low

glucose availability impacts T cell functionality in the TME[72–74]. Rendering tumor cells more glycolytic by increasing tumor cell glucose uptake makes CD8+ T cells less capable of controlling tumor growth[72]. It was also shown that tumor cell-specific checkpoint blockade reduces tumor cell glucose uptake, restoring glucose to the TME, which may be one reason for the success of co-inhibitory checkpoint blockade as an immunotherapeutic[72]. In addition, another recent study has shown that the glycolytic metabolite phosphoenolpyruvate is important for sustaining calcium-mediated nuclear factor of activated T cells (NFAT) signaling to enable conventional CD4+ T cell function in the tumor[73]. The low glucose TME has also been shown to decrease methyltransferase enhancer of zeste homolog 2 (EZH2) expression in T cells in the setting of ovarian cancer[74]. Low EZH2 expression led to a decreased ability of T cells to perform glycolysis and effector functions and also decreased T cell survival. Therefore, glucose is an essential metabolite for T cell function, but its limited availability in the TME contributes to metabolically-induced T cell dysfunction.

1.5.3 Hypoxia and Tumor-Infiltrating T Cell Function

Oxygen availability is low in the TME due to both poor vascularization of the tumor and the high oxygen consumption of proliferative tumor cells[21,22]. Decreased oxygen tension is a classic hallmark of the tumor microenvironment, but its effects of hypoxia on T cell function are still nebulous[1,75]. Much of our understanding of hypoxia's effect on T cells is derived from genetic manipulation of the hypoxia sensing machinery, including prolyl hydroxylase domain-containing proteins (PHD), Von Hippel-Lindau (VHL) and hypoxia inducible factor 1 alpha (HIF1α)[75]. HIF1α is stabilized in hypoxia, but it is also stabilized

upon T cell activation, due in part to Myc upregulation and consequent glycolytic reprogramming[51]. Thus, it is difficult to interpret how the deletion or overexpression of HIF1α might actually represent a T cell's response to hypoxia *in vivo*. Nevertheless, in several different types of experimental systems, low oxygen seems to result in decreased T cell proliferation, with variable effects on cell survival and function[76]. Oxygen availability and its impact on infiltrating CD8+ T cell function have also begun to be explored by giving supplemental oxygen to tumor-bearing mice to decrease TME hypoxia[77]. This led to increased T cell infiltration, increased proinflammatory cytokines and improved tumor regression and enhanced survival in mice. Overall, oxygen is an important metabolite needed both for T cell and tumor cell function and is robustly competed for in the TME.

Chapter 3 of this thesis further explores how tumor hypoxia inhibits T cell function, as well as response to immunotherapy, which has also been published[78]. We first compared the oxygen consumption rate (OCR) of two different tumor cell lines, B16 melanoma and MC38 adenocarcinoma, and found they had different inherent differences in their metabolism. We also confirmed that CD8 T cells functioned poorly in low oxygen (hypoxia) by culturing them in 1.5% oxygen *in vitro*, to mimic the TME. We found when tumor cells were treated with metformin, a type II diabetes drug that inhibits mitochondrial oxygen consumption, tumor cell hypoxia decreased both *in vitro* and *in vivo.* Interestingly, while metformin decreased tumor cell OCR, CD8+ TIL OCR increased with metformin. We hypothesized this was due to metformin being preferentially taken up by tumor cells, as B16 and MC38 had 100 fold higher expression of the metformin transporter, Slc22a1. Metformin decreased CD8+ TIL hypoxia, which

allowed for increased CD8+ TIL activation, but metformin alone did not improve tumor clearance and CD8+ TIL from metformin-treated animals actually had increased exhaustion. However, when metformin was used in combination with checkpoint blockade, T cell effector function was dramatically increased, 80% of mice experienced tumor regression, and 70% of mice became tumor-free. Our data shows that decreasing tumor hypoxia can improve immunotherapeutic efficacy, which may provide an explanation as to why some patients do not benefit from checkpoint blockade monotherapy and may help to inform future combinatorial therapies.

1.5.4 TME Metabolites and Tumor-Infiltrating T Cell Function

The TME has low or altered metabolites compared to other environments in the body. The TME has low availability of many amino acids, especially glutamine, due to its use as a primary fuel for tumor cells[79]. Because glutamine is an important amino acid for T cells and a lack of glutamine prevents T cell activation and differentiation, the low glutamine TME is detrimental for T cell function[80,81]. The amino acid tryptophan is also low in the TME, due to the tryptophan-metabolizing enzyme indoleamine 2,3-dioxygenase (IDO) expressed by tumor cells and regulatory immune cells[82]. Both the loss of tryptophan from the environment and the increase of the tryptophan catabolite kynurenine are immunosuppressive. The amino acid arginine is also low in the TME, due to its consumption by tumor cells and by myeloid cell arginase-mediated depletion, and arginine is required in activated and proliferating T cells[83,84]. Lactic acid, the byproduct of deregulated tumor cell glycolysis, is extraordinarily immunosuppressive, inhibiting T cell function and cytokine production through both pH-dependent changes,

as well as loss of cytosolic NAD+ regeneration[85]. In addition, extracellular adenosine has been shown to be immunosuppressive. Extracellular ATP, released from dying cells, can be metabolized to adenosine by CD39 and CD73 expressed on the surface of regulatory T cells, MDSCs and tumor cells[86]. This adenosine binds to the adenosine A2A receptor on the surface of T cells to suppress T cell activity and induce regulatory T cells. Thus, the TME has many metabolic deficiencies, every one of them detrimental on its own for T cell function. T cell activation may therefore be crippled in the TME due to this “perfect storm” of metabolically-suppressive signals, acting along many axes to restrain T cell function.

1.5.5 Mitochondria and Tumor-Infiltrating T Cell Function

Mitochondria are more than the “powerhouse” of the cell: they are biosynthetic factories, used to generate the material for daughter cells, which help to form a T cell “clonal army”[18]. Mitochondria also are essential for T cell effector function, especially to generate reactive oxygen species (ROS) for T cell cytolytic activity[87]. Recently, even the morphology of mitochondria has been linked to T cell fate. Activated effector T cells undergo dramatic mitochondrial remodeling, forming punctate mitochondria caused by fission, while memory T cells are characterized by a fused network of mitochondria under the control of mitochondrial fusion protein optic atrophy 1 (Opa1)[88]. These mitochondrial fusion networks have superior oxidative function, an important hallmark of T cell memory, and function better in solid tumors. It may be that these different mitochondrial morphologies impact T cell function directly, and future studies in mitochondrial and metabolic dynamics will identify how these crucial processes are

dynamically regulated and reprogrammed during the life of the T cell. However, these processes can be critically regulated in response to cancer.

Chapter 4 of this thesis further explores how T cells lose mitochondrial activity and mass upon entering the TME, which has also been published[89]. This loss of mitochondria is a process that correlates with upregulation of co-inhibitory checkpoint molecules (Figure 3). This loss is caused by decreased mitochondrial biogenesis, due in part to repression of the transcriptional co-activator PGC1α. Chronic Akt signaling was found to drive down PGC1α expression in tumor-infiltrating T cells, and PGC1α levels could be partially restored with Akt inhibition, consistent with the finding that Akt inhibition promotes the expansion of quantitatively and qualitatively better TIL for adoptive cell therapy[90]. Enforcing PGC1α expression via genetic reprogramming also increased mitochondrial fitness in TIL, improving T cell functionality and decreasing tumor burden when adoptively transferred into a melanoma mouse model[89]. Similar mitochondrial deficiencies have been observed in T cells during chronic viral infection, suggesting that repression of PGC1α is a driving factor for decreased mitochondrial activity[91]. Thus, improving mitochondrial quantity by programming biogenesis of mitochondria or improving their quality by promoting fusion and morphologic changes may endow T cells with greater persistence and function in the nutrient-dearth TME.

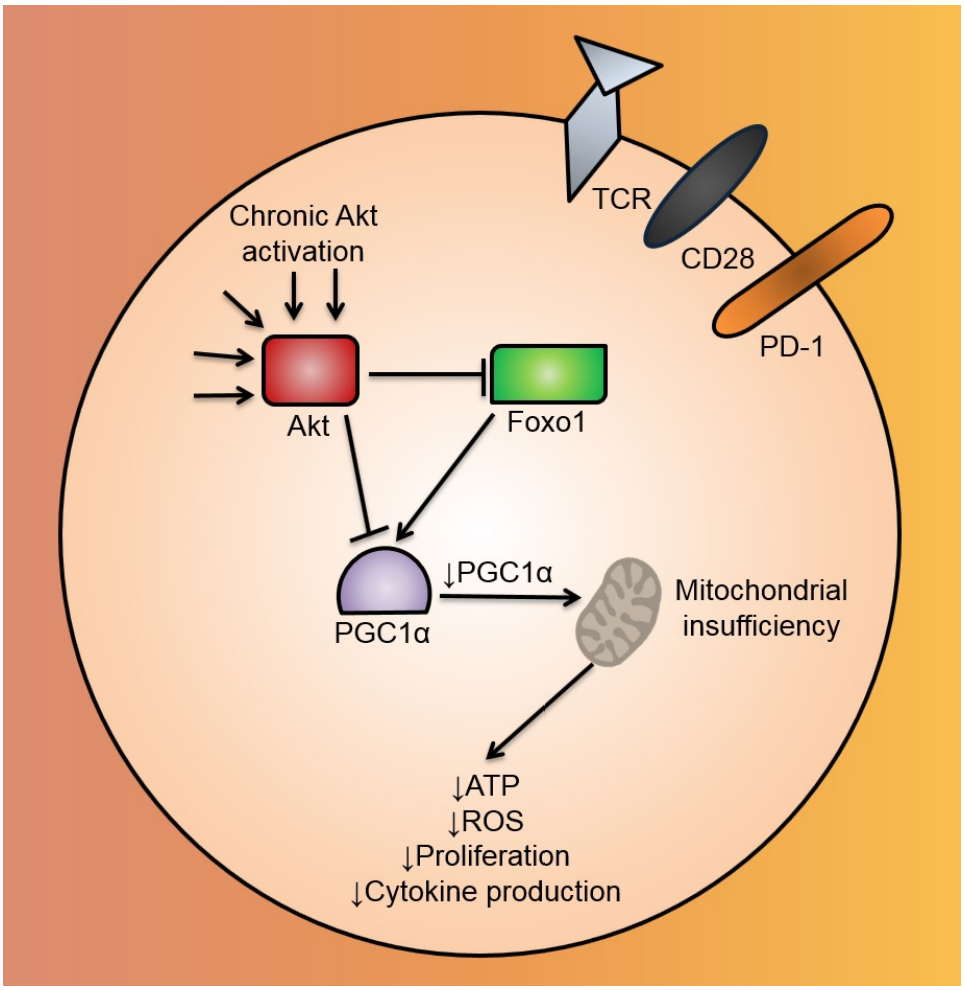

Figure 3. Mitochondrial biogenesis is repressed by Akt-mediated repression of PGC1α in CD8+ TIL

CD8+ TIL in the TME have chronically-activated Akt. Akt, either acting directly or indirectly via Foxo1, inhibits the mitochondrial biogenesis transcriptional coactivator, PGC1α. Repressed mitochondrial biogenesis leads to mitochondrial insufficiency, causing the CD8+ TIL to have functional defects, such as decreased ATP, ROS, cytokine production and proliferation. Abbreviations include tumor-infiltrating lymphocyte (TIL), tumor microenvironment (TME), Forkhead box protein o1 (Foxo1), PPAR gamma coactivator 1 alpha (PGC1α), and reactive oxygen species (ROS).

Chapter 5 of this thesis further explores how terminally exhausted T cells store rather than burn lipids, which is data that has not yet been published. In the TME, CD8+ T cells become exhausted due in part to chronic TCR engagement, in addition to the other environmental factors listed above. The T cells that experience prolonged T cell activation become what is known as terminally exhausted, or more severely dysfunctional. We found that this dysfunction includes decreased fatty acid oxidation, resulting in increased lipid storage as lipid droplets. This increase in lipid storage requires both chronic TCR activation and hypoxia, which we modeled in an *in vitro* T cell exhaustion assay. We have also found the metabolic defects in terminally exhausted T cells leads to changes in their epigenetic profile, causing exhausted T cells to have increased “poised” gene loci. The T cell exhaustion phenotype is driven by excess mitochondrial ROS, which causes both excess lipid storage and DNA damage. Finally, we show that targeting the excess lipid storage through both genetic and pharmacological means improves T cell function and outcomes in cancer.

1.6 CONCLUSIONS

The success of several immunotherapeutic approaches in cancer has generated incredible interest in tumor immunology, promoting the search for the next big checkpoint that might surpass PD-1. We would argue that along with the immune checkpoints that inhibit T cell responses in the TME, there are a variety of metabolic checkpoints that negatively impact TIL function. From low extracellular metabolites to

inhibitory metabolic signaling, the TME is an environment that by its basic nature prevents T cells from functioning adequately or killing their targets. While metabolic dysregulation is a relatively common phenotype of cancer cells, it is clear that there is considerable heterogeneity between patients and even intratumorally, suggesting that some patients may harbor more “metabolically aggressive” tumors than others. Thus, understanding the metabolic qualities of a patient’s tumor could provide clinicians with biomarkers to better understand the specific metabolically-inhibitory nature of a cancer. Furthermore, understanding the precise energetic defects in TIL and the effect of the microenvironment on these defects has the promise to not only synergize to improve existing immunotherapies, but potentially provide novel avenues to re-invigorate endogenous T cells by directly relieving these potent metabolic checkpoints.

2.0 EARLY TCR SIGNALING INDUCES RAPID AEROBIC GLYCOLYSIS ENABLING DISTINCT ACUTE T CELL EFFECTOR FUNCTIONS

2.1 FOREWORD

This chapter was adapted from a previously published manuscript in *Cell Reports*: Ashley V. Menk*, **Nicole E. Scharping*,** Rebecca S. Moreci, Xue Zeng, Cliff Guy, Sonia Salvatore, Heekyong Bae, Jianxin Xie, Howard A. Young, Stacy Gelhaus Wendell, and Greg M. Delgoffe. “Early TCR signaling induces rapid aerobic glycolysis enabling distinct acute T cell effector functions” *Cell Reports*, 2018. DOI: 10.1016/j.celrep.2018.01.040. ***Co-first authors**.

2.2 CHAPTER SUMMARY

To fulfill bioenergetic demands of activation, T cells perform aerobic glycolysis, a process common to highly proliferative cells in which glucose is fermented into lactate rather than oxidized in mitochondria. However, the signaling events that initiate aerobic glycolysis in T cells remain unclear. We show T cell activation rapidly induces glycolysis independent of transcription, translation, CD28, and Akt and not involving increased glucose uptake or activity of glycolytic enzymes. Rather, TCR signaling promotes

activation of pyruvate dehydrogenase kinase 1 (PDHK1), inhibiting mitochondrial import of pyruvate and facilitating its breakdown into lactate. Inhibition of PDHK1 reveals this switch is required acutely for cytokine synthesis but dispensable for cytotoxicity. Functionally, cytokine synthesis is modulated via lactate dehydrogenase, which represses cytokine mRNA translation when aerobic glycolysis is disengaged. Our data provide mechanistic insight to metabolic contribution to effector T cell function and suggest that T cell function may be finely tuned through modulation of glycolytic activity.

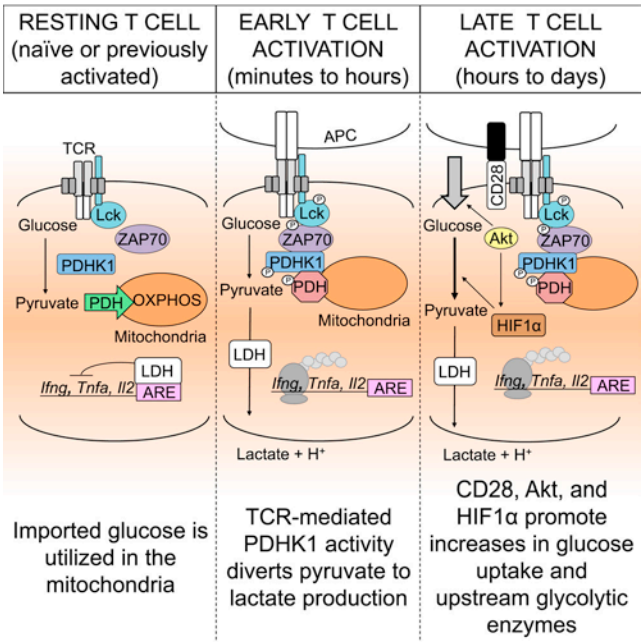

Figure 4. Graphical abstract for “Early TCR Signaling Induces Rapid Aerobic Glycolysis Enabling Distinct Acute T Cell Effector Functions”

2.3 INTRODUCTION

The activation of T cells to proliferate and develop into armed effector cells is a highly regulated process that relies on the balance of multiple signals. T cell receptor (TCR)

ligation triggers tyrosine kinase signaling, and costimulatory signals like CD28 can amplify these signals and engage important serine and threonine kinase cascades such as Akt and mTOR, leading to full T cell activation and proliferation[43]. Metabolic and nutrient sensing pathways also play a crucial role in T cell fate[28]. Effector phase T cells perform aerobic glycolysis, a metabolic state also adopted by rapidly dividing cells like cancer cells, in which despite the presence of oxygen, glucose is fermented into lactate rather than oxidized in the mitochondria[13]. Glycolysis rapidly keeps up with ATP demands in glucose-rich conditions[16], regenerates NAD+, and preserves the biosynthetic nature of the mitochondria to generate material to support proliferation[92]. However, aerobic glycolysis likely not only supports cellular function energetically but also interfaces with the acquisition of effector function through differentiation[93] and support of cytokine synthesis[27].

The molecular mechanism of the initiation of aerobic glycolysis in T cells and other cell types has been elusive[94]. Most of the glycolytic machinery is present in cells at baseline, although some proteins have isoforms that promote fermentative or oxidative pathways (pyruvate kinase M1 versus M2 and lactate dehydrogenase a versus b), suggesting that some transcriptional or post-transcriptional control might promote aerobic glycolysis[94]. Akt-mTOR signaling can also promote glycolysis through various mechanisms. Akt can phosphorylate GLUT1, facilitating its trafficking to the cell surface[95,96], modify glycolytic enzymes like hexokinase, and transcriptionally regulate metabolism through modulation of transcription factors[97]. mTOR can promote glycolysis through activation of hypoxia-inducible factor 1α (HIF1α), as well as Myc[98]. Yet it

remains unclear whether initiation or commitment to glycolytic metabolism is an early, post-translationally regulated event or a late, transcriptionally programmed process.

Thus, we sought to dissect signaling events that initiate aerobic glycolysis in T cells and understand whether the kinetics of its initiation might provide insight into molecular determinants for these events. We also wanted to determine which T cell effector functions may be under the influence of rapid glycolysis induced by T cell activation and how the glycolytic machinery might directly interact with these pathways. We found that TCR stimulation initiates a signaling event that allows T cells to immediately perform aerobic glycolysis. This rapid activation-induced glycolysis is directly linked to T cell effector function, allowing T cells to initiate effector responses shortly after activation.

2.4 METHODS

Mice

All animal work was done in accordance with the Institutional Animal Care and Use Committee of the University of Pittsburgh. All mice were housed in specific pathogen-free conditions before use. Both male and female mice were used, and mice were 6–8 weeks old at time of use. C57BL/6, OT-I, $Cd4^{Cre}$, and $Hif1a^{f/f}$ mice were obtained from The Jackson Laboratory. Mice lacking the ARE of *Ifng* were generated by Dr. Howard Young (National Cancer Institute [NCI]). $Rictor^{f/f}$ $Cd4^{cre}$ and littermate controls were obtained from Dr. Jonathan Powell (Johns Hopkins University).

T Cell Isolations

Spleen and lymph node CD4+ and CD8+ T cells were magnetically isolated from 6- to 8-week-old mice as previously described[89]. Naive T cells were isolated using CD44 (IM7)-biotin-activated magnetic depletion or by flow cytometric sorting (CD8+ or CD4+ CD62LhiCD44lo) on a Beckman Coulter Mo-Flo Astrios High Speed Cell Sorter.

PA-R T Cell Generation

To generate PA-R T cells, CD4+ or CD8+ T cells were freshly isolated from C57BL/6 and stimulated at 10×10^6/mL in complete RPMI with plate-bound anti-CD3 (3 μg/mL, BD Biosciences) and anti-CD28 (2 μg/mL, BD Biosciences), or spleen or node preparations harvested from OT-I mice were stimulated with 250 ng/mL SIINFEKL peptide (AnaSpec) in the presence of 50 U/mL IL-2 (PeproTech) for 24 hr. Cells were then expanded into complete RPMI supplemented with 50 U/mL IL-2 for 1 day, 25 U/mL IL-2 for an additional 4 days, and then 10 U/mL IL-2 for an additional 1–2 days. Some were also cultured with DCA (CAS 2156-56-1) (Fisher). Vaccinia-OVA, generated by J.R. Bennink[99] and provided by Dr. Jonathan Powell (Johns Hopkins University), was used as previously described to generate previously activated cells *in vivo*[89].

Metabolic Assays

Naive or PA-R T cells were plated on Cell-Tak-coated Seahorse Bioanalyzer XFe96 culture plates (300,000 or 100,000 cells/well, respectively) in assay media consisting of minimal, unbuffered DMEM supplemented with 1% BSA and 25 mM glucose, 2 mM glutamine, and for some experiments, 1 mM sodium pyruvate. Basal rates were taken

for 30 min, and then streptavidin-complexed anti-CD3bio at 3 μg/mL ± anti-CD28 at 2 μg/mL or PMA (CAS 16561-29-8) (Fisher) was injected and readings continued for 1–6 hr. In some experiments, oligomycin (2 μM), carbonyl cyanide p-trifluoromethoxyphenylhydrazone (FCCP) (0.5 μM), 2-deoxy-d-glucose (10 mM) rotenone/antimycin A (0.5 μM), and DCA (20 mM) were injected to obtain maximal respiratory and control values. Inhibitors used for some experiments include 5–50 mM DCA, 10 nM Lck inhibitor RK24466 (CAS 213743-31-8), 500 nM Akt inhibitor VIII (CAS 612847-09-3), 500 nM rapamycin (CAS 53123-88-9) (Cayman Chemical), 10 μM ERK inhibitor U0126 (CAS 109511-58-2), 10 μM PI3K inhibitor LY294002 (CAS 154447-36-6), 100 nM PKC inhibitor sotratorin (CAS 425637-18-9), EDTA (CAS 67526-95-8), actinomycin D (CAS 50-76-0), cycloheximide (CAS 66-81-9) (Cayman Chemical), 500 nM U-73122 PLCγ inhibitor (CAS 112648-68-7) (Sigma), and EGTA (CAS 67-42-5) (Fisher). For Jurkat T cell experiments, wild-type (WT) or ZAP-70-deficient cells were stimulated with OKT3 (BioLegend) complexed using anti-mouse immunoglobulin G (IgG). Because ECAR values tend to vary among experiments, most figure panels have both a representative trace and normalized data (calculated as the difference between maximal and basal ECAR values). Lactate was measured using the colorimetric kit from Abcam.

Retroviral RNA Interference

Short hairpin RNA (shRNA) retroviral constructs were purchased from OriGene, and OT-I T cells were transduced as previously described[89], except that puromycin (2 μg/mL) was used for selection.

Immunoblotting and Immunoprecipitation Analysis

Immunoblotting was performed as previously described[100]. Naive or PA-R T cells were stimulated with anti-CD3bio at 3 μg/mL complexed with streptavidin at 1.5 μg/mL (AnaSpec) for various times in the presence or absence of anti-CD28 at 2 μg/mL or with PMA. HEK293T cells transfected with combinations of Lck, LAT, ZAP-70, or PDHK1 overexpression vectors (A. Weiss) were used (no stimulation). All antibodies for IP or immunoblots (IBs) were obtained from Cell Signaling Technology except pPDH (S293) from Novus Biologicals and β-actin from Santa Cruz Biotechnology. IBs were detected via standard secondary detection and chemiluminescent exposure to film. Digitally captured films were analyzed densitometrically by ImageJ software.

Microscopy

Immunological synapse formation was analyzed in response to lipid bilayer stimulation as previously described[101]. Briefly, lipid bilayers containing ICAM-1 and Alexa Fluor (AF) 647-labeled anti-TCR antibodies were prepared. Resting OT-I CD8+ T cells were stimulated for 30 min before fixation with 4% paraformaldehyde, permeabilization with 0.1% T-100, and staining with antibodies overnight at 4°C. AF568-conjugated secondary antibodies and AF488-conjugated phalloidin (Fisher) were applied for 1 hr before analysis using TIRF microscopy. Images were acquired using an inverted TiE Nikon microscope equipped with a 100× 1.45 numerical aperture (NA) oil objective, motorized TIRF illumination, Andor DU-897 high-speed electron-multiplying charge-coupled device (EMCCD) camera, and Agilent laser launch. Analysis of fluorescent

intensities for each channel were determined for individual pixels using Nikon Elements software.

Functional Readouts

Cytokine production and proliferation were assessed as previously described[89], with some minor changes. CD8+ T cells were stimulated with 1 to 3 µg/mL plate-bound anti-CD3 and 2 µg/mL soluble anti-CD28 (for C57BL/6 T cells) or 250 ng/mL SIINFEKL peptide + antigen-presenting cells (for OT-I T cells) for 3–24 hr (final 4 hr in the presence of brefeldin A) and then stained intracellularly for cytokines, or secreted IFNγ was measured using an ELISA assay. For naive T cell functional assays, $CD62L^{hi}CD44^{lo}$ OT-I T cells were purified flow cytometrically, stimulated for 5 hr with T cell-depleted splenocytes and SIINFEKL peptide in the presence of brefeldin A, and then stained intracellularly for CCL3 (BioLegend). *In vitro* cytotoxicity was assessed as previously described[78]. *In vivo* cytotoxicity was measured as the change in the ratio of carboxyfluorescein succinimidyl ester $(CFSE)^{hi}$ (OVA peptide loaded) to $CFSE^{lo}$ (irrelevant control) cells after adoptive transfer of OT-I T cells and differentially CFSE-labeled target cells relative to naive mice.

RNA Immunoprecipitation

PA-R T cells were activated 18 hr with plate-bound anti-CD3 at 3 µg/mL and anti-CD28 at 2 µg/mL in the presence or absence of DCA. Cells were harvested and crosslinked with 1% formaldehyde 10 min at room temperature (RT). Cells were then lysed in RNA immunoprecipitation (RIP) lysis buffer (150 mM KCl, 25 mM Tris, 1 mM EDTA, 1% NP-

40) and precleared. Lysates were then incubated with 2 µg of anti-LDH A (LDHA) or its species-matched isotype control (Santa Cruz Biotechnology), rotating overnight at 4°C, followed by addition of 25 µL of protein A/G agarose. Beads were washed five times in RIP lysis buffer before elution with 1% SDS and 100 mM NaHCO3. Crosslinks were reversed with NaCl for 5 hr at 65°C before Trizol RNA extraction and cDNA generation.

Statistical Analysis

The p values were calculated using an unpaired Student's t test or Pearson's correlation. Values of $p < 0.05$ were considered significant. Values of $p < 0.05$ were ranked as $*p < 0.05$, $**p < 0.01$, $***p < 0.001$, and $****p < 0.0001$.

2.5 RESULTS

2.5.1 T Cell Activation Rapidly Induces Aerobic Glycolysis

To determine the glycolytic capacity of T cells in real time, we employed extracellular flux analysis using a Seahorse XFe96 bioanalyzer. Naive and previously activated, rested (PA-R) CD4+ and CD8+ T cells were activated for 6 hr *in vitro* with plate-bound anti-CD3 and anti-CD28, and oxidative metabolism (oxygen consumption rate [OCR]) and glycolysis (extracellular acidification rate [ECAR]) were measured. Consistent with previous findings[37], PA-R and naive T cells both switched metabolic states within 6 hr of activation (Figures 5A and 5B).

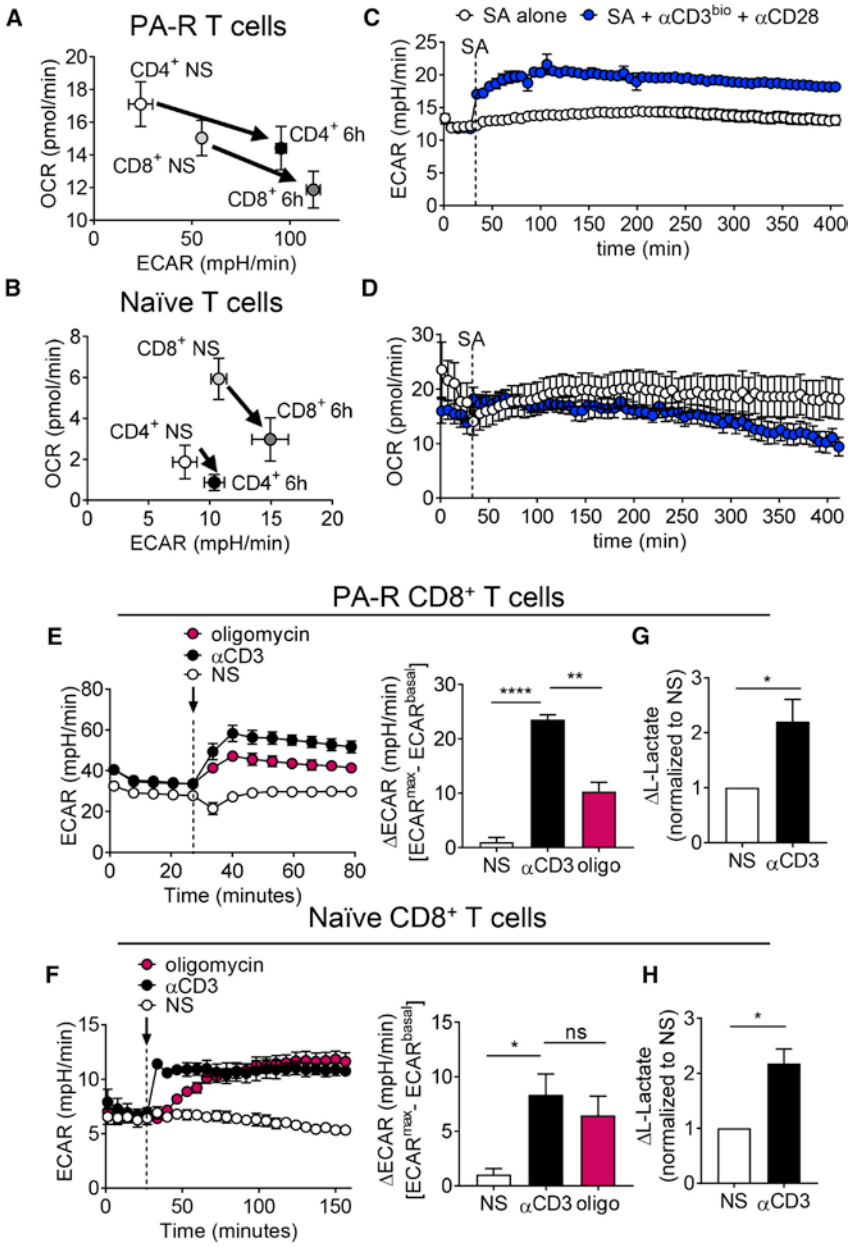

Figure 5. T Cells Rapidly Engage Aerobic Glycolysis upon Activation

(A) Extracellular. acidification rate (ECAR, x axis) and oxygen consumption rate (OCR, y axis) of PA-R T cells (plate-bound αCD3 + CD28 activation and expansion in IL-2) left resting (No Stimulation, NS) or stimulated for 6 hr with 3 μg/mL αCD3 and 2 μg/mL αCD28. (B) As in (A), but sorted naive (CD44lo) T cells. (C) ECAR trace of naive CD8+ T cells equilibrated in the Seahorse instrument and stimulated via injection of streptavidin or streptavidin-crosslinked αCD3 at 3 μg/mL and soluble αCD28 at 2 μg/mL. (D)

As in (C), but the OCR trace. (E) ECAR trace (left) and tabulated data (right) of PA-R CD8+ T cells stimulated with streptavidin (NS), streptavidin-crosslinked αCD3, or 1 μM oligomycin (which stimulates glycolytic reserve). (F) ECAR trace (left) and tabulated data (right) of naive CD8+ T cells stimulated as in (E). (G) Tabulated L-lactate measurements from PA-R CD8+ T cells stimulated for 1 hr with streptavidin or streptavidin-crosslinked αCD3 at 3 μg/mL. (H) As in (G), but with naive CD8+ T cells. Data are representative of 3 independent experiments. $*p < 0.05$, $**p < 0.01$, $***p < 0.001$. ns, not significant by unpaired t test. Error bars represent SEM.

To identify when during this 6-hr period glycolysis may be activated, naive CD8+ T cells were equilibrated in the Seahorse instrument for 30 min, and streptavidin-complexed anti-CD3 and anti-CD28 were injected to crosslink the TCR and ligate CD28. T cells engaged glycolysis within minutes of TCR activation, reaching a peak within 15 min and remaining glycolytic for the duration of the assay (Figure 5C). A concomitant loss of oxidative phosphorylation slowly occurred, reaching equilibrium around 2 hr post-stimulation (Figure 5D). Oligomycin treatment, which inhibits mitochondrial ATP synthase and stimulates cells to perform maximal levels of glycolysis, revealed that TCR ligation immediately engaged the entire glycolytic reserve of both PA-R and naive T cells (Figures 5E and 5F). ECAR activity correlated to increases in extracellular lactate concentration at time points consistent with this early change (Figures 5G and 5H). Thus, T cell activation induces a major metabolic change in the cell, *i.e*. the stimulation of nearly all capable aerobic glycolysis, within minutes.

2.5.2 TCR Signaling Alone Can Mediate Rapid Activation-Induced Glycolysis

CD28 signaling can sustain glycolysis partly through the activation of phosphatidylinositol 3-kinase (PI3K)-Akt signaling[33,95,102]. However, CD28 signaling was dispensable for the rapid initiation of aerobic glycolysis in both freshly isolated and PA-R CD8+ T cells (Figure 6A; Figure S31A). TCR signal strength determined the magnitude of glycolytic switching that occurred (Figure 6B; Figure S31B). Although CD28 has been shown to act as a signal amplifier for TCR-mediated signals, neither PA-R nor naive T cells showed enhancement of rapid activation-induced glycolysis when CD28 was combined with suboptimal TCR stimulation (Figure 6B; Figure S31B), potentially because CD8+ effector T cells are often considered co-stimulation independent[103]. Stimulating naive T cells in hours-long culture revealed that although the initial switch to glycolysis was independent of CD28 signaling (Figures 6A and 6B), sustained glycolytic function required CD28 signaling (Figure 6C), Thus, although CD28 signaling may be required for initiating transcriptional or translational changes in cellular metabolism, it is dispensable for the initiation of glycolysis that occurs just after TCR engagement.

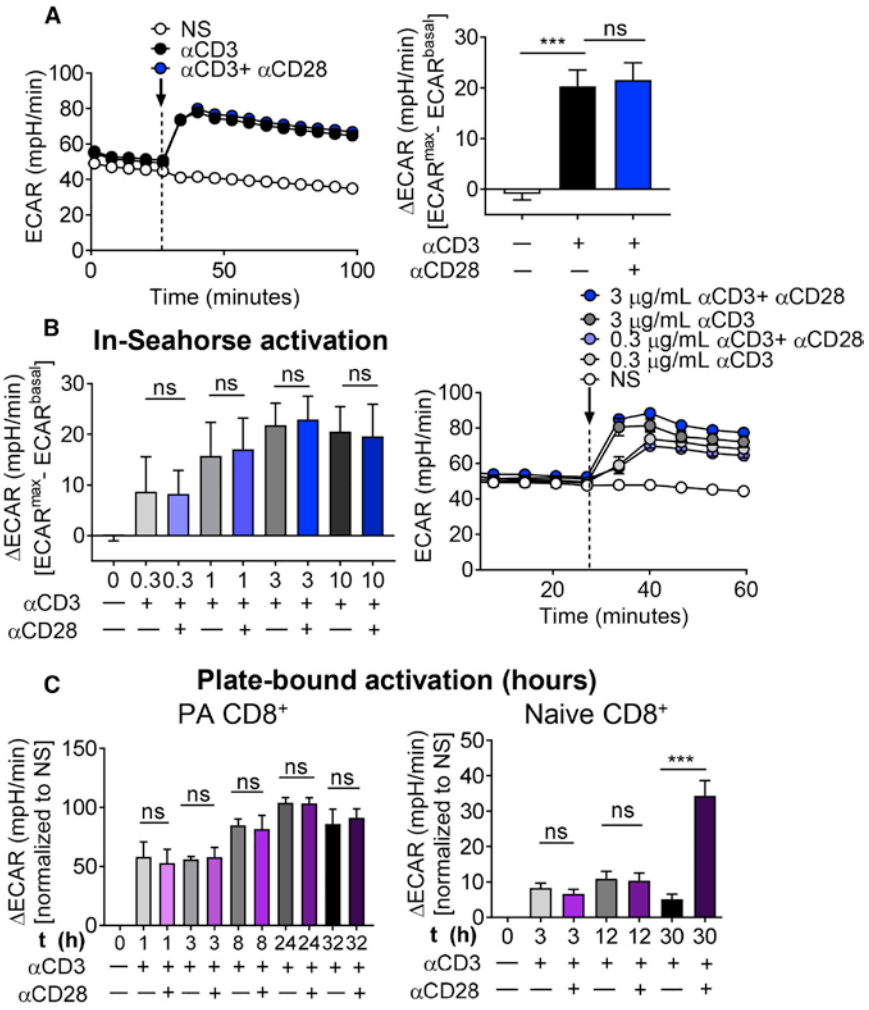

Figure 6. Initiation of Glycolysis in T Cells Is CD28 Independent

(A) ECAR trace of PA-R CD8+ T cells stimulated with streptavidin (No Stimulation, NS) or streptavidin-crosslinked αCD3 at 3 μg/mL in the presence or absence of 2 μg/mL αCD28 (left), and tabulated results (right). (B) Tabulated ECAR of PA-R CD8+ T cells stimulated with indicated amounts of streptavidin-crosslinked αCD3 in the presence or absence of αCD28 (left), and trace ECAR (right). (C) Tabulated ECAR levels of PA-R and naive CD8+ T cells stimulated for the indicated times with αCD3 in the presence or absence of 2 μg/mL αCD28 and then assayed in the Seahorse instrument. Results represent the mean of three (C) or four (A and B) independent experiments. ∗∗∗$p < 0.001$. ns, not significant by unpaired t test. Error bars represent SEM.

2.5.3 Rapid Activation-Induced Glycolysis Is Mediated by PDHK1 in a Manner Independent of Transcription, Translation, and Glucose Flux

To examine the nature of this TCR-induced glycolysis, T cells were treated with actinomycin D or cycloheximide before activation, showing that neither new transcription nor translation was necessary to initiate rapid glycolysis (Figure 7A). Furthermore, fluorescent 2-NBD-glucose uptake analysis showed glucose uptake was not elevated during these activation time points, occurring only late after stimulation (24 hr) (Figure 7B). Given that many enzymes in the glycolytic pathway can be post-translationally modified, TCR-induced changes in glycolytic enzyme phosphorylation upon T cell activation were measured. However, we observed no changes in phosphorylation of previously reported modified enzymes in the glycolytic pathway, including hexokinase, phosphoglycerasemutase, enolase, pyruvate kinase, or lactate dehydrogenase (LDH) (Figures S32A and S32B). This does not rule out other methods of modulation of glycolytic enzyme activity, but because TCR activation is driven by phosphorylation, its contribution is likely through this mechanism. These results suggested that the extracellular acidification observed immediately after T cell activation was not due to changes in glucose uptake or increases in glycolytic flux but rather due to changes in glucose processing.

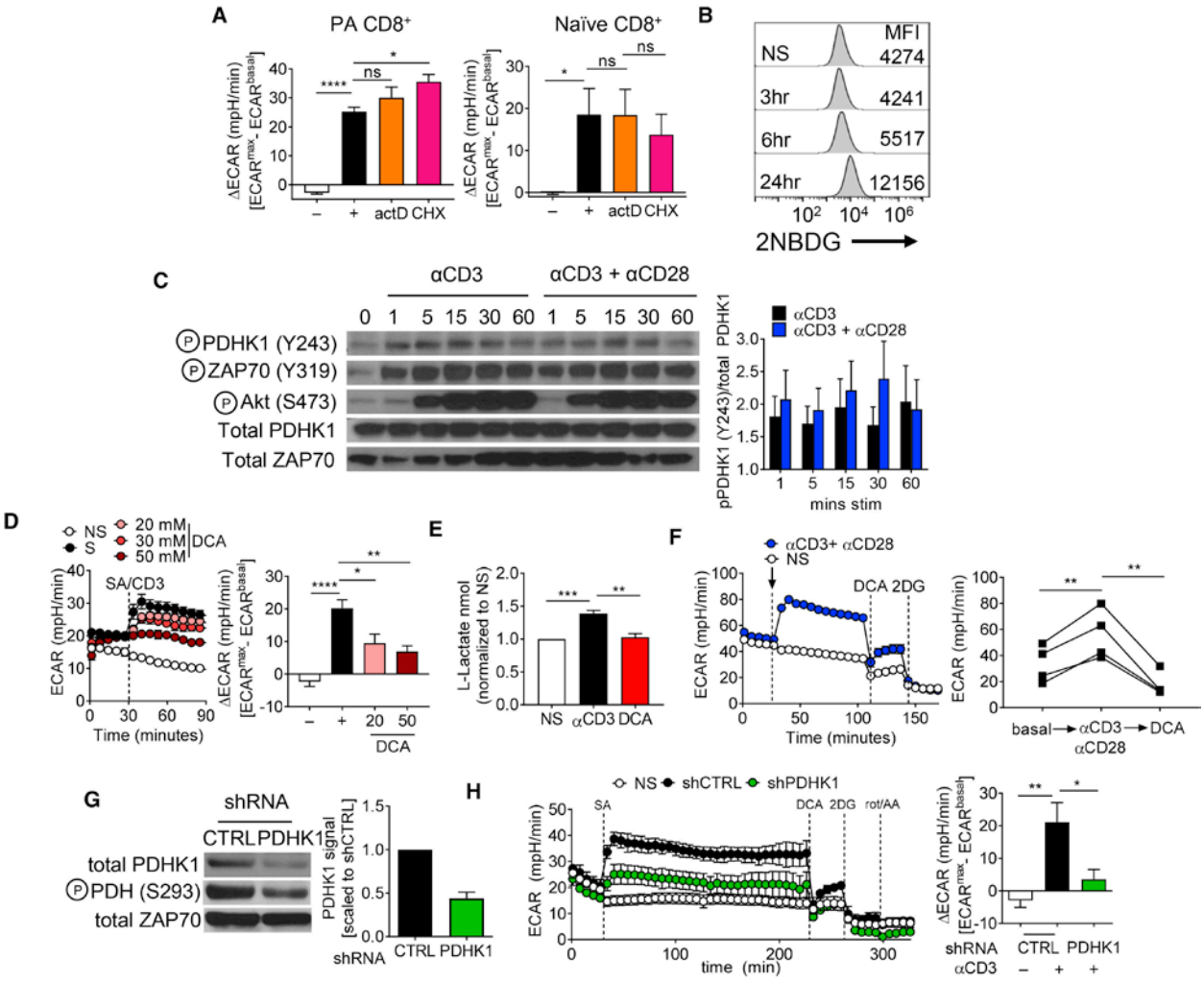

Figure 7. TCR-Induced Aerobic Glycolysis Occurs via PDHK1

(A) Tabulated ECAR of PA-R and naive CD8+ T cells stimulated with streptavidin or streptavidin-crosslinked αCD3 at 3 μg/mL in the presence or absence of transcription or translation inhibition (1 μM actinomycin D [ActD] or 10 μg/mL cycloheximide [CHX]). (B) Representative histogram of glucose uptake, using PA-R CD8+ T cells reactivated with 3 μg/mL plate-bound αCD3 + 2 μg/mL soluble αCD28 for the indicated times and then pulsed with 2NBDG. (C) Representative immunoblot (IB) of indicated phospho- or total proteins in lysates from PA-R CD8+ T cells stimulated for the indicated periods with streptavidin or streptavidin-crosslinked αCD3 at 3 μg/mL in the presence of 2 μg/mL αCD28 (left), and tabulated densitometry scanning (right). (D) ECAR trace of PA-R CD8+ T cells stimulated with streptavidin (No Stimulation, NS) or streptavidin-crosslinked αCD3 at 3 μg/mL and 2 μg/mL αCD28 in the presence or absence of the indicated amounts of dichloroacetate (DCA) (left), and tabulated ECAR (right). (E)

Tabulated L-lactate measurements from PA-R CD8+ T cells stimulated with streptavidin (NS) or streptavidin-crosslinked αCD3 at 3 μg/mL in the presence of absence of 20 mM DCA. (F) ECAR trace of PA-R CD8+ T cells stimulated as in (D) and then injected with 20 mM DCA (left), and tabulated ECAR (right). (G) Immunoblot of PDHK1, its enzymatic target pS PDH, and ZAP-70 (as a loading control) from CD8+ T cells retrovirally expressing scrambled control shRNA (shCTRL) or shRNA to Pdk1 (encoding PDHK1) (left), and tabulated densitometry scanning (right). (H) ECAR trace of cells from (G) stimulated with crosslinked αCD3 at 3 μg/mL, followed by 20 mM DCA, 10 mM 2-deoxy-d-glucose (2DG), and 500 nM rotenone/antimycin A (left), and tabulated ECAR (right). Results represent three (A–C, E, and G), four (F and H), or five (D) independent experiments. $*p < 0.05$, $**p < 0.01$, $****p < 0.0001$ by unpaired t test. ns, not significant. Error bars represent SEM.

Pyruvate flux into mitochondria is controlled by pyruvate dehydrogenase (PDH), which both facilitates pyruvate import into the mitochondria and catalyzes its conversion to acetyl-coenzyme A (CoA) for the tricarboxylic acid (TCA) cycle[104]. A prominent form of PDH regulation is modification by phosphorylation by the glycolytic gatekeeper pyruvate dehydrogenase kinase 1 (PDHK1, encoded by Pdk1)[104]. This results in inhibition of PDH function, blocking pyruvate flow into mitochondria, and facilitating lactic acid conversion by LDH. In cancer, PDHK1 can be phosphorylated by oncogenic tyrosine kinases, stimulating its function to promote glycolysis[105]. Tyrosine phosphorylation of PDHK1 (measured using a phosphotyrosine immunoprecipitation and immunoblotting, and a specific phosphotyrosine antibody in whole-cell lysates) was rapidly induced upon TCR ligation and in a CD28-independent manner in T cells (Figure 7C; Figure S32C). We employed dichloroacetate (DCA), a specific inhibitor of PDHK1, to block activity of PDHK1 in the presence of TCR signals[106–108]. Inhibition of PDHK1 with DCA prevented the initiation of glycolysis in PA-R T cells, shown both using

Seahorse ECAR and direct lactate measurements (Figures 7D and 7E). The activity of PDHK1, read out by its phosphorylation of PDH, was also increased upon T cell activation and inhibited by DCA treatment (Figure S32D). Furthermore, DCA treatment of T cells already undergoing rapid activation-induced glycolysis reduced ECAR to preactivation levels (Figure 7F).

To further support the hypothesis that activation-induced PDHK1 activity alters the path of glucose processing, freshly isolated T cells were stimulated with anti-CD3 alone in normal glucose-containing media for 30 min and then pulsed with uniformly labeled 13C-glucose for another 30 min to conduct isotopic flux analysis (Figure S32E). Glucose-derived pyruvate levels were unchanged at 30 min between resting and stimulated cells, confirming that glycolytic enzymatic activity that produces pyruvate from glucose was not altered by TCR activation (Figure S32F). 13C-labeled lactate was markedly increased in the media in response to TCR signaling in a DCA-dependent manner (and thus PDHK1-dependent manner) (Figure S32G). Finally, consistent with the notion that PDHK1 activation inhibits pyruvate processing in the mitochondria, less incorporation of labeled carbon was observed in the TCA cycle intermediates malate and citrate in response to stimulation, which was mitigated by DCA treatment (Figures S32H and S32I). However, only glucose-derived TCA cycle activity was inhibited, because the abundance of unlabeled TCA cycle intermediates remained unchanged regardless of treatment (Figure S32J).

Genetic targeting of PDHK1 was also employed to further define its role in glycolytic switching. PDHK1 was knocked down using retroviral RNA interference during CD8+ T cell expansion (Figure 7G). This revealed a significant decrease in activation-

induced glycolysis (Figure 7H). Thus, PDHK1 is an important signaling node induced by early T cell activation that facilitates the rapid switch in the bioenergetic fate of glucose.

2.5.4 The Glycolytic Gatekeeper PDHK1 Is Activated by Early TCR Signaling

TCR engagement induces tyrosine phosphorylation of several kinases and previous studies have suggested that in cancer, oncogenic receptor tyrosine kinases (RTKs) bind to and phosphorylate PDHK1, especially FGFR1[105]. Two TCR-induced kinases, ZAP-70 and Lck share significant homology with FGFR1, suggesting these might bind to PDHK1. Indeed, we found PDHK1 was coimmunoprecipitated with Lck at steady state and upon activation, PDHK1 bound to ZAP-70, suggesting these proteins might exist in a complex (Figure 8A). In addition, ZAP-70-deficient Jurkat T cells failed to engage rapid glycolysis upon stimulation with OKT3 (Figures S33A and S33B). To determine which early TCR signaling molecules PDHK1 directly interacted with upon T cell activation, HEK293T cells were transfected with different combinations of PDHK1, linker of activated T cells (LAT), and constitutively active Lck or Zap70 to study their interactions in a non-T cell system[109]. PDHK1 could bind directly to Lck or Lat, but interaction with Zap70 required the presence of Lck or LAT (Figure 8B). Total internal reflection fluorescence (TIRF) microscopy of PA-R T cells on stimulatory lipid bilayers revealed that total and phosphorylated PDHK1 were present at and were significantly associated with the T cell synapse upon T cell activation (Figure 8C).

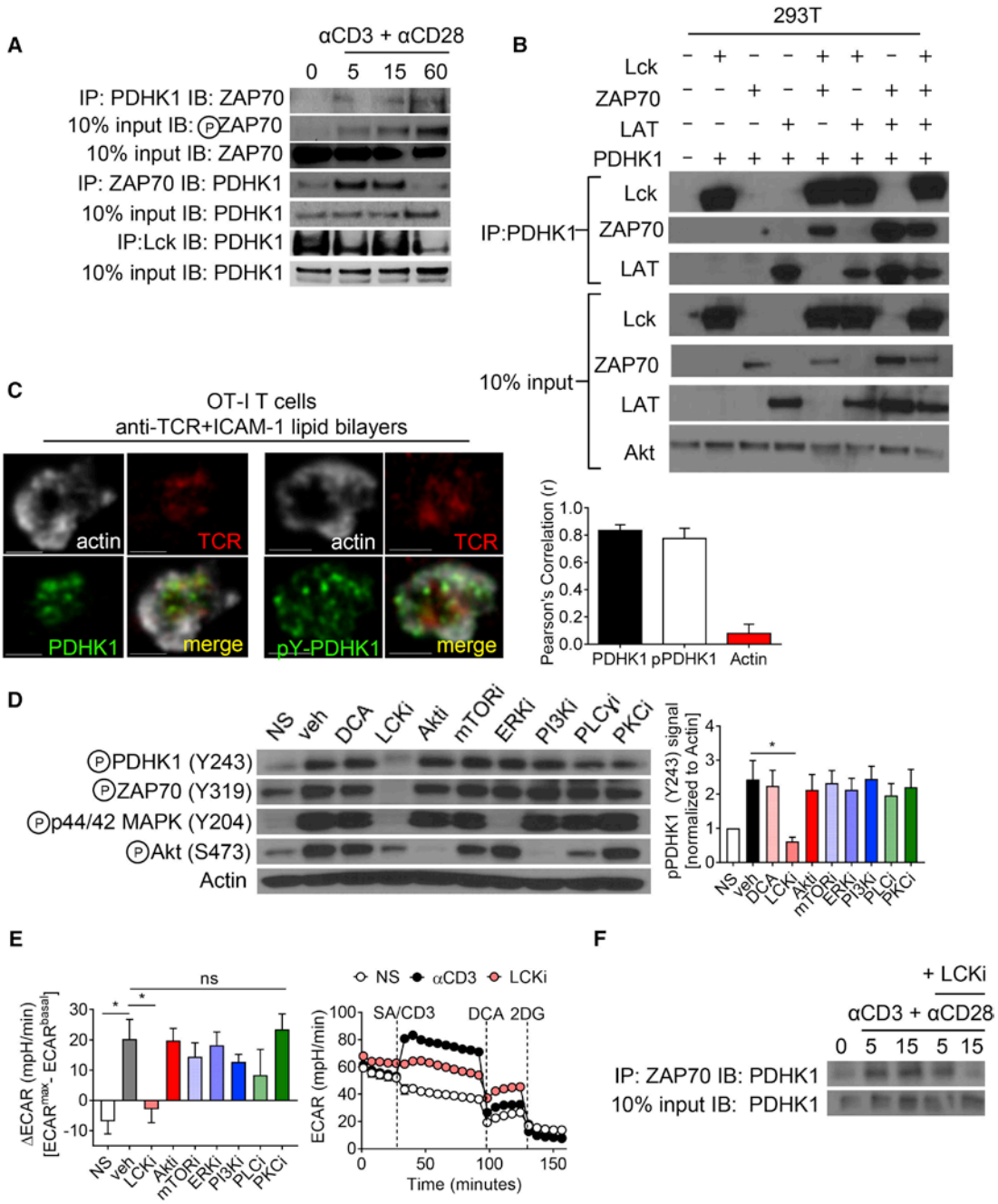

Figure 8. Proximal TCR Signaling Molecules Interact with PDHK1

(A) Immunoblot of immunoprecipitations of the indicated proteins in lysates from CD8+ T cells stimulated with streptavidin or streptavidin-crosslinked αCD3 at 3 μg/mL and αCD28 at 2 μg/mL for the indicated times. (B) Immunoblot of immunoprecipitations of PDHK1 from HEK293T cells transfected with the indicated combinations of Lck, LAT, ZAP-70, and PDHK1 expression vectors. (C) TIRF microscopy images of OT-I T cells stimulated on αTCR and ICAM-1 containing stimulatory lipid bilayers for 15 min

and then stained intracellularly for total and phospho-PDHK1 (left), and Pearson's correlation in proximity to TCR (right). (D) Immunoblot of indicated proteins in lysates from PA-R CD8+ T cells stimulated with streptavidin (No Stimulation, NS) or streptavidin-crosslinked αCD3 at 3 μg/mL in the presence or absence of the indicated inhibitors (left), and tabulated densitometry (right). (E) Tabulated ECAR of PA-R CD8+ T cells stimulated as in (D) in the presence or absence of the indicated inhibitors (left), and trace ECAR of Lck inhibition (right). (F) Immunoblot of immunoprecipitations of the indicated proteins in lysates from PA-R CD8+ T cells stimulated as in (A) for the indicated times in the presence or absence of 10 nM Lck inhibitor. Results represent the mean of three (A, D, and F), four (B), five (E), or seven (C) independent experiments. $*p < 0.05$ by unpaired t test. ns, not significant. Error bars represent SEM.

To determine whether more distal signaling pathways were engaging the glycolytic machinery, T cells were treated with the minimal effective doses of several reported signaling module inhibitors induced during TCR activation, confirming Lck inhibition prevented PDHK1 phosphorylation and rapid activation-induced glycolysis (Figures 8D and 8E) and preventing the interaction of PDHK1 and Zap70 (Figure 8F). In stark contrast, Akt, mTOR, ERK, PI3K, PLC, protein kinase C (PKC), and calcium flux were dispensable for induction of rapid glycolysis and phosphorylation of PDHK1 (Figures 8D and 8E; Figure S33C). These results were particularly surprising because Akt has been implicated in early-immediate glycolysis in human memory T cells[38]. PI3K-Akt was also not sufficient to induce glycolysis, because in-Seahorse stimulation of PI3K with a PTEN inhibitor did not engage glycolysis (Figure S33D). Likewise, T cells from $Rictor^{f/f}Cd4^{Cre}$ mice, in which Akt cannot be phosphorylated by mTORC2[50], were still able to initiate glycolysis after activation (Figure S33E).

Another previously reported contributor to glycolysis is HIF1α, which promotes glycolysis through transcriptional and post-translational changes, including the

upregulation of PDHK1[110]. Naive T cells from Hif1a$^{f/f}$ Cd4^{Cre} mice were able to initiate rapid glycolysis, as well as their wild-type counterparts (Figure S33F). Activation and expansion of HIF1α-deficient T cells revealed their basal glycolysis was lower than that of wild-type cells, consistent with the notion that HIF1α promotes a transcriptional glycolytic program (Figure S33G). However, these previously activated HIF1α-deficient T cells induce rapid glycolysis upon reactivation to the same degree relative to their basal levels, indicating that PDHK1's role in glycolysis is distinct from that of HIF1α (Figures S33G and S33H). Hyperactivation of PKC alone using the phorbol ester phorbol 12-myristate 13-acetate (PMA) can also initiate glycolysis in PA-R T cells, but to a lesser degree, with distinct kinetics and without engaging PDHK1 (Figures S33I and S33J). Thus, the initiation of glycolysis occurs directly downstream of the TCR in an Lck-dependent manner via the kinase PDHK1.

2.5.5 Rapid Activation-Induced Glycolysis Regulates Distinct Acute Effector Functions

Aerobic glycolysis has been previously shown to be critical for T cell effector function, as measured by cytokine production, but is used interchangeably with oxidative phosphorylation (OXPHOS) to meet the metabolic needs of T cell proliferation and expansion[27,94]. Consistent with these reports, at high doses, DCA-mediated PDHK1 inhibition had effects on proliferation after 96 hr (Figure S34A). Because this pathway is induced minutes after activation, its major importance may be to support the early-immediate, rapid effector function of T cells competent to produce cytokines.

Previous reports have suggested glycolysis is important for the synthesis of cytokine in typical stimulation conditions[27]. Inhibition of PDHK1 in the early phase inhibited the ability of effector CD8+ T cells to rapidly synthesize interferon gamma (IFNγ), interleukin (IL)-2, or tumor necrosis factor alpha (TNFα) early after TCR activation (1 hr–6 hr) (Figures 9A and 9B). DCA treatment also inhibited cytokine production in overnight activation, suggesting that although this switch is induced quickly upon activation, it is also used later into the activation phase to facilitate cytokine synthesis and secretion (Figure 9C). To fully interrogate effector function, the cytotoxic potential of T cells was also examined. Inhibition of PDHK1-mediated glycolysis had a minimal effect on cytolytic capacity (Figure 9D), and DCA-treated cells were still able to produce the cytolytic molecules perforin and granzyme B (Figure S34B). PDHK1 inhibition by DCA was not toxic to the cells (Figure S34C). Consistent with the role of PDHK1 as a gatekeeper enzyme rather than a promoter of glycolytic flux, PDHK1 inhibition did not change the ability of T cells to take up glucose (Figure S34D). PDHK1 inhibition had similar effects on in vivo-generated CD8+ effector T cells. Using OT-I transfer and ovalbumin (OVA)-expressing Vaccinia virus, we observed inhibition of cytokine production (Figure S34E) and preserved cytotoxic function *in vivo* (Figure 9E) in the presence of PDHK1 inhibition.

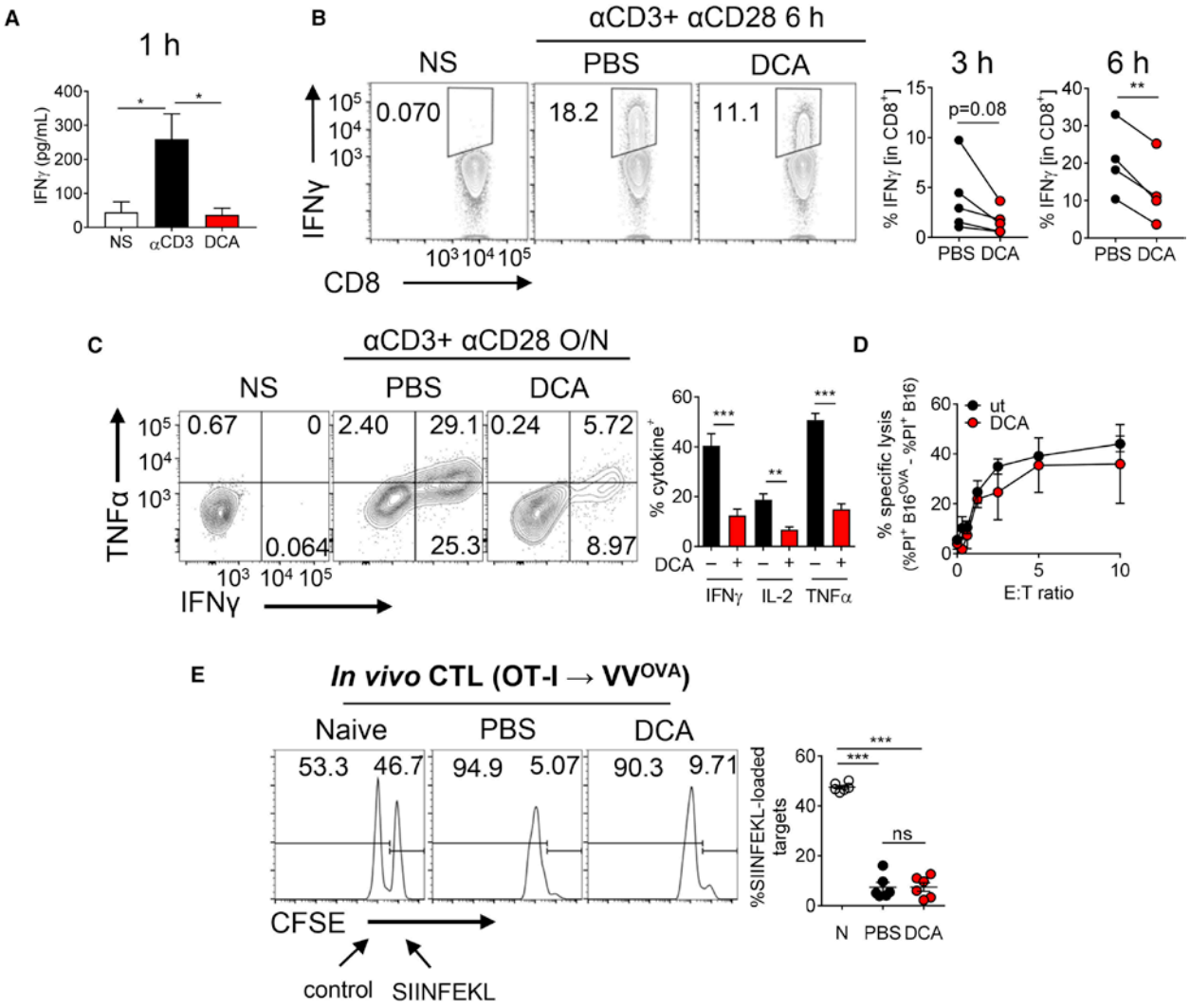

Figure 9. PDHK1-Mediated Glycolysis Is Required for Cytokine Production but Dispensable for Cytotoxic T Cell Function

(A) Tabulated IFNγ ELISA data from PA-R CD8+ T cells, in which cells were pretreated with 20 mM DCA 30 min before 1-hr activation via streptavidin-crosslinked αCD3 at 3 μg/mL. (B) Representative flow cytogram (left) and tabulated cytokine production (right) from PA-R CD8+ T cells stimulated for 6 hr with 3 μg/mL αCD3 and 2 μg/mL αCD28 in the presence or absence of 20 mM DCA. (C) Representative flow cytogram (left) and tabulated cytokine production (right) from PA-R CD8+ T cells stimulated overnight with 3 μg/mL αCD3 and 2 μg/mL αCD28 in the presence or absence of 5 mM DCA. (D) Quantified in vitro cytotoxicity assay using PA-R OT-I T cells cultured with OVA-expressing or parental B16 melanoma cells in the presence or absence of 5 mM DCA. (E) Representative cytogram (left) and tabulated results (right)

of an in vivo cytotoxicity assay in which OT-I cytotoxic T lymphocyte (CTL) were generated in vivo with vaccinia virus (VV)OVA, after which mice receive an adoptive transfer of control or cognate-peptide-loaded splenocyte targets differentially labeled with CFSE and an immunoprecipitation (IP) injection of either PBS or DCA. Results represent the mean of five (C), four (B), or three (A, D, and E) independent experiments. $*p < 0.05$, $**p < 0.01$, $***p < 0.001$ by unpaired t test. Error bars represent SEM.

Although we and others have shown that aerobic glycolysis promotes acute effector function of T cells, there have been reports that aerobic glycolysis also promotes IFNγ competency during Th1 differentiation through a long-term, epigenetic mechanism[93]. These studies were done with LDH-deficient animals, which have essentially irreversible inhibition of aerobic glycolysis. Employing pharmacological and reversible inhibition of aerobic glycolysis via DCA could thus both confirm the role of aerobic glycolysis in T cell differentiation and reveal a role for this pathway in acute effector function of T cells. Similar to previous reports using LDH-deficient T cells, inhibiting glycolysis for 7 days using the PDHK1 inhibitor DCA during PA-R T cell generation prevented T cell differentiation, as evidenced by an inability to produce IFNγ (Figure S34F). In addition, genetic targeting using retroviral RNA interference caused a decrease in cytokine production but had no effect on perforin or granzyme B production or the ability for the cells to kill target cells *in vitro* (Figures S34G–S34I). However, this inhibited cytokine synthesis occurred even when PDHK1 was active during the restimulation (DCA treatment during differentiation but washed out before restimulation) (Figure S34F). This suggests that aerobic glycolysis plays a secondary, long-term role in maintaining the T cell differentiation state in a manner distinct from the control of acute cytokine production we and others have observed.

Our previous data suggested that naive T cells also engaged this rapid glycolytic switch in response to TCR stimulation (Figures 5 and 6). Because naive T cells generally are not cytokine competent, we explored the contribution of this early glycolytic switch to their function, taking advantage of the reversibility of DCA-mediated PDHK1 inhibition. Washout experiments, in which DCA was only present during 12 hr of initial stimulation, revealed that this early glycolytic switch was dispensable for expansion of naive T cells, suggesting that its contribution might be limited to the acute phase (Figure S35A). In addition, when PDHK1 was inhibited only during activation, it did not negatively affect glucose uptake, mitochondrial mass or polarization, or the ability for T cells to produce IFNγ after restimulation, suggesting that PDHK1-mediated glycolysis is especially important for short-term functions in response to acute activation (Figures S35B and S35C). Although naive T cells do not synthesize cytokine, they rapidly make other chemical mediators, including chemokines like CCL3. Naive ($CD62L^{hi}CD44^{lo}$) OT-I T cells stimulated with peptide and antigen presenting cells (APCs) for 5 hr revealed CCL3 production was strikingly dependent on glycolysis (Figure S35D). Thus, it appears that this rapid metabolic change is important, both in naive and in PA-R effector T cells, in early, acute synthetic functions of T cells.

2.5.6 Rapid Activation-Induced Glycolysis Supports Post-transcriptional Control of Cytokine Synthesis through LDH

Although, aerobic glycolysis can contribute to effector function by promoting epigenetic changes supporting T cell differentiation, our data and others' also suggest a more immediate role for glycolysis in acute effector function. Although T cells undergo this

major metabolic change during their early cytokine-producing phase, they do not increase their ability to take up glucose (Figure 7B). This suggested that the ability to engage aerobic glycolysis and thus support effector function would depend on the availability of glucose in the environment, acting as a sensor for nutrient availability. To test this, PA-R T cells were stimulated for a short time (3 hr) in the Seahorse in various suboptimal concentrations of glucose, revealing that the extent of PDHK1-mediated aerobic glycolysis depended on the availability of glucose, reaching saturation around 5 mM, after which no more glucose could be fermented (Figure 10A). Measurement of IFNγ secretion from these same Seahorse assay wells by ELISA revealed that cytokine production, while occurring in even zero-glucose conditions, showed a substantial increase as glucose availability increased (Figure 10B). This is in agreement with previous data suggesting cytokine synthesis was linked to extracellular glucose availability[53]. DCA treatment during the assay revealed that this supplemental cytokine synthesis depended on the PDHK1-mediated switch (Figure 10B). However, neither glucose concentrations nor PDHK1 activity appreciably changed the mRNA levels of *Ifng* (or *Tnf* or *Il2*) cytokine transcripts, even though these cells produce lower amounts of these cytokines after either short-term (3 hr) or long-term (overnight) stimulation (Figures 10B and 10C; Figure S36). Previous studies have revealed a role for metabolic enzymes, especially GAPDH, in modulating cytokine mRNA stability[27]. However, GAPDH, an enzyme several steps upstream of pyruvate, is used for glucose processing regardless of whether pyruvate is oxidized in mitochondria or fermented into lactate, and DCA treatment fails to inhibit GAPDH activity[111]. However, LDH, which catalyzes the interconversion of pyruvate and lactate and is the only glycolytic enzyme with

differential function in DCA-treated cells, has also been shown to have RNA-binding function. Previously studies have shown that LDH, like GAPDH, binds the AU-rich element (ARE) in the 3′ UTR of mRNAs like granulocyte-macrophage colony stimulating factor (GM-CSF) and with greater affinity than GAPDH[112]. We activated PA-R CD8+ T cells overnight in the presence or absence of DCA and performed RNA immunoprecipitation using anti-LDH antibodies (Figure 10D). LDH bound mRNA transcripts for the cytokines IFNγ, TNFα, and IL-2 in resting T cells, but upon activation, this binding was significantly reduced. Inhibition of PDHK1-mediated glycolysis during activation resulted in enhanced binding of LDH to cytokine mRNA, suggesting that LDH may be mediating post-transcriptional regulation of these cytokine transcripts (Figure 10D). LDH failed to bind transcripts for the cytotoxicity gene Gzmb, which lacks an ARE in its 3′ UTR (Figure 10D), supporting the model that cytolytic capacity does not require glycolysis (Figure 9E; Figures S34B, S34H, and S34I). These experiments were conducted using a full overnight stimulation to induce optimal transcription and translation of cytokine rather than using an acute activation protocol. However, the PDHK1-mediated glycolytic switch is important for optimal elaboration of cytokine even in overnight stimulatory conditions (Figure 9C). To confirm the role of the ARE in LDH-mediated mRNA control, T cells were assayed from mice in which the *Ifng* 3′ UTR has been replaced with a scrambled nucleotide insertion, resulting in a transcript that is the same size as wild-type *Ifng* but lacks the ARE[113]. T cells with this mutation are resistant to DCA-mediated inhibition of IFNγ synthesis (Figures 10E and 10F). Specificity of this effect was confirmed, because IL-2 was still repressed with DCA treatment in $Ifng^{\Delta ARE}$ T cells (Figure 10F). Thus, the initiation of aerobic glycolysis in T cells promotes effector

cytokine production partly through the alleviation of LDH-mediated repression of mRNA translation.

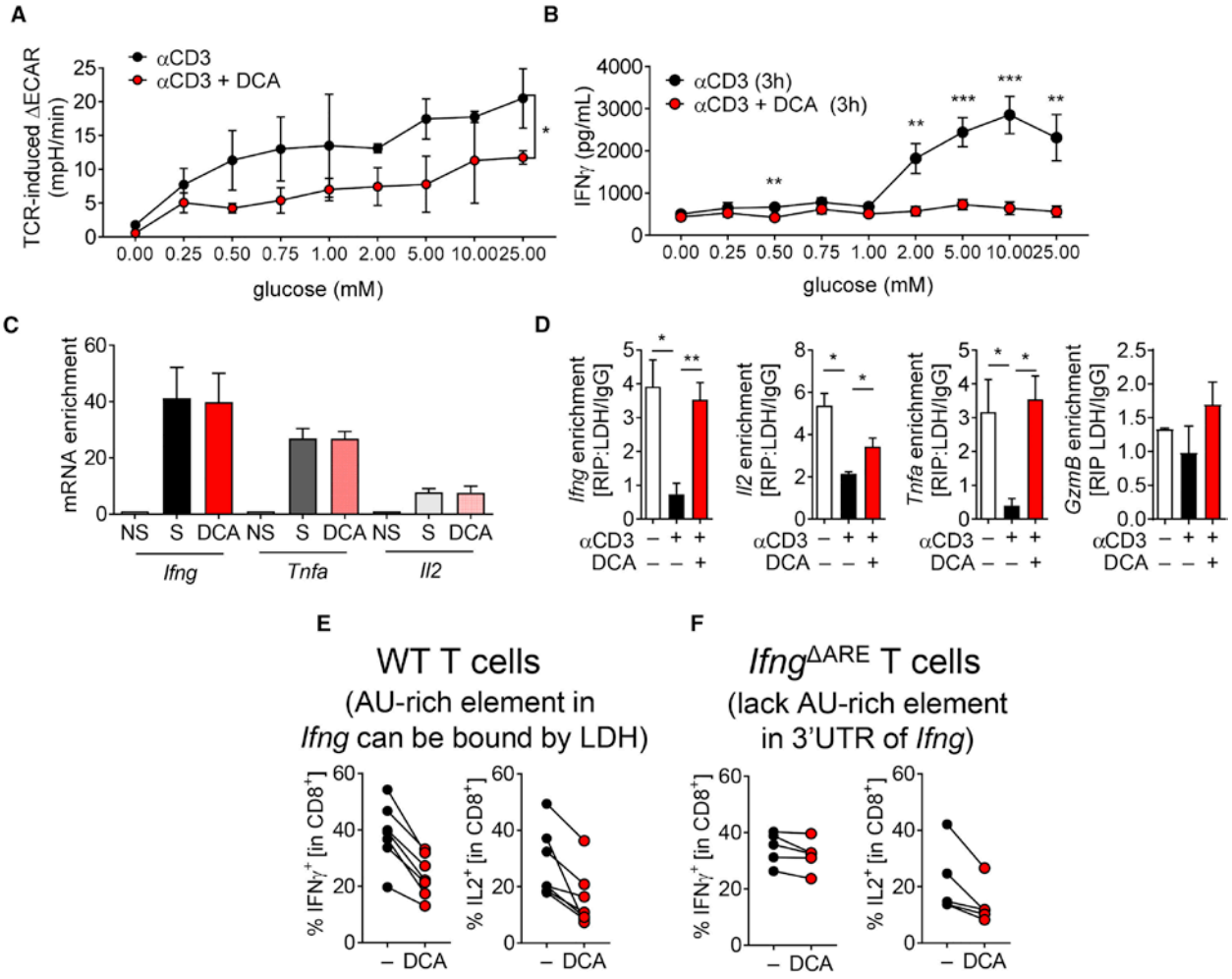

Figure 10. PDHK1-Mediated Aerobic Glycolysis Integrates Glucose Availability and LDH Activity to Control Cytokine Synthesis at the Post-transcriptional Level

(A) Tabulated ECAR generated from PA-R CD8+ T cells stimulated with streptavidin or streptavidin-crosslinked αCD3 at 3 μg/mL in the presence or absence of 20 mM DCA in the indicated concentration of glucose. (B) IFNγ production from supernatant collected from the flux analysis experiment in (A) measured by ELISA. (C) qPCR analysis of cDNA generated from RNA extracted from PA-R CD8+ T cells stimulated overnight with 3 μg/mL αCD3 and 2 μg/mL αCD28 in the presence or absence of DCA. mRNA levels of the indicated cytokines were standardized with Actb expression. (D) qPCR analysis of cDNA generated from RNA IP using LDHA-specific antibodies or a species-specific control. Precipitates were prepared from PA-R CD8+ T cells left resting or stimulated with 3 μg/mL αCD3 and 2 μg/mL αCD28 in the presence or absence of DCA overnight and then crosslinked with 1% formaldehyde before RNA IP. Results are expressed as fold enrichment over species-specific control (IgG). (E) IFNγ and IL-2

production (measured by flow cytometry) of WT CD8+ T cells stimulated with 3 μg/mL αCD3 and 2 μg/mL αCD28 in the presence of DCA. (F) IFNγ and IL-2 production of T cells stimulated with 3 μg/mL αCD3 and 2 μg/mL αCD28 from mice homozygous for a targeted deletion of the Ifng AU-rich element (ARE) (ΔA) or littermate controls. Results represent the mean of three (A–D) or two (E and F) (n = 5–7 mice per group) independent experiments. $*p < 0.05$, $**p < 0.01$, $***p < 0.001$ by two-way ANOVA (A) unpaired t test (B–F). Error bars represent SEM.

2.6 DISCUSSION

The immune response interfaces heavily with metabolic and nutrient sensing pathways, the study of which has garnered interest in recent years[114]. Although it has been known for decades that lymphocytes carry out aerobic glycolysis during activation[26], it has only recently become clear which signals may initiate or sustain this metabolism. In addition, the functional relevance of aerobic glycolysis, in particular the epigenetic and post-transcriptional control of effector function, has just been realized[27,37,93]. Our results reveal four previously unappreciated aspects of activation-mediated metabolic reprogramming.

First, our data suggest that rapid activation-induced glycolysis, occurring immediately after TCR ligation, bears hallmarks that make this metabolic pathway distinct from the aerobic glycolysis of actively proliferating T cells. Thus, this effect occurs in a transcription- and translation-independent manner and does not enhance or require increased glucose uptake in T cells. Rather, our studies support a model in which this rapid activation-induced glycolysis is a distinct metabolic switch promoting

pyruvate to lactate conversion immediately after activation, to support short-term effector function.

Second, although CD28 and Akt signaling were previously shown to be critical for the upregulation of metabolic machinery and the maintenance of glycolysis throughout T cell expansion[33,102,115], the initiating events of glycolysis, occurring almost immediately after T cell activation, are CD28 and Akt independent. Although Akt has been associated with rapid induction of glycolysis previously using effector memory cells[38], our studies using the minimal inhibitory dose of Akt/PI3K inhibition, as well as genetic deletion of the Akt kinase, reveal this pathway is dispensable for rapid activation-induced glycolysis, at least in murine effector T cells. It is possible that Akt may play a larger role in bona fide memory T cells (rather than *in vitro*-generated PA-R T cells) to promote this metabolic switch, suggesting additional complexity in the regulation of these signaling pathways in distinct differentiation states.

Third, our studies suggest that PDHK1-mediated initiation of aerobic glycolysis, while required for optimal cytokine production and secretion[27], is dispensable for other effector functions, such as proliferation and cytolytic function. Our studies are in agreement with previously published data implicating glycolysis in the post-translational control of cytokine translation[27,53] but reveal that cytotoxicity is an effector function that can be distinguished, metabolically, from cytokine production. Furthermore, using PDHK1 inhibition as a reversible inhibitor of LDH activity, we confirmed that aerobic glycolysis plays a role in the regulation of differentiation in a manner that is distinct from its control of acute effector function. This was accomplished using DCA, which reversibly inhibits PDHK1 activity. Although we confirmed the metabolic and functional

roles of PDHK1 using RNA interference, the irreversibility of genetic deletion made separating acute functional versus epigenetic or differentiation effects difficult. Future experiments will employ inducible genetic inhibition experiments to more specifically inhibit PDHK1's activity, which has been as important for PMA- and ionomycin-elicited IL-17 cytokine production in CD4+ helper T cells[116]. Our data in CD8+ T cells are largely in agreement with this previous work, although by stimulating using TCR crosslinking (anti-CD3 and/or cognate peptide), we have revealed that additional cytokines (Ifng, Il2, and Tnfa) are under control of PDHK1-mediated aerobic glycolysis. In addition, by using *in vivo*-generated effector T cells using Vaccinia virus, we highlight the link between our *in vitro*-generated findings *in vivo* biological significance, although more elegant detection methods will surely enable future functional and metabolic analysis of acutely activated T cells *in vivo*.

Fourth, our data support a role for LDH as a key node linking aerobic glycolysis and cytokine production. LDH, like GAPDH and other metabolic enzymes, binds AREs present in cytokine (and presumably chemokine) transcripts, repressing translation in a non-glycolytic state. Thus, part of the glycolytic phenotype is the relief of cytokine mRNA from LDH-mediated translational repression. Because key cytotoxic granule genes like Gzmb and Prf1 lack an ARE in their 3′ UTR, they are not regulated by aerobic glycolysis, in concordance with our functional data. Our data in naive T cells show that CCL3, a chemokine rapidly secreted in response to activation, is also under glycolytic control: it too bears an ARE in its 3′ UTR[117], suggesting that a range of proteins may be modulated in response to rapid glycolysis. These data provide evidence that rapid activation-induced glycolysis is a general T cell phenomenon,

regardless of differentiation state. It is the goal of future work to determine the full implication of these findings, such as other mRNA sequences regulated by glycolytic enzymes and differences in regulated mRNA between T cell types and differentiation states.

In agreement with previous reports[27], inhibition of aerobic glycolysis during short-term activation (30 min to 6 hr) does not repress cytokine production, resulting in a consistent 40%–50% reduction in cytokine levels. We believe this is not a technical issue, but rather indicative of real biology. This pathway, by its nature, does not increase glucose uptake or glycolytic processing; rather, it changes how pyruvate is metabolized, thereby affecting the activity of LDH. Thus, our data support a model in which, during early T cell activation, glycolysis acts as a rheostat or throttle for cytokine production, tuning the amount of cytokine translation to match the metabolic state of the microenvironment, which is consistent with our glucose titration experiments. This has wide-ranging implications for T cell activation in the tissues, which typically possess far lower concentrations of glucose than typical cell culture media. Of particular interest is activation in the tumor microenvironment, which has dramatically reduced concentrations of glucose and increased levels of lactic acid, which both may alter the ability of even optimally activated T cells to effectively synthesize cytokines[73,89]. It is the goal of future work to translate these mechanistic insights, identifying how glycolytic activity and subsequent effector molecule synthesis may be modulated during *in vivo* activation, especially in environments in which nutrients may be limited or abundant.

Many other cell types demonstrate rapid effector functions, synthesizing cytokines hours after activation, which may be regulated by this rapid activation-induced

glycolysis. In support of this, we have shown that mast cells stimulated through the FcεR rapidly trigger glycolysis that is important for their cytokine production[118]. We anticipate other rapid cytokine-producing cells will use similar tyrosine signaling cascades to promote rapid glycolysis, including FcγR-stimulated natural killer (NK) cells, invariant natural killer T (iNKT) cells, and B cells.

Previous studies have implicated glycolysis in T cell activation, avoidance of anergy, and regulate the balance of effector versus memory differentiation[33,37,38,95,102,119]. Many studies have used 2-deoxy-d-glucose (2DG), which inhibits the entire glycolytic pathway starting at hexokinase, as well as N-linked glycosylation[120]. Other studies have use galactose, which through the Leloir pathway can still enter the glycolytic process[121]. In addition, some studies have used steady-state genetic perturbations many of these enzymes[93]. Inhibition of PDHK1, in contrast, does not perturb glucose flux or enzymatically perturb any stage of glycolysis, thus effectively targeting only the activation-induced glycolytic pathways[122]. Furthermore, we believe that using pharmacological, reversible inhibition of this switch rather than genetic deletion has confirmed the role of this pathway in epigenetic control of differentiation, as well as acute control of effector function.

Our data support a model placing these early, key changes in glucose metabolism central to the execution of the acute effector T cell program in differentiated, cytokine competent cells, as well as early synthesis programs like chemokine production even in naive T cells. This is initiated by the TCR at the level of PDHK1 and is functionally modulatory at the level of LDH. This antigen receptor-mediated, rapid activation-induced glycolysis constitutes a metabolic pathway that is fundamentally

distinct from those longer-term, transcriptionally regulated changes that characterize proliferating T cells. Our work also suggests that different functions of lymphocytes may be effectively distinguished through metabolic means. As such, understanding how these distinct metabolic pathways interface with immune effector programs may allow for the use of metabolic intervention to functionally modulate the immune response with greater precision.

3.0 EFFICACY OF PD-1 BLOCKADE IS POTENTIATED BY METFORMIN-INDUCED REDUCTION OF TUMOR HYPOXIA

3.1 FOREWORD

This chapter was adapted from a previously published manuscript in *Cancer Immunology Research*: **Nicole E. Scharping**, Ashley V. Menk, Ryan D Whetstone, Xue Zeng, and Greg M. Delgoffe. “Efficacy of PD-1 blockade is potentiated by metformin-induced reduction of tumor hypoxia.” *Cancer Immunology Research*, 2017. DOI: 10.1158/2326-6066.CIR-16-0103.

3.2 CHAPTER SUMMARY

Blockade of the coinhibitory checkpoint molecule PD-1 has emerged as an effective treatment for many cancers, resulting in remarkable responses. However, despite successes in the clinic, most patients do not respond to PD-1 blockade. Metabolic dysregulation is a common phenotype in cancer, but both patients and tumors themselves are metabolically heterogeneous. We hypothesized that the deregulated oxidative energetics of tumor cells present a metabolic barrier to antitumor immunity through the generation of a hypoxic microenvironment and that normalization of tumor

hypoxia might improve response to immunotherapy. We show that the murine tumor lines B16 and MC38 differed in their ability to consume oxygen and produce hypoxic environments, which correlated with their sensitivity to checkpoint blockade. Metformin, a broadly prescribed type II diabetes treatment, inhibited oxygen consumption in tumor cells *in vitro* and *in vivo*, resulting in reduced intratumoral hypoxia. Although metformin monotherapy had little therapeutic benefit in highly aggressive tumors, combination of metformin with PD-1 blockade resulted in improved intratumoral T-cell function and tumor clearance. Our data suggest tumor hypoxia acts as a barrier to immunotherapy and that remodeling the hypoxic tumor microenvironment has the potential to convert patients resistant to immunotherapy into those that receive clinical benefit.

3.3 INTRODUCTION

Immunotherapy has emerged as a viable and effective treatment for a variety of cancer types. One of the major successes in cancer immunotherapy involves the antibody-mediated blockade of coinhibitory “checkpoint” molecules, negative regulators highly upregulated on the surface of tumor-infiltrating T cells[123]. The goal of these treatments is to relieve cell-intrinsic inhibition of a patient's own immune response to the cancer treatment. Antibodies targeting cytotoxic lymphocyte antigen 4 (CTLA-4) and programmed death 1 (PD-1) signaling, alone or in combination, have resulted in durable antitumor immunity and remarkable clinical responses[123].

It is now accepted that tumors generate a suppressive microenvironment that acts to evade and inhibit immune responses by a number of distinct factors, including

recruitment of suppressive populations like regulatory T cells, as well as secretion of suppressive cytokines[124]. However, it is now becoming clear that the metabolic nature of the tumor microenvironment also contributes to suppression of antitumor immunity[125]. Carrying out T-cell effector function is metabolically demanding, requiring intermediates necessary for proliferation, cytokine synthesis, and cytotoxicity[126]. The tumor microenvironment typically has low concentrations of glucose and other metabolites, an acidic interstitial pH, and low oxygen tension[127]. This is due to altered blood supply as well as deregulated energetics of tumor cells themselves[127]. Thus, in addition to being inhibited through immunosuppressive mechanisms, tumor-infiltrating T cells also may lack the fuel required for effector function.

Hypoxia is a well-known component of the tumor microenvironment and has been rigorously studied in a variety of experimental systems and patient samples[128]. Hypoxia is generally considered to be immunosuppressive, although previous studies employing HIF1α, VHL-, and PHD-deficient T cells have revealed that the role of these proteins in T-cell differentiation and function is complex[75,129]. The effects of “true” hypoxia remain unclear, as apparent roles for oxygen tension in T cell differentiation versus effector function can be disparate[130]. Still, oxidative phosphorylation (OXPHOS) is required for many aspects of T-cell function[131]. Thus, we examined how oxygen tension plays a role in responses to immunotherapy using murine models of cancer, coupled with metabolic analysis and pharmacologic modulation of the tumor microenvironment.

Here, we demonstrate mitigation of tumor hypoxia using the mitochondrial complex 1 inhibitor metformin. Remodeling of the tumor microenvironment this way

resulted in increased sensitivity to PD-1 blockade, increased intratumoral T-cell function, and tumor regression.

3.4 METHODS

Mice

All animal work was done in accordance with the Institutional Animal Care and Use Committee of the University of Pittsburgh (Pittsburgh, PA). All mice were housed in specific pathogen-free conditions. Six- to 8-week-old mice of similar weight and mixed genders were randomized prior to experimentation. C57/BL6, SJ/L (Thy1.1), and OT-I mice were obtained from The Jackson Laboratory.

Reagents and cell lines

B16-F10 cells were obtained from ATCC. MC38 cells were a gift from Dario Vignali (University of Pittsburgh). B16OVA (MO5) was obtained from Per Basse (University of Pittsburgh) and Lou Falo (University of Pittsburgh). Both MC38 and B16OVA have not been authenticated, but OVA expression was verified on $B16^{OVA}$ by immunoblot and flow cytometry. Cell lines were obtained in 2014, and Mycoplasma testing was performed in June 2014. Cell lines were not passaged more than three times before experimentation. Antibodies to CD8 (53-6.7), CD4 (GK1.5), PD-1 (29F.1812), Tim-3 (RMT3-23), CD44 (IM7), CD62L (MEL-14), TNFα (MP6-XT22), IFNγ (XMG1.2), CD11b (M1/70), CD11c (N4180), Ki67 (16A8), CD45 (30-F11), F4/80 (BM8), Ly6C (HK1.4), and propidium iodide were from BioLegend. Hypoxia staining was detected with an antibody

to pimonidazole (Hypoxyprobe). Antibody to PD-1 (J43) and its hamster IgG control were obtained from Bio X Cell. CellTrace Violet was purchased from eBioscience. 2-NBD-glucose and metformin were purchased from Cayman Chemical. In all in vivo studies, mice were injected with 2.5×10^5 tumor cells intradermally.

Metabolism assay

Using a Seahorse XFe96 Bioanalyzer (Agilent), B16 (50,000/well), MC38 (50,000/well), direct ex vivo sorted CD8+ lymph node cells and tumor-infiltrating lymphocytes (TIL; 100,000/well), or in vitro cultured OT1 CD8+ T cells (100,000/well) were plated on Seahorse culture plates in media consisting of minimal, unbuffered DMEM supplemented with 1% BSA and 25 mmol/L glucose, 1 mmol/L pyruvate, and 2 mmol/L glutamine. Basal oxygen consumption rates (OCR) were taken for 30 minutes. Cells were stimulated with 2 μmol/L oligomycin, 0.5 μmol/L FCCP, 100 mmol/L 2-deoxyglucose, and 100 μmol/L rotenone/antimycin A to obtain maximal respiratory and control values.

In vitro T-cell functional assays

Spleen and lymph node preparations from OT-I mice were stimulated with SIINFEKL peptide (250 ng/mL, AnaSpec) and IL2 (25 U/mL, PeproTech) for 24 hours. Cells were washed, expanded 10 fold into fresh media with IL2, and cultured for 7 days to generate previously activated cytotoxic T cells. To measure proliferation, OT-I T cells were labeled with the proliferation dye CellTrace Violet and stimulated for 72 hours with peptide and antigen-presenting cells (APC). To measure cytokine production, cells were

stimulated overnight with C57/B6 antigen-presenting cells plus SIINFEKL. Cell supernatants were analyzed by ELISA. To measure cytotoxicity, OT-I T cells were cocultured with B16 or $B16^{OVA}$ cells for 16 hours at ratios ranging from 10:1 (effector:target) to 1:2, then stained with propidium iodide to detect apoptosis in the target cells. For each assay, cells were cultured in either ambient normoxic or hypoxic conditions (1.5% O2, BioSpherix).

TIL analysis

When tumors reached ≥6 mm, mice were injected intraperitoneally with 50 mg/kg metformin (Cayman Chemical) on days −3 and −1. On day 0, mice were injected intravenously with pimonidazole (80 mg/kg, Hypoxyprobe) in PBS 1.5 hours before sacrifice. Nondraining and draining lymph nodes were harvested and manually disrupted to single-cell suspension. Explanted tumors were injected whole with a mixture of collagenase, dispase, and DNase I (Thermo Fisher Scientific), incubated at 37°C for 15 to 30 minutes, and then dissociated between two frosted glass slides to single-cell suspension. Suspensions of lymph node and tumor were filtered and vortexed at high speed for 1 minute prior to downstream analyses. Pimonidazole was visualized using anti-pimonidazole antibodies after 1% PFA fixation and 0.1% Triton X-100 permeabilization. Ki67 and cytokine staining was performed using the eBioscience Fix/Perm Kit. Cytokine staining was completed after 18-hour stimulation with PMA and ionomycin (Sigma; the final 4 hours in the presence of a protein transport inhibitor).

Histology

In some experiments, after tumor growth, metformin treatment, and pimonidazole pulsing, tumors were dissected and frozen at −80°C in Optimal Cutting Temperature Compound (OCT) (Tissue-Tek) and sectioned (Cryostat microtome). Tissue was fixed in histology-grade acetone (Fisher) at −20°C, then rehydrated in staining buffer, stained with hypoxyprobe (Hypoxyprobe) and DAPI (Life Technologies), and mounted with ProLong Diamond Antifade Mountant (Life Technologies). Sections were imaged with an Olympus IX83 microscope and analyzed with ImageJ.

Immunoblotting analysis

Direct ex vivo sorted CD8+ lymph node cells and TILs were lysed in lysis buffer (1% NP40, 150 mmol/L NaCl, 20 mmol/L Tris, 2 mmol/L EDTA, and 2 mmol/L EGTA). Lysates were denatured with lithium dodecyl sulfate and dithiothreitol. Lysates were loaded into 4%–12% Bis-Tris Plus Bolt PAGE Gels (Life Technologies). Gels were transferred to membranes using NuPAGE Bolt electroblotting in the presence of 2 mmol/L Tris, 192 mmol/L glycine, and 10% methanol. Membranes were blocked in 3% BSA in TBS with 0.1% Tween-20 (TBST). Primary antibodies to Hif1α (Cell Signaling Technology) or actin (Santa Cruz) were diluted in 3% BSA/TBST and incubated with membranes overnight. After three washes with TBST, secondary antibodies (Jackson ImmunoResearch) diluted in 3% BSA/TBST were incubated with membranes for 1 hour. After three TBST washes, membranes were incubated with Western Lightning ECL substrate and exposed to film. Digitally captured films were analyzed densitometrically by ImageJ software.

Real-time PCR

Direct *ex vivo* sorted CD8+ lymph node cells and TILs, in vitro activated CD8+ T cells, CD45-depleted direct ex vivo B16 cells, or in vitro cultured MC38 cells were lysed in TRIzol and RNA extracts were made. cDNA was reverse transcribed using the High-Capacity cDNA Reverse Transcription Kit (Applied Biosystems). Real-time PCR was performed with primers for Slc22a1 and Ppib (cyclophilin b), and quantitation was performed using the ΔΔCt method.

Metformin plus anti-PD-1 therapy

On day 5, when there were 1 to 10 mm2 palpable tumors, mice were started on either 0.2 mg anti-PD-1 or hamster IgG isotype control (Bio X Cell), injected every 4 days intraperitoneally, and metformin (50 mg/kg, Cayman Chemical) or PBS, injected every 2 days intraperitoneally. Cohorts were sacrificed when control mouse tumors reached 15 mm in any direction measured. For metformin drinking water cohorts, mice with 1 to 10 mm2 palpable tumors started on 1 g/L metformin drinking water and were injected with anti-PD-1 every 4 days intraperitoneally. Cohorts were sacrificed when control mouse tumors reached 15 mm in any direction measured.

3.5 RESULTS

3.5.1 Tumor hypoxia is variable between tumor types and inhibits T-cell function

The C57/BL6 tumor line B16-F10 (referred to here as B16) melanoma and MC38 colon adenocarcinoma are common transplantable murine tumor models and have different degrees of immunogenicity[132]. To determine whether these tumor lines also have different metabolic characteristics, we used a Seahorse Bioanalyzer to analyze the ability of these tumor cells to perform oxidative phosphorylation, read out as oxygen consumption rate (OCR). We found that B16 has a higher baseline OCR compared with MC38, as well as higher spare respiratory capacity (mitochondrial reserve induced by the uncoupling reagent FCCP; Fig. 11A). B16 and MC38 had minimal glycolytic differences, as measured by extracellular acidification rate (ECAR; Fig. 11B). The different OCR of these lines has *in vivo* effects, as CD8+ TILs display a higher degree of hypoxia in B16 tumors, as measured by binding of pimonidazole (an injectable, irreversible hypoxia tracer), than in MC38 tumors examined directly *ex vivo* (Fig. 11C). Thus, the capacity of a tumor cell to consume oxygen has effects on the TIL hypoxia phenotype.

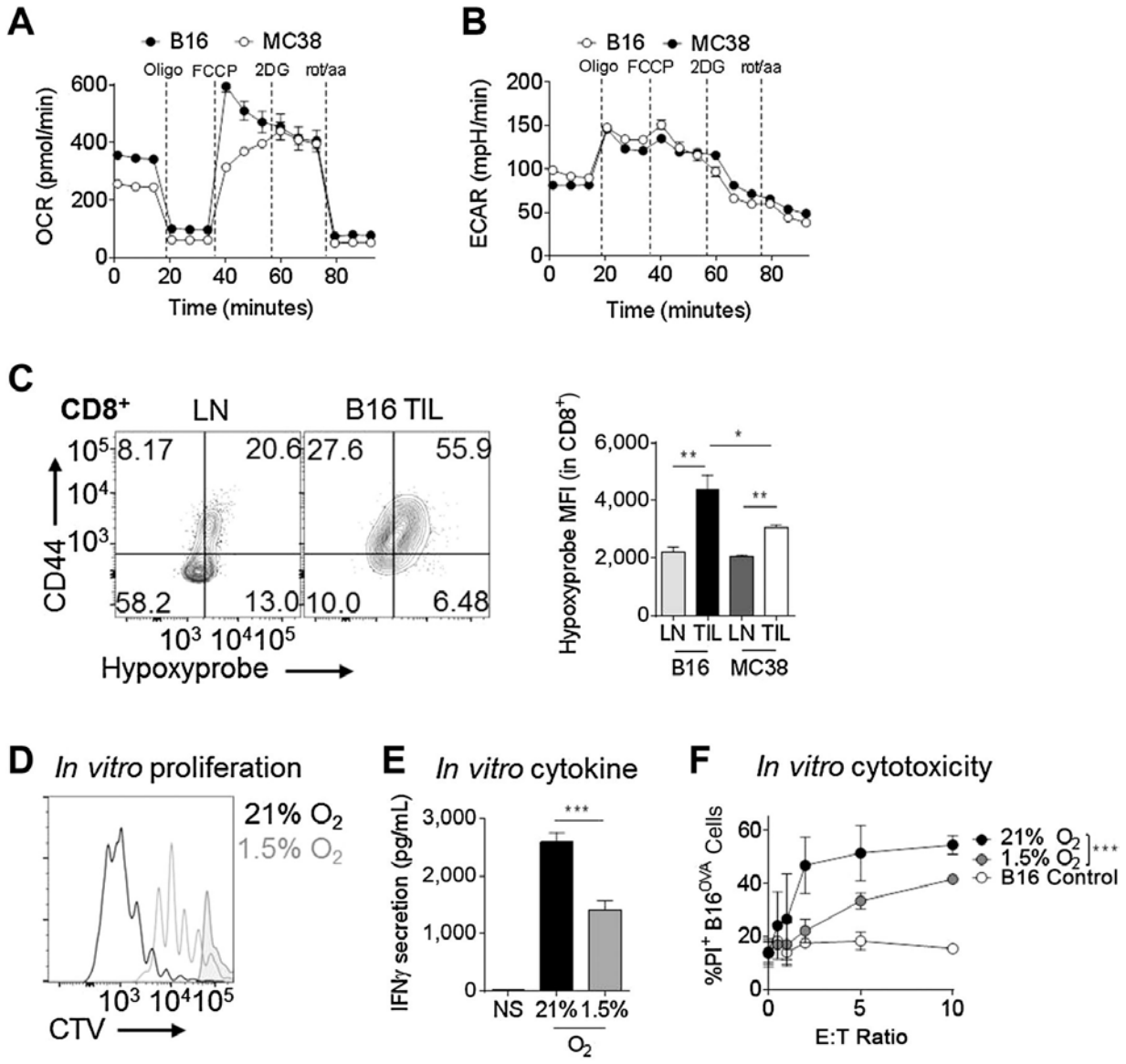

Figure 11. Tumor hypoxia is variable between tumor types and inhibits T cell function

A, OCR trace of B16 and MC38 cells (50,000 cells/well) interrogated for mitochondrial activity in the Seahorse instrument. B, ECAR trace of B16 and MC38 cells interrogated for glycolytic activity in the Seahorse instrument. C, Hypoxyprobe staining of T cells isolated from B16 and MC38 tumors. Results are tabulated to the right. LN, lymph node. D, CellTrace Violet (CTV) dye dilution showing proliferation of OT-I T cells activated with peptide in ambient normoxia (20%) or hypoxic (1.5%) conditions. Shaded histogram, unstimulated cells. E, Cytokine production of CD8+ T cell stimulated as in D overnight. NS, no stimulation. F, Cytotoxicity [propidium iodide (PI) staining] of parental or OVA-expressing B16 tumor cells incubated with previously activated, effector OT-I T cells overnight under conditions of normoxia or

hypoxia. *, P < 0.05; **, P < 0.01; ***, P < 0.001 by unpaired t test (C and E) or two-way ANOVA with repeated measures (F). Results represent three independent experiments.

As hypoxia has been shown to have various effects on T cells in culture (10), we tested the effects of hypoxia on antigen-specific (OT-I) T cells previously activated and rested in normoxia, then restimulated in vitro using a hypoxia chamber set at average tumor hypoxia (1.5%). We found that T cells proliferated less compared with T cells cultured in normoxic conditions (Fig. 11D). Cytotoxic T cells generated via peptide stimulation and expansion in normoxic conditions but restimulated in hypoxic conditions also synthesized significantly lower levels of IFNγ than their normoxic counterparts (Fig. 11E) and had lower cytolytic activity against antigen-expressing tumor targets (Fig. 11F). Thus, cytotoxic T cells in acutely hypoxic conditions are functionally impaired compared with T cells in normoxia.

3.5.2 Metformin treatment acts as an inhibitor of tumor oxygen consumption

To determine whether tumor hypoxia can be pharmacologically modulated, we used the mitochondrial complex I inhibitor metformin on B16 and MC38 tumor cells in metabolic flux assays, revealing that metformin decreases tumor cell OCR in both B16 and MC38 cells *in vitro* (Fig. 12A). B16 tumors isolated from mice treated with metformin, depleted of CD45+ cells, and assayed directly *ex vivo* had similar phenotypes (Fig. 12B). Immunofluorescent analysis of metformin-treated tumor-bearing mice with hypoxyprobe revealed that, in agreement with previously published data[133], metformin treatment

decreased overall tumor hypoxia (Fig. 12C). Thus, metformin acting on tumor cells induced a decrease in overall tumor hypoxia.

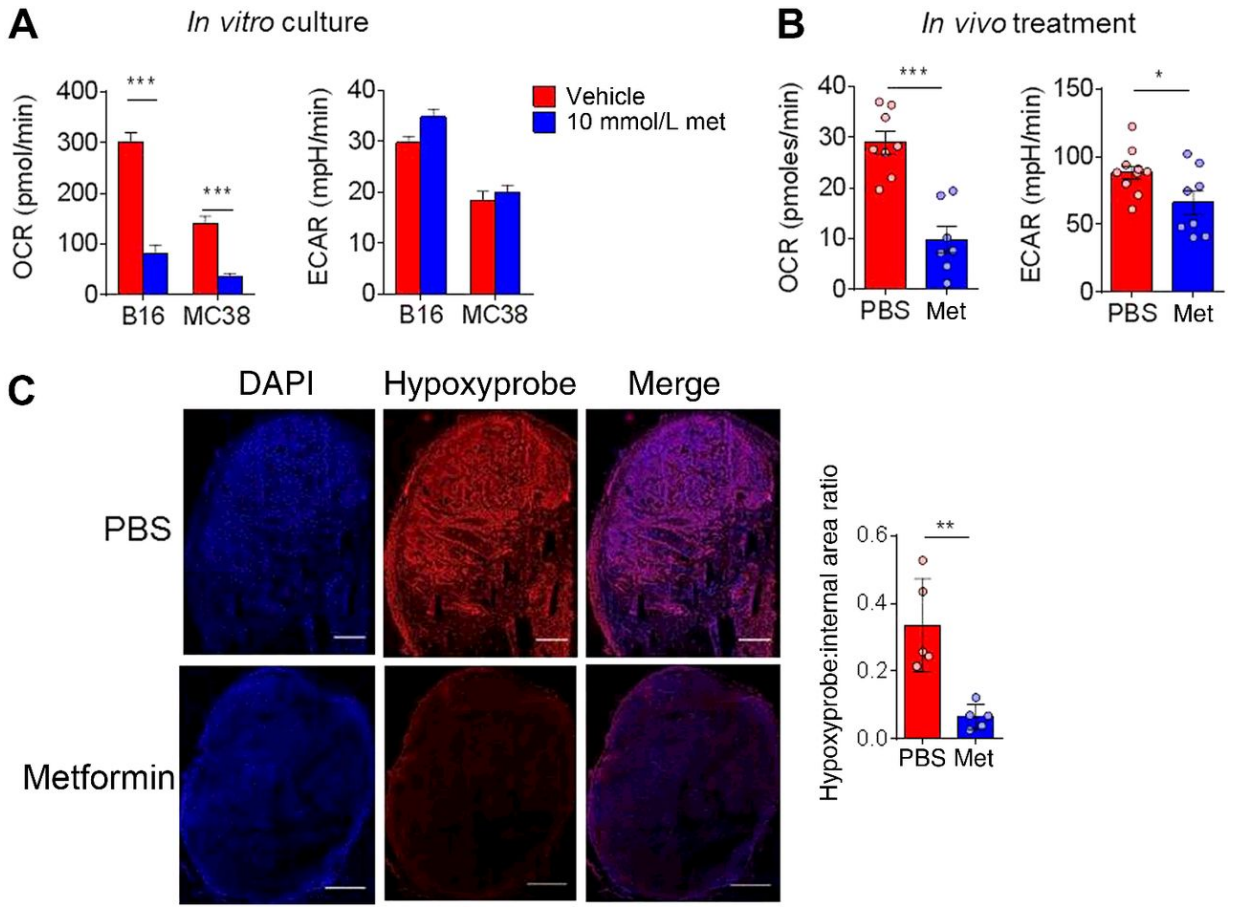

Figure 12. Metformin treatment acts as an inhibitor of tumor oxygen consumption

A, OCR of B16 or MC38 in vitro cultured cells (50,000 cells/well) treated overnight in the presence or absence of 10 mmol/L metformin. B, OCR of B16 tumor cells (CD45-depleted) plated directly ex vivo from mice bearing small tumors treated with PBS or metformin (Met; 50 mg/kg) for 3 days. C, Pimonidazole staining of full tumor sections (stitched from 300–500 individual panels) from mice bearing B16 tumors receiving PBS or metformin treatment for 3 days as in B. Tabulated results quantify the internal hypoxyprobe signal from a set threshold normalized for each day of imaging. Scale bar, 1 mm. *, $P < 0.05$; **, $P < 0.01$; ***, $P < 0.001$ by unpaired t test. Data represent the mean (A–C tabulation) or are representative (C, images) of at least three independent experiments.

3.5.3 Metformin treatment alters hypoxia-driven changes in T-cell phenotypes

After establishing that metformin decreased tumor hypoxia, in part by inhibiting cancer cell oxygen consumption, we sought to determine the effect of metformin treatment on tumor-infiltrating T cells *in vivo*. We have previously shown that T cells in the tumor microenvironment are at a metabolic disadvantage and repress oxidative metabolism[89]. Seahorse analysis of tumor cells and T cells sorted directly from untreated and metformin-treated tumors revealed that, in untreated animals, tumor cell oxidative metabolism dwarfs that of T cells (Fig. 13A). In contrast, metformin-induced inhibition of tumor cell metabolism results in similar OCRs for both tumor and tumor-infiltrating T cells: repression of tumor cell OCR and an increase in T-cell OCR (Fig. 13A). This opposite effect on T cells was intriguing and suggested T cells from the tumor microenvironment were affected by metformin indirectly. Metformin requires active transport by the organic cation transporter (OCT1, encoded by Slc22a1). Tumor cells express more of this transporter than T cells, suggesting that, especially in the tumor microenvironment, tumor cells preferentially take up metformin and are specifically inhibited by it (Supplementary Fig. S37A). Metformin treatment *in vitro* does impact T cell OCR, as high doses of metformin decreased T-cell OCR and increased ECAR (Supplementary Fig. S37B). Metformin can cause increases in glucose uptake, so we also analyzed the glucose uptake of tumor-infiltrating T cells by 2NBDG uptake, a fluorescent glucose tracer, and found that metformin did not induce increased glucose uptake *in vivo*, further suggesting the effect of metformin on tumor-infiltrating T cells was indirect (Supplementary Fig. S37C). We additionally found that metformin treatment of mice significantly decreased hypoxia experienced by TIL T cells, with no significant

effect on lymph node–resident populations (Fig. 13B). To determine whether metformin-induced changes in TIL hypoxia would impact tumor control or clearance, mice with small, palpable B16 tumors were treated therapeutically with metformin. Mice treated with metformin had no significant difference in tumor size compared with PBS-treated mice (Fig. 13C).

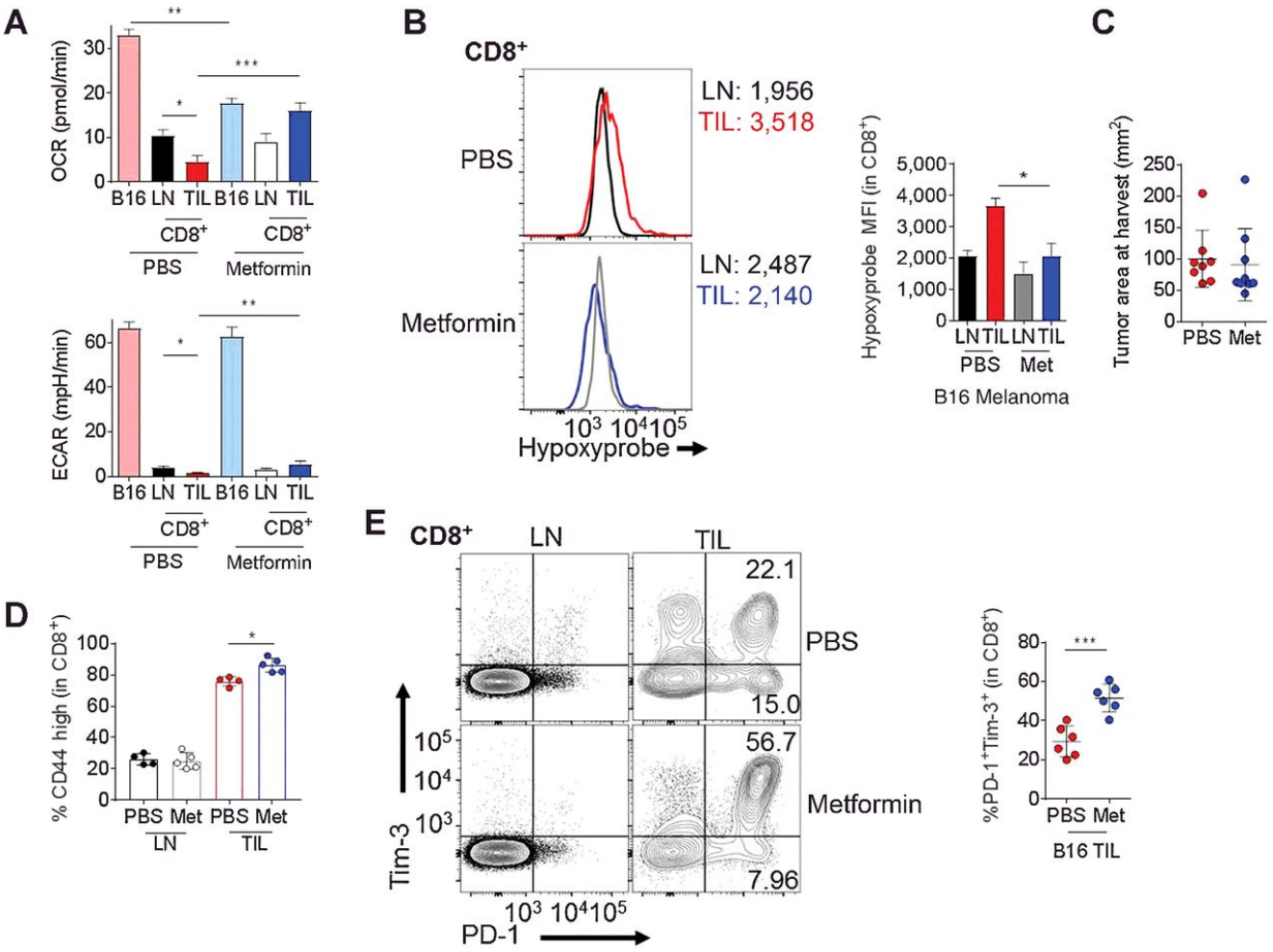

Figure 13. Metformin treatment reduces intratumoral T-cell hypoxia

A, OCR (top) or ECAR (bottom) from B16-bearing mice treated with metformin or vehicle for 3 days. CD45+CD8+ T cells were sorted by flow cytometry and assayed directly ex vivo, whereas B16 tumor cells were CD45-depleted before assaying. LN, lymph node. B, Flow cytogram (left) and tabulation (right) of pimonidazole staining in T cells from B16-bearing mice treated with metformin or vehicle for 3 days. C, Tumor area at 21 days for mice treated during tumor progression with PBS or metformin (Met). D and E, Quantification of CD44hi CD8+ T cells (D) from B16-bearing mice treated with metformin or vehicle for 3 days (E) PD-1 and Tim-3 expression in CD8+ T cells from mice treated as in D. *, $P < 0.05$; **, $P < 0.01$; ***, $P < 0.001$ by unpaired t test. Results are representative of three (A, B, D, and E) or four (C) independent experiments.

To investigate why T cells in more oxygenated environments were still unable to decrease tumor burden, we characterized the infiltrate from the tumors of metformin-treated mice. Metformin did not enhance the expression of any co-inhibitory molecules on antigen-presenting populations, nor did it change the percentage of tolerogenic myeloid-derived suppressor cells in the tumor (Supplementary Fig. S37D–S37F). However, tumor-infiltrating T cells from metformin-treated tumor-bearing mice had a small but significant increase in the number of activated T cells (CD44hi; Fig. 13D), suggesting that metformin treatment may promote increased T-cell activation. To supplement our hypoxia studies, we also examined the direct *ex vivo* protein quantity of HIF1α. Intriguingly, even though *in vivo* metformin treatment decreased tumor and T cell hypoxia (Figs. 12C and 13B), HIF1α protein in TIL was unaltered or increased (Supplementary Fig. S37G). HIF1α expression is usually associated with hypoxia, but T cells also upregulate HIF1α upon activation[134], so we believe the trend toward increased HIF1α in metformin-treated TIL may be a readout of increased T cell activation (Fig. 13D and Supplementary Fig. S37G). As chronic activation can lead to T cell dysfunction, we then assessed the expression of co-inhibitory “exhaustion” molecules and found coinhibitory molecules PD-1 and Tim-3 were elevated compared with control mice (Fig. 13E). Thus, although metformin treatment alone does not affect tumor burden in these aggressive models, metformin treatment may allow for increased activation of T cells, resulting in further upregulation of immunologic checkpoints on tumor-infiltrating CD8+ T cells.

3.5.4 Metabolic remodeling synergizes with checkpoint blockade to unleash antitumor immunity

Anti-PD-1 immunotherapy can cause tumor clearance in 40% of C57/BL6 mice with MC38 tumors, but has little beneficial effect on reducing tumor burden or causing tumor clearance in B16 tumors[132]. We hypothesized that normalization of tumor hypoxia with metformin might generate a microenvironment more permissive to anti-PD-1 immunotherapy. We treated mice with metformin or PBS in combination with anti-PD-1 or isotype control when mice developed palpable tumors (1–10 mm2) and continued therapy throughout the course of the experiment. We found that whereas anti-PD1 alone or metformin alone had no impact on tumor burden, the combination of anti-PD-1 and metformin induced regression in 80% of mice, and tumor clearance in 70% of the mice with B16 (Fig. 14A). Analysis of the TILs in these mice revealed that CD8+ T cells produced more effector cytokines (Fig. 14B and 14C) and were substantially more proliferative (Fig. 14D) than T cells from the single treatment or control groups. Although our study is a therapeutic model, sequencing studies in the B16 model have revealed that, like many immunotherapeutic strategies, a synergistic metformin and anti-PD-1 effect had a size threshold; when B16 tumors were large (>10 mm2) prior to treatment, they lost sensitivity to this treatment strategy (data not shown).

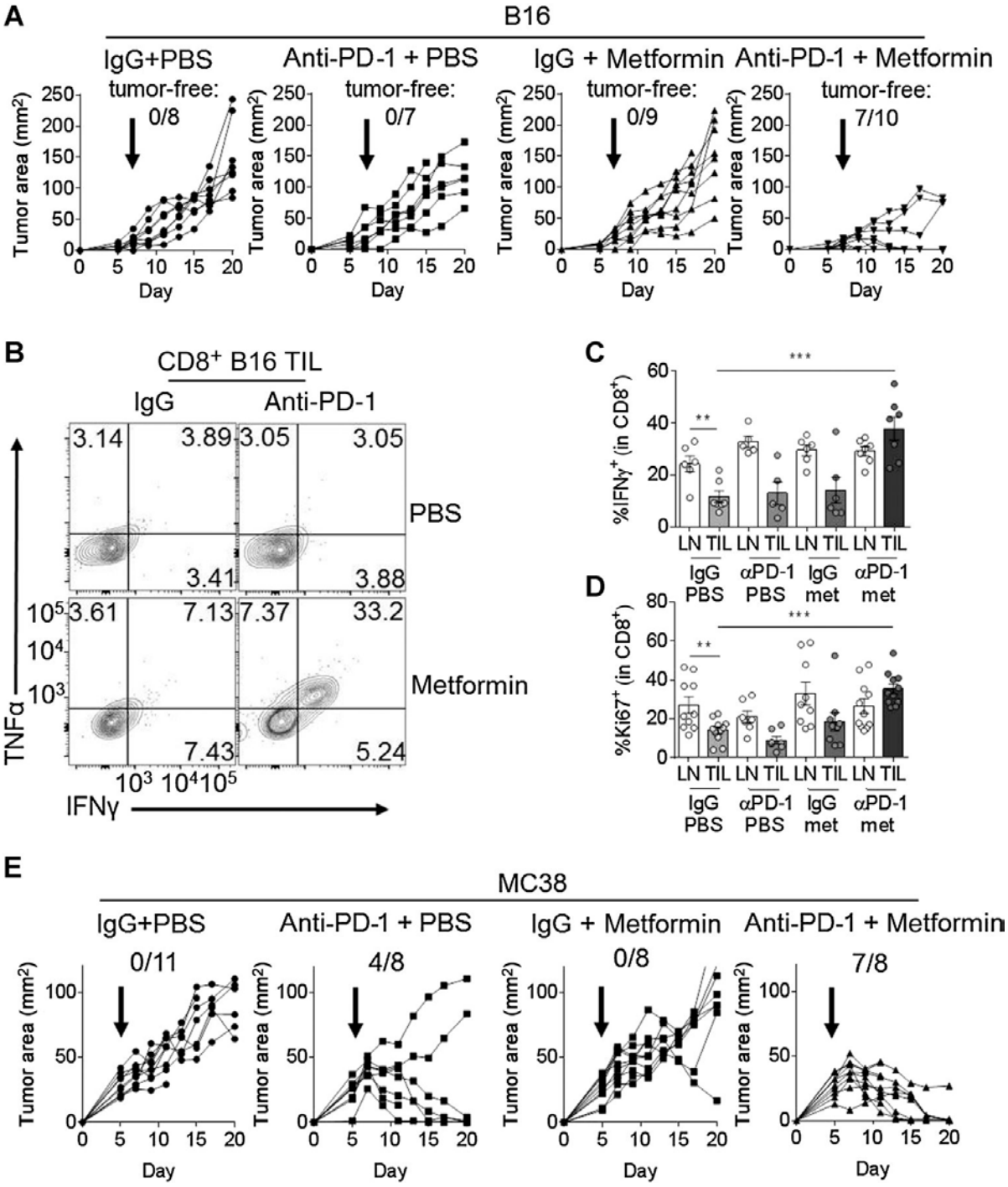

Figure 14. Metabolic remodeling synergizes with checkpoint blockade to affect antitumor immunity

Tumor measurements of C57/BL6 mice inoculated with B16 melanoma. Mice began receiving treatment on day 5 as indicated, receiving 0.2 mg anti-PD-1 or its isotype control every 4 days, and either metformin (met) or vehicle. Number of mice tumor-free of the total inoculated is reported. B, Representative flow

cytogram depicting IFNγ and TNFα production from CD8+ tumor-infiltrating T cells from B16-bearing mice treated as in A. C, Tabulated IFNγ staining from multiple mice; each dot represents one animal. D, Ki67 expression in CD8+ T cells from mice treated as in A as indicated. E, As in A, but mice were inoculated with MC38. **, $P < 0.01$; ***, $P < 0.001$ by unpaired t test. Results represent the mean (A, C, D, and E) or are representative of (B) three to five independent experiments.

Our studies were mostly conducted using intraperitoneal injection of metformin, but we also utilized metformin delivered in the drinking water (1 g/L). We observed similar synergy between these two treatments in B16 melanoma, although the effect was not as striking as with intraperitoneal injection (Supplementary Fig. S38). Given that our data suggest that tumor cells may be preferentially taking up metformin, the continually administrated nature of the drinking water treatment may start to have inhibitory effects on T cells.

MC38 is partially sensitive to PD-1 therapy, which we hypothesize is due at least in part to their less oxidative and thus hypoxic nature. We then asked whether the baseline response rate could be improved by further hypoxia mitigation with metformin. Indeed, mice with MC38 tumors fared even better with metformin and anti-PD-1 treatment than with anti-PD-1 alone; 88% of mice treated with anti-PD-1 and metformin showed complete tumor clearance, and every mouse experienced tumor regression (Fig. 14E). This suggests that tumor oxidative metabolism exists as a common barrier to immunotherapy. Thus, anti-PD-1 and metformin combination therapy shows synergistic effects on tumor clearance when compared with single-therapy treatment, increasing TIL T-cell activation and effector function.

3.6 DISCUSSION

Our study links the hypoxic nature of the tumor microenvironment with resistance to immunotherapy. We have revealed, as many others have shown, that oxygen is a vital metabolite for T-cell function, which is limiting in the tumor microenvironment. Remodeling the tumor microenvironment through inhibition of tumor cell oxidative metabolism resulted in increased sensitivity to immunotherapy, which unleashed the antitumor immune response to promote cancer regression.

Our data add to an increasing number of reports suggesting that the metabolic makeup of the tumor microenvironment is a critical inhibitory factor for T-cell function. Although T cells can be metabolically plastic, and are primed to utilize glucose in oxygen-poor conditions, glucose can also be limiting in the tumor microenvironment[72,135]. Thus, although immunotherapies like checkpoint blockade may allow for optimal activation, microenvironmental deficiencies may prevent T cells from generating enough energy to carry out effector function[89].

It is established that patients taking metformin for type II diabetes have a decreased risk of cancer[136,137] and that much of the antitumor metformin effect can be attributed to T cells[138]. However, the precise causes and extent of metformin's antitumor effect have been elusive, undoubtedly complicated by the fact that the mechanism of action of metformin is still unclear[139]. Whether through inhibition of complex I or activation of the energy charge sensor AMPK, however, it is clear that metformin treatment can inhibit the oxygen consumption of tumors, and consequent generation of hypoxia, in agreement with prior studies[133]. Although metformin likely has pleiotropic effects on a wide array of cellular functions, its effect on tumor hypoxia serves as an

important proof-of-concept study, suggesting pharmacologic inhibition of tumor cell oxidative metabolism or oxygen-diffusing drugs may serve as critical potentiators of antitumor immunity. An alternative approach, utilizing hyperoxygenation of mice, indeed suggests that antitumor immune function is improved when tumor hypoxia is mitigated[77]. Our data build on this foundation, suggesting that metformin-induced remodeling of microenvironment oxygen tension acts to create a “level playing field” for T- cell activation in response to immunotherapy.

Metformin can have immunosuppressive effects in a number of models, including GVHD, lupus, and graft rejection[140–142]. In these scenarios, T cells are the “dominant force” at the site of activation and may be experiencing either the systemic hypoglycemic or lactic acidotic effects of metformin. In the tumor microenvironment, where T cells are competing metabolically with cancer cells, metformin may simply be preferentially taken up by tumor cells. Our data showing that T cells demonstrate relatively low expression of the metformin transporter OCT-1 (Slc22a1) compared with tumor cells support this notion. Along these lines, our drinking water experiments suggest continual administration may mediate a less synergistic effect; translating these observations to the clinic will require dosing and sequencing experimentations to find optimal synergy with immunotherapeutic treatments.

Previous studies exploring the role of the HIF pathway have revealed somewhat surprising data regarding this oxygen-sensing pathway in T cell function. T cells lacking VHL, the upstream inhibitor of HIF1α, show increased T cell production of effector molecules like granzyme B and have enhanced antitumor activity, suggesting the hypoxia response might be advantageous for T cells[143]. Hypoxia may function to

promote aerobic glycolysis, which is tied to effector function epigenetically and posttranscriptionally[27,38,93]. However, in the tumor microenvironment, as glucose is limiting, only cells able to effectively compete for glucose would experience an enhanced response[72,135]. Hypoxia and HIF are not always linked in T cells, as HIF1α is also stabilized upon T cell activation and other downstream pathways[134]. Indeed, our data showing that tumor-infiltrating T cells from metformin-treated animals had similar amounts of HIF1α, even though they experienced less hypoxia, as shown by pimonidazole staining, support the notion that HIF1α, especially in T cells, is not always directly linked to true hypoxia.

As we identified hypoxia as a barrier to tumor immunity, our data also suggest that the degree of tumor hypoxia may predict the response to immunotherapy. This is in agreement with a report examining transcriptomes from patients receiving PD-1 blockade, identifying a hypoxia signature in innate resistance to immunotherapy[144].

Our study employing metformin as a method to modulate the oxygen tension of the tumor microenvironment showed substantial effects on the efficacy of PD-1 blockade immunotherapy. However, we hypothesize that, as hypoxia acts as a general barrier to T cell function, many forms of immunotherapy that aim to act by reinvigorating T cells at the tumor site will be improved through modulation of this aspect of the microenvironment. Future studies will explore how blockade of other checkpoints, stimulatory antibody treatment, or adoptive cell therapy might be improved by pharmacologic modulation of hypoxia.

Our data support a model in which a common phenotype of cancer cells, metabolic dysregulation, can mediate immune evasion and resistance to

immunotherapy through the generation of a nutrient-poor, hypoxic microenvironment. Remodeling the tumor microenvironment through modulation of cancer cell metabolism may have the potential to convert nonresponder patients into those that can receive the benefits of immunotherapeutic cancer treatment.

4.0 THE TUMOR MICROENVIRONMENT REPRESSES T CELL MITOCHONDRIAL BIOGENESIS TO DRIVE INTRATUMORAL T CELL METABOLIC INSUFFICIENCY AND DYSFUNCTION

4.1 FOREWORD

This chapter was adapted from a previously published manuscript in *Immunity*: **Scharping, Nicole E**., Ashley V. Menk, Rebecca S. Moreci, Ryan D. Whetstone, Rebekah E. Dadey, Simon C. Watkins, Robert L. Ferris, and Greg M. Delgoffe. "The Tumor Microenvironment Represses T Cell Mitochondrial Biogenesis to Drive Intratumoral T Cell Metabolic Insufficiency and Dysfunction." *Immunity*, 2016. DOI: 10.1016/j.immuni.2016.07.009.

4.2 CHAPTER SUMMARY

Although tumor-specific T cells recognize cancer cells, they are often rendered dysfunctional due to an immunosuppressive microenvironment. Here we showed that T cells demonstrated persistent loss of mitochondrial function and mass when infiltrating murine and human tumors, an effect specific to the tumor microenvironment and not merely caused by activation. Tumor-infiltrating T cells showed a progressive loss of

PPAR-gamma coactivator 1α (PGC1α), which programs mitochondrial biogenesis, induced by chronic Akt signaling in tumor-specific T cells. Reprogramming tumor-specific T cells through enforced expression of PGC1α resulted in superior intratumoral metabolic and effector function. Our data support a model in which signals in the tumor microenvironment repress T cell oxidative metabolism, resulting in effector cells with metabolic needs that cannot be met. Our studies also suggest that modulation or reprogramming of the altered metabolism of tumor-infiltrating T cells might represent a potential strategy to reinvigorate dysfunctional T cells for cancer treatment.

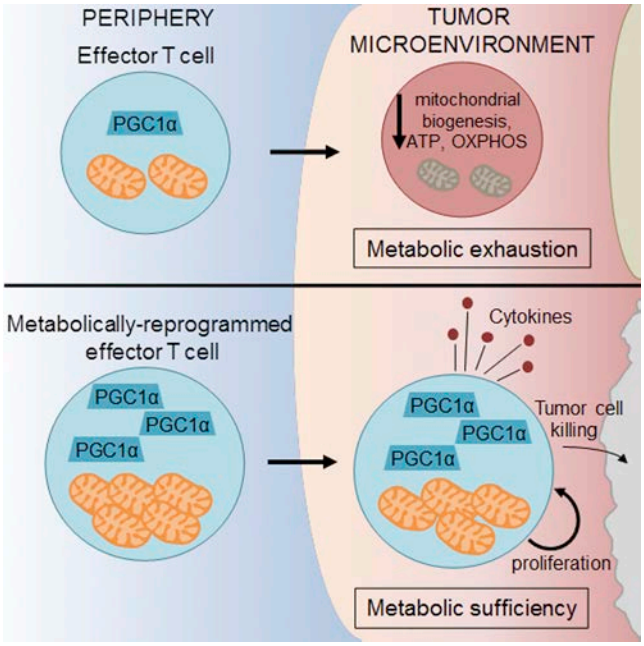

Figure 15. Graphical abstract for "The Tumor Microenvironment Represses T Cell Mitochondrial Biogenesis to Drive Intratumoral T Cell Metabolic Insufficiency and Dysfunction"

4.3 INTRODUCTION

The immune system has evolved multiple cellular mechanisms for the detection and elimination of abnormal or stressed cells in a wide array of environments. Early detection of cancer, via immunosurveillance, can occur almost anywhere, facilitating destruction of early transformed cells expressing neoantigens. However, as cancers edit and escape this initial immune detection, they also generate an immunosuppressive microenvironment which restricts T cell infiltration, activation, and effector function both through direct repression (via cytokines, adenosine, prostaglandins, glucose restriction, etc.) as well as the recruitment of immunosuppressive populations tasked with maintaining immune tolerance[145]. The result is an ineffectual antitumor immune response and consequent tumor progression.

Recent advances in cancer immunotherapy have revealed that the T cell response to cancer can be reinvigorated in a variety of ways, resulting in durable and effective benefit in a wide array of cancer types[146–148]. These include engineering chimeric antigen receptors redirect T cells to tumors, personalized antigen vaccines to persistent neoepitopes, and, probably most prominently, antibody-mediated blockade of co-inhibitory “checkpoint” molecules, like programmed death-1 (PD-1), cytotoxic T lymphocyte antigen 4 (CTLA-4), lymphocyte activation gene 3 (LAG-3), T cell immunoglobulin and mucin-containing gene 3 (Tim-3), among others[146]. These molecules are highly upregulated on tumor-infiltrating T cells and are thought to negatively regulate T cell activation and effector function. This elevated and sustained expression of co-inhibitory molecules is indicative of a hyporesponsive phenotype, originally discovered in chronic viral infection, termed T cell exhaustion[149]. Antigen

persistence results in continued TCR and cytokine signals, which promote upregulation of these receptors, resulting in a hyporesponsiveness functionally similar to anergy but mechanistically distinct[150,151]. Importantly, T cells can still have an exhausted phenotype in the absence of co-inhibitory molecules[152,153], shedding light on the fact that while these co-inhibitory molecules have been extensively studied at the molecular and biochemical levels, it is still unclear what the contribution of co-inhibitory molecule signaling is to the initiation or maintenance of the exhausted phenotype. Thus for improving the treatment of cancer, chronic viral infections, and other diseases, it is critical to understand the mechanisms behind the dysfunction in chronically activated T cells[154]. This is especially important considering that, while checkpoint blockade has had remarkable success in the clinic, the majority of patients still do not respond to these therapies[146].

Carrying out effector function is a metabolically demanding process[28]. T cells must efficiently divide and replicate their genome rapidly and with fidelity, synthesize high levels of cytokines, and deliver cytotoxic payload to target cells. Recent discoveries of T cell dependence on nutrient sensing and metabolic flux have shown that metabolism represents a key mechanism by which the immune system can be regulated[126]. They also suggest that the fate and function of T cells are intrinsically tied to their metabolism and that a T cell (like any other cell) requires the machinery to generate bioenergetic intermediates to support proliferation and effector function[126].

During their effector phase, T cells utilize aerobic glycolysis, diverting glucose into lactate fermentation rather than mitochondrial acetyl-CoA oxidation to support their expansion and proliferation[26,28]. The precise contributions of this pathway and its

teleology remain the subject of much study, but nevertheless the mitochondria remain an essential component of T cell metabolism. Effector T cells significantly upregulate oxidative activity and memory T cell precursors become increasingly dependent on mitochondria to mediate fatty-acid oxidation over time[36,37]. Furthermore, the mitochondria remain important organelles for biosynthesis, calcium buffering, and mediating programmed cell death[155,156]. Thus, while T cells might divert glucose metabolism away from mitochondrial pathways during activation, mitochondria are still critical for maintaining the health and integrity of the T cell in both the effector and memory phases of a T cell response.

While the effects of glucose deprivation in tumor microenvironments on both glycolytic metabolism and T cell function have garnered much recent interest, the mitochondrial phenotype of T cells infiltrating tumors remains unclear[72,74,125,135]. We have observed that tumor-infiltrating T cells display metabolic insufficiency, characterized most prominently by a persistent loss of mitochondrial function and mass. Loss of mitochondrial function in tumor-reactive T cells occurred specifically in the tumor microenvironment, largely independently of PD-1 blockade or regulatory T cell suppression, and due to a defect in PPAR-gamma coactivator 1α (PGC1α)-programmed mitochondrial biogenesis. This defect was due in part to chronic protein kinase B (Akt) signaling, inhibited Foxo transcription factor activity, and consequent PGC1α repression. Metabolic reprogramming of T cells through enforced PGC1α expression rescued mitochondrial function and induced superior antitumor responses characterized by cytokine production and tumor control. These findings show the chronic activation associated with the anti-cancer response represses oxidative

metabolism, suggesting that the dysfunction of tumor-infiltrating T cells might be linked to an ability to generate sufficient metabolic intermediates for cellular function.

4.4 METHODS

Mice

Animal work was done in accordance with the Institutional Animal Care and Use Committee of the University of Pittsburgh. All mice were housed in specific pathogen free conditions prior to use. C57/BL6, SJ/L (Thy1.1), Ppargc1a$^{f/f}$, Cd4^{Cre}, Foxp3$^{GFP.Cre.ERT2}$, Foxp3$^{DTR.GFP}$, and OT-I mice were obtained from The Jackson Laboratory.

Cell Lines, Antibodies, and Other Reagents

B16-F10 and LLC were obtained from ATCC. MC38 was obtained from Dario Vignali. B16OVA (MO5) was obtained from Per Basse and Lou Falo. OVA-expressing Vaccinia virus was originally generated by Yewdell and Bennink and obtained from Jonathan Powell. Most antibodies for flow cytometry were obtained from BioLegend. MitoTracker Green FM, MitoTracker Deep Red FM, tetramethylrhodamine ester (TMRE), and H2-DCFDA were obtained from ThermoFisher. VDAC antibody was obtained from Abcam. LC3B, pAktS473, pFoxo1/3a antibodies were obtained from Cell Signaling Technologies and detected after surface staining with simultaneous fixation and permabilization in 1.5% PFA made up in 1X Permeabilization buffer (eBioscience). 2-NBD-glucose, m-divi-1, and Akt inhibitor VIII were purchased from Cayman Chemical. PGC1α antibody (H-

300) was obtained from Santa Cruz Biotechnology, and was detected using the Foxp3 Fix/Perm kit (eBioscience) and Alexa Fluor 647 or Alexa Fluor 488-conjugated anti-rabbit immunoglobulin G (IgG) (Jackson Immunoresearch). Anti-PD-1 blocking antibody (J43) and its hamster IgG control were obtained from Bio-X-Cell. CellTrace Violet was purchased from eBioscience, and CFSE was purchased from BioLegend.

T Cell Isolations from Lymph Node and Tumor and Adoptive Transfer

Spleen and lymph node CD8+ T cells were isolated from 6- to 8-week-old OT-I (Thy1.2 or Thy1.1) mice. Tissue was harvested, mechanically disrupted, and incubated with a biotinylated antibody cocktail consisting of antibodies (BioLegend) to B220, CD11b, CD11c, CD16/32, CD19, CD25, CD105, NK1.1, TCRγδ, and CD4. After a wash step, cells were incubated with streptavidin-coated magnetic nanoparticles (BioLegend). After washing, CD8+ cells were isolated by applying a magnetic field and removing untouched cells. These OT-I CD8+ T cells were also labeled with the proliferation dye CellTrace Violet according to the manufacturer's protocol. Mice bearing B16OVA tumors or immunized with VVOVA received cells intravenously. To obtain single-cell suspensions of tumor infiltrating lymphocytes, excised, we injected whole tumors repeatedly using 20G needles with 2 mg/mL collagenase type VI, 2 U/mL hyluronidase (Dispase), and 10 U/mL DNase I (Sigma) in buffered RPMI with 10% FBS and incubated them for 30 min at 37°C. Tumors were mechanically disrupted between frosted glass slides and filtered to remove particulates, then vortexed for 2 min. In many experiments (especially prior to sorting), tumor homogenates were debulked of tumor cells using CD105-biotin mediated magnetic depletion.

Human Peripheral Blood Lymphocyte or Tumor Infiltrating Lymphocyte Isolation

After approval by Institutional Review Board (University of Pittsburgh Cancer Institute (UPCI) protocol 99-069], informed consent was obtained from each patientt before blood withdrawal. Blood from patients with HNC treated with cetuximab during or within 1 month of treatment (UPCI clinical trial #08-013 NCT 01218048). Fresh tumors from patients with HNC were minced into small pieces manually, transferred to 70 μm cell strainers (BD), and mechanically separated using the plunger of a 5 ml syringe. Lymphocytes were purified by Ficoll-Paque PLUS centrifugation following standard protocol (Amersham Biosciences), pulsed with 2NBDG, and stained for flow cytometry.

Metabolism Assays

Nondraining and draining lymph node or tumor preparations were pulsed with 20 μM 2-NBDG (Cayman Chemical) in 5% FBS-containing media for 30 min at 37°C. Cells were surface stained and loaded with MitoTracker FM (ThermoFisher) dyes or TMRE to measure mitochondrial mass and function.

T cells were plated on Cell-Tak coated Seahorse culture plates (50,000 or 100,000 T cells/well) in assay media consisting of minimal, unbuffered DMEM supplemented with 1% BSA and 25 mM glucose, 1 mM pyruvate, and 2 mM glutamine and analyzed using a Seahorse XFe96 (Agilent). Basal extracellular acidification and oxygen consumption rates were taken for 30 min. Cells were stimulated with oligomycin (2 μM), FCCP (0.5 μM), 2-deoxyglucose (100mM) and rotenone/antimycin A (100 μM) to obtain maximal

respiratory and control values. Spare respiratory capacity is measured as the difference between basal OCR values and maximal OCR values obtained after FCCP uncoupling.

Electron Microscopy

CD8+ T cells were sorted from LNs and TIL and fixed in 4% glutaraldehyde and stained for electron microscopy as previously described[157].

Retroviral Expression

PGC1α was originally generated by B. Spiegelman, obtained from Addgene (plasmid 1026)[158], and cloned into an MSCV-driven retroviral expression vector which also encodes an IRES-mCherry cassette, from Dario Vignali. This vector was transiently transfected into Phoenix ecotropic cells. OT-I splenocytes were stimulated with SIINFEKL peptide at 250 ng/mL in the presence of 100U/mL IL-2 for 24 hr. Retroviral supernatants were harvested, and filtered, and supplemented with 6 μg/mL polybrene. OT-I T cell cultures were spinduced with the retroviral supernatant for 90 min at 2,500 rpm. 24 hr later spinduction this was repeated. Cells were expanded and sorted by mCherry prior to analysis and adoptive transfer.

4.5 RESULTS

4.5.1 Tumor-Infiltrating T cells Have Decreased Mitochondrial Mass

To assess the metabolic capacity of tumor-infiltrating T cells, we measured mitochondrial function and mass by flow cytometry using MitoTracker Deep Red FM (a membrane permeable, carbocyanine-based dye for mitochondria used previously to stain mitochondrial mass[159]). Competency for glucose uptake was determined using fluorescent 2-NBD-glucose (2NBDG) in T cells infiltrating implantable tumors. While MitoTracker Deep Red has been shown to be membrane potential sensitive in some systems, uncoupling using carbonyl cyanide m-chlorophenyl hydrazine (CCCP) showed that, using our staining protocols, MitoTracker Deep Red was highly resistant to collapse of membrane potential, especially compared to tetramethylrhodamine ester (TMRE), a well-known membrane-potential sensitive dye (Figure S39A). C57/BL6 mice were inoculated with B16 melanoma, and at day 12, lymph node and tumor preparations were pulsed with 2-NBDG and stained for flow cytometric analysis. Whereas T cells in the lymph nodes, both non-draining (ndLN) and tumor draining (dLN), effectively took up glucose and had relatively high MitoTracker FM staining, CD8+ tumor infiltrating lymphocytes (TILs) showed a dramatic reduction of mitochondrial mass and glucose uptake (Figures 16A and 16B). To confirm the phenotype we were observing was due to loss of mitochondrial mass and not to mitochondrial depolarization, we employed both MitoTracker Green FM (another carbocyanine-based dye) and antibodies to the mitochondrial outer membrane protein Voltage Dependent Anion Channel (VDAC), both of which revealed similar losses

(Figure S39B). T cells of various effector and memory phenotypes have been shown to have distinct mitochondrial masses[36], which we confirmed with our dyes; however, these differences are substantially smaller than those observed within the tumor microenvironment (Figure S39C). For clarity, throughout this study we primarily gate solely on CD8+ T cells and without further subdivision, unless explicitly stated. This insufficiency was largely specific to CD8+ T cells, as CD4+ T cells retained most of their mitochondrial mass in B16 tumors. This phenotype was common to three different implantable tumor models inoculated into B6 mice, including MC38 adenocarcinoma and Lewis Lung Carcinoma (LLC), with some notable differences. We also observed loss of MitoTracker FM staining in a proportion of CD4+ T cells in LLC, and no significant differences in glucose uptake (Figure 16B and Figures S39D and S39E). This loss of mitochondrial mass was confirmed by transmission electron microscopy, which revealed that tumor-infiltrating CD8+ T cells not only showed lower mitochondrial mass, but also abnormal mitochondrial morphology (Figure 16C). We also examined metabolism in T cells infiltrating human head and neck squamous cell carcinoma (HNSCC) and found a similar loss of mitochondrial staining when compared to peripheral blood T cells (Figure 16D).

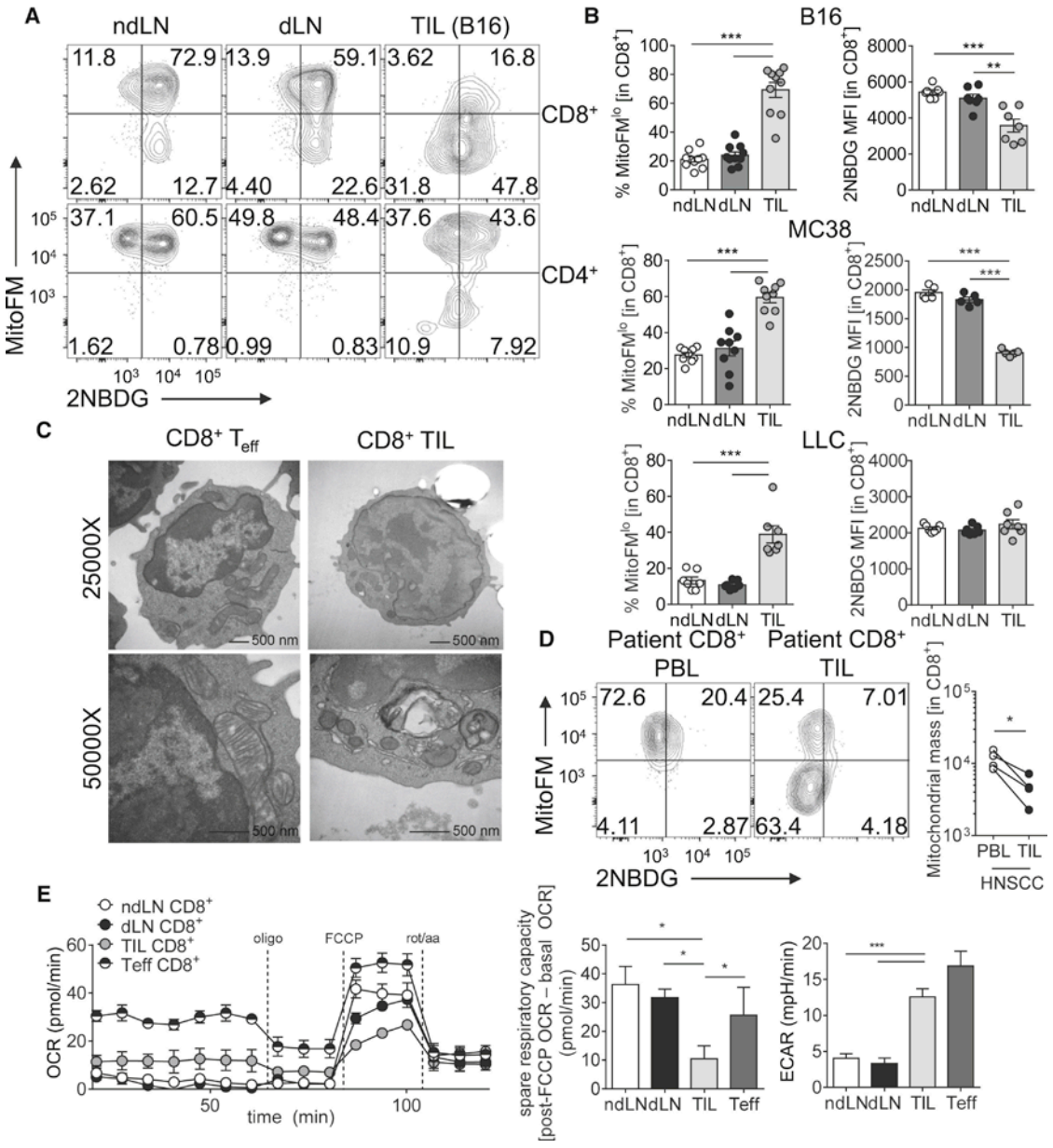

Figure 16. Tumor-Infiltrating CD8+ T Cells Display Suppressed Mitochondrial Function and Mass

(A) Representative flow cytogram of nondraining (ndLN), draining (dLN) lymph node, or tumor-infiltrating lymphocyte (TIL) preparations from C57BL/6 mice inoculated with B16 melanoma cells 12 days prior, gated on CD8 or CD4 as indicated. (B) Tabulated flow cytometric data from CD8+ T cells isolated from mice bearing the indicated tumor types. Each circle represents an individual animal. (C) Transmission electron microscopy of activated or tumor-infiltrating CD8+ T cells. (D) MitoTracker FM staining of CD8+ T cells from peripheral blood lymphocyte (PBL) or TIL of HNSCC patients. (E) Oxygen consumption rate

(OCR) trace (left) and metabolic analysis panels (middle, right) from CD8+ T cells isolated from the indicated sites from B16-bearing animals. T cells activated 24 hr with anti-CD3/anti-CD28 (Teff) are included as a control. Spare respiratory capacity (SRC) is calculated as the difference between initial, basal OCR values, and the maximal OCR values achieved after FCCP uncoupling. Data represent the mean or are representative of 3–5 independent experiments. $*p < 0.05$, $**p < 0.01$, $***p < 0.001$ by unpaired t test. Error bars indicate SEM.

We next examined the metabolic output of tumor-infiltrating T cells using a Seahorse extracellular flux analyzer. Metabolic flux analysis of effector, LN-resident, or tumor-infiltrating CD8+ T cells confirmed a defect in oxygen consumption (OCR), with substantial loss of spare respiratory capacity (a measure of mitochondrial reserve, measured as the difference between basal and uncoupled maximal oxygen consumption) compared to naive, LN-resident cells, or previously activated effector T cells (Figure 16E). This resulted in an increased dependence on glycolytic metabolism, as evidenced by increased extracellular acidification rate (Figure 16E). Thus, T cells infiltrating mouse and human tumors showed a loss of mitochondrial mass and dependence on glycolytic metabolism, rendering them unable to carry out critical cellular functions in the glucose-poor tumor microenvironment.

4.5.2 Loss of Mitochondrial Function Is Specific T Cell Responses in the Tumor Microenvironment

We next wanted to determine whether the mitochondrial dysfunction in tumors was specific to the anti-tumor response or if it occurred in other types of robust effector responses. To do this, we utilized an adoptive transfer system of naive, congenically

mismatched ovalbumin (OVA)-specific TCR transgenic (OT-I) T cells into mice bearing OVA-expressing B16 ($B16^{OVA}$) tumors or mice infected with OVA-expressing Vaccinia virus (VV^{OVA}) for 6 days. This experiment was designed to compare the chronic activation seen in cancer to a robust acute *in vivo* response in which antigen is effectively cleared[50]. Consistent with our data generated in polyclonal populations from mouse and human tumors, OT-I T cells infiltrating tumors showed decreased MitoTracker FM staining relative to their LN-resident counterparts (Figure 17A, 17B). In contrast, OT-I T cells responding to VV^{OVA} infection in the spleen had *increased* mitochondrial mass compared to splenic OT-I T cells adoptively transferred into non-infected mice, as evidenced by increased MitoTracker FM and intracellular VDAC staining (Figure 17A, Figure S40A). T cells responding to OVA in the context of VV^{OVA} also increased basal oxygen consumption (OCR) and spare respiratory capacity (Figure 17B). VV^{OVA}-responsive T cells also displayed heightened glycolytic function, even compared to OT-I T cells isolated from tumors (Figure 17B). Comparisons of ATP reserves from OT-I T cells responding in $B16^{OVA}$ tumors compared to VV^{OVA}-infected spleens revealed that TILs showed an inability to maintain ATP reserves, while this pool was dramatically increased in cells responding to viral infection (Figure 17C). Functionally this led to different patterns of cytokine production upon peptide or phorbol 12-myristate 13-acetate/ionomycin restimulation (Figure S40B). The phenotype of mitochondrial insufficiency observed in tumor-infiltrating lymphocytes was quite stable; OT-I T cells isolated from $B16^{OVA}$ tumors retained a phenotype of low mitochondrial mass, even when isolated and transferred into a new, VV^{OVA} infected mouse for 7 days

(Figure 17D). Thus, T cell dysfunction associated with loss of mitochondria occurred specifically in the context of chronic activation within the tumor microenvironment.

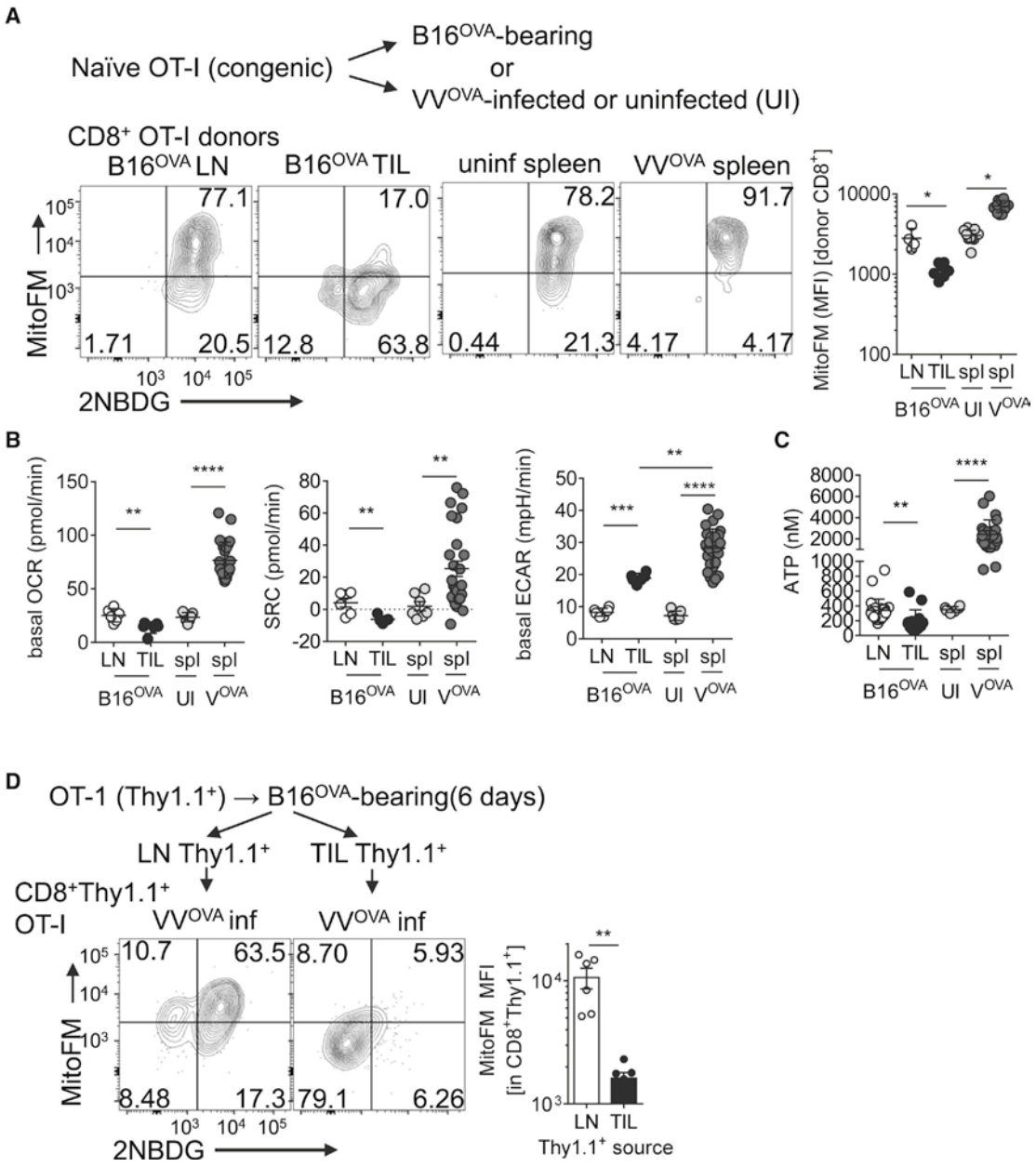

Figure 17. Loss of Mitochondrial Function and Mass Is Not Simply a Phenotype of Robust Activation In Vivo

(A) Representative flow cytogram and tabulated results of 2NBDG uptake and MitoTracker FM measurements of OT-I T cells injected into B16OVA-bearing or VVOVA-infected, or uninfected congenically mismatched hosts for 6 days. Plots are gated on CD8+ T cells and the congenic allele marker (Thy1). (B) Seahorse measurements (OCR, SRC, and ECAR) from cells in (A). (C) ATP measurements from purified donor cells from (A). (D) Flow cytogram of glucose uptake and mitochondrial

mass of OT-I (Thy1.1+) T cells adoptively transferred into B16OVA bearing mice for 6 days, isolated from either LN or tumor, then transferred into VVOVA-infected mice for 6 days. Flow cytogram depicts splenic CD8+Thy1.1+ cells. $*p < 0.05$, $**p < 0.01$, $***p < 0.001$ by unpaired t test. Results represent four (A–C) or three (D) experiments. Circles represent individual animals. UI = uninfected VOVA = VVOVA-infected (1 × 106 PFU IP), spl = spleen. Error bars indicate SEM.

4.5.3 Mitochondria Become Dysfunctional as T Cells Are Activated in Tumors.

We next utilized the above OT-1 T cell adoptive transfer model to explore the metabolic consequences of activated T cells as they enter the tumor microenvironment versus those T cells responding to acute infection. Naive, OT-I Thy1.1+ T cells were labeled with CellTrace Violet (CTV) to monitor proliferation and transferred into $B16^{OVA}$-bearing or VV^{OVA}-infected C57BL/6 (Thy1.2+) mice for 72 hr. This resulted in robust proliferation in both scenarios, with OT-I T cells undergoing as many as seven cell divisions (Figure 18A). We also observed loss of mitochondrial mass as T cells enter the tumor microenvironment, just as we had shown with longer incubations (6 days, Figure 17A). Experiments employing dichlorofluorescin diacetate (DCFDA), a cellular reactive oxygen species (ROS) indicator, and TMRE, a mitochondrial membrane potential-sensitive dye (Figure S39A), indicated that T cells responding to antigen in the tumor microenvironment showed mitochondrial depolarization as well as a loss of ROS production (Figures 18B and 18C). Because mitochondrial depolarization can lead to autophagy, we then asked whether mitophagy may be mediating the loss of mitochondria in tumor-infiltrating T cells. However, we did not observe any significant increases in Light Chain 3B (LC3B) staining in permeabilized OT-I T cells, suggesting

that autophagic processes are likely not overtly deregulated in these cells (Figure 18D). We also treated tumor-bearing mice 24 hr after transfer with the mitophagy and mitochondrial fission inhibitor m-divi-1[160]; this also failed to improve mitochondrial staining in tumor-infiltrating T cells (Figure 18E). We also asked whether loss of mitochondrial function could occur *in vitro* in response to co-culture with tumor cells, and found that response of naive or previously activated OT-I T cells to B16OVA tumor cells *in vitro* did not result in mitochondrial loss (Figures S41A and S41B). Thus, T cells responding to cancer lost oxidative metabolism relatively rapidly, but this required signals that are present specifically in the tumor microenvironment.

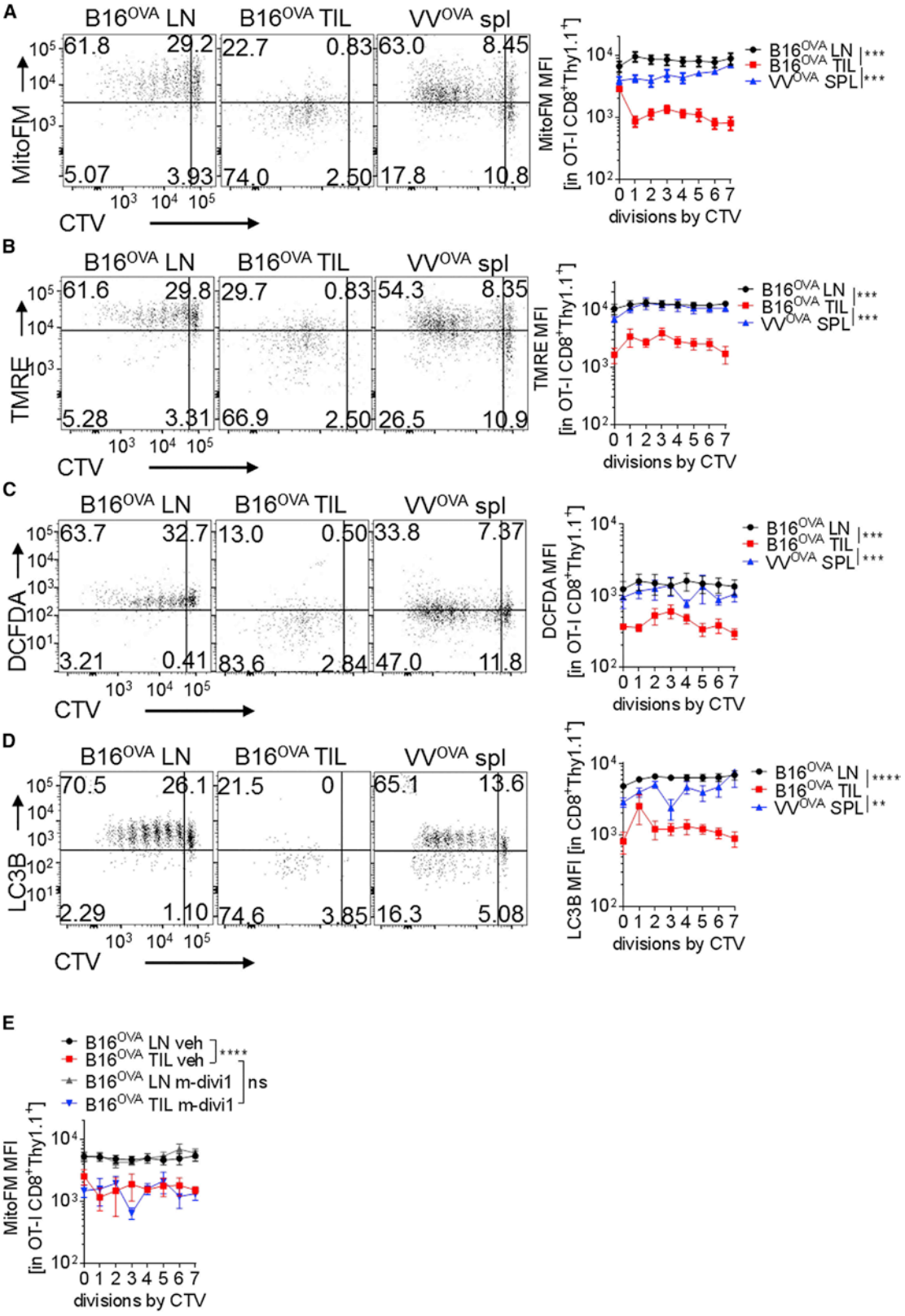
A
B16OVA LN
B16OVA TIL
VVOVA spl
MitoFM
CTV
61.8
29.2
5.07
3.93
22.7
0.83
74.0
2.50
63.0
8.45
17.8
10.8
MitoFM MFI [in OT-I CD8+Thy1.1+]
divisions by CTV
B16OVA LN ***
B16OVA TIL ***
VVOVA SPL ***
B
TMRE
61.6
29.8
5.28
3.31
29.7
0.83
66.9
2.50
54.3
8.35
26.5
10.9
TMRE MFI [in OT-I CD8+Thy1.1+]
C
DCFDA
63.7
32.7
3.21
0.41
13.0
0.50
83.6
2.84
33.8
7.37
47.0
11.8
DCFDA MFI [in OT-I CD8+Thy1.1+]
D
LC3B
70.5
26.1
2.29
1.10
21.5
0
74.6
3.85
65.1
13.6
16.3
5.08
LC3B MFI [in CD8+Thy1.1+]
B16OVA LN ****
B16OVA TIL **
E
B16OVA LN veh
B16OVA TIL veh
****
B16OVA LN m-divi1
B16OVA TIL m-divi1
ns
MitoFM MFI [in OT-I CD8+Thy1.1+]

Figure 18. T Cell Mitochondrial Dysfunction Is Induced upon Entry into the Tumor Microenvironment

(A) Representative flow cytogram and tabulated data of LN and TIL of naive, CellTrace Violet (CTV)-labeled, OT-I (Thy1.1+) CD8+ T cells transferred into B16OVA-bearing mice (5–7 mm tumors), or the spleens of the same progenitor cells transferred into B6 mice infected with 1 × 106 PFU VVOVA for 72 hr. Cells were stained with MitoTracker Deep Red FM. (B) As in (A), but with the mitochondrial membrane potential dye TMRE. (C) As in (A), but with the cellular ROS indicator DCFDA. (D) As in (A), but cells were permeabilized and stained intracellularly for LC3B. (E) Representative data from experiments as in (A), but some mice received mitophagy inhibitor m-divi-1. Results represent the mean of three or four independent experiments, with n = 7–9 mice per group. $**p < 0.01$, $***p < 0.001$, $***p < 0.0001$ by two-way ANOVA. Error bars indicate SEM.

4.5.4 Loss of Mitochondrial Mass Correlates with Upregulation of Co-inhibitory Molecules

As loss of mitochondrial function was progressive and specific to the tumor microenvironment, we next sought to determine the relationship between the loss of mitochondria seen in tumor-infiltrating T cells and the expression of molecular markers for dysfunctional, exhausted T cells. B16 melanoma is highly enriched for dysfunctional T cells expressing high levels of PD-1, LAG-3, and Tim-3 (Figure 19A). Mitochondrial loss in the polyclonal T cell response appeared to be progressive, as T cells expressing more co-inhibitory molecules had decreased mitochondrial mass, as evidenced by MitoTracker FM staining as well as staining for VDAC (Figures 19B, 19C, and S42A). Whereas mitochondrial mass was inversely correlated with upregulation of coinhibitory molecules, glucose competency was consistently depressed in tumor-infiltrating T cells

and did not specifically correlate with these markers (Figure 19D), in agreement with previous reports[72,135]. This resulted in a failure to maintain a sufficient reserve of ATP (as measured directly *ex vivo*) (Figure 19E). We observed similar results in MC38 and LLC tumors (Figures S42B and S42C). Although LLC did not induce similar sustained co-inhibitory molecule expression in CD8+ T cells (compared to the other two models) (Figure S42C), there was still a significant mitochondrial defect (Figures 16B and S39). CD8+ T cells infiltrating head-and-neck cancers exhibited decreased MitoTracker staining compared to peripheral blood lymphocyte T cells (Figure 16D) and high levels of coinhibitory molecule expression (Figure 19F) that correlated with mitochondrial loss (Figure 19G). In order to directly determine whether lower MitoTracker FM staining correlated with poor cytokine production, we sorted tumor-infiltrating T cells based on MitoTracker FM staining, stimulated them *in vitro*, and monitored cytokine production. Consistent with their exhausted phenotype, T cells having lowest mitochondrial staining had the lowest cytokine production (Figure S42D). Thus, T cells infiltrating solid tumors showed a progressive loss of mitochondrial mass and function, such that the most exhausted cells also showed the lowest mitochondrial activity.

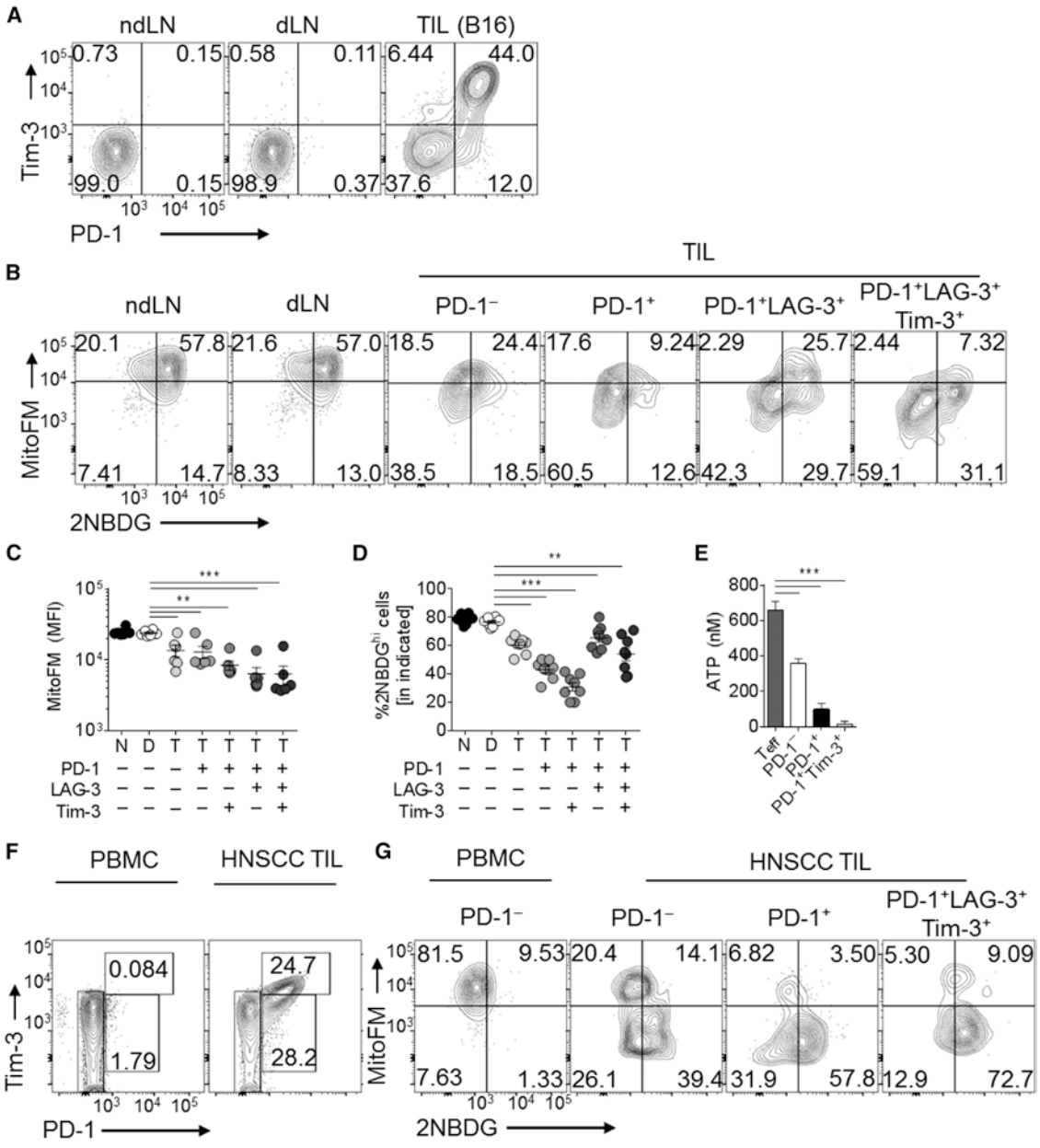

Figure 19. Mitochondrial Dysfunction in Intratumoral T Cells Is Progressive and Correlates with Coinhibitory Molecule Expression in Mouse and Human Tumors

(A) Representative flow cytogram of CD8+ T cells isolated from day 14 B16-bearing C57/BL6 mice. (B) Flow cytogram showing mitochondrial mass and glucose competency of CD8+ T cell subsets. (C and D) Tabulated data from (B). (E) ATP measurements from CD8+ T cells sorted directly ex vivo from tumors based on the indicated expression. Results are compared to LN CD8+CD44hi cells (Teff). (F) Cytogram of coinhibitory molecules and (G) mitochondria/glucose status of CD8+ cells from PBL or TIL from

HNSCC patients. Data represent the mean or are representative of 3–5 independent experiments. $*p < 0.05$, $**p < 0.01$, $***p < 0.001$ by unpaired t test. Error bars indicate SEM.

4.5.5 Loss of T Cell Oxidative Metabolism in Cancer Is Largely Independent of PD-1 Signaling and Treg Cells

PD-1 blockade can reverse tumor-induced T cell dysfunction and lead to heightened antitumor immunity and cancer regression[146]. We thus wanted to determine whether PD-1 blockade might rescue loss of mitochondrial function in tumor-infiltrating T cells. We employed mice bearing B16 tumors, in which PD-1 therapy is ineffective, despite the presence of large numbers of PD-1+ T cells, as well as those bearing MC38 tumors, which is sensitive to PD-1 monotherapy[132]. Mice were inoculated with B16 or MC38 and received anti-PD-1 (200 μg, thrice weekly) or isotype control when palpable tumors were present (1 × 1 mm). Regardless of treatment or tumor type, tumor-infiltrating T cells showed similar decreases in mitochondrial mass (Figures 20A and 20B). Our PD-1 blockade strategy was therapeutically effective, resulting in 40% regression in MC38 bearing mice (Figure 20C). In order to determine whether PD-1 signaling might impact the mitochondrial sufficiency of recent T cell entrants into the tumor, we transferred dye-labeled OT-I T cells into mice bearing established $B16^{OVA}$ tumors under the cover of PD-1 blockade or its control for 72 hr. We observed a temporary and incomplete recovery of MitoTracker FM staining in later cell divisions (Figure 20D). However, these changes were statistically significant only when broken down by cell division and were not detected past 72 hr (data not shown). Thus, although PD-1 might play a role in

modulation of metabolism, blockade of PD-1 was not sufficient to reverse mitochondrial insufficiency observed in tumor-infiltrating T cells.

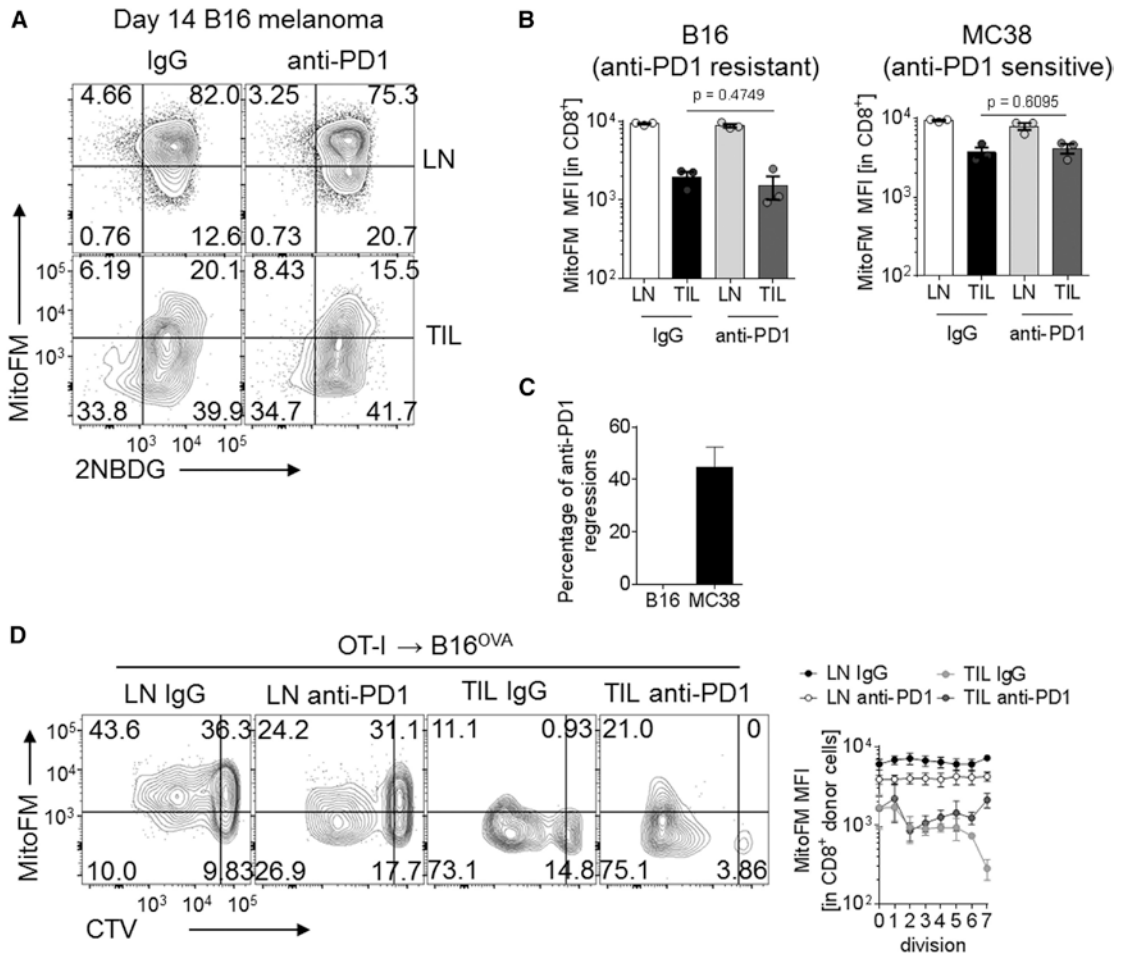

Figure 20. PD-1 Blockade Does Not Rescue Metabolic Dysfunction in Intratumoral T Cells

(A) Representative flow cytogram of CD8+ T cells from LN and TIL preparations in B16-bearing mice receiving thrice-weekly injections of 200 μg anti-PD1 or its isotype control. (B) Tabulated results from (A) as well as MC38-bearing mice. Each dot represents a mouse in this experiment. (C) Percentage of mice experiencing tumor regression in several experiments conducted as in (B). (D) Flow cytogram and tabulated values of MitoTracker FM staining during cell division of OT-I T cells transferred into established $B16^{OVA}$ tumors under the cover of anti-PD1 or its isotype control. Data are representative of five (A and B) or represent the mean of three (C and D) independent experiments. Error bars indicate SEM.

Regulatory T cells (Treg) also represent a major immunosuppressive player in the tumor microenvironment[157]. Thus, we asked whether Treg cells mediate metabolic

insufficiency in the tumor microenvironment by examining CD8+ TILs from Foxp3$^{DTR.GFP}$ mice which carry a diphtheria toxin receptor and green fluorescent protein (GFP) knocked into the 3′ UTR of Foxp3, allowing for conditional deletion of Treg cells upon treatment with diphtheria toxin (DT)[161]. Treatment of B16-bearing Foxp3$^{DTR.GFP}$ mice with DT resulted in near complete depletion of tumor-infiltrating Treg cells (Figure S43A) but no significant increases in CD8+ T cell MitoTracker FM staining (Figure S43B). In agreement with these *in vivo* findings, CD8+ T cells cultured *in vitro* by purified Treg cells also maintained mitochondrial sufficiency (Figure S43C). Thus, metabolic insufficiency in CD8+ TILs appeared to be driven in a manner independent of “classic” immunosuppressive mechanisms in the tumor microenvironment.

4.5.6 PGC1α-Mediated Mitochondrial Biogenesis Is Repressed by Akt in Tumor-Infiltrating T Cells

Having found that PD-1 and Treg cells did not appear to be responsible for the mitochondrial dysfunction seen in tumor-infiltrating T cells, we next sought to determine the molecular mechanism for this metabolic phenotype. Our kinetic analyses showed that these T cells divided extremely rapidly in response to tumor antigen in the LNs, so we hypothesized that T cells failed to properly program mitochondrial biogenesis during rapid cell division upon entry into the tumor microenvironment. Mitochondrial replication is programmed in part by the mitochondrial transcription factor A (TFAM) and regulated by the transcriptional coactivator PGC1α (encoded by *Ppargc1a*)[162,163]. Intracellular staining and quantitative PCR analysis revealed tumor infiltrating CD8+ T cells exhibit decreased PGC1α protein and *Ppargc1a* expression, respectively (Figure 21A and

Figure S44A). Kinetic analysis of dye-labeled, naive OT-I cells injected into $B16^{OVA}$-bearing mice showed PGC1α downregulation occurred concomitant with cell division specifically in the tumor microenvironment, suggesting microenvironment-derived signals promoted downregulation of mitochondrial biogenesis during T cell proliferation (Figure 21B). Repression of PGC1α occurred even in the presence of PD-1 blockade, suggesting another dominant signal present in the tumor microenvironment suppresses PGC1α expression (Figure S44B). Analysis of PGC1α-deficient T cells ($Ppargc1a^{f/f}$ $Cd4^{Cre}$ mice) revealed progressive losses of mitochondrial mass in vitro after activation, resulting in decreased OCR (Figures S44C and S44D). Comparison of cytokine production in LN- and TIL OT-I T cells responding to cognate peptide revealed that the small proportion of PGC1α+ cells in tumor-infiltrating compartments marked the T cells that were competent to produce cytokines, indicating that this pathway is important for intratumoral T cell function (Figure 21C). In agreement with this observation, T cells showing repressed PGC1α staining also exhibited decreased T-bet and Ki-67 staining, consistent with a model in which PGC1α repression is concomitant with a terminally exhausted phenotype (Figure S44E and S44F).

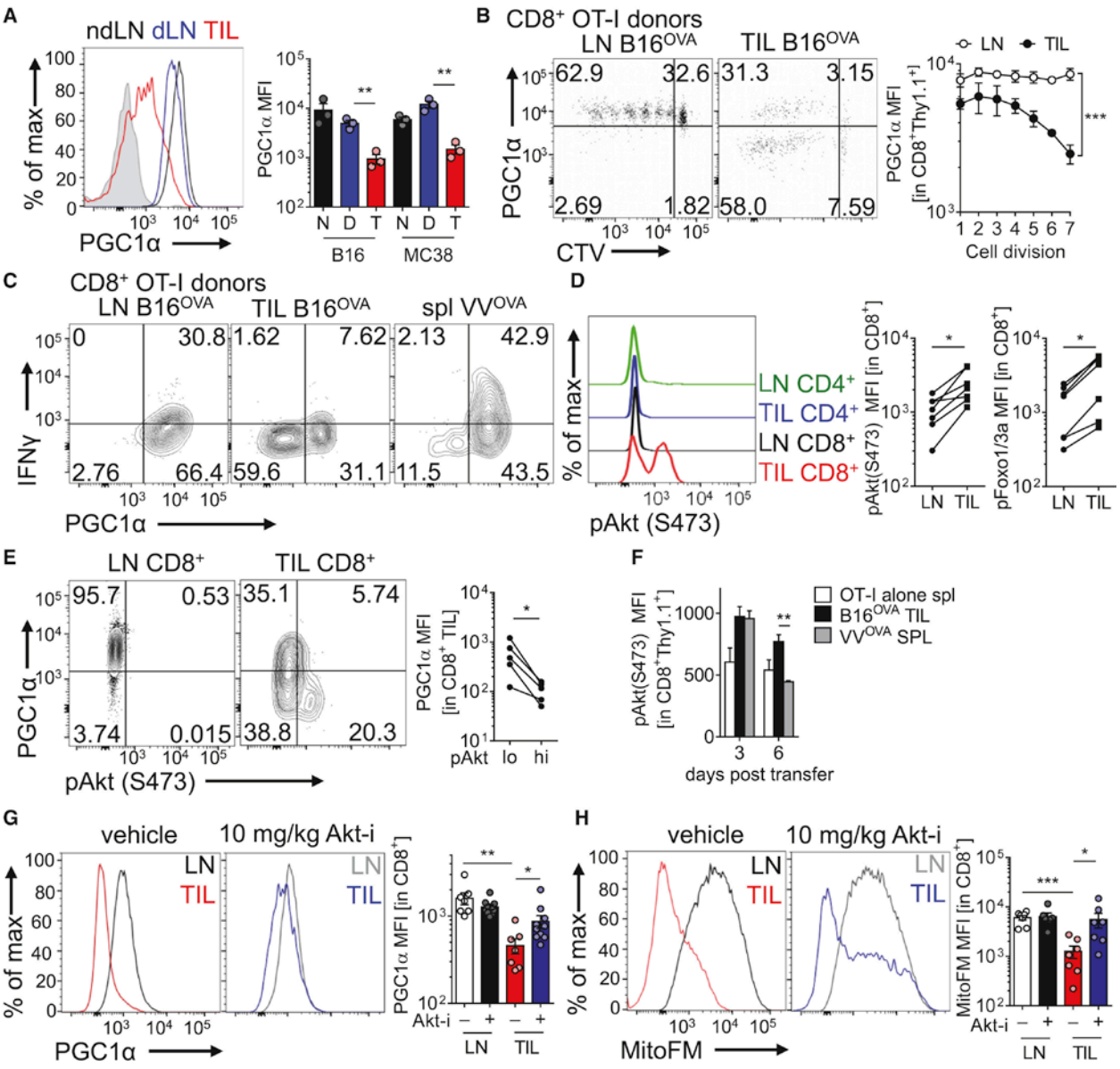

Figure 21. Intratumoral T Cell Mitochondrial Biogenesis Is Repressed by Chronic Akt-Mediated Repression of PGC1α

(A) Flow cytogram (left) and tabulated data (right) of PGC1α intracellular staining in CD8+ T cells isolated from nondraining or draining LNs or TIL preparations from B16 or MC38 bearing mice. Shaded histogram indicates isotype control. (B) Flow cytogram of PGC1α expression in CTV-labeled, naive OT-I T cells adoptively transferred into B16OVA bearing mice for 72 hr. Tabulation for multiple experiments is to the right. (C) Flow cytogram of cytokine production of congenically mismitached WT OT-I T cells transferred into B16OVA-bearing or VVOVA-infected mice for 96 hr, then restimulated with SIINFEKL peptide. (D)

Representative and tabulated phospho-Akt (S473) and phospho-Foxo1(T24)/3a(T32) staining of the indicated cell populations in mice bearing 14-day B16 tumors. MFI is reported. (E) Representative flow cytogram and tabulated data indicating PGC1α staining in pAkt low or high cells. (F) MFI of pAkt staining in naive OT-I T cells, or OT-I T cells transferred for 3 or 6 days into a B16OVA-bearing or VVOVA infected mouse. (G) PGC1α levels and (H) mitochondrial mass of CD8+ T cells from LN and TIL of 14-day B16-bearing mice treated for 60 hr with Akt inhibitor VIII or its vehicle. Results are representative of five (A, B, and D), three (C, E, G, and H), or two (F) independent experiments. $*p < 0.05$, $**p < 0.01$, $***p < 0.001$ by unpaired t test (A, F, G, and H) or paired t test (D, E, G, and H). $***p < 0.001$ by two-way ANOVA. Error bars indicate SEM.

PGC1α is dynamically regulated by a number of signaling pathways relevant to T cell activation, with Akt being a prominent repressive pathway[164]. Akt upregulates glycolytic metabolism through a variety of mechanisms, but it also can actively repressive oxidative programs, particularly through the phosphorylation and inactivation of Foxo family transcription factors, shown previously to promote PGC1α expression[165,166]. Thus, we sought to examine the status of Akt activity in tumor-infiltrating T cells, hypothesizing that the chronic activation signals mediated by persistent antigen in cancer might promote Akt activation and repress the oxidative phenotype programmed by Foxo. CD8+ T cells infiltrating B16 tumors showed increased Akt activation (as measured by phosphorylation at serine 473) and Akt-mediated inhibitory Foxo phosphorylation compared to LN (where the vast majority of T cells are resting) (Figure 21D). Comparison of Akt activation to PD-1 status revealed that Akt is highest in tumor-infiltrating T cells that are PD-1 intermediate as well as those having high PD-1 and LAG-3 surface expression. This suggests that Akt is persistent in newly activated T cells as well as those receiving chronic stimulation and differentiating

toward terminal exhaustion (Figure S44G). Importantly, intratumoral cells that have high levels of Akt activation are particularly low in PGC1α protein levels (Figures 21E). We also examined early (3 day) and late (6 day) responses of T cells responding to $B16^{OVA}$ or VV^{OVA}, and found that while Akt activation in acute viral infection was transient, T cells activated in the tumor microenvironment appeared to show chronic Akt signaling, persisting 6 days after adoptive transfer (Figure 21F). Short-term treatment (72 hr) of B16-bearing mice with a potent Akt kinase inhibitor revealed that Akt, at least in part, mediated losses in PGC1α and mitochondrial sufficiency (Figures 21G and 21H). Thus, T cells responding to antigen in tumor microenvironments repressed mitochondrial biogenesis through repression of PGC1α, driven in part by chronic Akt activation and consequent repression of Foxo activity.

4.5.7 Metabolic Reprogramming of Tumor-Specific T Cells Results in Increased Antitumor Immunity

Having demonstrated that PGC1α acted as a node of dysregulation for mitochondrial sufficiency in tumor-specific T cells, we thus wondered whether reprogramming T cells to favor mitochondrial biogenesis would result in increased intratumoral T cell persistence and function. To this end, we generated retroviral vectors to overexpress PGC1α in OT-I T cells. PGC1α overexpression significantly increased mitochondrial mass early (48 and 96 hr) after transduction in *in vitro* culture, although during the expansion phase, empty-vector transduced cells initiated mitochondrial biogenesis and eventually catch up to PGC1α-transduced T cells (Figure 22A). However, even at this later stage, PGC1α-reprogrammed T cells showed significantly increased OXPHOS

(Figure 22A). These cells also exhibited upregulation of spare respiratory capacity (Figure 22A), indicating high mitochondrial reserve and priming of mitochondrial biogenesis. We did not observe any significant increases in aerobic glycolysis (ECAR), although we did observe an upward trend in some experiments (Figure 22A). We then determined whether any particular carbon source dominated this increase in SRC. FCCP-uncoupled T cells were treated with inhibitors of pyruvate, fatty acid, or glutamine oxidation, which revealed that the increased respiratory capacity did not preferentially apply to a particular carbon source. These findings point to a general increase in mitochondrial capacity when PGC1α expression was enforced (Figure S45A). *In vitro*, these T cells exhibited similar effector function as their control counterparts, suggesting that in this environment where nutrients are not limiting, T cells are operating more or less at maximal capacity (Figure S45B). OT-I T cells overexpressing PGC1α transferred into mice with established $B16^{OVA}$ tumors were resistant to loss of mitochondrial sufficiency and were highly enriched in the tumor microenvironment (Figure 22B). Restimulation with OVA peptide showed that these metabolically reprogrammed T cells were superior at producing type 1 cytokines, compared to their wild-type counterparts (Figure 22C). Notably, these reprogrammed T cells expressed (at even higher levels than EV) co-inhibitory molecules, suggesting retention of mitochondrial function promoted further activation and upregulation of these checkpoint molecules (Figure S45C). Having found that PGC1α-reprogrammed T cells displayed increased effector function, we then tested whether these T cells had better therapeutic efficacy. Mice bearing small (2–6 mm2) $B16^{OVA}$ tumors received an adoptive transfer of 250,000 (if tumor was < 4 mm2) or 500,000 (if starting tumor was > 4 mm2) PGC1α or empty-

vector transduced OT-I T cells, and tumor growth was measured over time. PGC1α-reprogrammed T cells showed enhanced antitumor efficacy, resulting in significantly prolonged survival and higher incidence of complete regressions (20%) in this aggressive tumor model (Figures 22D and 22E). Thus, reprogramming tumor-specific T cells to favor mitochondrial biogenesis protected them from the loss of function observed in the tumor microenvironment.

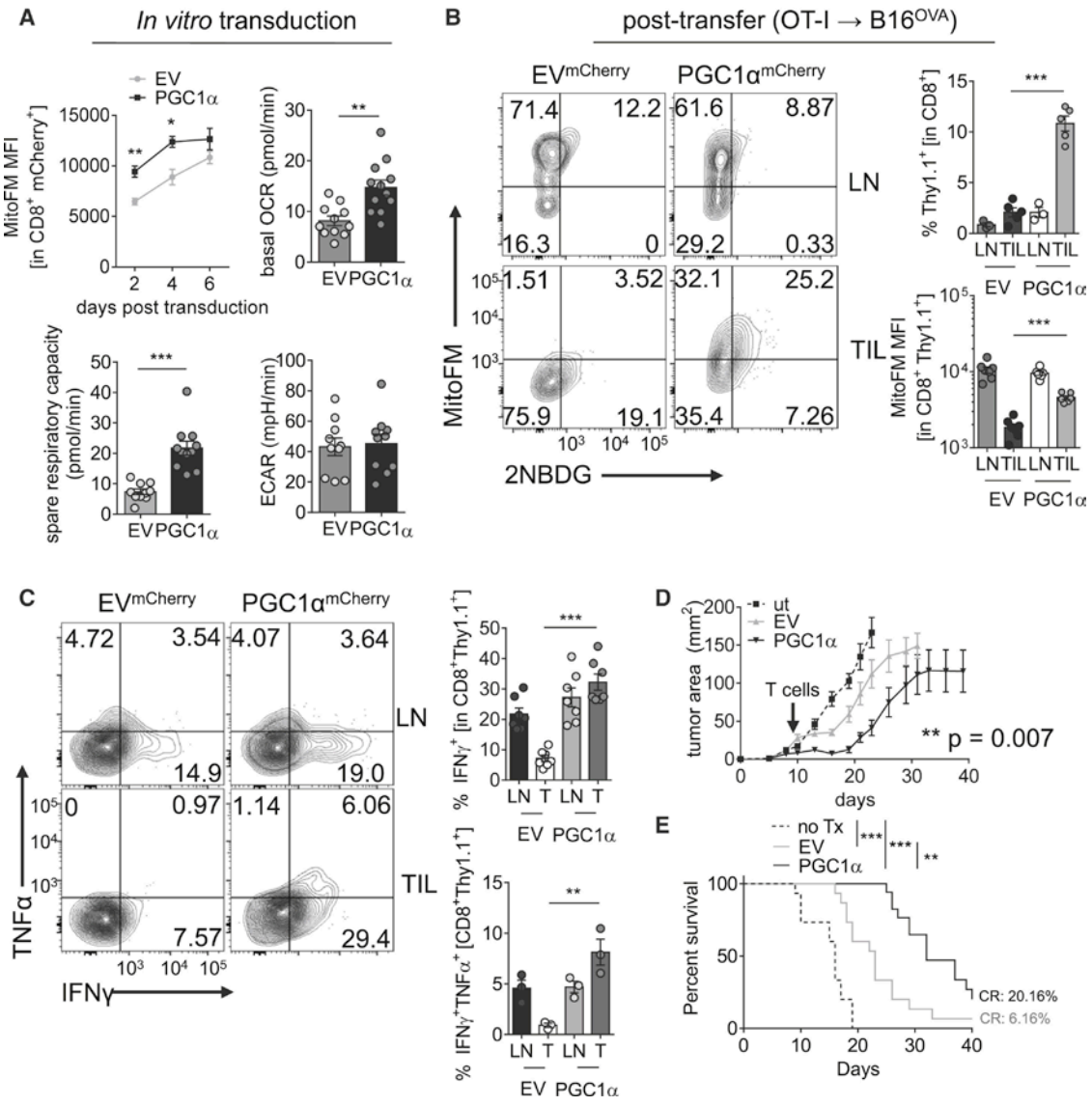

Figure 22. Bolstering Mitochondrial Biogenesis Improves Intratumoral T Cell Function

(A) Metabolic analysis of OT-I T cells retrovirally transduced with an empty mCherry vector (EV) or one encoding PGC1α. MitoTracker FM staining at various time points post transduction is indicated. OCR, SRC, and ECAR values are from day 5–7 post transduction. (B) Representative flow cytogram of LN- and TIL-resident OT-I T cells transduced as in (A) and transferred into $B16^{OVA}$ bearing C57/BL6 mice. Proportion of the transferred cells in LN and TIL and tabulated MitoTracker FM staining is reported. (C) Flow cytogram depicting cytokine synthesis in OT-I T cells transferred as in (B) and restimulated directly ex vivo with cognate peptide. Results are tabulated to the right. (D) Tumor growth plot of $B16^{OVA}$ bearing mice treated therapeutically upon detection of palpable tumors on day 7 with 250,000 (< 4mm2) or

500,000 (> 4mm2) of PGC1α or control-expressing cells. (E) Survival plot from e. n = 15–17 mice per group. Results represent six (A and B), four (C), or three (D and E) independent experiments. $**p < 0.01$, $***p < 0.001$ by unpaired t test (A–C), two-way ANOVA with repeated-measures (D), or log-rank test (E). Error bars indicate SEM.

4.6 DISCUSSION

Our data indicate a central place for persistence and function of mitochondria in sustaining effector function of T cells, especially those under continual stimulation as in cancer or chronic viral infections. We observed progressive and persistent loss of mitochondrial function and mass, observed most prominently in CD8+ T cells specifically in the tumor microenvironment. At least in the time course of rapidly growing tumor, this effect could be observed concomitantly with PD-1 upregulation but largely independently of treatment with anti-PD-1, with only mild and temporary increases in response to blockade of this particular checkpoint. Rather, Akt signaling associated with chronic activation, resulted in repression of oxidative metabolism, thus driving an unsustainable metabolic program. Our data reveal the metabolic nature of T cell dysfunction, in cancer and in general.

While glucose metabolism, especially aerobic glycolysis, has been heavily studied as a key mediator of T cell effector fate and function, our study suggests that mitochondrial function and mass are dynamically regulated and required to maintain optimal effector function. This is consistent with recent data suggesting mitochondrial

membrane potential may predict stemness in tumor-infiltrating T cells, and that cytokine production might be increased in T cells that display high mitochondrial activity[167].

As mentioned previously, there is some debate whether MitoTracker Deep Red FM is a potentiometric dye or one that stains for mitochondrial mass irrespective of membrane potential[168]. Our data employing uncoupling agents such as CCCP indicated that although Deep Red FM might show some sensitivity for membrane potential at high doses, this compound was much less robust than TMRE, a true potentiometric dye. We believe our corollary data employing MitoTracker Green and VDAC antibodies indeed confirm that T cells infiltrating tumors exhibit losses of mitochondrial function and total mass, consistent with repressed PGC1α-mediated mitochondrial biogenesis. Whereas effector T cells have been shown to possess fewer mitochondria than their memory counterparts[36,37], it is unclear how chronic stimulation might alter this fate. Our data suggest that the continued activation of T cells in cancer promotes a defect in mitochondrial biogenesis, mediated in part by Akt-controlled inhibition of Foxo-programmed PGC1α transcription. While Akt does repress oxidative metabolism, more traditional roles for Akt suggest its potential as an *in vivo* therapeutic target might be limited, because T cells might require Akt and downstream signaling *in situ* to mediate effector functions[169]. However, recent studies have revealed that this might not be the case. Akt inhibition has been employed in preclinical and translational settings as a means to reinvigorate TIL expansion, in part through modulating oxidative metabolism[90]. In addition, T cells lacking the mammalian target of rapamycin complex 2, the kinase for the hydrophobic motif (serine 473, measured in this study) of Akt, show superior effector function and increased oxidative metabolism. This suggests full Akt activation might not

be acutely required for effector function[50]. Thus, our data identify PGC1α as a crucial mechanistic link between Akt and repressed oxidative metabolism in tumor-infiltrating T cells. In addition, Akt inhibitors, which are currently being evaluated in clinical trials as anti-cancer agents, might have immunomodulatory effects that could synergize with immunotherapies.

PD-1 has been shown to inhibit mammalian target of rapamycin complex 1 signaling (which has metabolic consequences), as well as modulating metabolism at the genetic level[149]. However, we only observed association between PD-1 upregulation and mitochondrial insufficiency, with mild and short-lived effects on mitochondrial metabolism arising from anti-PD-1 treatment. In the tumor, there might be too many other signals to be offset by PD-1 blockade alone; alternatively, other co-inhibitory molecules like LAG-3 or TIGIT might be playing additional roles in modulating lymphocyte metabolism. Likewise, we failed to see any effect of regulatory T cell suppression on mitochondrial function and mass, both using a genetic model of Treg cell depletion, as well as coculture of purified Treg cells with activated CD8+ T cells.

Our data point to PGC1α as a key node of signal integration tying a diverse array of cellular signals (including Akt signaling) to mitochondrial biogenesis. Type I and type II interferons, tumor necrosis factor, interleukin-12, energy charge, and low NAD+/NADH or oleate/palmitate ratios have been shown to repress PGC1α expression, localization or transcriptional activity through a variety of signaling pathways[170–175]. PGC1α is post-translationally modified by a number of signaling pathways important in T cell biology (Akt, p38-MAPK, AMPK, SIRT1, PRMT1)[164]. Thus, the balance of these

signals in the inflammatory milieu might determine the ability of PGC1α to program mitochondrial biogenesis.

This study adds to a growing number of reports that collectively suggest that the T cell exhaustion observed in chronic activation has underpinnings in basic cellular processes like metabolism. Unlike anergy (induced by minimal signaling through TCR ligation alone in a non-inflammatory environment), persistent, inflammatory activation in cancer and chronic viral infections promote an effector state that T cells cannot sustain[145,149,151]. This is especially perilous in the tumor microenvironment, because chronic inflammatory signals might drive a sustained reliance on glycolysis in a tissue site where glucose levels are extremely low[125]. We and others reveal that tumor-infiltrating T cells show depressed glucose uptake compared to LN-resident cells. These cells also have decreased glycolysis compared to virus-activated cells, suggesting that T cell exhaustion in general is characterized by metabolic insufficiency[72,74,135]. Teleologically, T cells in metabolic distress might upregulate co-inhibitory molecules as a means to prevent terminal loss of metabolic sufficiency or survival, a model consistent with results obtained in chronic viral infection[67]. These metabolic defects can persist even when the cells are removed from the suppressive microenvironment, which might provide a potential explanation for situations in which concomitant tumor immunity is lost at distal sites.

Finally, our data provide strong support for modulation and reprogramming of the metabolic state as a strategy for the improvement of immunotherapy for cancer. While advances in checkpoint blockade and other types of immunotherapy have revealed that the mechanisms blocking immune cell activation can be altered by therapeutic

intervention, tumors present a harsh microenvironment that is immunosuppressive by its basic nature. Further, our data suggest that the metabolic status of individual tumor microenvironments and their respective T cell infiltrates, which can vary from model to model or, more importantly, patient to patient, might help predict the response to immunotherapies like checkpoint blockade. While our study demonstrates that the direct metabolic reprogramming of T cells can have efficacy, it might be advantageous to adopt other strategies to remodel the metabolism of the microenvironment itself in order to create a more permissive environment for T cell activity.

Metabolism is central to cellular function, so it is largely unsurprising that T cells fail in nutrient-poor conditions. Our results and others' have shed light on the fact that during chronic activation, as in cancer, T cells are driven to proliferate and perform effector function at the expense of their continued persistence and longevity. Development of strategies to modify the bioenergetics of T cells or the tumor microenvironment itself has the promise to improve and synergize with other forms of immunotherapy to increase the efficacy of the treatment of cancer.

5.0 CHRONIC T CELL ACTIVATION UNDER HYPOXIA CAUSES ROS-MEDIATED T CELL DYSFUNCTION AND INAPPROPRIATE CARBON STORAGE IN EXHAUSTED T CELLS

5.1 FOREWORD

This chapter contains data that will be published in future manuscripts. This work would not be possible without the following co-authors: Natalie Rittenhouse, Yiyang (Steve) Wang, Mara Sullivan, Xue (Lucy) Zeng, Rhodes Ford, Ashley V. Menk, Ronal Peralta, Roderick J. O'Sullivan, Simon Watkins, Amanda C. Poholek, and Greg M. Delgoffe.

5.2 CHAPTER SUMMARY

In chronic viral infection and cancer, CD8+ T cells become exhausted due to chronic TCR engagement and other environmental factors. The T cells that experience prolonged T cell activation become what is known as terminally exhausted, becoming severely dysfunctional and are unable to be rescued by current therapies. This dysfunction includes metabolic dysfunction, where CD8+ T cells lose mitochondrial mass and function. We found that this metabolic dysfunction in terminally exhausted T cells includes decreased fatty acid oxidation, resulting in increased lipid storage as lipid

droplets. We have also found this increased in lipid storage requires both chronic TCR activation and hypoxia, which can be modeled in our *in vitro* T cell exhaustion assay. We have also found the metabolic defects in terminally exhausted T cells leads to changes in their epigenetic profile, causing exhausted T cells to have increased poised gene loci. The T cell exhaustion phenotype is driven by increased mitochondrial reactive oxygen species (ROS), which causes both excess lipid storage and DNA damage. Finally, we show that targeting the excess lipid storage through both genetic and pharmacological means improves T cell function and outcomes in cancer. Together, we have found terminally exhausted T cells store carbons as lipids rather than utilizing them for fuel, and by modulating lipid utilization we can improve TIL function.

5.3 INTRODUCTION

When CD8+ T cells become activated in response to MHCI plus cognate peptide, environmental factors can influence the T cells' functional outcome. In the setting of acute viral infection, CD8+ T cells transition from effector T cells to memory T cells, which retain proliferative capacity, cytokine production, memory markers, and have the capacity to persist and reactivate in response to future TCR stimulation[149,176]. In contrast, exhausted T cells found in chronic viral infection and cancer do not transition from effector to memory; instead they transition to the exhaustion state where they lose proliferative and cytokine potential, upregulate co-inhibitory receptor expression, and become reliant on antigen, or chronic TCR activation, to persist. Therefore, memory and exhausted T cells can be thought of as opposing differentiation states, whereby the

tumor microenvironment causes T cells to differentiate into exhausted T cells, rather than memory.

Within exhausted T cells, we can further define two main populations of cells: one that is more stem-like – PD1mid, TCF7 high, Tbet high, TOXlo, can respond to checkpoint blockade – and another population that is terminally exhausted – PD1+Tim3+, TCF7lo, EOMEShi, TOXhi, and a static epigenetic profile, of which do not show evidence of rejuvenation after checkpoint blockade[177–187]. Exhausted T cells, in addition to the attributes above, also suffer from a metabolic disadvantage. We have previously shown exhausted T cells lose mitochondrial mass and function, have decreased oxygen consumption, and lower ATP[89,91]. Only by metabolically bolstering the T cells before they enter the tumor microenvironment (TME) can one prevent the negative effects of T cell exhaustion, allowing T cells to be more cytokine competent, decreasing tumor burden, and increasing patient survival. This metabolic defect is in contrast to memory T cells, where increased mitochondrial content, increased oxygen consumption rate, and reliance on fatty acid oxidation are defining characteristics of memory T cells[89,188].

This led us to ask what aspect of mitochondrial function is essential for CD8+ tumor-infiltrating lymphocyte (TIL) function, or alternatively, what aspect of dysfunctional mitochondria contribute to TIL dysfunction. Mitochondria are more than ATP factories; they also play an essential role in synthesizing all the building blocks required for new organelles and daughter cells such as fatty acids, nucleotides, and amino acids[87,189–191]. Mitochondria are recruited to the T cell synapse and locally buffer calcium signaling upon T cell activation. They also generate epigenetic intermediates for modifying the

epigenome, and they produce reactive oxygen species (ROS), which at low levels is essential for normal T cell signaling, and they make iron-sulfer clusters, which are essential for nuclear DNA enzyme functionality[192]. We wanted to dissect the metabolic and immunologic factors that drive T cell exhaustion and determine what are the metabolic consequences of T cell exhaustion.

We found that terminally exhausted T cells have suppressed fatty acid oxidation genes, which leads them to inappropriately store their carbon as lipids. This lipid storage is due to chronic T cell activation under hypoxia, generating excessive mitochondrial ROS and damaging DNA. By enforcing fatty acid oxidation in TIL, either genetically or pharmacologically, we were able to improve both TIL function and survival in mouse cancers. Terminally exhausted T cells also suffer from an altered epigenetic profile due to metabolic disadvantage.

5.4 METHODS

Mice

Animal work was done in accordance with the Institutional Animal Care and Use Committee of the University of Pittsburgh. All mice were housed in specific pathogen free conditions prior to use. C57/BL6, SJ/L (Thy1.1), Cd4Cre, and Cy Tg(TcraTcrb)8Rest/J (pmel) mice were obtained from The Jackson Laboratory. Prdm1 f/f mice were a gift from the Poholek lab.

Cell Lines, Antibodies, and Other Reagents

B16-F10 was obtained from ATCC. Zombie viability dye and anti-CD8 (53.6.7), anti-Tim3 (RMT3-23), anti-PD1 (29F.1A12), anti-IFNγ (XMG1.2) and anti-TNFα (MP6-XT22) antibodies were obtained from BioLegend. BODIPY neutral lipid dye 493/503 (4,4-Difluoro-1,3,5,7,8-Pentamethyl-4-Bora-3a,4a-Diaza-s-Indacene), MitoSOX Red Mitochondrial Superoxide Indicator, Dynabeads Mouse T-Activator CD3/CD28 for T-Cell Expansion and Activation, and anti-Tox (TXRX10) and anti-Blimp1 (5E7) antibody was obtained from Fisher. Rotenone and Antimycin A were obtained from Sigma. VDAC antibody was obtained from Abcam. Anti-acetylated lysine antibody was obtained from Cell Signaling Technologies and detected after surface staining with brief fixation first with 4% PFA, followed by fixation and permeabilization with the Foxp3 Fix/Perm kit (eBioscience), staining with the unconjugated antibody, then Alexa Fluor 647 or Alexa Fluor 488-conjugated anti-rabbit immunoglobulin G (IgG) (Jackson Immunoresearch). Rosiglitazone was purchased from Cayman Chemical. PGC1α antibody (H-300) was obtained from Santa Cruz Biotechnology, and was detected using the Foxp3 Fix/Perm kit (eBioscience) and anti-rabbit immunoglobulin G (IgG) (Jackson Immunoresearch). Anti-PD-1 blocking antibody (J43) and its hamster IgG control were obtained from Bio-X-Cell. Anti-phospho Histone H2A.X (Ser139) antibody was obtained from Millipore.

Immunoblotting Analysis

Immunoblotting was performed as previously described[100]. Antibodies for immunoblots were obtained from Cell Signaling Technology (Blimp1) and Santa Cruz Biotechnology (PGC1α). Immunoblots were detected via standard secondary detection and

chemiluminescent exposure to film. Digitally captured films were analyzed densitometrically by ImageJ software.

T Cell Isolations from Lymph Node and Tumor

Lymph node T cells were isolated from 6- to 8-week-old B16-bearing mice and mechanically disrupted. To obtain single-cell suspensions of tumor infiltrating lymphocytes, we injected whole tumors repeatedly using 20G needles with 2 mg/mL collagenase type VI, 2 U/mL hyluronidase (Dispase), and 10 U/mL DNase I (Sigma) in buffered RPMI with 10% FBS and incubated them for 25 min at 37°C. Tumors were mechanically disrupted between frosted glass slides and filtered to remove particulates, then vortexed for 30 seconds. In many experiments (especially prior to sorting), tumor homogenates were debulked of tumor cells using CD105-biotin mediated magnetic depletion.

In vitro exhaustion assays

For the bead-based exhaustion assay (called Chronic Stim + Hypoxia Assay), lymph node and spleen T cells were isolated from 6- to 8-week-old mice, mechanically disrupted, and sorted on CD8+ CD44hi. Cells were then activated at 20,000 T cells per 96 well plate round bottom wells with an equivalent number of CD3/CD28 washed dynabeads, 25U/ml IL2, and 10ng/ml IL-12 in 200uL complete RPMI + 10% serum. Cells were activated for 24hr, beads were magnetically removed, then cells were divided into 4 conditions: no dynabeads in regular incubator (acute activation in normoxia), no dynabeads in 1.5% oxygen hypoxia chamber (acute activation in

hypoxia), with 200,000 dynabeads in the regular incubator (chronic activation in normoxia), and with 200,000 dynabeads in 1.5% oxygen hypoxia chamber (chronic activation in hypoxia). Cells were continued to be cultured in 25U/ml IL2 in 200uL complete RPMI + 10% serum in 96-well round bottom plates. After 24 hours (d3), more media + IL2 was added. After 24hr (d4), cells were split, more beads were added, and fresh media + IL2 was added. After 48hr (d6), cells were split, more beads were added, and fresh media + IL2 was added. After 24hr (d7), cells were assayed after beads were removed.

For antimycin A-based exhaustion assay, CD8 T cells were isolated, activated for 24hr with 3ug/ml plate-bound CD3, soluble CD28, and 50U/ml IL2. After activation, cells were cultured in either media + 25U/ml IL2 alone, or with 0.02uM Antimycin A, or 0.02uM Rotenone + 0.02uM Antimycin A. Cells were cultured for 5 days in conditions, then assayed.

Luminescence assay

The PGC1α plasmid was originally generated by B. Spiegelman, obtained from Addgene (plasmid 8887)[193]. The Blimp1 plasmid was a gift from the Poholek lab. 293T cells were co-transfected with the plasmids, then next day, the ONE-Glo EX Luciferase Assay System (Promega) was used to assay luminescence.

Gene Expression Profiling by RNaseq

LN or TIL was dissociated from tissue as described above, then sorted based on CD8+ CD44hi in LN, and CD8+ and PD1 vs Tim3 expression for TIL. Cells were lysed, mRNA

converted into cDNA, and cDNA was prepared using the SMARTer Ultra Low Input RNA Kit for Sequencing - v3 user manual (Clontech Laboratories). Sequencing libraries were prepared using Nextera XT DNA Library Preparation kit (Illumina), normalized at 2nM using Tris-HCl (10mM, pH 8.5) with 0.1% Tween20, diluted and denatured to a final concentration of 1.8nM using the Illumina Denaturing and Diluting libraries for the NextSeq 500 protocol Revision D (Illumina). Cluster generation and 75bp paired-end dual-indexed sequencing was performed on Illumina NextSeq 500 system. RNA-seq was analyzed using standard methods including alignment to the genome using HISAT2, gene expression values (TPM) calculated using Subread and identification of differentially expressed genes (DEG) using DEseq2 with a cutoff of 2 fold and p value<0.05.

Cleavage Under Targets & Release Using Nuclease (CUT&RUN)-Sequencing

LN or TIL was dissociated from tissue as described above, then sorted based on CD8+ CD44hi in LN, and CD8+ and PD1 vs Tim3 expression for TIL. DNA at specific chromatin modifications was then extracted as described[194]. In brief, sorted cells were washed, concanavalin-coated magnetic beads (Bangs Laboratories) added, and incubated with appropriate antibody overnight (anti-H3K9ac, H3K27ac, H3K27me3, H3K4me3, IgG control Cell Signaling; anti-γH2AX Abcam). Next day, cells were washed with digitonin buffer, and protein A micrococcal nuclease was added to cleave DNA at sites of bound antibody and incubated for 1hr. Cells were washed, chilled to 0°C, and 100mM $CaCl_2$ was added to cleave and release the DNA. Cells were centrifuged, supernatant with released DNA fragments collected, DNA extracted, and barcoded

libraries for Illumina sequencing with Tru-Seq adaptors were used to amplify DNA library. Size distribution of library was quantified by Agilent 4200 TapeStation analysis, and paired-end Illumina sequencing of the barcoded libraries was performed.

CUT&RUN data was aligned to the genome using Bowtie2, redundant reads removed, and normalized to spike-in controls. Peaks were called with MACS using p-value threshold of 1e10-5. Regions identified in both replicates will be identified as true and compared to IgG control group. Peak intensity (tags) were normalized as tags per 1milions reads. Differential peaks were identified using DiffBind with cutoff of 2 fold and FDR < 0.01. Downstream analysis was performed with HOMER, bedtools, and custom R scripts.

Electron Microscopy

CD8+ T cells were sorted from LNs and TIL and fixed in 4% glutaraldehyde and stained for electron microscopy as previously described[157].

Retroviral Expression

The PPARγ plasmid was obtained from origene, and cloned into an MSCV-driven retroviral expression vector which also encodes an IRES-mCherry cassette, from Dario Vignali. This vector was transiently transfected into Plat-E ecotropic cells. Pmel lymph node and splenocytes were harvested, mechanically disrupted, and incubated with a biotinylated antibody cocktail consisting of antibodies (BioLegend) to B220, CD11b, CD11c, CD16/32, CD19, NK1.1, TCRγδ, and CD4. After a wash step, cells were incubated with streptavidin-coated magnetic nanoparticles (BioLegend). After washing,

CD8+ cells were isolated by applying a magnetic field and removing untouched cells. These pmel CD8+ T cells were stimulated with 5ug/ml plate-bound CD3 and 2ug/ml soluble CD28 in the presence of 50U/mL IL-2 for 24 hr. Retroviral supernatants were harvested, and filtered, and supplemented with 6 μg/mL polybrene. Pmel T cell cultures were spinduced with the retroviral supernatant for 120 min at 2,200 rpm. Cells were expanded and sorted by mCherry prior to analysis and adoptive transfer.

Rosiglitazone + adoptive T cell transfer therapy

Mice were given 250,000 B16 melanoma cells injected intradermally on day 0. On day 5 (1-10mm^2 tumors), mice began 1mg/kg rosiglitazone (Cayman Chemical) or sterile PBS, given every day for 3 days. On day 7, after 3 days treated with rosiglitazone, mice were given 10 million previously activated pmel T cells intravenously. Mice were sacrificed when tumors reached 15mm in any direction.

Rosiglitazone + anti-PD1 therapy

Mice were given 250,000 MC38 adenocarcinoma cells injected intradermally on day 0. On day 5 (1-10mm^2 tumors), mice started on 1mg/kg rosiglitazone (Cayman Chemical) once a day for 3 days. On day 8, mice began either isotype control or 0.2mg anti-PD1 (G4), every 4 days IP. Mice were sacrificed when tumors reached 15mm in any direction.

5.5 RESULTS

5.5.1 Exhausted tumor-infiltrating T cells have increased carbon storage as lipids

We have previously reported CD8+ T cells in mouse and human cancers show decreased mitochondrial mass and function, with more terminally exhausted TIL showing the greatest decrease in mitochondrial mass[89]. We wanted to further explore this metabolic dysfunction in terminally exhausted TIL. In our mouse model of B16 melanoma, we find terminally exhausted CD8+ TIL by day 14, which we define by PD1+ Tim3+ (Figure 23A, red box). When we further subset these cells by PD1 versus Tim3 expression to define recently infiltrated (PD1mid) CD8+ T cells versus terminally exhausted (PD1+Tim3+) CD8+ T cells, we see our subsets are in agreement with recent work showing terminally exhausted T cells as TOX high, an essential transcription factor for programming exhausted T cells[183] (Figure 23B).

By subsetting TIL into different groups based on PD1 vs Tim3 expression, we were able to explore the functional effects of decreased mitochondria. We compared the transcriptome of LN CD8+ T cells and TIL subset as PD1lo, PD1mid, PD1hi, and PD1+Tim3+ terminally exhausted T cells, and found exhausted TIL have decreased expression of fatty acid oxidation genes (Figure 23C). This was a particularly striking finding, as memory T cells rely on fatty acid oxidation, further highlighting the metabolic differences between memory and exhausted T cells[188] When looking for the phenotypic correlates of expression of genes responsible for decreased breakdown of lipids, we found exhausted TIL have increased lipid content, as measured by BODIPY neutral lipid

dye (Figure 23D). Exhausted TIL also have increased acetylated lysine (Figure 23E), with acetylation being another readout for increased carbon storage. Exhausted TIL also have more cellular content as measured by granularity (Figure 23F). Finally, by electron microscopy, we see that terminally exhausted TIL have increased lipid droplets (Figure 23G, lipid droplets highlighted with white dotted line) which cells may accumulate in an attempt to protect mitochondria from lipotoxic damage[195]. Taken together, we show that exhausted TIL have excessive carbon storage, as highlighted by increased lipid content in these cells.

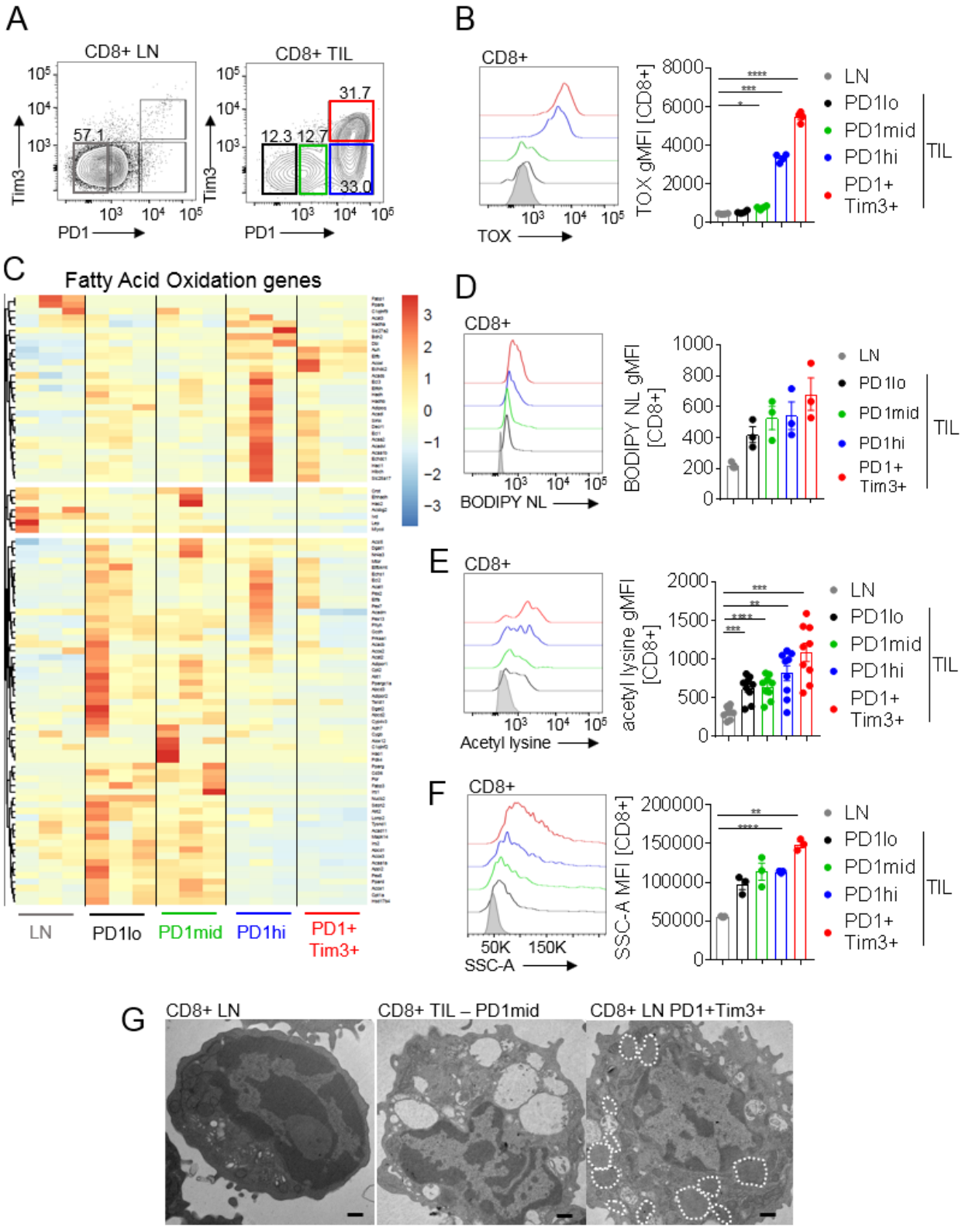

Figure 23. Exhausted tumor-infiltrating T cells have increased carbon storage as lipids

(A) Flow cytograms of LN and TIL PD1 vs Tim3 expression. (B) (left) Overlaid histograms of LN and TIL based on PD1 vs Tim3 expression, showing TOX expression, (right) quantification of TOX geometric mean fluorescent intensity. (C) LN and TIL sorted based on PD1 vs Tim3 expression, mRNA sequenced, then gene expression showed based on Gene Ontology term fatty acid oxidation (GO:0019395). (D) (left) Overlaid histograms of LN and TIL based on PD1 vs Tim3 expression, showing BODIPY neutral lipid (BODIPY NL) staining, (right) quantification of BODIPY NL geometric mean fluorescent intensity. (E) (left) Overlaid histograms of LN and TIL based on PD1 vs Tim3 expression, showing acetylated lysine expression, (right) quantification of acetylated lysine geometric mean fluorescent intensity. (F) (left) Overlaid histograms of LN and TIL based on PD1 vs Tim3 expression, showing side scatter area (SSC-A), (right) quantification of SSC-A geometric mean fluorescent intensity. (G) Electron microscopy representative images of CD8+ T cells sorted from LN and TIL, based on PD1 vs Tim3 expression.

5.5.2 Exhausted T cells inappropriately store lipids due to chronic T cell activation in a low oxygen environment

Next, we wanted to determine what TME factors were causing exhausted T cells to accumulate stored lipids. We developed an *in vitro* system to generate exhausted T cells, focusing on an immunologic driver (chronic T cell activation) and a metabolic driver (hypoxia). We isolated CD8+CD44hi T cells from mice, activated them in normal conditions, then divided the cells into acute vs chronic activation conditions (no further activation vs continuous activation with CD3/CD28-coated beads), carried out either in normoxic or hypoxic conditions (atmospheric oxygen vs 1.5% hypoxia chamber, similar to tumor hypoxia[196]) (Figure 24A). Using this *in vitro* system, we see that only the group that received chronic T cell activation in hypoxic conditions upregulated the highest PD1 and Tim3 expression, similar to terminally exhausted TIL (Figure 24B, 23A).

Transcriptionally, T cells that experience chronic T cell activation in hypoxic conditions have a subset of genes similarly expressed in exhausted TIL (Figure 24C). We also find that the *in vitro* exhausted T cells that experience chronic T cell activation in hypoxia also have the highest BODIPY neutral lipid staining, the highest acetyl lysine content, and are the most granular compared to the other groups (Figure 24D, 24E, 24F). Together, we see that we can use the *in vitro* system to generate an exhausted T cell phenotypically similar to exhausted TIL. Our results suggest that chronic T cell activation in hypoxia is the cause of excess carbon storage in exhausted T cells.

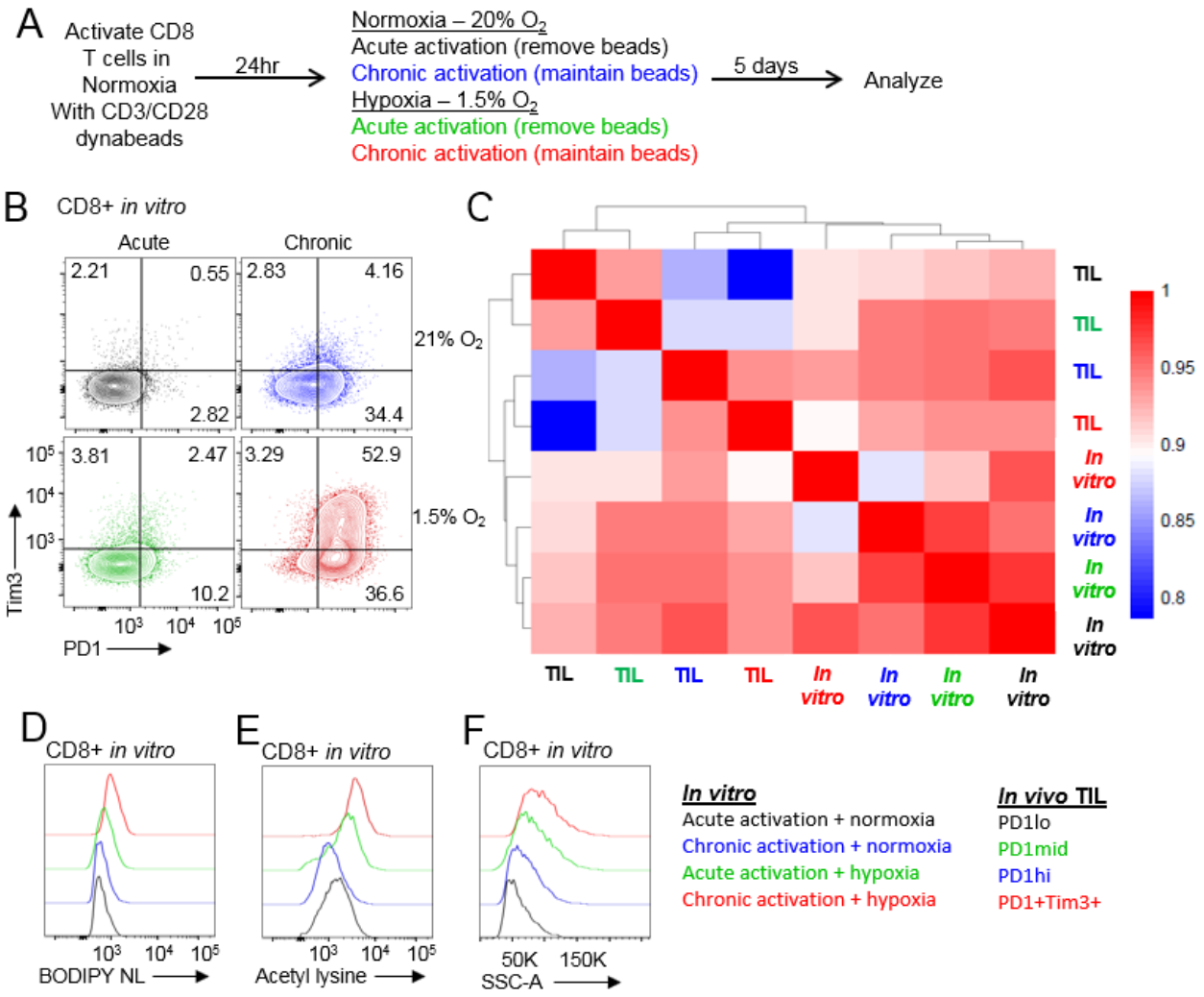

Figure 24. Exhausted T cells inappropriately store lipids due to chronic T cell activation in a low oxygen environment

(A) Visual schematic of *in vitro* T cell exhaustion assay. (B) Representative flow cytograms of CD8+ T cells PD1 vs Tim3 expression of *in vitro* exhausted T cell assay. (C) LN and TIL sorted based on PD1 vs Tim3 expression and T cells from *in vitro* T cell exhaustion assay sorted on live cells, mRNA sequenced, then gene expression compared using Pearson Correlation and plotted to show similarities and differences visually. (D) Overlaid histograms of *in vitro* T cell exhaustion assay, showing BODIPY NL staining. (E) Overlaid histograms of *in vitro* T cell exhaustion assay, showing acetyl lysine expression. (F) Overlaid histograms of *in vitro* T cell exhaustion assay, showing Side Scatter Area (SSC-A).

5.5.3 Chronic activation alters the response to hypoxia via Blimp-mediated repression of PGC1α

To further explore the transcriptional program contributing to the exhaustion phenotype, we focused on a transcriptional repressor found in exhausted T cells – Blimp1[197]. Blimp1 is well known to govern cell fate between plasma and memory B cells, but also plays a role in T cell differentiation, and is highly expressed in exhausted T cells[197,198]. In our mouse model of cancer, Blimp1 is most highly expressed in terminally exhausted TIL, as well as *in vitro* cultured cells experiencing chronic T cell activation in hypoxia (Figure 25A, 25B). Since Blimp1 is a transcriptional repressor, we wanted to determine if it could be contributing to the metabolically suppressed phenotype seen in the *in vitro* exhausted T cells. Consistent with our previous work showing that PGC1α, the master regulator of mitochondrial biogenesis, mitochondrial fusion, and antioxidant gene programs, is repressed in CD8+ TIL[89], we found the most terminally exhausted TIL have the lowest PGC1α expression (Figure 25C). We found a similar phenotype in our *in vitro* T cell exhaustion assay, showing T cells experiencing chronic T cell activation under hypoxia have the lowest PGC1α expression (Figure 25D). Linking these findings together, we found that Blimp1 can directly suppress the PGC1α promoter when tested in an *in vitro* luciferase reporter assay (Figure 25E). Thus, increasing amounts of Blimp1 lead to a step-wise decrease in both PGC1α promoter luciferase activity and endogenous PGC1α protein expression. Taken together, these results suggest that Blimp1 is at least partly responsible for the repression of metabolic genes in terminally exhausted TIL, since Blimp1 can suppress PGC1α expression.

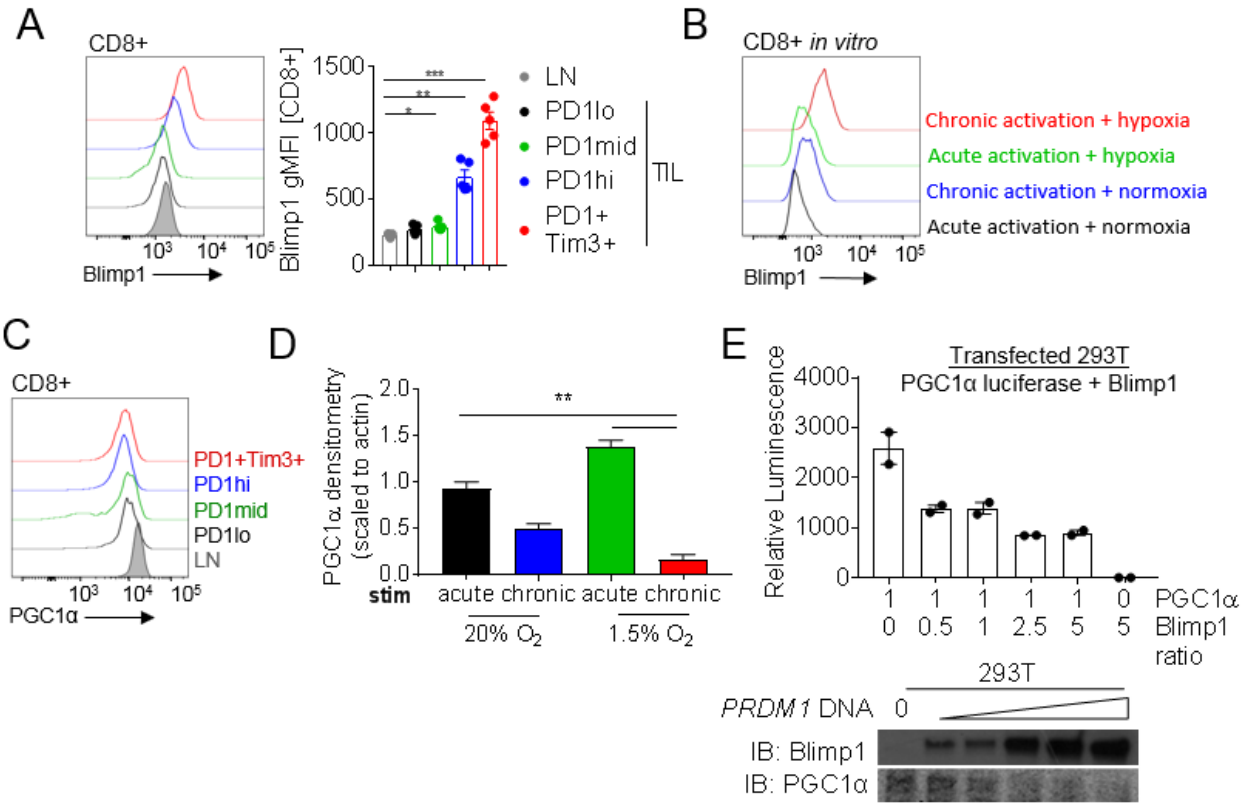

Figure 25. Chronic activation alters the response to hypoxia via Blimp-mediated repression of PGC1α

(A) (left) Overlaid histograms of LN and TIL based on PD1 vs Tim3 expression, showing Blimp1 expression, (right) quantification of Blimp1 geometric mean fluorescent intensity. (B) Overlaid histograms of *in vitro* T cell exhaustion assay, showing Blimp1 expression. (C) Overlaid histograms of LN and TIL based on PD1 vs Tim3 expression, showing PGC1α expression. (D) CD8+ T cells from *in vitro* T cell exhaustion assay in immunoblot assay, with PGC1α expression quantified. (E) 293T cells were co-transfected overnight with mouse PGC1α promoter on luciferase + mouse Blimp1 plasmid, at the indicated ratios. Cells were then lyse and luminescence quantified as well as relative protein visualized via immunoblot.

5.5.4 Exhausted T cells have altered T cell epigenetics, resulting in increased poised gene promoters on terminally-exhausted T cells

As we have now established a link between terminally exhausted T cells and metabolic dysfunction, we wanted to explore how this metabolic dysfunction could be impacting the epigenetic landscape of exhausted T cells. Mitochondria make the epigenetic products needed to modify the epigenome[199,200], and oxygen is needed to demethylate histones, so we hypothesized that there would be global changes in the epigenetic landscape of CD8+ TIL[199,200]. Others have explored exhausted T cell epigenetics via the Assay for Transposase-Accessible Chromatin using sequencing (ATACseq)[177,182]. Due to low cell number input, this is an excellent tool for phenotyping the low immune cell yields from mouse tumors, although it is limited in that it can only show open vs closed chromatin regions. This can be a great starting point, but open or closed chromatin does not resolve which chromatin modification are present at specific gene loci, i.e. genes that appear open by ATACseq may not yield the corresponding transcripts via RNAseq.

To determine the specific identity of histone modifications at gene loci, we have utilized the new epigenetic profiling strategy called Cleavage under targets and release using nuclease (CUT&RUN) developed by Peter Skene, Jorja Henikoff, and Steven Henikoff[194], and adapted it to use with CD8+ TIL from mouse B16 melanoma. Utilizing CUT&RUN, we looked at histone modifications H3K9ac for active transcription, H2K27ac for active enhancers, H3K27me3 for repressed transcription, and H3K4me3 as a mark of promoters and enhancers in the genome[200]. Using LN (CD8+ CD44hi) and CD8+ TIL sorted by PD1 vs Tim3 expression, we found, contrary to our original hypothesis, that there were *not* global epigenetic changes in exhausted TIL. Instead

most regions of the genome were repressed – as expected for differentiated cells – and only when we analyzed our sequencing data by looking at genomic areas that were different between populations did we see variations between the populations (called differential peak analysis, Figure 26A, 26B, 26C, 26D). Further analysis of chromatin modifications specifically at the transcription start site (TSS) of genes found that terminally exhausted TIL had both high H3K27me3 and H3K4me3 histone modifications at the same TSS, indicating that these gene loci were uniquely poised for gene expression (Figure 26E). Taken together, these data show that exhausted T cells have a unique epigenetic profile and exhausted T cells have an increased number of poised genes in their epigenome.

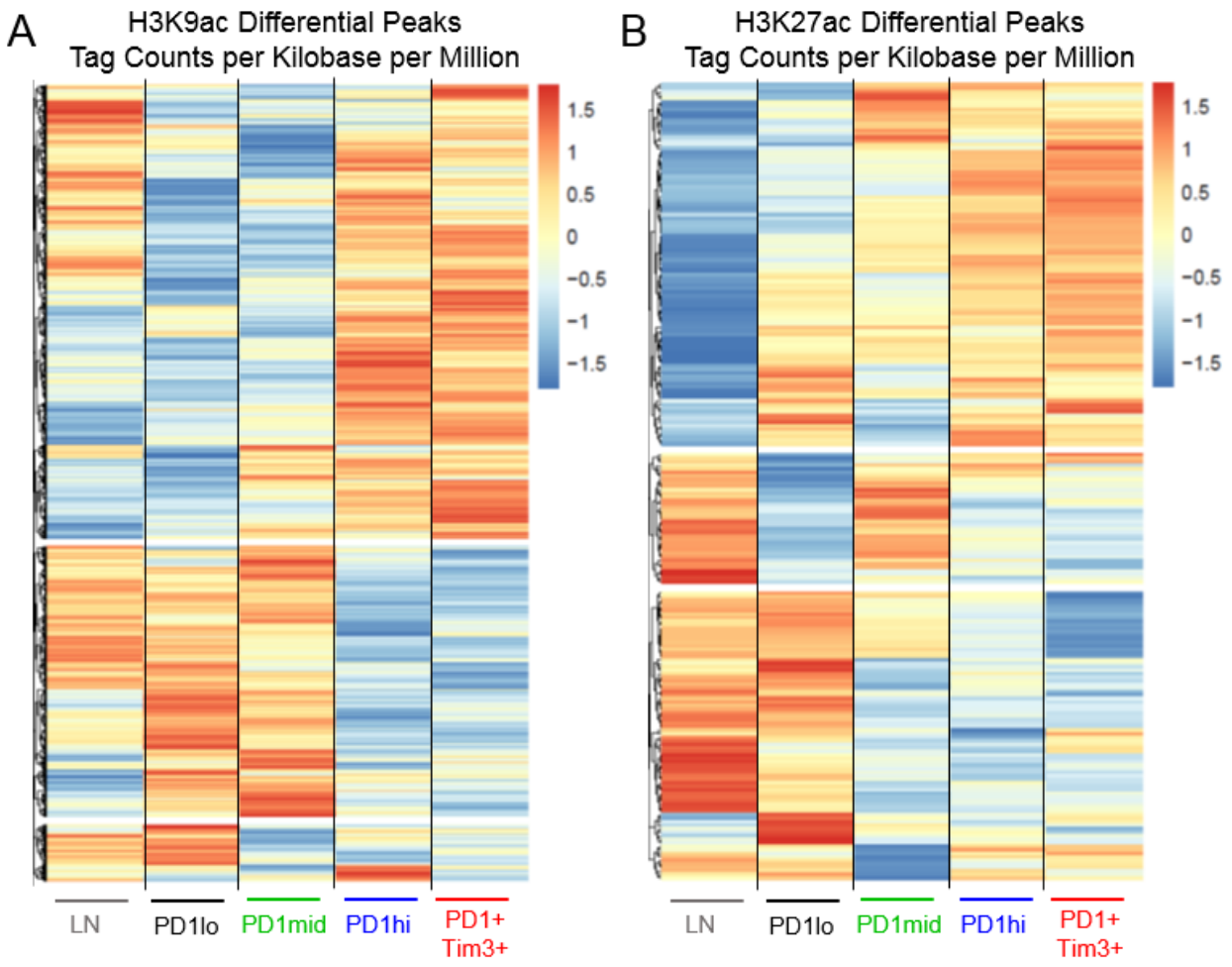
A
H3K9ac Differential Peaks
Tag Counts per Kilobase per Million
1.5
1
0.5
0
−0.5
−1
−1.5
LN
PD1lo
PD1mid
PD1hi
PD1+
Tim3+
B
H3K27ac Differential Peaks
Tag Counts per Kilobase per Million
1.5
1
0.5
0
−0.5
−1
−1.5
LN
PD1lo
PD1mid
PD1hi
PD1+
Tim3+

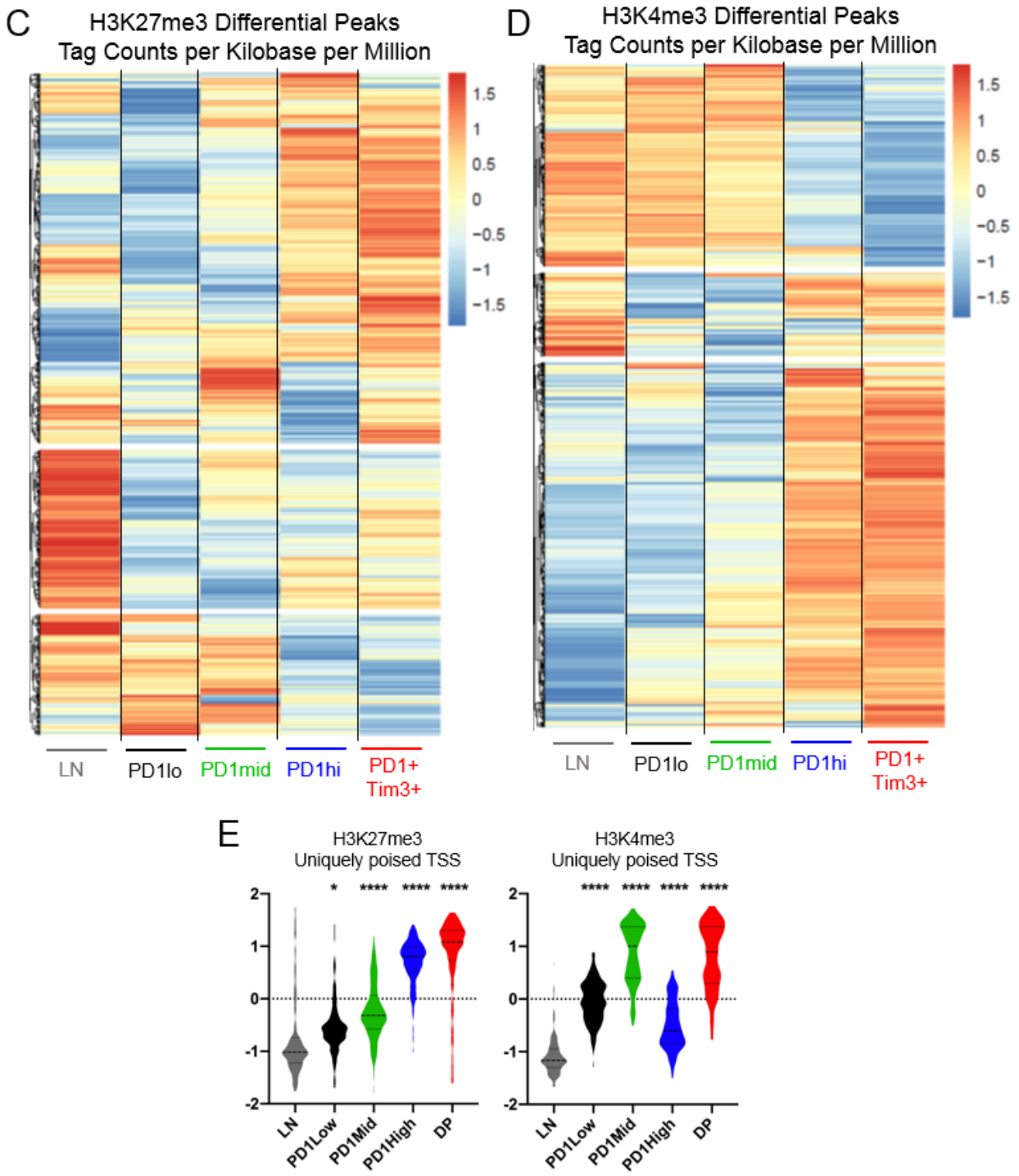

Figure 26. Exhausted T cells have altered T cell epigenetics, resulting in increased poised gene promoters on terminally-exhausted T cells

LN and TIL sorted based on PD1 vs Tim3 expression, epigenetic marks quantified via CUT&RUN assay, and populations quantified for reproducible and differential expression of indicated histone modification.

(A) H3K9ac, (B) H3K27ac, (C) H3K27me3, and (D) H3K4me3. Heat map shown as tag count per million base pairs. (E) Graph showing violin plots from list of genes first screened from PD1+Tim3+ terminally exhausted TIL population (called DP) that had H3K27me3 and H3K4me3 at the transcription start site (TSS). The violin plot shows unique gene subsets scaled to heat map row organized in the same order for both H3K27me3 and K3K4me3 (i.e. not the heatmaps in C & D).

5.5.5 Exhausted T cell dysfunction is due to mitochondrial ROS, which cause inappropriate carbon storage as lipids

Our previous work has shown terminally exhausted T cells have low oxygen consumption and altered mitochondrial morphology, but not an absence of mitochondria[89]. We wanted to investigate whether dysfunctional mitochondria in exhausted T cells are actively producing metabolic byproducts that are detrimentally contributing to overall TIL dysfunction. To explore this question, assessed whether exhausted T cells had different mitoROS production. Others have shown exhausted T cells can produce ROS[201–203] and, in agreement with the literature, we found terminally exhausted T cells produce more mitochondrial ROS (Figure 27A). We made similar findings in our *in vitro* T cell exhaustion assay, where T cells that experience chronic T cell activation under hypoxia had the highest mitochondrial ROS (Figure 27B). We also found that the increase in mitochondrial ROS may be due to a decrease in oxidative stress genes expressed in terminally exhausted TIL, preventing the cells from handling the excessive ROS produced during chronic T cell activation in hypoxia (Figure 27C). To explore how excessive ROS can directly affect T cells, we developed an *in vitro* assay to increase mitochondrial ROS in T cells. By treating T cells with low-dose

mitochondrial complex III inhibitor for 5 days, we see an increase in mitochondrial ROS (Figure 27D). This increase in ROS is absent when T cells are co-cultured in low-dose Antimycin A with mitochondrial complex I inhibitor Rotenone (Figure 27D). Strikingly, culturing T cells in Antimycin A increased expression of PD1 and Tim3, led to increased BODIPY neutral lipid staining and acetyl lysine content, and caused an increase in granularity, all similar to terminally exhausted T cells (Figure 27E, 27F). This phenotype was mitigated with the addition of an additional inhibitor (Rotenone). Taken together, this implicates mitochondrial ROS as the driver of the exhaustion phenotype, causing increases in co-inhibitory marker expression and causing T cells to store their carbons as lipids rather than utilize them as fuel.

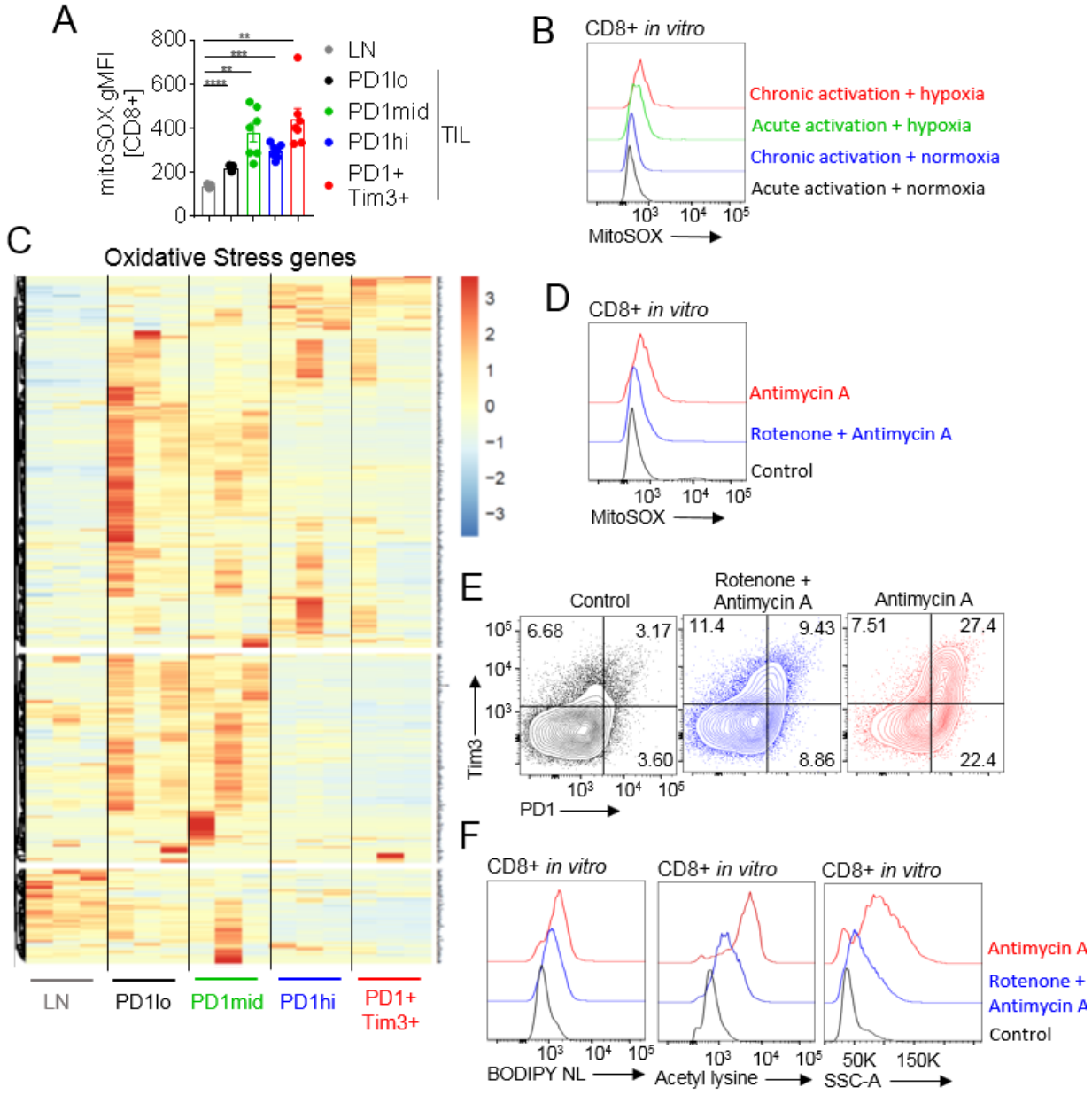

Figure 27. Exhausted T cell dysfunction is due to mitochondrial reactive oxygen species (ROS), which cause inappropriate carbon storage as lipids

(A) LN and TIL based on PD1 vs Tim3 expression, quantification of mitoSOX geometric mean fluorescent intensity. (B) Overlaid histograms of *in vitro* T cell exhaustion assay, showing mitoSOX staining. (C) LN and TIL sorted based on PD1 vs Tim3 expression, mRNA sequenced, then gene expression showed based on Gene Ontology term response to oxidative stress (GO:0006979). (D) Overlaid histograms of

CD8+ T cells cultured in nothing (control), 0.02μM Antimycin A, or 0.02μM Rotenone + 0.02μM Antimycin A for 5 days, showing mitoSOX staining. (E) As in D, showing representative flow cytograms of PD1 vs Tim3 expression. (F) As in D, showing histogram overlays of BODIPY NL staining, Acetylated lysine expression, and side scatter area (SSC-A).

5.5.6 Excessive reactive oxygen species increases DNA damage in exhausted T cells

To further explore the negative effects of mitochondrial ROS on T cells, we wanted to determine if terminally exhausted TIL also experience more DNA damage. DNA damage is most often quantified by an increase in γH2AX, a phosphorylation on histone H2AX that promotes recruitment of DNA damage repair machinery to the site of a double-stranded DNA break[204]. The link between ROS and DNA damage has been well established in other settings, including cancer, Parkinson's disease, Alzheimer's disease, diabetes, multiple sclerosis, rheumatoid arthritis, and systemic lupus erythematosus[205]. Increased DNA damage in TIL has also been observed by other groups[203,206]. In agreement with these findings, we see increased γH2AX staining by flow in TIL, specifically in terminally exhausted TIL (Figure 28A). We also see increases in γH2AX staining in our *in vitro* model of T cell exhaustion, where T cells that experience chronic T cell activation under hypoxia have the highest γH2AX staining, and T cells treated with low-dose Antimycin A to cause excessive mitochondrial ROS also have the highest γH2AX staining (Figure 28B, 28C). To look specifically at gene loci experiencing DNA damage rather than global DNA damage by γH2AX staining for flow, we utilized our new epigenetic profiling technique CUT&RUN with γH2AX. We

found that terminally exhausted TIL have more DNA damage at distinct gene loci than other LN and TIL populations (Figure 28D). Taken together, we see that terminally exhausted T cells experience DNA damage at specific gene loci, which may be due to chronic T cell activation under hypoxia causing excessive mitochondrial ROS.

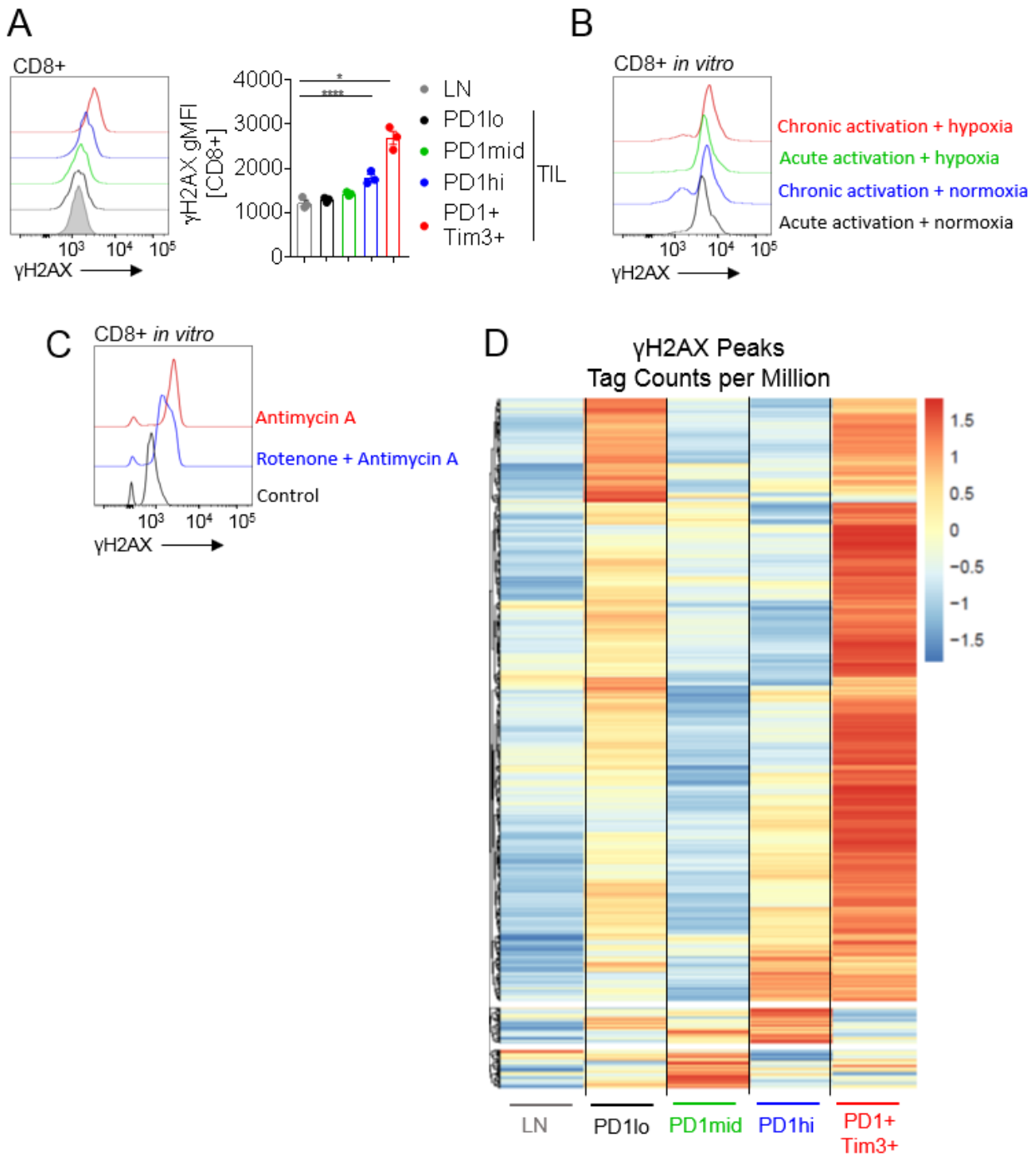

Figure 28. Excessive reactive oxygen species increases DNA damage in exhausted T cells

(A) (left) Overlaid histograms of LN and TIL based on PD1 vs Tim3 expression, showing γH2AX expression, (right) quantification of γH2AX geometric mean fluorescent intensity. (B) Overlaid histograms of *in vitro* T cell exhaustion assay, showing γH2AX expression. (C) Overlaid histograms of CD8+ T cells cultured in nothing (control), 0.02μM Antimycin A, or 0.02μM Rotenone + 0.02μM Antimycin A for 5 days,

showing γH2AX expression. (D) LN and TIL sorted based on PD1 vs Tim3 expression, γH2AX epigenetic mark quantified via CUT&RUN assay, and populations quantified for reproducible expression of γH2AX histone modification. Heat map shown as tag count per million base pairs.

5.5.7 Reprogramming TIL to utilize fatty acid oxidation improves TIL function

Finally, we wanted to explore the therapeutic potential of our findings in an *in vivo* model of cancer. Because fatty acid oxidation genes are decreased in terminally exhausted TIL (Figure 23C), we hypothesized that enforcing expression of a master regulator of the peroxisomal beta-oxidation pathway of fatty acids would improve TIL function. We chose to overexpress Peroxisome Proliferator Activated Receptor Gamma (PPARγ) in gp100-specific pmel T cells via retroviral transduction, and adoptively transfer the T cells into mice with gp100-expressing B16 mouse melanoma (Figure 29A). Seven days post-transfer, we sacrificed the tumor-bearing animals and analyzed the transferred cells. We found the transferred cells were less exhausted by TOX expression when compared to empty vector-transduced control cells (Figure 29B), and were more functional by cytokine expression (Figure 29C, 29D).

To address the effects of increasing fatty acid oxidation in TIL, we utilized adoptive cell therapy (B16 melanoma with gp100-specfic pmel T cells) as a model of immunotherapy. We first transferred pmel T cells into tumor-bearing mice treated with the PPARγ agonist Rosiglitazone (RSG) injected every other day IP, and found that pmel T cells + RSG improved mouse survival (Figure 29E). We then utilized an immunotherapy-sensitive model of cancer (MC38 adenocarcinoma) with PD1

checkpoint blockade and found three doses of RSG before the start of immunotherapy was sufficient to improve response to immunotherapy and increase survival (Figure 29F). Taken together, we found that increasing fatty acid oxidation either genetically or pharmacologically improves T cell function and, when combined with immunotherapy, improves therapeutic outcomes.

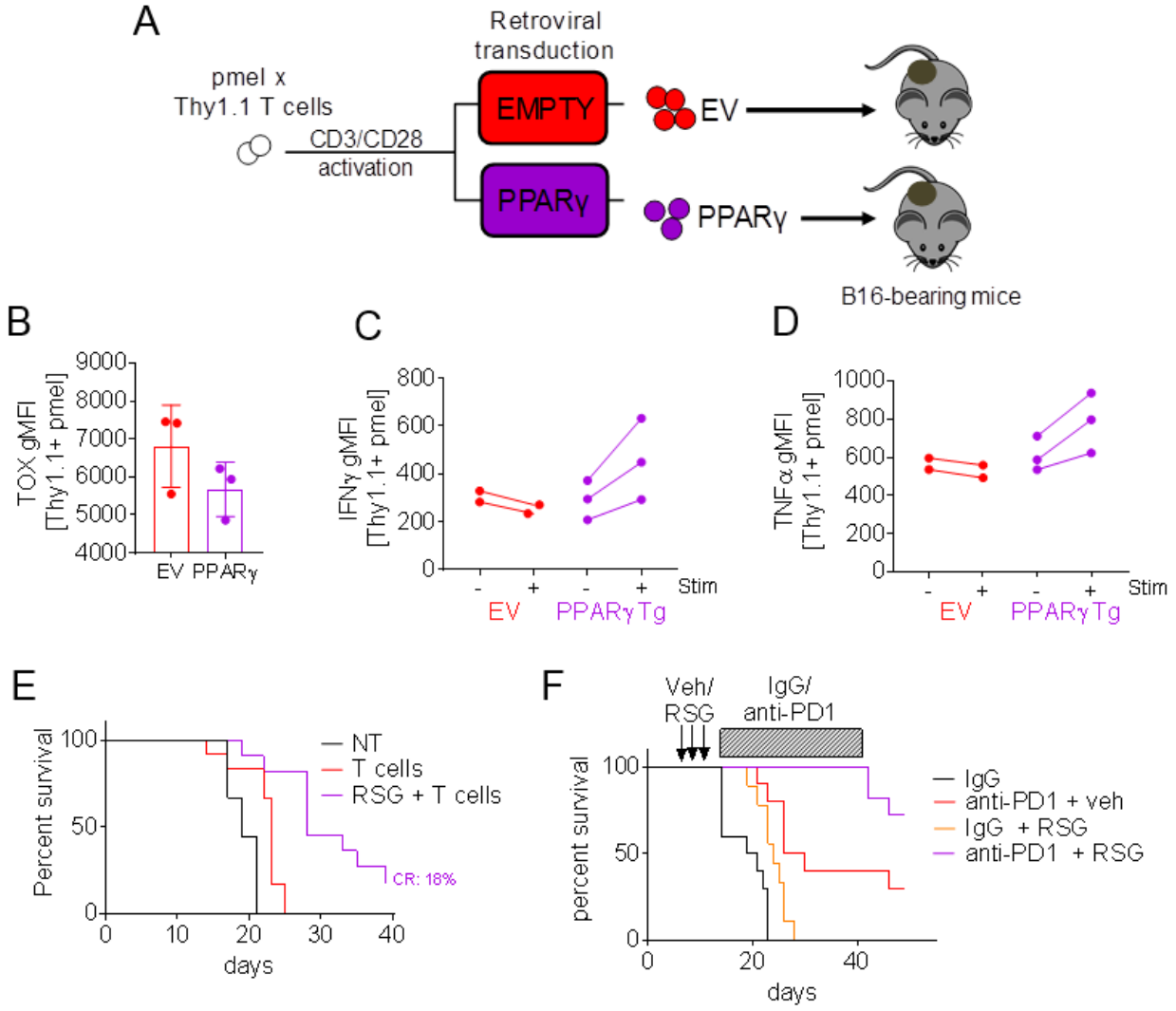

Figure 29. Reprogramming TIL to utilize fatty acid oxidation improves TIL function

(A) Visual schematic of T cell transduction and adoptive T cell transfer experiment. (B) Quantification of TOX geometric mean fluorescent intensity from empty vector (EV) and PPARγ-overexpressing pmel T cells after 7 days in B16 melanoma tumors. (C) Quantification of IFNγ geometric mean fluorescent intensity from empty vector (EV) and PPARγ-overexpressing pmel T cells cultured O/N in the presence or absence of their cognate peptide (gp100), with golgiplug include in the last 5 hours. (D) As in C, but Quantification of TNFα geometric mean fluorescent intensity. (E) Mice were given B16 melanoma d0, treated with PBS and Rosiglitazone (RSG) by IP for 3 days before adoptive T cell transfer of activated pmel T cells via IV injection on d5. Rosiglitazone was given every 2 days for the duration of the

experiment, and survival was quantified. (F) Mice were given MC38 adenocarcinoma on d0, treated with PBS or RSG by IP for 3 days before starting anti-PD1 therapy on d5. Anti-PD1 or isotype control was administered IP every 4 days and survival was quantified.

5.6 DISCUSSION

We found that terminally exhausted CD8+ T cells in the TME store carbons as lipids rather than burn them. This storage of lipids in terminally exhausted T cells is driven in the TME by chronic T cell activation in the presence of hypoxia, as we were able to recapitulate this phenotype *in vitro* with those two TME conditions. The role of lipids in T cell metabolism has been explored in the context of T cell memory, where it has been characterized that memory T cells upregulate both mitochondrial biogenesis and fatty acid oxidation pathways. Indeed, breakdown of lipids via lysosomal degradation is required for their function[188,207]. The inability of exhausted T cell to metabolize lipids therefore may be a major reason why in the setting of cancer and chronic viral infection we see exhausted T cells rather than memory. The lipid content of immune cells in the context of cancer has been explored in NK cells, where Michelet *et. al* has shown adipocyte-associated NK cells to be less functional in obesity and obesity plus cancer, but attributed the NK dysfunction to obesity[208]. In chronic viral infection, Bettonville *et. al* have shown that exhausted CD4+ T cells also had increased lipid content, but they did not target lipids in the context of therapy[209].

Acetyl lysine staining was also used to show an increase in excessive carbon storage, but the implications of this have yet to be fully explored. Acetyl lysine is well

characterized as a histone modification, but in recent years researchers have been exploring acetylation as a post-translational modification that may alter the function of proteins[210]. Acetyltransferases can add acetyl groups to proteins to change gene transcription by modifying transcription factor activity, cell cycle genes, DNA damage repair, enzymatic cell signaling, cytoskeletal organization, protein folding and aggregation, RNA processing, and autophagy. Depending on the protein and where the acetylation is added, acetylation can inhibit or enhance catalytic activity, promote protein degradation, change protein-protein interactions, or even subcellular protein localization. There are many avenues to explore how increased acetylation may be impacting exhausted T cell function, and it will be the subject of future work to explore the consequences of excessive acetylation in exhausted T cells.

To better understand the signaling events that drive T cell exhaustion, we have shown that Blimp1 is most highly increased in our *in vitro* model of chronic T cell activation under hypoxia, and Blimp1 can repress PGC1α. Blimp expression has been previously shown in exhausted T cells[197,198], but here we show a link to metabolism through its ability to suppress PGC1α. More studies are needed to understand if Blimp1 is directly repressing PGC1α: although we have previously shown Akt inhibition can partially rescue PGC1α[89], the signaling network between Blimp1, Akt, and PGC1α needs to be elucidated. This will be the study of future work.

Repression of PGC1α expression can lead to widespread changes in gene expression, which helps explain why a decrease in mitochondria in exhausted T cells could still affect fatty acid oxidation (an enzymatic process that occurs in the cytosol of cells). PGC1α is not only the master regulator of mitochondrial biogenesis, but it initiates

gene programs responsible for mitochondrial fusion, expression of antioxidant genes, and oxidative metabolism in general[163]. The link between mitochondrial dysfunction and loss of fatty acid oxidation has already been established in the context of inflammation with dextran sulfate sodium (DSS)-induced colitis, where Baixauli *et. al* found knockout of transcription factor A, mitochondrial (TFAM) in T cells led to a decrease in mitochondrial mass and function and dysfunction of lysosomes[59]. Lysosomes are an integral component of fatty acid oxidation, as they are the subcellular location where lipids are broken down[211]. In our TIL exhausted T cells, we see some evidence for decreases in the number of lysosomes, in our RNAseq data as well as in the EM images, where the TIL PD1mid population has large lysosomes throughout the cell, while the PD1+Tim3+ terminally exhausted cells have almost no lysosomes and accumulate lipid droplets instead (Figure 23G). Future work will explore this lysosomal phenotype in exhausted T cells, and whether increasing the lysosomal gene program via overexpression of lysosomal biogenesis transcription TFEB can improve TIL function.

Looking to the epigenetics of exhausted T cells, we are still elucidating the full phenotype and its implications in ongoing work, but we have found that exhausted TIL have increased poised transcriptional start sites (*i.e*. a combination of H3K4me3 and H3K27me3 histone modifications). It will be the subject of future work to understand if genes that are poised for expression in exhausted TIL only need the right combination of therapy to allow for gene expression. We hypothesize that to convert poised genes to expressed genes, we will need not only checkpoint blockade but additional therapy, as the Wherry lab has already shown PD1 checkpoint blockade does not change the

epigenome in exhausted T cells during chronic viral infection[177]. As H3K27me3 methylation needs to be removed to convert a poised gene to one available for transcription initiation, and demethylation requires oxygen for both ten-eleven translocation (TET) and Jumonji C (JmjC) family demethylases to work, future studies will determine if the combination of decreasing tumor hypoxia plus immunotherapy can change the epigenome of exhausted T cells[212]. We also know that there are not dramatic global changes to chromatin histone acetylation, even though there is more lipid accumulation and cellular acetyl lysine in terminally exhausted T cells. As extra-mitochondrial pools of acetyl CoA feed into lipid synthesis and histone acetylation, further work is needed to better understand the destination of acetyl CoA in exhausted T cells. Mitochondrial enzymes in the nucleus are responsible for metabolites for epigenetic modifications, so there is evidence for distinct acetyl CoA pools within cells[213].

Our data suggest that ROS alone can cause the T cell exhaustion phenotype, shown by culturing T cells in low dose antimycin A, and this ROS can lead to inappropriate carbon storage as lipids. It was previously shown that ROS can inhibit tyrosine phosphatase activity, which could lead to increased tonic T cell signaling[214]. ROS also can lead to increases in NFAT, which without its binding partner AP1, is well known to drive an exhaustion gene program[215,216]. Alternatively, the TCA cycle enzyme aconitase is exquisitely sensitive to ROS-mediated inhibition[217]. Inhibition of aconitase could be preventing the TCA cycle from moving forward to break down carbons for ATP, allowing TCA cycle intermediate acetyl CoA to leave the mitochondria and be used to build lipids. ROS can also oxidize lipids, which could change how lipids are structured,

the makeup of cell membranes, or the overall charge of the cell. Oxidized lipids can also modify DNA bases, which would have many deleterious side effects for overall basic biological functions in exhausted T cells[218,219]. For cancer immunotherapy, it will be important to target ROS in T cell directly, as exogenous antioxidants in mouse models of cancer have actually increased tumor burden, so whole-body antioxidant therapy is not a viable treatment strategy[220,221].

Both *in vitro* and *in vivo* exhausted T cells show evidence of DNA damage, and our CUT&RUN sequencing of exhausted TIL shows evidence that exhausted TIL have increased DNA damage in a specific subset of genes. Further analysis will be needed to understand the implications of these findings, as the DNA damage identified by γH2AX CUT&RUN is found in regions of the genome that have mRNA transcripts in exhausted TIL, according to RNAseq. We have also found that the DNA damage can be characterized as small, discrete peaks rather than 10KB+ fragments found in 'true', or well-characterized DNA damage induced by known damaging agents such as ionizing raditation[222]. This leads us to ask, what does γH2AX mean in exhausted T cells? Is exhausted T cell γH2AX revealing DNA damage or something more nuanced, such as transcriptional stress in the TME? And as our cells sorted *ex vivo* for CUT&RUN are a polyclonal population, it will be important to perform single-cell epigenetics and transcriptomics to determine if an individual exhausted T cell with γH2AX is actually not producing a mRNA transcript, but such technology does not exist (yet).

Targeting lipid accumulation directly via genetically overexpressing PPARγ in antigen-specific T cells made for less exhausted T cells that were more functional. This was also seen pharmacologically with the PPARγ-agonist rosiglitazone, in mice treated

either with rosiglitazone alone or in combination with checkpoint blockade. It is unclear from the data whether we actually improved function of terminally exhausted T cells, or simply gave TIL a better start upon entering the TME. It is still not well understood, but it is believed that different PPAR family members can be more beneficial when building lipids (PPARγ) versus burning lipids (PPARα and PPARδ)[223–225], future work will need to dive deeper into characterization of PPAR family members to determine if different ones would better serve exhausted TIL therapy.

Can we only prevent T cell exhaustion, or can we actually rescue terminally exhausted T cells? If we target exhausted T cells via metabolism, allowing them to utilize their stored lipids, would that not only help them function better, but change their epigenetic state and convert them into memory T cells? This answer could have a great impact in the field of TIL immunotherapy, as it could help us better understand when T cells we need to target for checkpoint blockade immunotherapy. It could also reveal how to improve exhausted TIL for adoptive T cell immunotherapy, how to prevent exhaustion in designer T cell therapies (such as Chimeric Antigen Receptor T cells), and allow patients to better retain memory T cells specific to their cancer, giving them lifelong protection from reoccurrence.

6.0 SUMMARY & FUTURE DIRECTIONS

This work taken together describes some of the immunometabolic requirements of T cell activation and exhaustion, revealing many important aspects of T cell biology through the dysfunction caused by cancer. While by no means a complete view on the subject, it describes fundamental aspects of the inextricably intertwined relationship between T cell function and metabolism, how inappropriate cues from the T cell's environment can change this mechanism, and how by better understanding the link between cell function and metabolism we can design better therapies, not only for cancer, but other diseases characterized by T cell metabolic dysfunction. This last chapter provides a summation of the work and highlights future studies still needed.

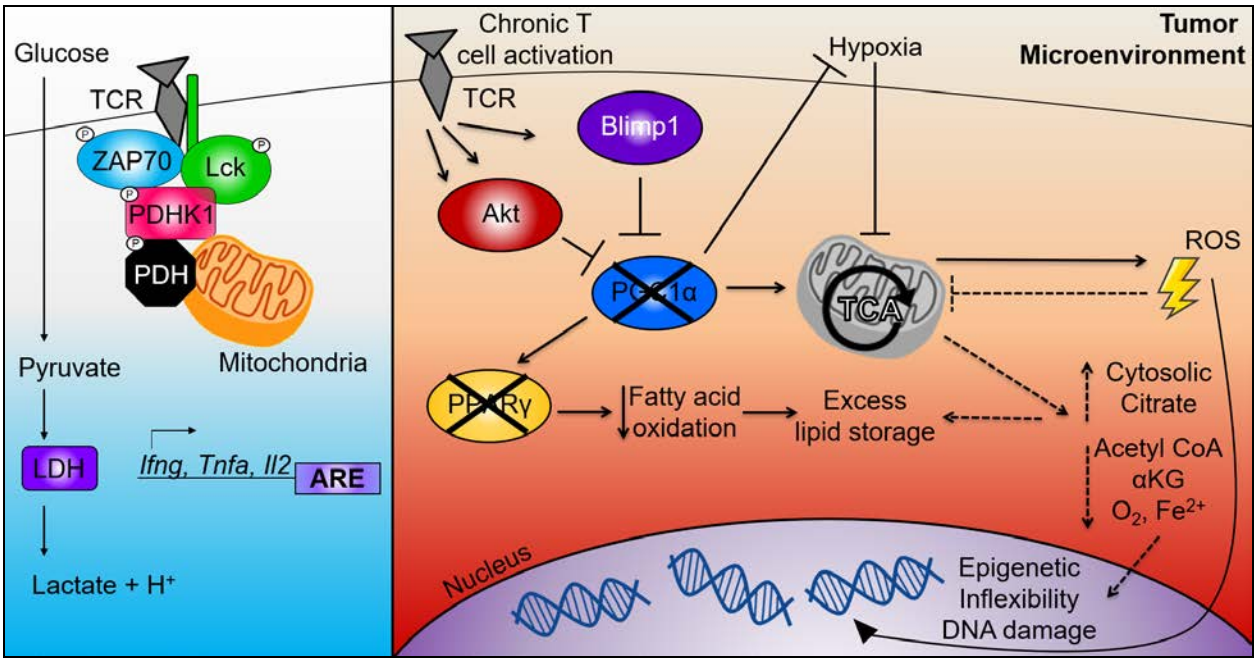

Figure 30. Model for the immunometabolic requirements of T cell activation and exhaustion

Figure includes data in thesis summarized into one model diagram. On the left, T cells receive acute activation, causing PDHK1 to initiate aerobic glycolysis. Glycolytic enzyme LDH then releases cytokine mRNA from regulation, allowing it to be translated. On the right, T cells receive chronic T cell activation under hypoxia, causing an increase in Akt and Blimp1-mediated repression of PGC1α. This prevents mitochondrial biogenesis, preventing T cells from handling the negative effects of mitochondrial ROS, including DNA damage. Loss of PGC1α also leads to the loss of PPARγ, which decreases fatty acid oxidation and leads to increased lipid storage. Dotted lines indicated hypothesized effects, whereby dysfunctional mitochondrial could cause a buildup of cytosolic citrate, which could contribute to the buildup of lipids. Increases in lipids could mean a decrease in epigenetic intermediates, which could negatively impact epigenetic flexibility.

When a T cell initially becomes activated, it immediately (>5 minutes) switches to prioritizing glycolysis. We see this immediate switch into utilizing exogenous glucose as a source of fuel not only leads to quicker ATP generation via glycolysis, but it also releases mRNA from regulation, as glycolytic enzymes moonlight as RNA binding

molecules when not processing carbons from glucose. This allows protein synthesis to occur minutes after activation, which allows cytokine mRNA to be released from regulation and immediately synthesized and for T cells to rapidly produce effector molecules. We found that the IL2, TNFα, and IFNγ cytokine mRNA held in check by glycolytic enzyme LDH has an AU-rich element (ARE) in the 3′ UTR, while granzyme B mRNA does not have an ARE, and therefore was not regulated by LDH. It will be important in future work to determine what other mRNA is regulated by LDH or other glycolytic enzymes. Is it only cytokine mRNA? Are different mRNAs restrained depending on the T cell type or differentiation state? Do other immune cells, especially those capable of targeted cytokine secretion, also do this? And why is only cytokine mRNA held in metabolic regulation, but cytotoxic mRNA (Granzyme B) not regulated by glycolysis? Is cytotoxic mRNA regulated by a different metabolic process at different point in synthesis?

We also found that the immediate switch to glycolysis upon activation not only led to immediate effector function, but that this switch was occurring only at the T cell synapse and not throughout the cell. Presumably in a normal biological setting, this helps direct effector function at the target cell presenting MHCI+peptide, and limits bystander killing. Many interesting biological processes related to this event are still unexplored, and will be the subject of future work. For example, what role does the byproduct of glycolysis, *i.e.* lactic acid, play at the synapse? Is it simply a waste product? Or does the low pH or lactic acid molecule itself play a role in mediating effector function? Perhaps the lactic acid lowers the pH between the T cell and target cell, helping to prevent cytotoxic granules from killing the T cell on its way to killing the

target cell? And finally, how does our understanding of glycolysis, lactic acid, and low pH inform our knowledge of T cell killing in the TME, where the pH is already lower than normal tissue? Does this low pH prevent T cells from effectively killing tumor cells, allowing them to be protected from T cell cytotoxicity?

We and others have shown that chronic T cell activation leads to dysfunction. In the setting of cancer, the TME plays and additional role in mediating this dysfunction through soluble and ligand-receptor mediated inhibitory signals from both suppressive immune cells and cancer cells, and from the decrease in essential environmental metabolites needed to fuel function. How all of these signals and factors contribute to CD8+ T cell dysfunction is still incompletely known, but is an actively studied area in the field. One major problem is that it is difficult to dissect the role of each inhibitory factor in dysfunction, as not everyone agrees on what the essential drivers of T cell dysfunction in the TME are. One technique that may help elucidate the impact of the TME on T cell exhaustion is the *in vitro* T cell exhaustion assay described in chapter five. Choosing immunologic and metabolic TME factors to drive T cell exhaustion, we have found that chronic T cell activation and hypoxia are both required to generate an exhausted T cell. This assay is a starting point to dissect exhausted T cell biology, but the phenotype of these cells is not a 1:1 copy of exhausted T cells from the tumor. Future work will improve upon the *in vitro* T cell exhaustion assay to determine what other factors are needed to get *in vitro* exhausted T cells that are phenotypically and functionally as similar to *ex vivo* exhausted TIL as possible. This will include testing addition of specific TME factors, like PDL1 or TGFβ, but will also include an RNAseq comparison between *ex vivo* terminally exhausted TIL and *in vitro* generated exhausted T cells. Genes that

are similar between the two groups will help us determine which genes are changed due to chronic T cell activation in hypoxia, but the genes that are different between TIL and *in vitro* will help us determine the assay's missing components.

The importance of oxygen (in all its forms) in T cell biology and function are a common theme throughout this thesis. We see lack of intercellular oxygen consumption in exhausted T cells, as characterized by the loss of mitochondrial mass and function in exhausted TIL *ex vivo*. The loss of mitochondria in exhausted T cells to due to repression of mitochondrial biogenesis, mediated by PGC1α. Interestingly, the remaining dysfunctional mitochondria are still utilizing oxygen, but are paradoxically making ROS. This is an interesting phenomenon, as exhausted T cells are already in a hypoxic environment, and it seems that the little oxygen available is utilized "incorrectly". We hypothesize that this increase in ROS in exhausted T cells is due to two biological problems. One, that the electron transport chain (the mitochondrial component that utilizes oxygen to make ATP) can actually run in reverse in hypoxia, which is known to generate ROS[226], and two, that because both chronic T cell activation and hypoxia are needed to generate the highest amount of ROS, chronic T cell activation is driving a gene program that is unable to handle the reverse flow of the ETC and excessive ROS. We already know from our RNAseq data that terminally exhausted TIL have decreased expression of a large number of antioxidant genes. We also know, in addition to PGC1α being responsible for mitochondrial biogenesis, that it is responsible for turning on antioxidant genes as well. Additionally, from our *in vitro* exhaustion assay, when cells are cultured in antimycin A alone, we can directly generate ROS and cause T cell exhaustion, but antimycin A plus rotenone together does not. These data together seem

to highlight the importance of intercellular antioxidants and the severe negative effect of long-term exposure to ROS. It is still unclear if it is best to prevent T cells from receiving chronic ROS exposure, or if we can take a terminally exhausted T cell and then decrease ROS to improve the T cell's functionality. Future work will explore the timing of ROS exposure and therapy in exhausted T cells. It will also be important to think about limiting ROS exposure in our designer T cell therapies, such as Chimeric Antigen Receptor (CAR) T cells.

We have also shown that targeting the lack of extracellular oxygen in the TME by using the complex I inhibitor metformin is also another method of improving TIL functionality *in vivo*. Metformin treatment decreased tumor hypoxia, but only with the combination of checkpoint blockade were we able to see a decrease (or even clearance) of tumor burden. Based on these preclinical models, we have initiated a clinical trial in collaboration with Dr. Yana Najjar (ClinicalTrials.gov Identifier NCT03311308) in which patients with melanoma receive Pembrolizumab and metformin. We have also been exploring how TME metabolism impacts T cells, focusing on how different tumors from different patients have heterogeneous tumor metabolic profiles, which can greatly impact T cell functionality and their response to immunotherapy[227]. Going forward, it will be important to do careful translational studies, as both tumor heterogeneity and other factors our mice do not model (such as age or obesity) could impact TME hypoxia and TIL functionality.

Lack of oxygen can also impact exhausted T cell epigenetics. Oxygen is required for TET dioxygenases and JmjC family demethylases to function, therefore the hypoxic TME may be either keeping chromatin repressed, actively converting open chromatin to

repressed chromatin, or keeping otherwise expressed genes in a poised state. Future work will explore how reducing tumor hypoxia could help change TIL epigenetics. It is currently unclear if we can simply prevent TIL from repressing chromatin by oxygenating the TME, or if we can rescue the terminally exhausted TIL epigenetic profile. We hypothesize that reducing hypoxia alone would not be enough to change TIL epigenetics, as the TME still has a variety of other suppressive factors, but could potentially work in tandem with checkpoint blockade. The future work exploring exhausted T cell epigenetics will also need to include a better understanding of how environmental factors, especially TME metabolites and soluble/ligand signals impact T cell differentiation and epigenetics, and how depending on T cell type (e.g. effector T cell vs Treg), the environmental factors may be interpreted differently by the T cells to impact differentiation and epigenetics.

Finally, we have explored how T cell metabolism can impact cell biology, leading us to explore the dramatic cell biological differences in exhausted T cells. Exhausted T cells accumulate lipids and acetylated lysine, as well as becoming larger and more granular. How all these biological changes impact T cell function will be the subject of extensive future study. Lipids, especially oxidized lipids caused by excess ROS, can be toxic to cells, and acetylated lysine has extensive effects on a variety of enzymatic functions. We also still do not understand how T cell exhaustion impacts basic biological functions, e.g. does the lack of mitochondria in exhausted T cells mean the building blocks for new organelles are not available? Does decreased function occur for essential organelles like endoplasmic reticulum or the Golgi apparatus, further negatively impacting exhausted TIL function? By RNAseq and electron microscopy, we

also see a decrease in lysosomes, which may explain why lipids accumulate in exhausted T cells, as lysosomes are essential for lipid catabolism. But what about other catabolic processes, e.g. the ability for exhausted T cells to catabolize themselves? Autophagy has been studied in T cells in various disease contexts, but not in exhausted T cells. Do exhausted T cells have the ability to break down and recycle cellular components? Understanding these basic biology questions would help us both better understand exhausted T cell dysfunction and to design therapeutic strategies to improve their function.

Many of the data discussed in this thesis have direct therapeutic implications, some of which are already being translated by industry collaborations. For example, we are including PGC1α in human CAR T cells, in collaboration with Bluebird Bio. Metabolically programming CAR T cells is an active area of exploration in the field of immunotherapy, stemming from the discovery that different CAR signaling domains led not only to different CAR T cell metabolism, but different T cell phenotypes and patient outcomes[228–230]. CAR T cells that include the 4-1BB signaling domain have a more oxidative phenotype, are more memory-like, and persist longer in patients than CAR T cells that only include the CD28 signaling domain. These findings are in agreement with our data, elucidating the signaling pathway of 4-1BB[231]. By using anti-4-1BB antibodies in conjunction with anti-PD1 in mouse melanoma, we found 4-1BB increases mitochondrial mass and fusion by signaling through PGC1α, allowing for increased TIL functionality and survival by generating T cells that are more memory-like. Designing CAR T cells with PGC1α as part of the construct has the ability to further improve CAR T cell persistence, and ideally make CAR T cells more metabolically fit and functional in

solid tumors, rather than only functional in hematologic malignancies as they are at present[232].

As a whole, it will be important for the field of immunometabolism to transition from describing a type of metabolism in a specific cell to understanding what that specific cell metabolism means for cell function. The early days of immunometabolism have described how a type of metabolism is inherent to a type of cell (or at least a differentiation state): glycolysis is for effector T cells, oxidative phosphorylation is for memory T cells, etc. But we have come to appreciate this is too simplistic an approach. It would better benefit our understanding to reframe the discussion, to think about how a specific type of metabolism drives functional outcome. A highly glycolytic T cell can be an effector T cell because it is using a 100x faster way to generate ATP than oxidative phosphorylation, it generates byproducts for building blocks for daughter cells and for massive epigenetic remodeling, and is holding cytokine mRNA in regulation, so it *can* be an effector T cell as a result. A highly oxidative T cell can be a memory T cell because it has the necessary machinery in place (mitochondria) to respond to its cognate antigen when it encounters it in the future. Metabolism drives function; function does not choose metabolism.

The field of cancer immunometabolism has made exciting progress, but still has far to go to understand how metabolism and environment can drive specific T cell function and what environmental signals can not only change the metabolism utilized by T cells, but how metabolism changes the T cells' capacity to function. Only by knowing these fundamental details can we improve existing immunotherapy with more rational combinations and make designer T cells that can take wrong fuel/wrong environmental

signals/wrong metabolic cues and give the correct functional readout, decrease tumor burden, and improve survival in cancer.

APPENDIX A

SUPPLEMENTAL DATA

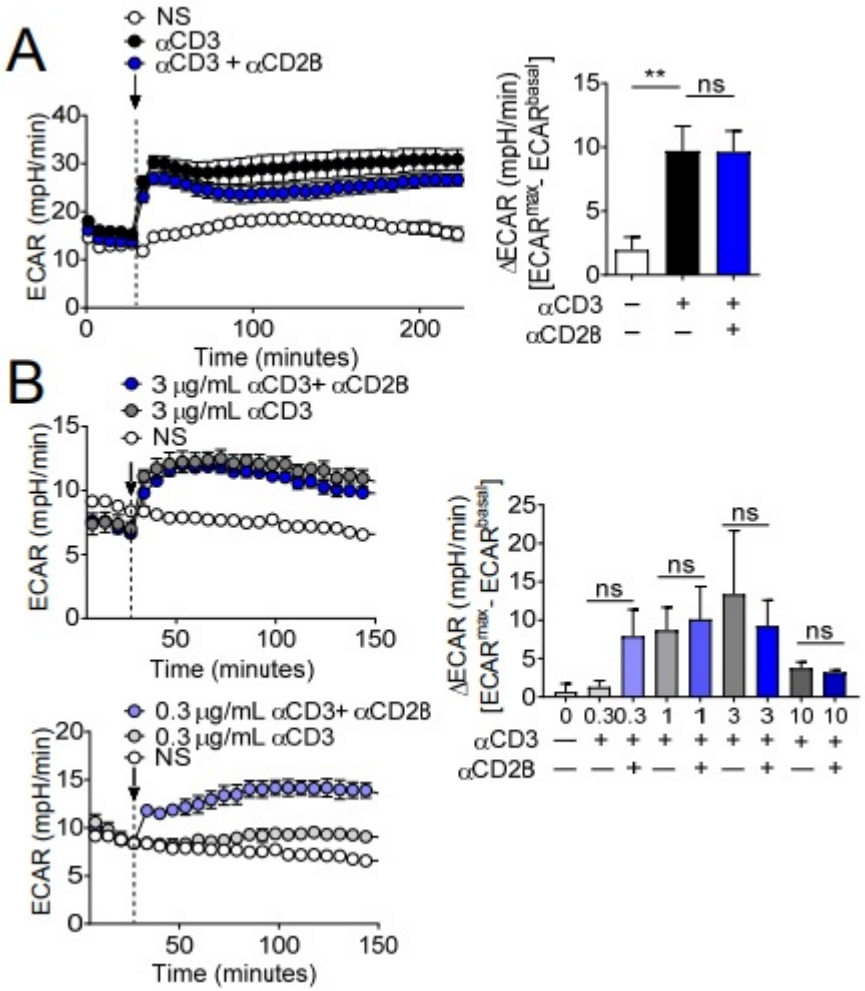

Figure 31. CD28 is not required for TCR-mediated rapid glycolysis in naïve nor previously activated CD8+ T cells

A, (Left) ECAR trace of naïve, CD8+ T cells stimulated with streptavidin or streptavidin crosslinked- αCD3 at 3 μg/ml in the presence or absence of 2 μg/ml αCD28, (right) tabulated results from multiple experiments. B, (Right) tabulated ECAR of naïve, CD8+ T cells stimulated with indicated amounts of streptavidin-crosslinked αCD3 in the presence or absence of αCD28, (left, top) trace ECAR of optimal TCR activation, (left, bottom) trace ECAR of suboptimal activation. Results represent the mean of five (A)

or three (B) independent experiments. ** $p < 0.01$ ns, not significant by unpaired t-test. Error bars represent SEM.

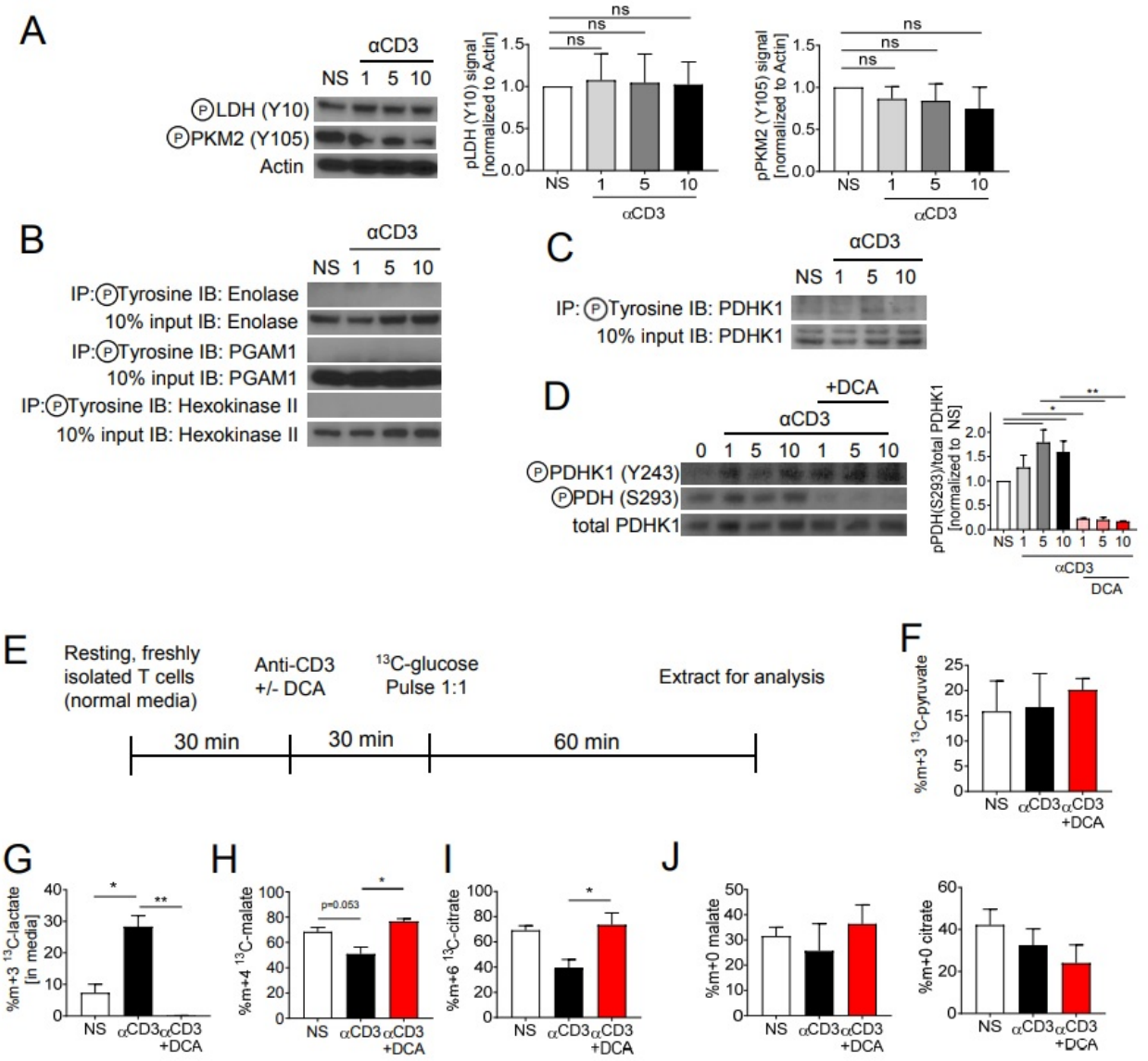

Figure 32. TCR signaling does not induce phosphorylation of glycolytic enzymes but rather reroutes glucose processing

A, (Left) representative immunoblot (IB) of indicated phospho or total proteins in lysates from previously activated, CD8+ T cells stimulated for the indicated periods with streptavidin-crosslinked αCD3 at 3 μg/ml, (right) tabulated densitometry scanning. B, IB of immunoprecipitations of phospho-tyrosine in lysates from PA-R CD8+ T cells stimulated as in A. C IB of immunoprecipitation of phospho-tyrosine in lysates from PA-R CD8+ T cells stimulated as in A. D, (Top) representative IB of indicated phospho or total proteins in lysates from PA-R CD8+ T cells stimulated as in A for the indicated periods in the presence or absence of

20 mM DCA, (bottom) tabulated densitometry scanning. E, Flow chart for 13C-glucose experiment. Freshly isolated CD8+ T cells were rested 30 min in Seahorse media containing glucose, stimulated with 3 ug/mL anti-CD3 for 30 minutes, and then pulsed with an equimolar concentration (10 mM) of 13C-uniformly labeled glucose. Metabolites were extracted 1 h after pulse. F, 13C labeled pyruvate from experiment described in E. G, 13C labeled lactate from experiment described in E. H, 13C labeled malate from experiment described in E. I, 13C labeled citrate from experiment described in E. J, Unlabeled (m+0) malate and citrate levels from E. Results represent three independent experiments. NS, not significant by unpaired t-test.

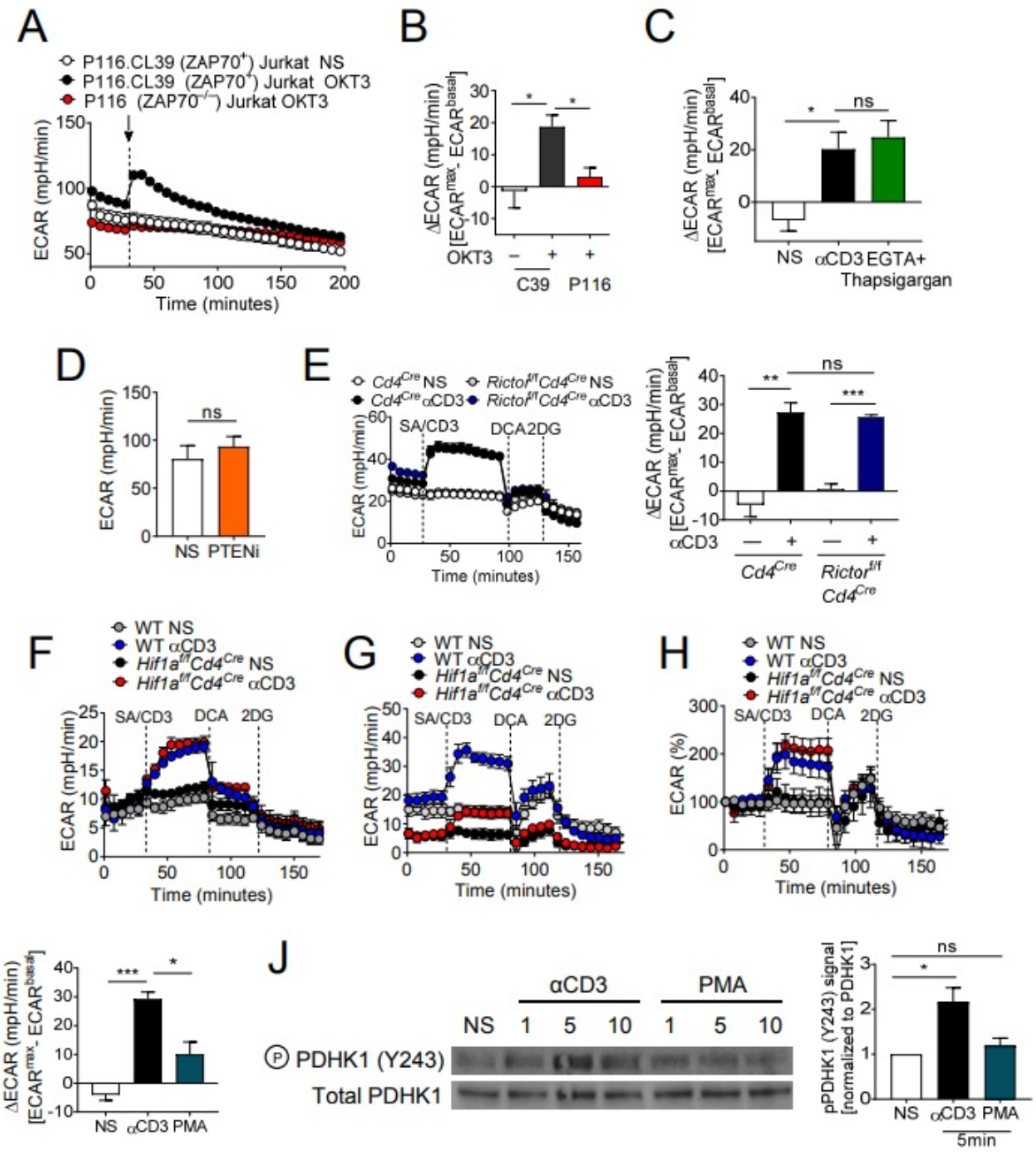

Figure 33. ZAP70 is required, but Akt, HIF1α, and calcium flux are dispensable for rapid activation-induced glycolysis

A, ECAR trace of ZAP70-deficient (P116) or ZAP70-reconstituted (P116.CL39) Jurkat T cells stimulated with OKT3 crosslinked with αIgG. B, Tabulated results from multiple experiments as in A. C, Tabulated ECAR from multiple experiments of PA-R CD8+ T cells stimulated with streptavidin-crosslinked αCD3 at 3 μg/ml in the presence or absence of 0.5 mM EGTA and 10 nM thapsigargan. D, Tabulated ECAR from

multiple experiments of PA-R CD8+ T cells in the presence or absence of 5 μM PTENi. E, Trace (left) and tabulated ECAR (right) of PA-R CD8+ T cells from Cd4Cre or Rictorf/f Cd4Cre mice stimulated with streptavidin cross-linked αCD3 at 3 μg/ml. F, Trace ECAR from naïve CD8+ T cells from Hif1af/f Cd4Cre or Hif1af/f stimulated with streptavidin-crosslinked αCD3 at 3 μg/ml. G, Trace ECAR from PA-R CD8+ T cells from Hif1af/f Cd4Cre or Hif1af/f stimulated as in F. H, Normalized ECAR from cells in G. I, Tabulated ECAR from multiple experiments of PA-R CD8+ T cells stimulated with streptavidin cross-linked αCD3 at 3 μg/ml or 33.3 ng/ml PMA. J, (Left) Immunoblot of indicated proteins in lysates of PA-R CD8+ T cells stimulated as in I for the indicated periods. (Right) tabulated densitometry results from multiple experiments. Results represent the mean of four (D, C, I) two (A, B, F, G, H) or three (E, J) experiments. * $p < 0.05$, ** $p < 0.01$, ***, $p < 0.001$, ns, not significant by unpaired t-test. Error bars represent SEM.

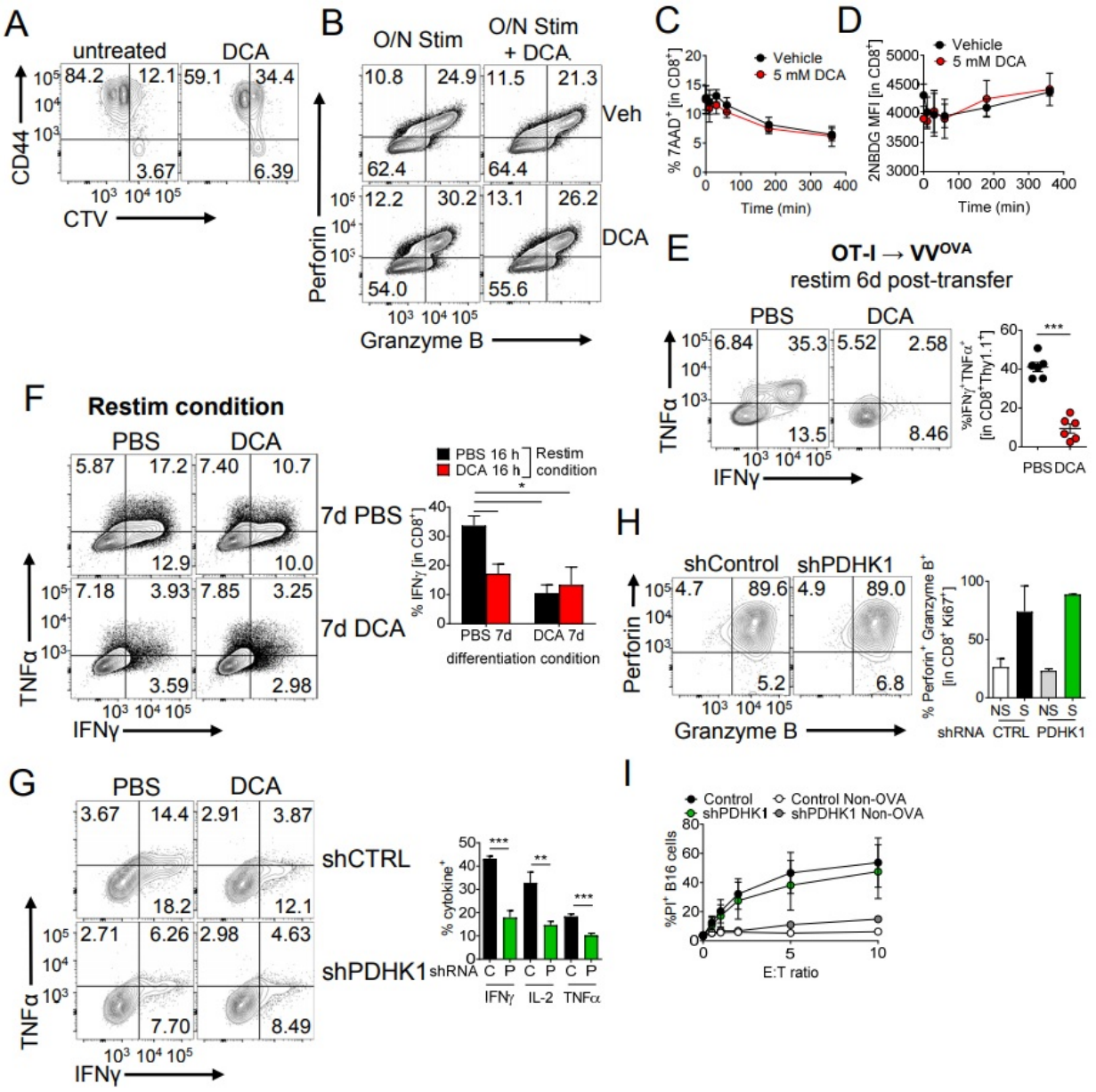

Figure 34. PDHK1-mediated rapid activation induced glycolysis influences cytokine production, but not cytotoxicity

A, Proliferation dye (CTV) labeled OT-I T cells cultured with cognate peptide in the presence of 5 mM DCA. B, Perforin and granzyme B production of PA-R T cells stimulated overnight as indicated. C, 7-AAD staining of PA-R T cells stimulated for the indicated times in the presence or absence of DCA. D, As in C, but cells were removed from stimulation and pulsed with 2NBDG.. E, Representative flow cytogram and tabulated data of Thy1.1+ OT-I T cells adoptively transferred into congenically mismatched mice infected with OVA-expressing Vaccinia virus (VVOVA) and restimulated with cognate peptide in the +/– 5 mM

DCA. F, Cytokine production of cells either differentiated in PBS or DCA-containing media (7d PBS or 7d DCA), then washed and restimulated +/– DCA. G, Cytokine production of CD8+ T cells retrovirally expressing scrambled control shRNA (shCTRL) or shRNA to Pdk1 (encoding PDHK1). H, Perforin and granzyme B staining of cells in G, I, In vitro cytotoxicity assay using PA-R OT-I T cells transduced as in G, cultured with OVA-expressing or parental B16 melanoma cells. Results represent the mean of three (A, C, D, E, G, H, I) experiments, or are representative of four (B, F) experiments. ** $p < 0.01$, *** $p < 0.001$ by unpaired t-test. Error bars represent SEM.

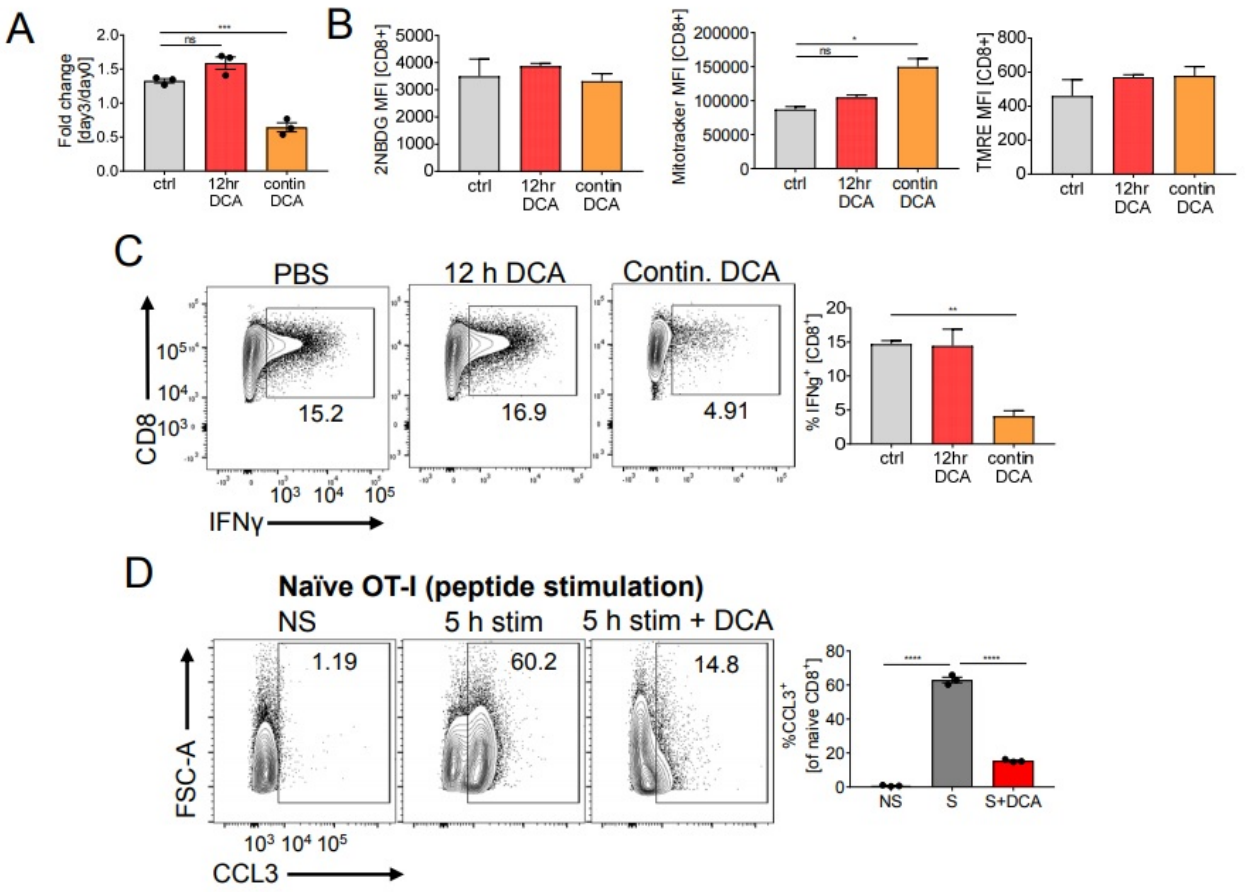

Figure 35. PDHK1-mediated rapid activation induced glycolysis influences early chemokine production in naïve CD8+ T cells

A, Tabulated fold change of naïve T cells sorted by CD8+, CD44lo, and CD62L+ expression and activated with plate-bound αCD3 at 3 μg/ml and 2 μg/ml soluble αCD28 in the presence of PBS or 20 mM DCA for 12 hours. After 12 hours, cells were removed from activation and were either cultured in the absence (ctrl, 12hr DCA groups) or presence of 20 mM DCA (continuous DCA group). Cell numbers were quantified after 3 days. B, As in A, but cells were stained with 2NBDglucose, MitoTracker FM, or TMRE. C, As in A, but cells were re-activated overnight with PMA + Ionomycin D, Representative flow cytogram of CCL3 staining from naïve OT1 T cells sorted as in A then co-cultured with antigen-presenting cells (T celldepleted splenocytes) at a 10:1 APC:naïve T cell ratio. T cells were activated with SIINFEKL peptide, protein transport inhibition, and in the presence or PBS or 50 mM DCA for 5hr. Results represent the mean of two (B, C) or three (A, D) independent experiments. * $p < 0.05$, ** $p < 0.01$, *** $p < 0.001$ by unpaired t-test. Error bars represent SEM.

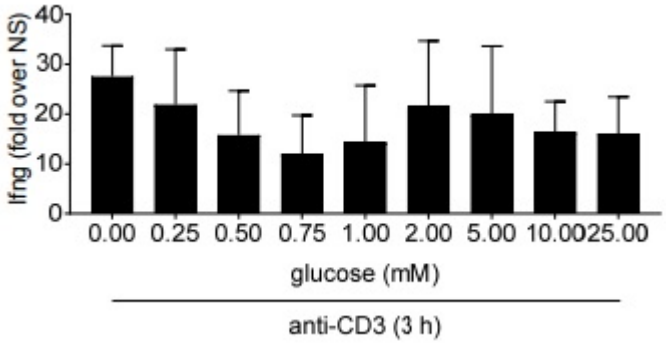

Figure 36. Fluctuations in glucose concentrations do not change Ifng mRNA levels.

A, Tabulated qPCR generated from PA-R CD8+ T cells stimulated with streptavidin or streptavidin-crosslinked αCD3 at 3 μg/ml in the indicated concentration of glucose for 3 h. Ifng was normalized to Actb expression and scaled to the no stim control. Results represent a mean of three experiments.

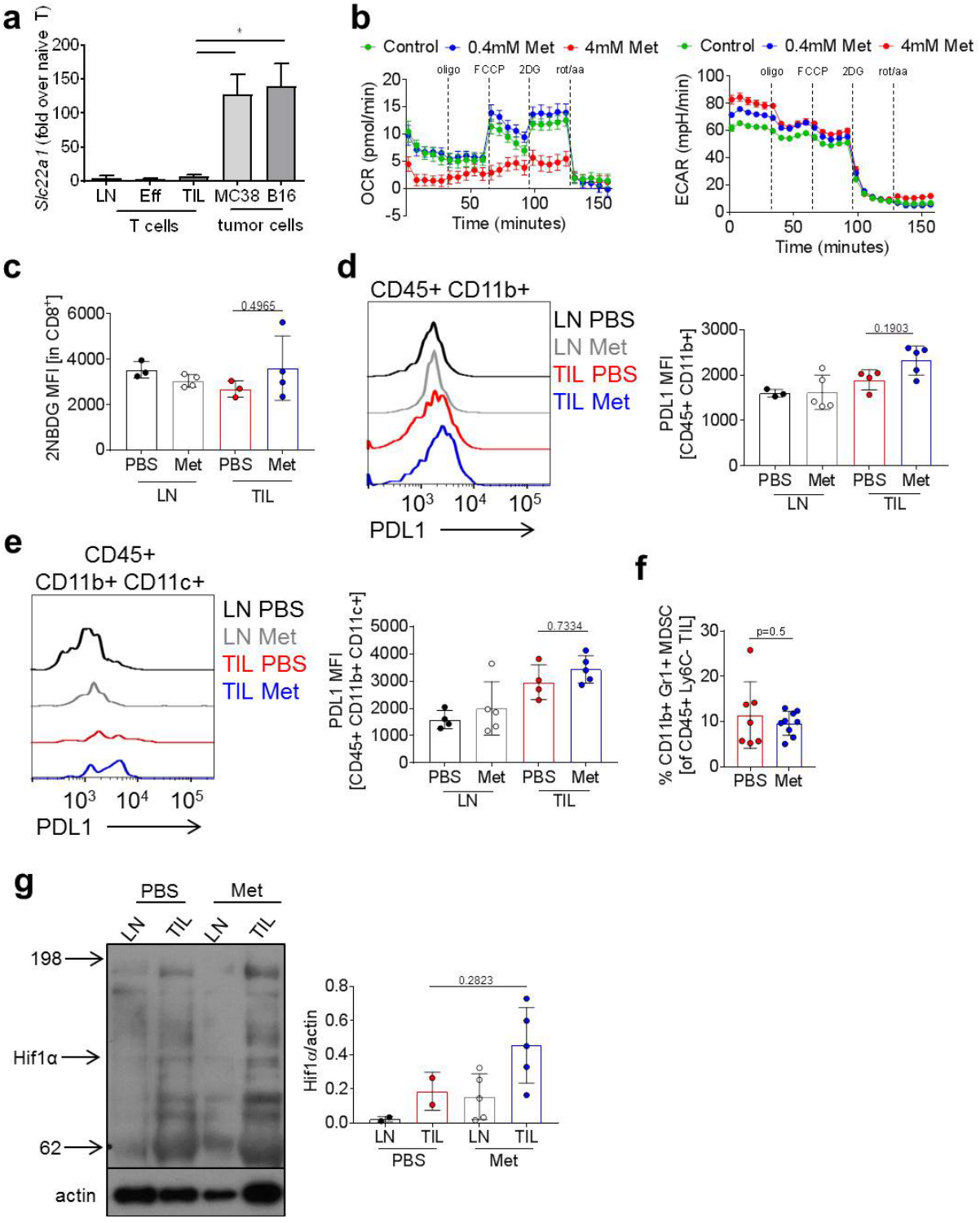

Figure 37. Metformin has indirect effects on immunity in the tumor microenvironment

(a) mRNA expression of Slc22a1 was quantified from direct ex vivo sorted CD8+ LN and TIL, in vitro activated CD8 T cells, CD45- direct ex vivo B16, or in vitro cultured MC38. Slc22a1 expression is graphed

as fold change over naïve T cell expression scaled to a endogenous control gene (PPIB) using the ΔΔCt method. (b) Oxygen consumption rate trace (left) or extracellular acidification rate trace (right) of in vitro OT-1 activated T cells cultured for 3 days in the presence of the indicated metformin concentrations. (c) Quantification of ex vivo 2NBDG glucose tracer uptake in CD8+ T cells from B16-bearing mice treated with metformin or vehicle for 3 days. (d) Histogram (left) and quantification (right) of PDL1 expression on CD45+ CD11b+ cells from B16-bearing mice treated as in c. (e) Histogram (left) and quantification (right) of PDL1 expression on CD45+ CD11b+ CD11c+ cells from B16-bearing mice treated as in c. (f) Quantification of % CD11b+ Gr1+ MDSCs from CD45+ Ly6C– cells from B16-bearing mice treated as in c. (g) Immunoblot (left) and quantification (right) of Hif1α and actin in CD8+ T cells from B16-bearing mice treated as in c. * $p < 0.05$ by unpaired t-test. Results are representative (a, b) or represent the mean (c-g) of 2 (a-c, g) or 3 (d-f) independent experiments.

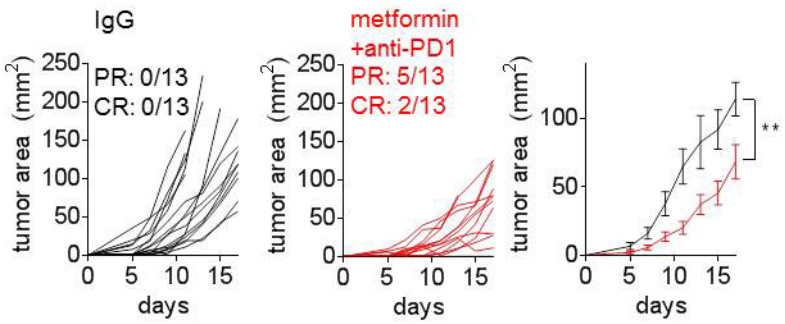

Figure 38. Metformin in the drinking water enhances PD-1 therapy in B16 melanoma

Tumor measurements of C57/BL6 mice inoculated with B16 melanoma. Mice began receiving treatment on d5, receiving 0.2mg anti-PD1 or its isotype control every 4 days. Mice receiving anti-PD1 also got 1g/L metformin drinking water. Number of partial responders (PR) and complete responders (CR) of the total inoculated mice is reported, as well as average tumor growth curve for all mice (far right). ** $p < 0.01$ by or two-way ANOVA with repeated-measures. Results represent 4 independent experiments.

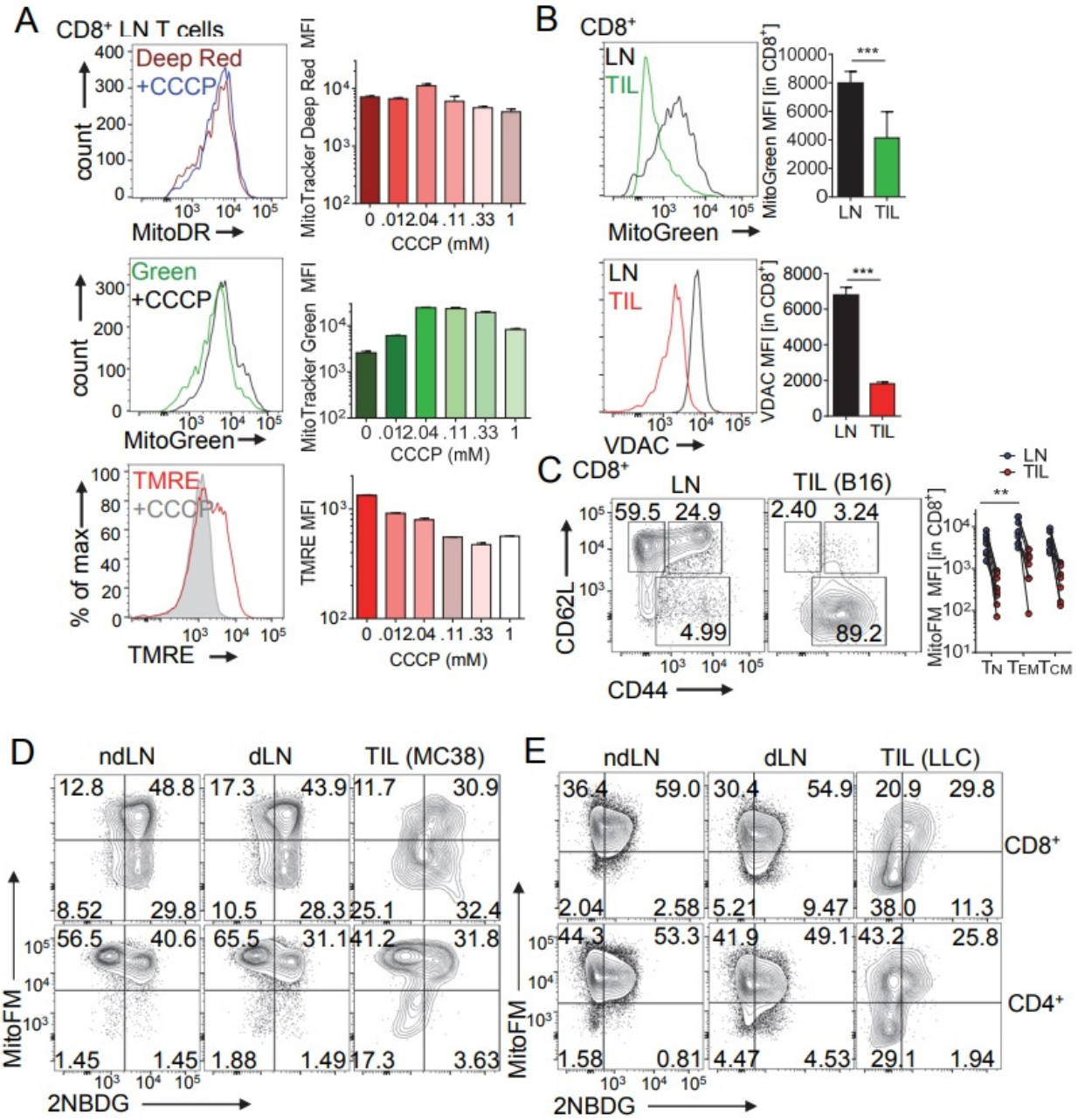

Figure 39. Tumor infiltrating T cells lose mitochondrial mass

(A) MitoTracker Deep Red FM, MitoTracker Green FM, and TMRE staining of CD8+ T cells from spleen and LNs. The indicated histogram represents T cells pre-incubated with 100-111 μM CCCP, which collapses membrane potential. Results from CCCP titration are tabulated below. (B) MitoTracker Green FM and intracellular VDAC staining of LN and TIL from d14 B16 tumors. (C) MitoTracker Deep Red FM staining of naïve (CD62LhiCD44lo), effector memory (CD62LloCD44hi), and

central memory (CD62LhiCD44hi) CD8+ T cells from LN and tumor-infiltrating compartments. (D) 2NBDG uptake and MitoTracker FM staining measurements from CD8+ and CD4+

T cells infiltrating day 18 MC38 tumors or (E) LLC tumors or from the nondraining or draining LN. Results represent 3 (A, B, D, E), or 6 (C) independent experiments. ** $p < 0.01$, **** $p < 0.001$ by unpaired (B) or paired (C) t test. Error bars indicate s.e.m.

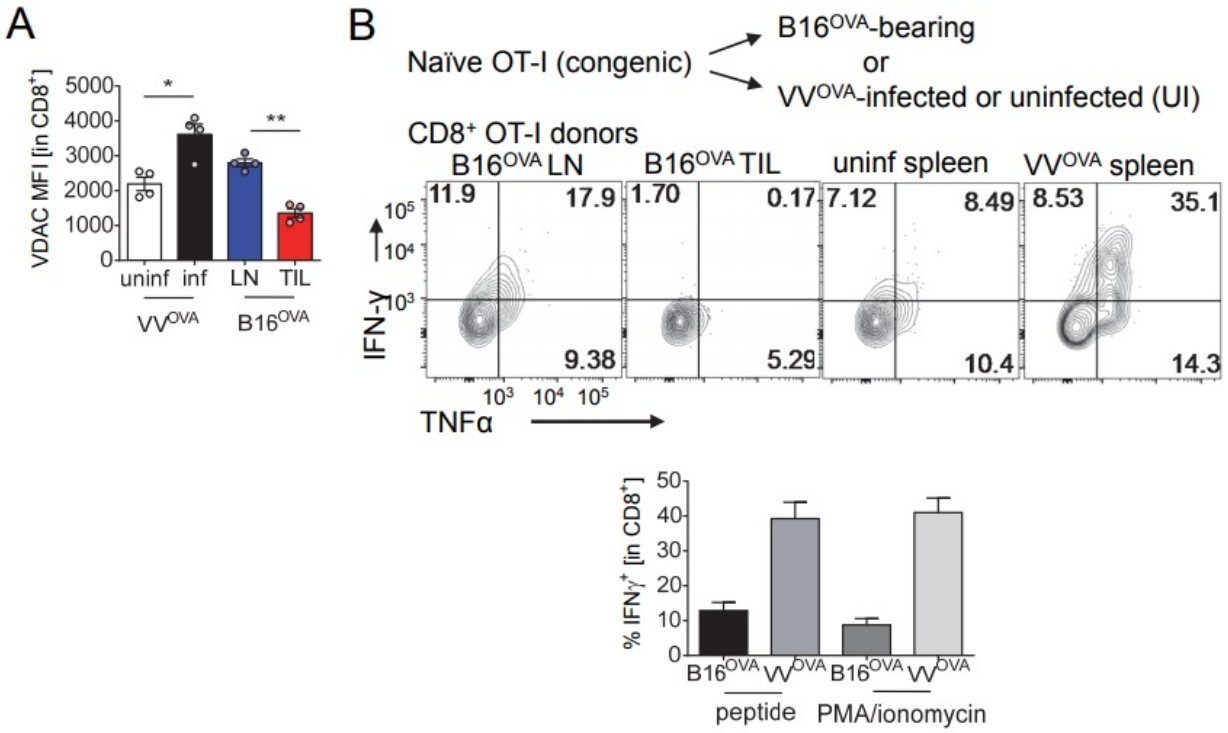

Figure 40. Tumor infiltrating T cells lose mitochondrial mass and do not efficiently elaborate cytokines

(A) VDAC staining of OT-I T cells cells. (B) Cytokine production of OT-I T cells. Some were rechallenged with cognate peptide overnight and others were stimulated with PMA/ionomycin, as tabulated below from TIL or spleen of VVOVA infected miceError bars indicate s.e.m.

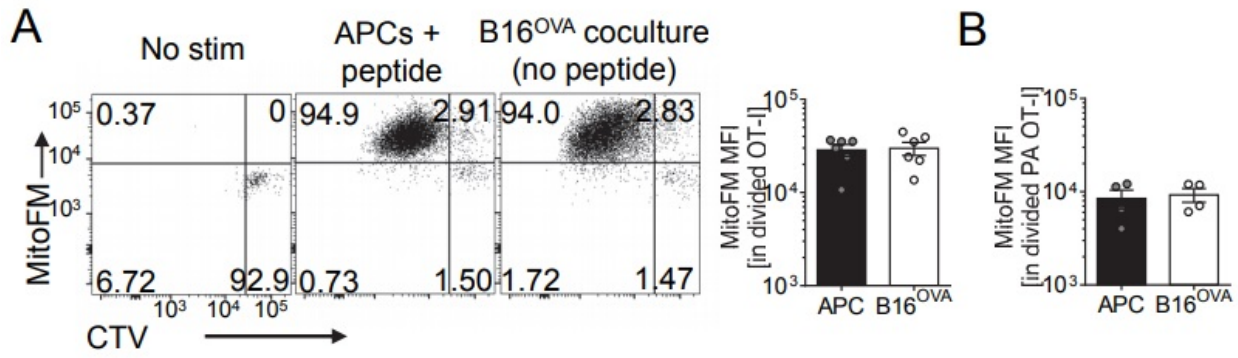

Figure 41. OT-I T cells do not lose mitochondrial activity when activated by tumor cells in vitro

(A) Flow cytogram and tabulated data of CTV-labeled OT-I splenocytes cocultured with either 25 ng/mL SIINFEKL peptide or in a 1:4 ratio with B16OVA cells, seeded 8 h prior to coculture, in the presence of 10 U/mL IL-2. (B) As in A, but using previously activated, purified effector OT-I T cells. Results represent the mean of 3 (of 8) independent experiments. Error bars indicate s.e.m.

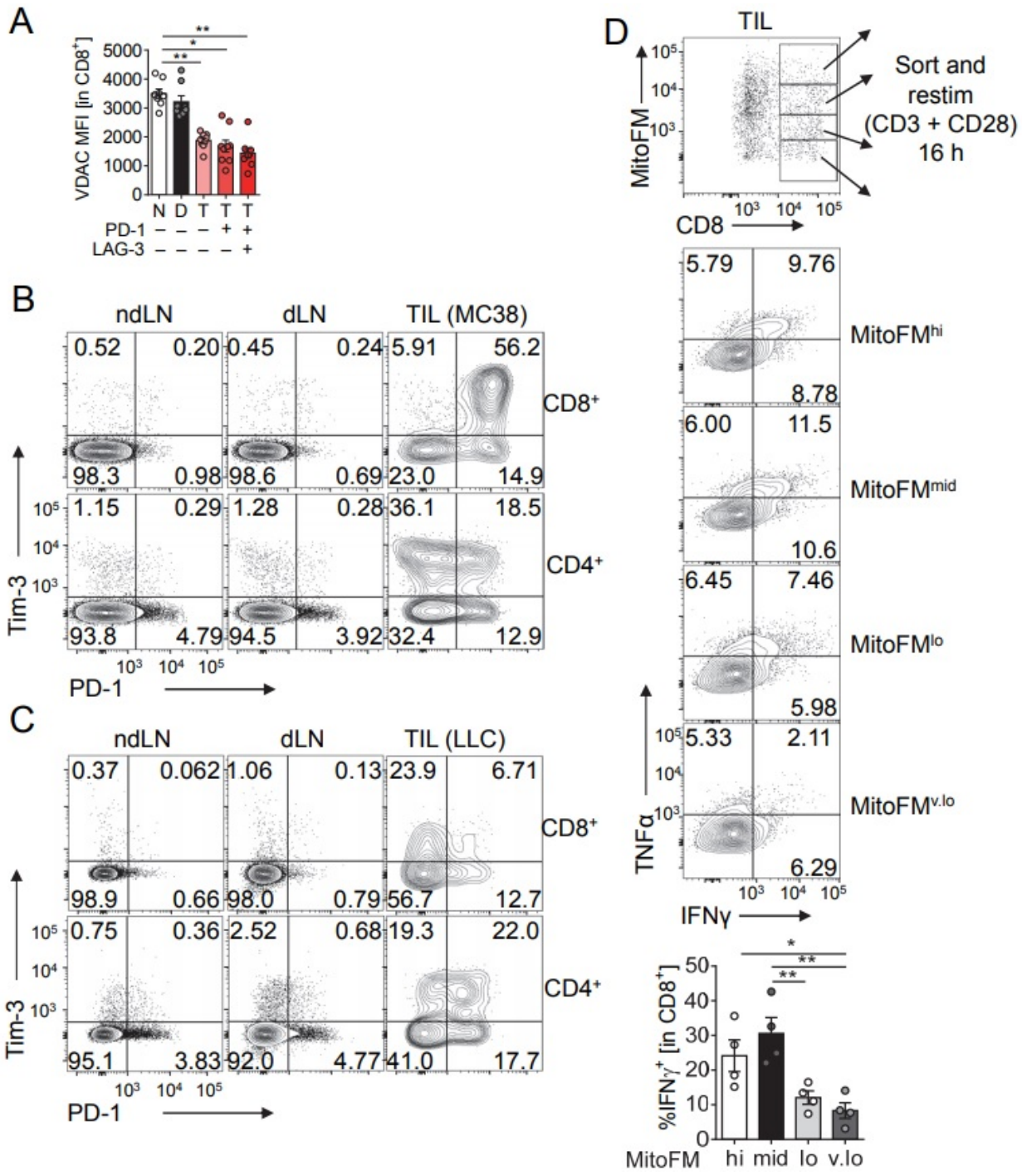

Figure 42. Mitochondrial mass loss is a characteristic of exhausted T cells

(A) VDAC staining of LN or TIL CD8+ T cells from B16-bearing mice expressing coinhibitory molecules PD-1 and LAG-3. (B) Co-inhibitory molecule expression on CD8+ and CD4+

T cells that are LN-resident or infiltrating MC38 or (C) LLC tumors on day 18 post inoculation (7-10 mm diameter tumors). (D) CD8+ T cells were sorted flow cytometrically from B16-bearing animals based on

MitoFM staining and washed extensively. Cells were then stimulated with anti-CD3/anti-CD28 for 16 h (final 4 h in the presence of a protein transport inhibitor), and then stained intracellularly for cytokines. Tabulated results for IFNγ staining are shown below. Results represent the mean of four independent experiments. Error bars indicate s.e.m. * < p 0.05, ** p < 0.01 by unpaired t test.

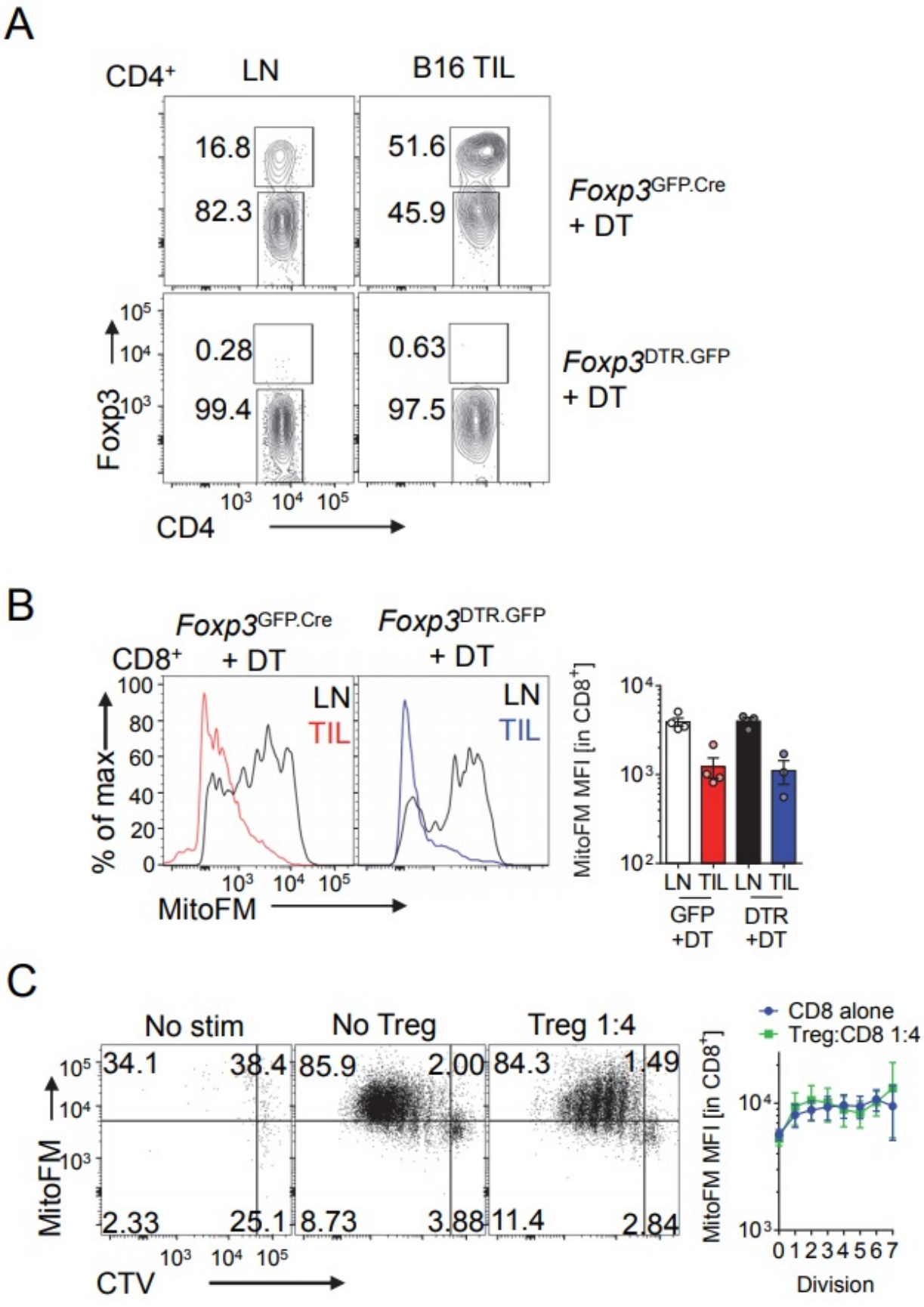
A
CD4+
LN
B16 TIL
16.8
82.3
51.6
45.9
Foxp3GFP.Cre
+ DT
0.28
99.4
0.63
97.5
Foxp3DTR.GFP
+ DT
Foxp3
CD4
B
Foxp3GFP.Cre
+ DT
Foxp3DTR.GFP
+ DT
CD8+
LN
TIL
% of max
MitoFM
MitoFM MFI [in CD8+]
LN TIL LN TIL
GFP +DT
DTR +DT
C
No stim
No Treg
Treg 1:4
34.1
38.4
2.33
25.1
85.9
2.00
8.73
3.88
84.3
1.49
11.4
2.84
MitoFM
CTV
CD8 alone
Treg:CD8 1:4
MitoFM MFI [in CD8+]
Division

Figure 43. Regulatory T cells do not mediate mitochondrial dysfunction in tumorinfiltrating CD8+ T cells

(A), Flow cytogram of CD4+ T cells from day 14 B16-bearing Foxp3GFP.Cre.ERT2 or Foxp3DTR.GFP mice treated for 3 days with diphtheria toxin. (B), Representative flow cytogram and tabulated data of MitoTracker FM staining in CD8+ T cells from mice in A. (C), Flow cytogram and tabulated data of CellTrace Violet labeled CD8+ T cells stimulated with anti-CD3 and antigen presenting cells (CD4–CD8– splenocytes) in the presence or absence of flow-cytometrically purified Treg cells (CD4+ GFP+ cells from a Foxp3GRP mouse). Results are representative of (A), or represent the mean of (B, C) two of three independent experiments. Error bars indicate s.e.m.

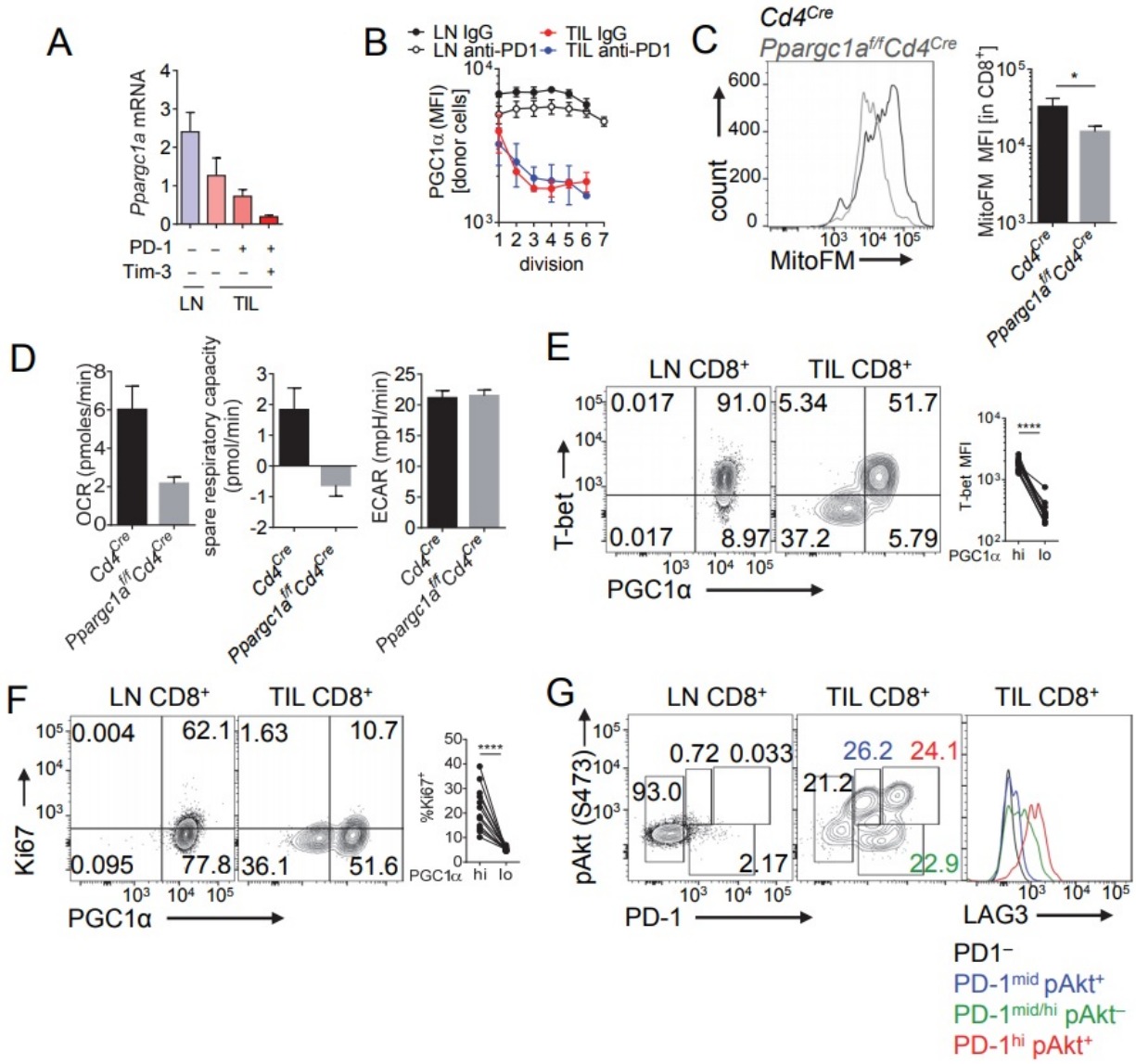

Figure 44. PGC1α is repressed progressively upon entry into the tumor microenvironment

(A) qPCR analysis of Ppargc1a (encoding PGC1α) from CD8+ T cells sorted from the indicated compartments based on co-inhibitory molecule expression from day 14 B16 tumors. Results are normalized to cyclophilin B expression and scaled to LN-resident CD4+ T cells. (B) PGC1α MFI (per division) of congenically mismatched, CTV-labeled OT-I T cells transferred into B16OVA bearing mice for 72 h under the cover of antiPD1 treatment or its isotype control. (C) Representative flow cytogram of MitoFM staining of CD8+ T cells isolated from Ppargc1af/fCd4Cre mice or Cd4Cre controls after in vitro expansion. (D) Metabolic flux measurements (Seahorse) from the cells in C. (E) Representative flow cytogram and tabulated results of PGC1α versus T-bet and (F) Ki67 staining. (G)

Representative flow cytogram depicting phospho-Akt (S473) activation as a function of PD-1 status. Results are representative of three (A, C, E, F), five (B, G), or two (D) independent experiments. * $p < 0.05$, **** $p < 0.0001$ by unpaired (C) or paired (E,F) t test. Error bars indicate s.e.m.

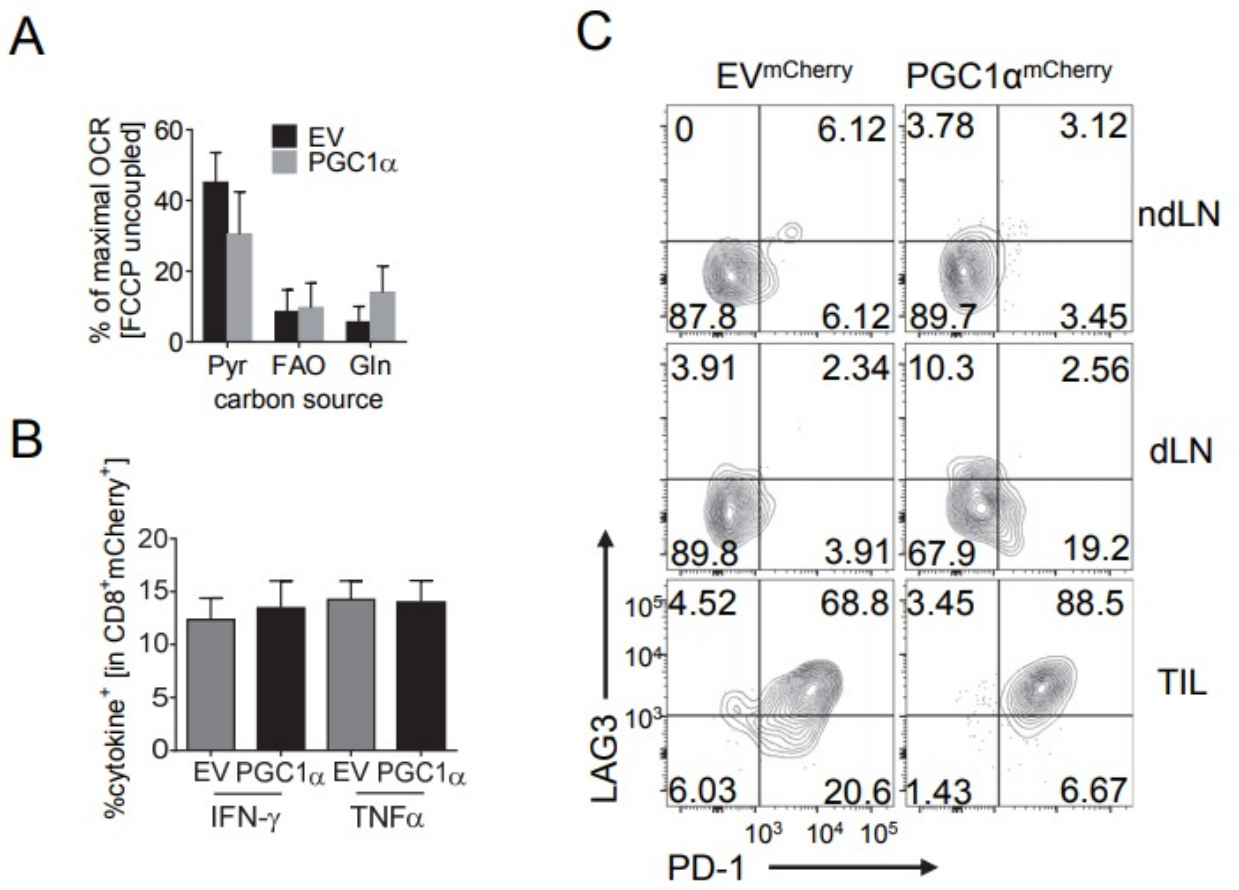

Figure 45. Enforced PGC1α expression results in general increases in mitochondrial function

(A) Fuel usage test of PGC1α- or EV-expressing OT-I T cells. Cells were uncoupled with FCCP and then subjected to sequential inhibition of pyruvate oxidation (UK5099), fatty acid oxidation (etomoxir), and glutaminolysis (BPTES). Results are displayed as % of FCCP-uncoupled OCR sensitive to the appropriate inhibitor. (B) IFNγ and TNFα production of EV or PGC1α expressing T cells prior to adoptive transfer. (C) Expression of PD-1 and LAG-3 on LN or TIL-resident reprogrammed T cells. Results represent the mean of three (A, B) or are representative of five (C) independent experiments. Error bars indicate s.e.m.

APPENDIX B

SUPPLEMENTAL METHODS

Sample preparation for LC-MS analysis

Monophasic extraction was performed for metabolomics analysis. For simultaneous extraction of polar and nonpolar metabolites, 1 mL of a solution containing methanol/water/dichloromethane (3/1/1, v/v/v) were added to the cell pellet or growth medium (200 µL), centrifuged at 1600 X g for 10 min at 4 °C, and the supernatant was transferred to a new vial and dried under nitrogen. Samples were re-suspended in 150 µL of 5% methanol in water for analysis.

LC-MS analysis

Samples were analyzed using ion-pairing reversed phase chromatography on a Vanquish ultra-high pressure liquid chromatography (UHPLC) coupled to a high resolution Q Exactive mass spectrometer (Thermo Scientific, Waltham, MA). Metabolites were resolved using a Phenomenex Luna C18(2) reversed phase column (2 x 150 mm, 5 µm particle size). The gradient solvent system consisted of solvents (A): H2O containing 10mM Hexylamine (pH:5) and (B): acetonitrile at a flow rate 150 uL/min.

Samples were applied to the column at 3% B (3 min) and eluted with a linear increase in solvent B (3%-95 B in 22 min), the gradient was held at 95%B for 4 min, following and additional increase to 100% B. This was followed by a wash step using 100% B for 3 min. The gradient then returned to starting conditions at 3% B for 2 min. The mass spectrometer was equipped with a HESI electrospray source and was operated in negative ion mode using the following parameters: aux gas heater temperature 300 °C, capillary temperature 325 °C, sheath gas flow 40, auxiliary gas flow 11, sweep gas flow 2, spray voltage 4 kV, S-lens RF level 50 %, full MS scans were obtained between 85–900 m/z. Analyte identification was confirmed by high resolution accurate mass.

B16^{OVA} in vitro stimulation

Freshly isolated OT-I splenocytes or purified, previously activated OT-I CD8+ T cells were CellTrace Violet labeled and plated at various ratios on B16 or B16^{OVA} cells in 10% RPMI for 72h. Proliferation and mitochondrial mass of the T cells was examined flow cytometrically.

Treg cell suppression assay

Lymph nodes and spleens from Foxp3 reporter mice (Foxp3DTR.GFP) were sorted based on expression of CD4 and GFP, then cocultured with CellTrace Violet-labeled CD8+ T cells from WT mice at a 1:4 ratio (Treg:Teff cell) in the presence of antigen presenting cells (CD4–CD8– splenic cells at a 2:1 APC:T cell ratio) and 1 µg/mL anti-CD3. After 72 h, proliferation and mitochondrial mass of the CD8+ T cells were analyzed by flow cytometry.

Fuel usage test

100,000 previously activated, transduced T cells were plated on CellTak-coated Seahorse plates in minimal, unbuffered Seahorse media containing glucose, and glutamine. Basal measurements were taken and then cells were uncoupled with FCCP and subjected to inhibition by UK5099, etomoxir, and BPTES. S7A depicts the percentage of the total FCCP uncoupled OCR inhibited by these agents.

APPENDIX C

EXTENDED METHODS

This appendix gives detailed experimental protocols for methods I helped design or optimize during my graduate school career.

C.1 IN VITRO T CELL EXHAUSTION (CHRONIC STIM + HYPOXIA ASSAY)

Hypothesis: Chronic stim + hypoxia are both required to cause T cell exhaustion.

Method:

D0

- Isolate previously-activated CD8+ T cells from mouse spleen and lymph nodes by sorting out CD44 hi CD8+ T cells. To activate, place 20K T cells in a round bottom plate with 0.5ul CD3/CD28 washed dynabeads (at 40K per ul, also 20K beads) + 25U/ml IL2 and 1:1000 IL-12 in 200uL R10. Allow 24hr for activation in normoxia.

D1

- After 24hr, recombine all cells and use a magnet to remove all dynabeads. Now place cells into various conditions:
    - Acute activation - (no dynabeads) in normoxia and hypoxia
    - Chronic 1:1 activation - (add back dynabeads) at a 1:1 bead:cell ratio in normoxia and hypoxia
    - Chronic 1:10 activation - (add back dynabeads) at a 1:1 bead:cell ratio in normoxia and hypoxia
- Continue culturing groups of cells in 200uL R10 + 25U/ml IL2 in round bottom plates.

D2

- Add 100ul R10 + 25U/ml IL2 to all wells

D3

- Divide all groups in half by pipetting 150ul (of 300ul well) into a new well, so that you now have double the wells per group. Spin down all cells in centrifuge, and flick off old media. Give all groups 300uL fresh R10 + 25U/ml IL2. For chronic stim groups, add back beads so the ratio will remain ~1:1 bead:cell

D4

- Leave cells alone

D5

- Divide all groups in half by pipetting 150ul (of 300ul well) into a new well, so that you now have double the wells per group. Spin down all cells in centrifuge, and

flick off old media. Give all groups 300uL fresh R10 + 25U/ml IL2. For chronic stim groups, add back beads so the ratio will remain ~1:1 bead:cell

D6

- Assay cells.

C.2 MOUSE CD8 T CELL TRANSDUCTION

Purpose: To introduce genetic modifications to in vitro cultured mouse T cells.

Timeline

Day -4

1. Break out Platinum-E Retroviral Packaging Cells for Ecotropic virus (Plat-E cells), stored in the liquid nitrogen.

    a. Thaw cells in 37 degree waterbath until no longer frozen (2-3 minutes)

    b. REMOVE TUBE FROM SHARED DRIVE DATABASE

    c. Move cells to 15 ml conical, add fresh D10 media to wash.

    d. Spin cells down at 1500 RPM for 5 minutes, then plate onto 15cm plate with 15-20 ml D10. Culture at 37 degrees.

Day -2

2. Trypsinize cells from plate (5ml trypsin [Trypsin-EDTA, Mediatech] for 3 minutes, stop with 5ml D10), count cells, and plate $1x10^6$ onto 10cm plates (for as many transductions as needed).

Day -1

3. Transfect Plat-E cells

a. Put 400uL serum-free DMEM (SF-DMEM) into a 1.5ml epiendorf, warm to room temperature

b. Add 6ug plasmid of interest and 2ug pCL-ECO helper plasmid to SF-DMEM. Pipette to mix well

c. Add 24uL room-temperature Mirus Bio TransIT-LT1 Transfection Reagent (Fisher) to SF-DMEM. Pipette to mix well.

d. Let sit at room temperature for 20 minutes to allow micelles to form.

e. Drip SF-DMEM onto previously-plated Plat-E cells, as well as 25uM chloroquine (Sigma, stock at 25mM, 1:1000 dilution)

f. After 6 hours, change plat-E media to fresh D10. Do not change media again until transduction, as you are now collecting retrovirus.

Day 0

4. Activate T cells

a. Coat a flat-bottom plate with 5ug/ml anti-CD3 leaf (Biolegend) in sterile PBS. Allow anti-CD3 to adhere to the plastic by incubating at 37 degrees for at least 3 hours.

b. Sacrifice mice, dissect spleen and lymph nodes according to the dissection protocol, and isolate CD4 or CD8 T cells according to T cell isolation protocol or sorting protocol.

c. Resuspend the cells at ~5x10^6/ml in R10, and add 2ug/ml anti-CD28 leaf (Biolegend) and 50U/ml IL-2 (Peprotech, stock at 100,000U/ml, 1:2000 dilution)

d. Aspirate off PBS from flat-bottom plate (DO NOT WASH). Gently add cells, trying not to disturb CD3 coating.

e. Let cells activate at least 24 hours at 37 degrees.

Day 1

5. Transduce T cells

a. Take media off transfected plat-E cells and filter using a 10ml syringe and 0.45um filter (Corning). Add 50U/ml IL-2 and 1:2000 polybrene (Fisher) to filtered media.

b. Spin down activated cells, and resuspend in filtered viral media. Put cells in a new flat bottom plate, wrap plate in cellophane, and spin the cells at 2200 RPM at 30 degrees for 2 hours.

c. After spin is complete, unwrap cellophane and put cells back into 37 degree incubator. Allow cells to recover for 2 hours.

d. After recovery, plate cells in fresh R10 + 50U/ml IL-2, at a concentration of 1x106/ml.

Day 2-10

6. Culturing T cells

a. Keep cells at 0.5x10^6/ml by counting every day. When cells need to expand, spin down cells and resuspend in fresh R10 + IL-2.

b. 3-4 days after activation, switch cells to 25U/ml IL-2 (1:4000 dillution) to become more rested.

c. Cells should continue to proliferate until 7-10 days after activation. Cells will stop proliferating but still be viable 10-14 days after activation. For cells that need to go longer than 14 days, or cytokine competency needs to be assessed post day 7, the cells will need to be reactivated.

C.3 MOUSE DISSECTION FOR LN, SPLEEN, AND TUMOR

Purpose: To isolate lymph node (LN), spleen, and tumor tissue to be processed for single cell suspension and further experimental analysis.

Mouse LN

1. Prepare collection tubes – aliquot 5ml serum free media into 15ml conical for every mouse being sacrificed. Place tubes on ice.

2. Take ice bucket and mouse locker key to mouse facility. Find chosen mice by checking ear tags in corresponding cage, then place mice into new cage by themselves.

3. Place mouse cage into CO2 chamber. Sacrifice by CO2 at gas flow rate of 3L/min (should take 3-5 minutes, watch chest to determine when respiration completely suppressed).

4. Use secondary method of sacrifice by utilizing cervical dislocation. Hold deceased mouse down by the head on the tabletop by pushing down with thumb

and first finger. Using your other hand, grab the tail and sharply pull spine up and away from your other hand to sever spinal cord.

5. Place mouse on its back, wet fur with 70% ethanol. Blot excess ethanol dry. Starting at the bottom of the abdomen, cut skin (but not peritoneal cavity) in a straight line up to the chin. Pull skin away from the animal (see below).

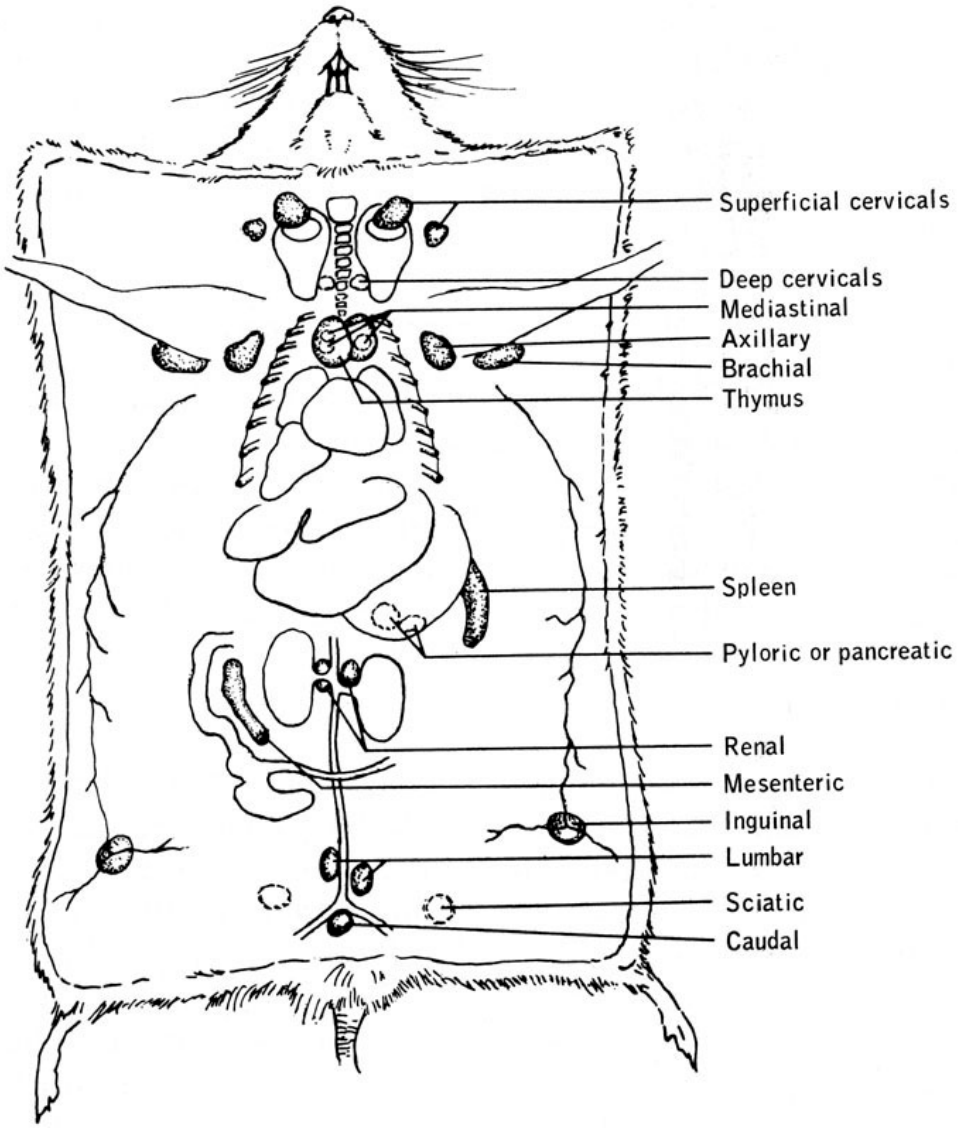

Figure 46. Schematic of mouse lymph nodes

Picture from "Dunn, T.B. Normal and pathologic anatomy of the reticular tissue in laboratory mice, with a classification and discussion of neoplasms. *J. Nat. Cancer Inst*. **14**: 1281-1434 (1954)."

6. Using mouse dissection forceps (pointy-end tweezers), locate cervical, axillary, brachial, and lnguinal LN, and pull sharply upwards to remove LN from surrounding tissue. Collect LNs on glove while dissection in progress.

7. After LNs have been removed and collected on glove, place LNs into collection tube. Keep on ice until ready to process.

8. After dissection, clean instruments, clean bench top, put equipment and dirty cages away, and collect mouse carcass in “dead bag” – plastic bag with date, Delgoffe, and protocol number (17071235).

9. Place mouse carcass in carcass freezer.

Mouse Spleen

1. Prepare collection tubes – aliquot 5ml serum free media into 15ml conical for every mouse being sacrificed. Place tubes on ice.

2. Take ice bucket and mouse locker key to mouse facility. Find chosen mice by checking ear tags in corresponding cage, then place mice into new cage by themselves.

3. Place mouse cage into CO2 chamber. Sacrifice by CO2 at gas flow rate of 3L/min (should take 3-5 minutes, watch chest to determine when respiration completely suppressed).

4. Use secondary method of sacrifice by utilizing cervical dislocation. Hold deceased mouse down by the head on the tabletop by pushing down with thumb and first finger. Using your other hand, grab the tail and sharply pull spine up and away from your other hand to sever spinal cord.

5. Place mouse on its back, wet fur with 70% ethanol. Blot excess ethanol dry. Starting at the bottom of the abdomen, cut skin (but not peritoneal cavity) in a straight line up to the chin. Pull skin away from the animal.

6. Locate spleen (see above), dissect away from connective tissue, and place into collection tube. Keep on ice until ready to process.

7. After dissection, clean instruments, clean bench top, put equipment and dirty cages away, and collect mouse carcass in “dead bag” – plastic bag with date, Delgoffe, and protocol number (17071235).

8. Place mouse carcass in carcass freezer.

Mouse Tumor

1. Prepare collection tubes – aliquot 5ml serum free media into 15ml conical for every mouse being sacrificed. Place tubes on ice.

2. Take ice bucket and mouse locker key to mouse facility. Find chosen mice by checking ear tags in corresponding cage, then place mice into new cage by themselves.

3. Place mouse cage into CO2 chamber. Sacrifice by CO2 at gas flow rate of 3L/min (should take 3-5 minutes, watch chest to determine when respiration completely suppressed).

4. Use secondary method of sacrifice by utilizing cervical dislocation. Hold deceased mouse down by the head on the tabletop by pushing down with thumb and first finger. Using your other hand, grab the tail and sharply pull spine up and away from your other hand to sever spinal cord.

5. Add Nair to the tumor mass, wait 2-3 minutes, then wipe off excess hair with a paper towel. Measure tumor size and record.

6. Using the forceps and scissors, carefully cut tumor mass off of the mouse, making sure to keep it fully intact. Place the tumor in the collection tube. Keep on ice until ready to process.

7. After dissection, clean instruments, clean bench top, put equipment and dirty cages away, and collect mouse carcass in “dead bag” – plastic bag with date, Delgoffe, and protocol number (17071235).

8. Place mouse carcass in carcass freezer.

C.4 CD8 T CELL ACTIVATION CULTURING, AND RESTIMULATION

Purpose: To activate T cells in vitro to generate previously-activated rested T cells.

I. T cell activation

a. Plate-bound CD3 activation

i. Coat a flat-bottom plate with 3ug/ml anti-CD3 leaf (Biolegend) in sterile PBS. Allow anti-CD3 to adhere to the plastic by incubating at 37 degrees for at least 3 hours.

ii. Sacrifice mice, dissect spleen and lymph nodes according to the dissection protocol, and isolate CD4 or CD8 T cells according to T cell isolation protocol or sorting protocol.

iii. Resuspend the cells at 5-10x10^6/ml in R10, and add 2ug/ml anti-CD28 leaf (Biolegend) and 50U/ml IL-2 (Peprotech, stock at 100,000U/ml, 1:2000 dilution)

iv. Aspirate off PBS from flat-bottom plate (DO NOT WASH). Gently add cells, trying not to disturb CD3 coating.

v. Let cells activate at least 24 hours at 37 degrees, but no longer than 48 hours.

b. Peptide activation

i. Sacrifice TCR transgenic mice (OT1+ or Pmel1 mice), dissect spleen and lymph nodes according to the dissection protocol.

ii. Resuspend cells at 5-10x106/ml in R10, add 50U/ml IL-2 (Peprotech, stock at 100,000U/ml, 1:2000 dilution) and appropriate peptide:

1. OT1 T cells: SIINFEKL peptide 250ng/ml (Anaspec, stock at 500ug/ml, 1:2000 dilution)

2. Pmel1 T cells: gp100 peptide 1uM (Anaspec, stock at 1mM, 1:1000 dilution)

iii. Add cells to a plate, let cells activate at least 24 hours at 37 degrees, but no longer than 48 hours.

c. Soluble CD3 activation

i. Sacrifice mice, dissect spleen and lymph nodes according to the dissection protocol, and deplete either CD4 T cells if activating CD8, or CD8 T cells if activating CD4, according to T cell isolation protocol or sorting protocol.

ii. Resuspend the cells at 5-10x106/ml in R10, and add 1ug/ml anti-CD3 leaf (Biolegend) and 50U/ml IL-2 (Peprotech, stock at 100,000U/ml, 1:2000 dilution)

iii. Add cells to a plate, let cells activate at least 24 hours at 37 degrees, but no longer than 48 hours.

d. PMA/Ionomycin activation

i. Sacrifice mice, dissect spleen and lymph nodes according to the dissection protocol, and isolate CD4 or CD8 T cells according to T cell isolation protocol or sorting protocol.

ii. Resuspend the cells at 5-10x106/ml in R10, and add 0.1ug/ml PMA (Fisher, stock at 1mg/ml, 1:10,000 dilution), 1ug/ml Ionomycin (Fisher, stock at 1mg/ml, 1:1000 dilution), and 50U/ml IL-2 (Peprotech, stock at 100,000U/ml, 1:2000 dilution)

iii. Add cells to a plate, let cells activate at least 24 hours at 37 degrees, but no longer than 48 hours.

II. T cell culturing

a. Timeline

i. After activation, spin down cells and aspirate off old media. Expand 10x volume in R10 and 50U/ml IL-2.

ii. Keep cells at $1x10^6$/ml by counting every day. When cells need to expand, spin down cells and resuspend in fresh R10 + IL-2.

iii. 3-4 days after activation, switch cells to 25U/ml IL-2 (1:4000 dillution) to become more rested.

iv. Cells should continue to proliferate until 7-10 days after activation. Cells will stop proliferating but still be viable 10-14 days after activation. For cells that need to go longer than 14 days, or cytokine competency needs to be assessed post day 7, the cells will need to be reactivated.

III. T cell restimulation

a. Plate-bound CD3 activation

i. Coat a flat-bottom plate with 3ug/ml anti-CD3 leaf (Biolegend) in sterile PBS. Allow anti-CD3 to adhere to the plastic by incubating at 37 degrees for at least 3 hours.

ii. Isolate live cells by density gradient (“Ficoll” the cells):

1. Condense in vitro cell culture into 5ml media (do not condense more than 50ml to 5ml, or you will overload your gradient) in a 15ml conical tube.

2. Gently layer 5ml Lymphocyte Separation Media (Mediatech) into the bottom of the 15ml conical, being careful to keep a distinct interface between the R10 and Lymphocyte Separation Media by pipetting slowly and preventing air bubbles.

3. Spin cells at 2200 RPM for 15 minutes.

4. After the spin, the live cells can be found at the interface between the R10 and Lymphocyte Separation Media, while the dead cells will be found at the bottom of the tube. Using a pipette bulb, carefully remove live cells into a fresh tube, wash cells with additional R10, and spin down again.

iii. After live cells have been isolated, resuspend the cells at 5-10x10^6/ml in R10, and add 2ug/ml anti-CD28 leaf (Biolegend) and 50U/ml IL-2 (Peprotech, stock at 100,000U/ml, 1:2000 dilution)

1. NOTE: If assaying for cytokines, DO NOT ADD IL-2.

iv. Aspirate off PBS from flat-bottom plate (DO NOT WASH). Gently add cells, trying not to disturb CD3 coating.

v. Let cells activate at least 24 hours at 37 degrees, but no longer than 48 hours.

b. PMA/Ionomycin activation

i. Isolate live cells by density gradient ("Ficoll" the cells):

1. Condense in vitro cell culture into 5ml media (do not condense more than 50ml to 5ml, or you will overload your gradient) in a 15ml conical tube.

2. Gently layer 5ml Lymphocyte Separation Media (Mediatech) into the bottom of the 15ml conical, being careful to keep a distinct interface between the R10 and Lymphocyte Separation Media by pipetting slowly and preventing air bubbles.

3. Spin cells at 2200 RPM for 15 minutes.

4. After the spin, the live cells can be found at the interface between the R10 and Lymphocyte Separation Media, while the dead cells will be found at the bottom of the tube. Using a pipette bulb, carefully remove live cells into a fresh tube, wash cells with additional R10, and spin down again.

ii. After live cells have been isolated, resuspend the cells at 5-10x10^6/ml in R10, and add 0.1ug/ml PMA (Fisher, stock at 1mg/ml, 1:10,000 dilution), 1ug/ml Ionomycin (Fisher, stock at 1mg/ml, 1:1000 dilution), and 50U/ml IL-2 (Peprotech, stock at 100,000U/ml, 1:2000 dilution)

1. NOTE: If assaying for cytokines, DO NOT ADD IL-2.

iii. Add cells to a plate, let cells activate at least 24 hours at 37 degrees, but no longer than 48 hours.

C.5 PROTOCOL FOR NEGATIVE SELECTION WITH BIOLEGEND MOJO BEADS

1. Process tissue and lyse red blood cells.

2. Count cells and resuspend cells at 40 x 10^6 cells/mL in 1X Mojo Sort Buffer.

3. Add Biotin antibodies to your cells/Mojo Sort Buffer. Use 1:1000 dilution for anti-CD19, anti-CD11c, anti-Ly-6G/Ly-6C, anti-CD11b, and anti-TCR γ/δ, and use 1:500 dilution for anti-CD45R/B220, anti-Pan-NK (CD49b), anti-CD105, anti-CD24, and anti-CD16/32.

Other antibodies:

- If selecting for CD8+ cells, add 1:1000 of CD25 and CD4 (CD25 is a marker of Tregs, somewhat redundant to add)
- If selecting for CD4+ cells, add 1:1000 of CD8a and CD8b.2
- If selecting for naïve cells, add 1:2500 of CD44

4. Mix well and incubate on ice for 15 minutes.

5. Wash cells with 1X Mojo Sort Buffer, 4X the volume currently in the tube. Spin down at 1500 rpm for 5 minutes.

6. Resuspend cells at 1 x 10^8 cells/mL in 1X Mojo Sort Buffer. Add MojoSort Streptavidin Nanobeads (5 µL/10 x 10^6 cells). Be sure to vortex the beads before adding them. BioLegend instructs to "vortex the beads at full speed for 5 touches."

    a. Example: If you have 260 x 10^6 cells, add 130 µL of beads.

7. Incubate on ice for 15 minutes.

8. Wash cells/beads with 1X Mojo Sort Buffer, 4X the volume currently in the tube, and spin down at 1500 rpm for 5 minutes.

9. Resuspend cells/beads in 3 mL of 1X Mojo Sort Buffer and place in 5 mL polystyrene tube. Place in magnet for 5 minutes.

10. After 5 minutes, pour out liquid and collect in 15 mL conical tube. Do not discard! These are your cells of interest. If needed, you can repeat steps 10-11 two more times.

11. Resuspend and count.

C.6 PROTOCOL FOR TIL ISOLATION – CD105 DEPLETION PRIOR TO SORT

1. Process tumors according to protocol above, making sure to add in a 30 second vortex step after red cell lysis. This helps separate tumor cells from immune cells and will increase your immune cell yield.

2. Follow negative selection protocol, but only use CD105 biotin antibody at 1:500.

3. Filter cells with 40µM filter after selection, and stain cells with antibodies needed for sorting in fancy sort buffer.

a. Don’t forget single stain controls for the sorter!

C.7 IMMUNOHISTOCHEMISTRY FOR TISSUE SECTIONS

1. Cut blocks of tissue to obtain spleen, lymph node, and tumor sections. Cryostat should be set to -20 degrees C, sections at 7um thickness

- If getting tissue fracturing, adjust temperature [try warmer] and thickness of section
- Can also try very briefly warming surface of OCT block by rubbing it with your thumb to decrease tissue fracturing

2. Fix slides in -20° acetone for 20 minutes at -20° (put back into freezer). Blot excess acetone off edges by pressing into a paper towel, and let air dry for 10 minutes (or until visibly dry). At this point you can store slides at -80° indefinitely (make sure slides stay dry).

3. To stain, let slides come up to room temperature, then draw a circle around tissue with a hydrophobic pen. Allow at least 10 minutes for hydrophobic line to dry.

4. Rehydrate tissue with staining buffer by adding ~200uL buffer to each tissue circle. Let sit at RT for 30 minutes. Make the staining buffer as follows:

<u>Staining Buffer</u>

100ml 1x PBS

1ml (1%) normal rat serum (as needed by antibody isotype)

1ml (1%) normal mouse serum (as needed by antibody isotype)

1g (1%) BSA

100ul (0.1%) Tween-20

5. Use aspirator to remove staining buffer, then blot with a kim wipe to get slide as dry as possible, making sure to not touch the tissue.

6. Aliquot primary antibodies (diluted in ~100ul staining buffer), and incubate in humidity chamber (foil-covered baking tray lined with damp paper towels) for 30 minutes at RT.

7. Wash slides first with a stream of PBS (using a transfer pipette) to get rid of excess antibody, then place slides in staining buffer and set on rotator to wash for 10 minutes. Gently blot next to sample area to remove excess liquid. If there is still excess liquid, it can be removed via aspiration. Renew the hydrophobic line if necessary (if staining with different secondaries on the same slide). Aliquot secondary antibodies (diluted in ~100ul staining buffer) and stain for 30 minutes at RT.

8. Wash slides again as previously, the counterstain with DAPI. DAPI stock is frozen at -20 at 5mg/ml stock concentration. To make a long-term working solution, dilute 50ul stock 1:50 in PBS (this solution can be stored in fridge for up to 6 months). Stain tissue with working solution for ~1minute.

9. Mount samples using prolong diamond anti-fade mounting media (add 3 evenly-spaced drops of mounting media to the coverslip, then place the coverslip on the slide). Let the mounting media cure for 24 hours (or at least overnight) at room temperature, protected from light.

10. Slides should be viewed with fluorescent microscope ASAP. For long term storage of stained slides, place them wrapped in foil at -80°.

C.8 ATP DETERMINATION ASSAY PROTOCOL

1. Prepare all reagents in biosafety cabinet, using sterile technique. Some reagents are light sensitive, so work with the light off.

2. Count cells and determine plate layout. In our hands, we have been able to get accurate ATP reads from 10K cells. Enter plate layout into luminometer software.

3. Prepare Somatic Cell ATP Release Agent (Sigma, FLSAR-1VL) by adding 90ml dH2O to 10ml concentrate. Reagent can be stored at 4deg indefinitely.

4. Prepare reagents from ATP Determination Kit (Fisher, A22066).

5. Prepare 100mM DTT stock solution by adding 1.62ml dH2O to 25mg DTT. Make 160uL aliquots and freeze at -20deg. Aliquots are stable for 6 months to 1 year.

6. Prepare 1x reaction buffer (50uL of 20x solution into 950uL dH2O) to add to 1 vial of 10mM D-Luciferin. Resuspended D-Luciferin is stable for several weeks at -20deg.

7. ATP standard is at 5mM. To make a 1uM → 1nM standard, take 1uL ATP stock and add it to 99uL dH2O to make 50uM stock (good for several weeks at -20deg). Then take 2uL of the 50uM diluted stock and add to 98uL dH2O to get 1uM. Do 1:1 serial dilutions for 11 wells to get standard curve from 1uM to 1nM. Well 12 should be water alone (blank).

8. Make up standard reaction solution as follows (for 10mL):

- 8.9ml dH2O
- 500uL 20x reaction buffer
- 100uL 0.1M DTT
- 500uL 10mM D-Luciferin
- 2.5uL firefly luciferase

9. Gently invert tube to mix. DO NOT VORTEX. Firefly luciferase can be easily denatured by vortexing. Allow reagents to sit at room temperature.

10. Plate correct number of cells (resuspended in PBS) in regular 96 well plate, in desired plate layout. Spin down, flick off liquid in sink.

11. Resuspend cells in Release Agent. Cells can only make up 10% of overall reaction (10uL of 100uL reaction), so resuspend cells accordingly, accounting for pipetting error.

12. Plate dH2O for standard, do serial dilutions with diluted ATP, leaving the blank well untouched.

13. Plate 90uL standard reaction solution in black luminometer plate (Perkin Elmer, 6005660). Add 10uL cells or standard to reaction solution, cover plate in foil, and place on rotating platform at 300RMP for ~2 minutes.

14. Read plate on luminometer. Make sure to manually adjust the luminometer to read for 5 seconds, and increase the reading sensitivity (we use a value of 130). ATP should be read within 30 minutes for highest accuracy.

BIBLIOGRAPHY

1. Hanahan, D. & Weinberg, R. A. Hallmarks of cancer: The next generation. *Cell* **144,** 646–674 (2011).

2. Dunn, G. P., Bruce, A. T., Ikeda, H., Old, L. J. & Schreiber, R. D. Cancer immunoediting: from immunosurveillance to tumor escape. *Nat. Immunol.* **3,** 991–998 (2002).

3. Dunn, G. P., Old, L. J. & Schreiber, R. D. The immunobiology of cancer immunosurveillance and immunoediting. *Immunity* **21,** 137–148 (2004).

4. Mittal, D., Gubin, M. M., Schreiber, R. D. & Smyth, M. J. New insights into cancer immunoediting and its three component phases-elimination, equilibrium and escape. *Curr. Opin. Immunol.* **27,** 16–25 (2014).

5. Dunn, G. P., Old, L. J. & Schreiber, R. D. The three Es of cancer immunoediting. *Annu. Rev. Immunol.* **22,** 329–60 (2004).

6. Lindau, D., Gielen, P., Kroesen, M., Wesseling, P. & Adema, G. J. The immunosuppressive tumour network: Myeloid-derived suppressor cells, regulatory T cells and natural killer T cells. *Immunology* **138,** 105–115 (2013).

7. Zarour, H. M. Reversing T-cell Dysfunction and Exhaustion in Cancer. *Clin. Cancer Res.* **22,** 1856–1864 (2016).

8. Baumeister, S. H., Freeman, G. J., Dranoff, G. & Sharpe, A. H. Coinhibitory Pathways in Immunotherapy for Cancer. (2016). doi:10.1146/annurev-immunol-032414-112049

9. Hodi, F. S. *et al.* Improved Survival with Ipilimumab in Patients with Metastatic Melanoma. *N. Engl. J. Med.* **363,** 711–723 (2010).

10. Topalian, S. L. *et al.* Safety, Activity, and Immune Correlates of Anti–PD-1 Antibody in Cancer. *N. Engl. J. Med.* **366,** 2443–2454 (2012).

11. Yuan, J. *et al.* Novel technologies and emerging biomarkers for personalized cancer immunotherapy. *J. Immunother. Cancer* (2016). doi:10.1186/s40425-016-0107-3

12. Warburg, O. On the Origin of Cancer Cells. *Science (80-.).* **123,** 309–314 (1956).

13. Kim, J. W. & Dang, C. V. Cancer's molecular sweet tooth and the warburg effect. *Cancer Res.* **66,** 8927–8930 (2006).

14. Heiden, M. G. Vander *et al.* Understanding the Warburg Effect : Cell Proliferation. *Science (80-.).* **324,** 1029–1034 (2009).

15. Gogvadze, V., Orrenius, S. & Zhivotovsky, B. Mitochondria in cancer cells: what is so special about them? (2008). doi:10.1016/j.tcb.2008.01.006

16. Thomas Pfeiffer, Stefan Schuster, S. B., Pfeiffer, T., Schuster, S. & Bonhoeffer, S. Cooperation and Competition in the Evolution of ATP-Producing Pathways. *Science* **292,** 504–507 (2001).

17. Martinez-Outschoorn, U. E., Peiris-Pagés, M., Pestell, R. G., Sotgia, F. & Lisanti, M. P. Cancer metabolism: a therapeutic perspective. *Nat. Rev. Clin. Oncol.* (2016). doi:10.1038/nrclinonc.2016.60

18. Basan, M. *et al.* Overflow metabolism in Escherichia coli results from efficient proteome allocation. *Nature* **528,** 99–104 (2015).

19. Helmlinger, G., Sckell, A., Dellian, M., Forbes, N. S. & Jain, R. K. Acid Production in Glycolysis-impaired Tumors Provides New Insights into Tumor Metabolism Acid Production in Glycolysis-impaired Tumors Provides New Insights into Tumor Metabolism 1. **8,** 1284–1291 (2002).

20. Kato, Y. *et al.* Acidic extracellular microenvironment and cancer. *Cancer Cell Int.* **13,** 89 (2013).

21. Wilson, W. R. & Hay, M. P. Targeting hypoxia in cancer therapy. *Nat Rev Cancer* **11,** 393–410 (2011).

22. Kouidhi, S., Noman, M. Z., Kieda, C., Elgaaied, A. B. & Chouaib, S. Intrinsic and tumor microenvironment-induced metabolism adaptations of T cells and impact on their differentiation and function. *Front. Immunol.* **7,** 1–10 (2016).

23. Unruh, A. *et al.* The hypoxia-inducible factor-1 a is a negative factor for tumor therapy. 3213–3220 (2003). doi:10.1038/sj.onc.1206385

24. Kim, J., Gao, P., Liu, Y., Semenza, G. L. & Dang, C. V. Hypoxia-Inducible Factor 1 and Dysregulated c-Myc Cooperatively Induce Vascular Endothelial Growth Factor and Metabolic Switches Hexokinase 2 and Pyruvate Dehydrogenase Kinase 1. **27,** 7381–7393 (2007).

25. Ganeshan, K. & Chawla, A. Metabolic Regulation of Immune Responses. *Annu. Rev. Immunol.* **32,** 609–634 (2014).

26. Roos, D., Loos, J. A. Changes in the carbohydrate metabolism of mitogenically stimulated human peripheral lymphocytes. *Exp. Cell Res.* **77,** (1973).

27. Chang, C. H. *et al.* Posttranscriptional control of T cell effector function by aerobic glycolysis. *Cell* **153,** 1239–1251 (2013).

28. Pearce, E. L., Poffenberger, M. C., Chang, C. & Jones, R. G. Fueling Immunity : Insights into Metabolism and Lymphocyte Function. **342,** (2013).

29. Wofford, J. a *et al.* IL-7 promotes Glut1 trafficking and glucose uptake via STAT5-mediated activation of Akt to support T cell survival IL-7 promotes Glut1 trafficking and glucose uptake via STAT5-mediated activation of Akt to support T cell survival. *Blood* **111,** 2101–2112 (2007).

30. Fox, C. J., Hammerman, P. S. & Thompson, C. B. Fuel feeds function: energy metabolism and the T-cell response. *Nat. Rev. Immunol.* **5,** 844–52 (2005).

31. Greiner, E. F., Guppy, M. & Brand, K. Glucose is essential for proliferation and the glycolytic enzyme induction that provokes a transition to glycolytic energy production. *J. Biol. Chem.* **269,** 31484–31490 (1994).

32. Macintyre, A. N. *et al.* The glucose transporter Glut1 is selectively essential for CD4 T cell activation and effector function. *Cell Metab.* **20,** 61–72 (2014).

33. Zheng, Y., Delgoffe, G. M., Meyer, C. F., Chan, W. & Powell, J. D. Anergic T cells are metabolically anergic. *J. Immunol.* **183,** 6095–6101 (2009).

34. Hentze, M. W. Enzymes as RNA-binding proteins: a role for (di)nucleotide-binding domains? *Trends Biochem. Sci.* 101–103 (1994).

35. Menk, A. V. *et al.* Early TCR Signaling Induces Rapid Aerobic Glycolysis Enabling Distinct Acute T Cell Effector Functions. *Cell Rep.* **22,** (2018).

36. van der Windt, G. J. W. *et al.* Mitochondrial Respiratory Capacity Is a Critical Regulator of CD8 + T Cell Memory Development. *Immunity* **36,** 68–78 (2011).

37. van der Windt, G. J. W. *et al.* CD8 memory T cells have a bioenergetic advantage that underlies their rapid recall ability. *Proc. Natl. Acad. Sci. U. S. A.* **110,** 14336–41 (2013).

38. Gubser, P. M. *et al.* Rapid effector function of memory CD8+ T cells requires an immediate-early glycolytic switch. *Nat. Immunol.* **14,** 1064–72 (2013).

39. Pearce, E. L. *et al.* Enhancing CD8 T-cell memory by modulating fatty acid metabolism. *Nature* **460,** 103–107 (2009).

40. Pollizzi, K. N. *et al.* Asymmetric inheritance of mTORC1 kinase activity during division dictates CD8 + T cell differentiation. **17,** 2–11 (2016).

41. Verbist, K. C. *et al.* Metabolic maintenance of cell asymmetry following division in activated T lymphocytes. *Nature* **532,** 389–393 (2016).

42. Chang, J. T. *et al.* Asymmetric T lymphocyte division in the initiation of adaptive immune responses. *Science* **315,** 1687–1691 (2007).

43. Powell, J. D. & Delgoffe, G. M. The Mammalian Target of Rapamycin: Linking T Cell Differentiation, Function, and Metabolism. *Immunity* **33,** 301–311 (2010).

44. Martel, R. R., Klicius, J. & Galet, S. Inhibition of the immune response by rapamycin, a new antifungal antibiotic. *Can. J. Physiol. Pharmacol.* **55,** 48–51 (1977).

45. Powell, J. D., Lerner, C. G. & Schwartz, R. H. Inhibition of cell cycle progression by rapamycin induces T cell clonal anergy even in the presence of costimulation. *J. Immunol.* **162,** 2775–2784 (1999).

46. Zheng, Y. *et al.* A Role for Mammalian Target of Rapamycin in Regulating T Cell Activation versus Anergy. *J. Immunol.* (2007). doi:10.4049/jimmunol.178.4.2163

47. Delgoffe, G. M. *et al.* The mTOR Kinase Differentially Regulates Effector and Regulatory T Cell Lineage Commitment. *Immunity* **30,** 832–844 (2009).

48. Araki, K. *et al.* mTOR regulates memory CD8 T-cell differentiation. *Nature* **460,** 108–112 (2009).

49. Delgoffe, G. M. *et al.* The kinase mTOR regulates the differentiation of helper T cells through the selective activation of signaling by mTORC1 and mTORC2. *Nat. Immunol.* **12,** 295–303 (2011).

50. Pollizzi, K. N. *et al.* mTORC1 and mTORC2 selectively regulate CD8 + T cell differentiation. 1–19 doi:10.1172/JCI77746DS1

51. Wang, R. *et al.* The Transcription Factor Myc Controls Metabolic Reprogramming upon T Lymphocyte Activation. *Immunity* **35,** 871–882 (2011).

52. Rolf, J. *et al.* AMPKa1: A glucose sensor that controls CD8 T-cell memory. *Eur. J. Immunol.* **43,** 889–896 (2013).

53. Blagih, J. *et al.* The Energy Sensor AMPK Regulates T Cell Metabolic Adaptation and Effector Responses In Vivo. *Immunity* **42,** 41–54 (2015).

54. Kidani, Y. *et al.* Sterol regulatory element-binding proteins are essential for the metabolic programming of effector T cells and adaptive immunity. *Nat. Immunol.* **14,** 489–99 (2013).

55. Choi, J. M. & Bothwell, A. L. M. The nuclear receptor PPARs as important regulators of T-cell functions and autoimmune diseases. *Mol. Cells* **33,** 217–222 (2012).

56. Clark, R. B. *et al.* The nuclear receptor PPAR gamma and immunoregulation: PPAR gamma mediates inhibition of helper T cell responses. *J. Immunol. (Baltimore, Md 1950)* **164,** 1364–1371 (2000).

57. Housley, W. J. *et al.* Peroxisome Proliferator-Activated Receptor Is Required for CD4+ T Cell-Mediated Lymphopenia-Associated Autoimmunity. *J. Immunol.* **187,** 4161–4169 (2011).

58. Roczniak-Ferguson, A. *et al.* The transcription factor TFEB links mTORC1 signaling to transcriptional control of lysosome homeostasis. *Sci. Signal.* **5,** ra42 (2012).

59. Baixauli, F. *et al.* Mitochondrial respiration controls lysosomal function during inflammatory t cell responses. *Cell Metab.* **22,** 485–498 (2015).

60. Cunningham, J. T. *et al.* mTOR controls mitochondrial oxidative function through a YY1–PGC-1α transcriptional complex. *Nature* 736–740 (2007). doi:10.1038/nature06322

61. Teft, W. A., Chau, T. A. & Madrenas, J. Structure-Function analysis of the CTLA-4 interaction with PP2A. *BMC Immunol.* **10,** 23 (2009).

62. Kuo, Y. C. *et al.* Regulation of phosphorylation of Thr-308 of Akt, cell proliferation, and survival by the B55α regulatory subunit targeting of the protein phosphatase 2A holoenzyme to Akt. *J. Biol. Chem.* **283,** 1882–1892 (2008).

63. Wlodarchak, N. & Xing, Y. PP2A as a master regulator of the cell cycle. *Crit Rev Biochem Mol Biol* **51,** 229–262 (2016).

64. Chemnitz, J. M., Parry, R. V., Nichols, K. E., June, C. H. & Riley, J. L. SHP-1 and SHP-2 Associate with Immunoreceptor Tyrosine-Based Switch Motif of Programmed Death 1 upon Primary Human T Cell Stimulation, but Only Receptor Ligation Prevents T Cell Activation. *J. Immunol.* **173,** 945–954 (2004).

65. Wu, C. J. *et al.* The tyrosine phosphatase SHP-2 is required for mediating phosphatidylinositol 3-kinase/Akt activation by growth factors. *Oncogene* **20,** 6018–6025 (2001).

66. Zhang, S. Q. *et al.* Receptor-specific regulation of phosphatidylinositol 3'-kinase activation by the protein tyrosine phosphatase Shp2. *Mol. Cell. Biol.* **22,** 4062–72 (2002).

67. Staron, M. M. *et al.* The Transcription Factor FoxO1 Sustains Expression of the Inhibitory Receptor PD-1 and Survival of Antiviral CD8+ T Cells during Chronic Infection. *Immunity* **41,** 802–814 (2014).

68. Lee, J. *et al.* Phosphotyrosine-dependent coupling of tim-3 to T-cell receptor signaling pathways. *Mol. Cell. Biol.* **31,** 3963–3974 (2011).

69. Vander Heiden, M. G. *et al.* Growth factors can influence cell growth and survival through effects on glucose metabolism. *Mol. Cell. Biol.* **21,** 5899–5912 (2001).

70. Rathmell, J. C. *et al.* Akt-directed glucose metabolism can prevent Bax conformation change and promote growth factor-independent survival. *Mol. Cell. Biol.* **23,** 7315–28 (2003).

71. Maciver, N. J. *et al.* Glucose metabolism in lymphocytes is a regulated process with significant effects on immune cell function and survival. *J. Leukoc. Biol.* **84,** 949–957 (2008).

72. Chang, C. H. *et al.* Metabolic Competition in the Tumor Microenvironment Is a Driver of Cancer Progression. *Cell* **162,** 1229–1241 (2015).

73. Ho, P. C. *et al.* Phosphoenolpyruvate Is a Metabolic Checkpoint of Anti-tumor T Cell Responses. *Cell* **162,** 1217–1228 (2015).

74. Zhao, E. *et al.* Cancer mediates effector T cell dysfunction by targeting microRNAs and EZH2 via glycolysis restriction. **17,** (2016).

75. Zhang, Y. & Ertl, H. C. J. Starved and asphyxiated: How can CD8+ T cells within a tumor microenvironment prevent tumor progression. *Front. Immunol.* **7,** 1–7 (2016).

76. Mcnamee, N. & Korns, D. Hypoxia and hypoxia-inducible factors as regulators of T cell development, differentiation, and function. *Immunol. Res.* 58–70 (2013). doi:10.1007/s12026-012-8349-8

77. Hatfield, S. M. *et al.* Immunological mechanisms of the antitumor effects of supplemental oxygenation. *Sci. Transl. Med.* **7,** 277ra30–277ra30 (2015).

78. Scharping, N. E. N. E., Menk, A. V. A. V. V., Whetstone, R. D. R. D., Zeng, X. & Delgoffe, G. M. G. M. M. Efficacy of PD-1 Blockade Is Potentiated by Metformin-Induced Reduction of Tumor Hypoxia. *Cancer Immunol. Res.* **5,** 9–16 (2017).

79. Altman, B. J., Stine, Z. E. & Dang, C. V. From Krebs to clinic: glutamine metabolism to cancer therapy. *Nat. Publ. Gr.* (2016). doi:10.1038/nrc.2016.71

80. Carr, E. L. *et al.* Glutamine uptake and metabolism are coordinately regulated by ERK/MAPK during T lymphocyte activation. *J. Immunol.* **185,** 1037–44 (2010).

81. Sinclair, L. V *et al.* Control of amino-acid transport by antigen receptors coordinates the metabolic reprogramming essential for T cell differentiation. *Nat. Immunol.* **14,** 500–8 (2013).

82. Platten, M., Wick, W. & Van Den Eynde, B. J. Tryptophan catabolism in cancer: Beyond IDO and tryptophan depletion. *Cancer Res.* **72,** 5435–5440 (2012).

83. Lind, D. S. Arginine and Cancer. *J. Nutr.* **134,** 2837S–2841 (2004).

84. Munder, M. Arginase: An emerging key player in the mammalian immune system: REVIEW. *Br. J. Pharmacol.* **158,** 638–651 (2009).

85. Choi, S. Y. C., Collins, C. C., Gout, P. W. & Wang, Y. Cancer-generated lactic acid: A regulatory, immunosuppressive metabolite? *J. Pathol.* **230,** 350–355 (2013).

86. Ohta, A. A metabolic immune checkpoint: Adenosine in Tumor Microenvironment. *Front. Immunol.* **7,** 1–11 (2016).

87. Sena, L. A. *et al.* Mitochondria Are Required for Antigen-Specific T Cell Activation through Reactive Oxygen Species Signaling. *Immunity* **38,** 225–236 (2013).

88. Buck, M. D. *et al.* Mitochondrial Dynamics Controls T Cell Fate through Article Mitochondrial Dynamics Controls T Cell Fate through Metabolic Programming. *Cell* **166,** 63–76 (2016).

89. Scharping, N. E. *et al.* The Tumor Microenvironment Represses T Cell Mitochondrial Biogenesis to Drive Intratumoral T Cell Metabolic Insufficiency and Dysfunction. *Immunity* **45,** 374–388 (2016).

90. Crompton, J. G. *et al.* Akt inhibition enhances expansion of potent tumor-specific lymphocytes with memory cell characteristics. *Cancer Res.* **75,** 296–305 (2015).

91. Bengsch, B. *et al.* Bioenergetic Insufficiencies Due to Metabolic Alterations Regulated by the Inhibitory Receptor PD-1 Are an Early Driver of CD8 + T Cell Exhaustion. *Immunity* **45,** 1–16 (2016).

92. Delgoffe, G. M. & Powell, J. D. Sugar, fat, and protein: new insights into what T cells crave. *Curr. Opin. Immunol.* **33,** 49–54 (2015).

93. Peng, M. *et al.* Aerobic glycolysis promotes T helper 1 cell differentiation through an epigenetic mechanism. *Science (80-.).* **6284,** 481–485 (2016).

94. Palmer, C. S., Ostrowski, M., Balderson, B., Christian, N. & Crowe, S. M. Glucose Metabolism Regulates T Cell Activation, Differentiation, and Functions. *Front. Immunol.* **6,** 1–6 (2015).

95. Jacobs, S. R. *et al.* Glucose uptake is limiting in T cell activation and requires CD28-mediated Akt-dependent and independent pathways. *J. Immunol.* **180,** 4476–4486 (2008).

96. Heather L. Wieman, Jessica A. Wofford, and J. C. R. Cytokine Stimulation Promotes Glucose Uptake via Phosphatidylinositol-3 Kinase/Akt Regulation of Glut1 Activity and Traffickin. *Mol. Biol. Cell* **18,** 1437–1446 (2007).

97. Eijkelenboom, A. & Burgering, B. M. T. FOXOs: Signalling integrators for homeostasis maintenance. *Nat. Rev. Mol. Cell Biol.* **14,** 83–97 (2013).

98. Pollizzi, K. N. & Powell, J. D. Integrating canonical and metabolic signalling programmes in the regulation of T cell responses. *Nat. Rev. Immunol.* **14,** 435–446 (2014).

99. Bacik I, Cox JH, Anderson R, Yewdell JW, B. J. TAP (Transporter Associated with Antigen Processing)- Independent Presentation of Endogenously Synthesized Peptides Is Enhanced by Endoplasmic Reticulum Insertion Sequences Located at the Amino- but not Carboxyl-Terminus of the Peptide. *J. Immunol.* **152,** 381 (1994).

100. Delgoffe, G. M., Kole, T. P., Cotter, R. J. & Powell, J. D. Enhanced interaction between Hsp90 and raptor regulates mTOR signaling upon T cell activation. *Mol. Immunol.* **46,** 2694–2698 (2009).

101. Guy, C. S. *et al.* Distinct TCR signaling pathways drive proliferation and cytokine production in T cells. *Nat. Immunol.* **14,** 262–270 (2013).

102. Frauwirth, K. A. *et al.* The CD28 Signaling Pathway Regulates Glucose Metabolism of metabolism in response to changes in cellular condi- tions. However, it has recently been shown that signals from cell surface receptors are required to control the ability of resting cells to tak. *Immunity* **16,** 769–777 (2002).

103. Flynn, K. & Müllbacher, A. Memory alloreactive cytotoxic T cells do not require costimulation for activation in vitro. *Immunol. Cell Biol.* **74,** 413–420 (1996).

104. Patel, M. S., Nemeria, N. S., Furey, W. & Jordan, F. The pyruvate dehydrogenase complexes: Structure-based function and regulation. *J. Biol. Chem.* **289,** 16615–16623 (2014).

105. Hitosugi, T. *et al.* Tyrosine Phosphorylation of Mitochondrial Pyruvate Dehydrogenase Kinase 1 Is Important for Cancer Metabolism. *Mol. Cell* **44,** 864–877 (2011).

106. Mithilesh Kumar Jha, K. S. Pyruvate dehydrogenase kinase as a Potential Therapeutic Target for Malignant Gliomas. *Brain Tumor Res Treat* **1,** 57–63 (2013).

107. Kankotia, S. & Stacpoole, P. W. Dichloroacetate and cancer: New home for an orphan drug? *Biochim. Biophys. Acta - Rev. Cancer* **1846,** 617–629 (2014).

108. Michelakis, E. D., Webster, L. & Mackey, J. R. Dichloroacetate (DCA) as a potential metabolic-targeting therapy for cancer. *Br. J. Cancer* **99,** 989–994 (2008).

109. Levin, S. E., Zhang, C., Kadlecek, T. A., Shokat, K. M. & Weiss, A. Inhibition of ZAP-70 kinase activity via an analog-sensitive allele blocks T cell receptor and CD28 superagonist signaling. *J. Biol. Chem.* **283,** 15419–15430 (2008).

110. Lee, K. E. & Simon, M. C. From stem cells to cancer stem cells: HIF takes the stage. *Curr. Opin. Cell Biol.* **24,** 232–235 (2012).

111. Schmidt, M. M., Rohwedder, A. & Dringen, R. Effects of chlorinated acetates on the glutathione metabolism and on glycolysis of cultured astrocytes. *Neurotox. Res.* **19,** 628–637 (2011).

112. Pioli, P. A., Jonell Hamilton, B., Connolly, J. E., Brewer, G. & Rigby, W. F. C. Lactate dehydrogenase is an AU-rich element-binding protein that directly interacts with AUF1. *J. Biol. Chem.* **277,** 35738–35745 (2002).

113. Hodge, D. L. *et al.* IFN-gamma AU-rich element removal promotes chronic IFN-gamma expression and autoimmunity in mice. *J. Autoimmun.* **53,** 33–45 (2014).

114. Jeffrey C. Rathmell. Metabolism and Autophagy in the Immune System: immunometabolism comes of age. *Immunol Rev.* **249,** 5–13 (2012).

115. Rathmell, J. C., Elstrom, R. L., Cinalli, R. M. & Thompson, C. B. Activated Akt promotes increased resting T cell size, CD28-independent T cell growth, and development of autoimmunity and lymphoma. *Eur. J. Immunol.* **33,** 2223–2232 (2003).

116. Gerriets, V. & Kishton, R. Metabolic programming and PDHK1 control CD4+ T cell subsets and inflammation. *J. …* **125,** 1–14 (2014).

117. Kang, J.-G. *et al.* Zinc Finger Protein Tristetraprolin Interacts with CCL3 mRNA and Regulates Tissue Inflammation. *J. Immunol.* **187,** 2696–2701 (2011).

118. Phong, B., Avery, L., Menk, A. V., Delgoffe, G. M. & Kane, L. P. Cutting Edge: Murine Mast Cells Rapidly Modulate Metabolic Pathways Essential for Distinct Effector Functions. *J. Immunol.* **198,** 640–644 (2017).

119. Sukumar, M. *et al.* Inhibiting glycolytic metabolism enhances CD8+ T cell memory and antitumor function. *J. Clin. Invest.* **123,** 4479–4488 (2013).

120. Zhang, D. *et al.* 2-Deoxy-D-glucose targeting of glucose metabolism in cancer cells as a potential therapy. *Cancer Lett.* **355,** 176–183 (2014).

121. PEDERSEN, E. B. A. P. L. High aerobic glycolysis of rat hepatoma cells in culture: Role of mitochondrial hexokinase. *Proc. Natl. Acad. Sci.* **74,** 3735–3739 (1977).

122. Zhang, S. L., Hu, X., Zhang, W., Yao, H. & Tam, K. Y. Development of pyruvate dehydrogenase kinase inhibitors in medicinal chemistry with particular emphasis as anticancer agents. *Drug Discov. Today* **20,** 1112–1119 (2015).

123. Topalian, S. L., Drake, C. G. & Pardoll, D. M. Immune checkpoint blockade: A common denominator approach to cancer therapy. *Cancer Cell* **27,** 451–461 (2015).

124. Gajewski, T. F. *et al.* Cancer immunotherapy strategies based on overcoming barriers within the tumor microenvironment. *Curr. Opin. Immunol.* **25,** 268–276 (2013).

125. Siska, P. J. & Rathmell, J. C. T cell metabolic fitness in antitumor immunity. *Trends Immunol.* 1–8 (2015). doi:10.1016/j.it.2015.02.007

126. Delgoffe, G. M. & Powell, J. D. Feeding an army: The metabolism of T cells in activation, anergy, and exhaustion. *Mol. Immunol.* **68,** 492–496 (2015).

127. Justus, C. R., Sanderlin, E. J. & Yang, L. V. Molecular connections between cancer cell metabolism and the tumor microenvironment. *Int. J. Mol. Sci.* **16,** 11055–11086 (2015).

128. Ackerman, D. & Simon, M. C. Hypoxia, lipids, and cancer: Surviving the harsh tumor microenvironment. *Trends Cell Biol.* **24,** 472–478 (2014).

129. Tao, J.-H., Barbi, J. & Pan, F. Hypoxia-inducible factors in T lymphocyte differentiation and function. A Review in the Theme: Cellular Responses to Hypoxia. *Am. J. Physiol. - Cell Physiol.* **309,** C580–C589 (2015).

130. Caldwell, C. C. *et al.* Differential Effects of Physiologically Relevant Hypoxic Conditions on T Lymphocyte Development and Effector Functions. *J. Immunol.* **167,** 6140–6149 (2001).

131. Noman, M. Z. *et al.* Hypoxia: a key player in antitumor immune response. A Review in the Theme: Cellular Responses to Hypoxia. *Am. J. Physiol. - Cell Physiol.* **309,** C569–C579 (2015).

132. Woo, S. R. *et al.* Immune inhibitory molecules LAG-3 and PD-1 synergistically regulate T-cell function to promote tumoral immune escape. *Cancer Res.* **72,** 917–927 (2012).

133. Zannella, V. E. *et al.* Reprogramming metabolism with metformin improves tumor oxygenation and radiotherapy response. *Clin. Cancer Res.* **19,** 6741–6750 (2013).

134. Phan, A. T. & Goldrath, A. W. Hypoxia-inducible factors regulate T cell metabolism and function. *Mol. Immunol.* **68,** 527–535 (2015).

135. Ho, P. *et al.* Phosphoenolpyruvate Is a Metabolic Checkpoint of Article Phosphoenolpyruvate Is a Metabolic Checkpoint of Anti-tumor T Cell Responses. *Cell* **162,** 1217–1228 (2015).

136. Bodmer, M., Meier, C., Krähenbühl, S., Jick, S. S. & Meier, C. R. Long-term metformin use is associated with decreased risk of breast cancer. *Diabetes Care* **33,** 1304–1308 (2010).

137. Josie M M Evans, Louise A Donnelly, Alistair M Emslie-Smith, Dario R Alessi, A. D. M. Metformin and reduced risk of cancer in diabetic patients. *Br. Med. J.* **330,** 1304–1305 (2005).

138. Eikawa, S. *et al.* Immune-mediated antitumor effect by type 2 diabetes drug, metformin. *Proc. Natl. Acad. Sci. U. S. A.* **112,** 1809–1814 (2015).

139. He, H. *et al.* Metformin, an old drug, brings a new era to cancer therapy. *Cancer J. (United States)* **21,** 70–74 (2015).

140. Park, M. J. *et al.* Metformin attenuates graft-versus-host disease via restricting mammalian target of rapamycin/signal transducer and activator of transcription 3 and promoting adenosine monophosphate–activated protein kinase-autophagy for the balance between T helper 17 an. *Transl. Res.* **173,** 115–130 (2016).

141. Yin, Y. *et al.* Normalization of CD4+ T cell metabolism reverses lupus. *Sci. Transl. Med.* **7,** 274ra18–274ra18 (2015).

142. Lee, C. F. *et al.* Preventing Allograft Rejection by Targeting Immune Metabolism. *Cell Rep.* **13,** 760–770 (2015).

143. Doedens, A. L. *et al.* Hypoxia-inducible factors enhance the effector responses of CD8 + T cells to persistent antigen. *Nat. Immunol.* **14,** 1173–1182 (2013).

144. Hugo, W. *et al.* Genomic and Transcriptomic Features of Response to Anti-PD-1 Therapy in Metastatic Melanoma. *Cell* **165,** 35–44 (2016).

145. Jiang, Y., Li, Y. & Zhu, B. T-cell exhaustion in the tumor microenvironment. *Cell Death Dis.* **6,** 1–9 (2015).

146. La-Beck, N. M., Jean, G. W., Huynh, C., Alzghari, S. K. & Lowe, D. B. Immune Checkpoint Inhibitors: New Insights and Current Place in Cancer Therapy. *Pharmacotherapy* **35,** 963–976 (2015).

147. Mahoney, K. M., Rennert, P. D. & Freeman, G. J. Combination cancer immunotherapy and new immunomodulatory targets. *Nat. Rev. Drug Discov.* **14,** 561–584 (2015).

148. Ribas, A. Adaptive immune resistance: How cancer protects from immune attack. *Cancer Discov.* **5,** 915–919 (2015).

149. Wherry, E. J. & Kurachi, M. Molecular and cellular insights into T cell exhaustion. *Nat. Rev. Immunol.* **15,** 486–499 (2015).

150. Crespo, J., Sun, H., Welling, T. H., Tian, Z. & Zou, W. T cell anergy, exhaustion, senescence, and stemness in the tumor microenvironment. *Curr. Opin. Immunol.* **25,** 214–221 (2013).

151. Schietinger, A. & Greenberg, P. D. Tolerance and exhaustion: Defining mechanisms of T cell dysfunction. *Trends Immunol.* **35,** 51–60 (2014).

152. Legat, A., Speiser, D. E., Pircher, H., Zehn, D. & Fuertes Marraco, S. A. Inhibitory receptor expression depends more dominantly on differentiation and activation than 'exhaustion' of human CD8 T cells. *Front. Immunol.* **4,** 1–15 (2013).

153. Odorizzi, P. M., Pauken, K. E., Paley, M. A., Sharpe, A. & Wherry, E. J. Genetic absence of PD-1 promotes accumulation of terminally differentiated exhausted CD8 $^{+}$ T cells. *J. Exp. Med.* **212,** 1125–1137 (2015).

154. Pauken, K. E. & Wherry, E. J. Overcoming T cell exhaustion in infection and cancer. *Trends Immunol.* **36,** 265–276 (2015).

155. Rizzuto, R., De Stefani, D., Raffaello, A. & Mammucari, C. Mitochondria as sensors and regulators of calcium signalling. *Nat. Rev. Mol. Cell Biol.* **13,** 566–578 (2012).

156. Wenner, C. E. Targeting mitochondria as a therapeutic target in cancer. *J. Cell. Physiol.* **227,** 450–456 (2012).

157. Liu, C., Workman, C. J. & Vignali, D. A. A. Targeting regulatory T cells in tumors. *FEBS J.* **283,** 2731–2748 (2016).

158. Monsalve, M. *et al.* Direct coupling of transcription and mRNA processing through the thermogenic coactivator PGC-1. *Mol. Cell* **6,** 307–316 (2000).

159. Cottet-Rousselle, C., Ronot, X., Leverve, X. & Mayol, J. F. Cytometric assessment of mitochondria using fluorescent probes. *Cytom. Part A* **79 A,** 405–425 (2011).

160. Cui, M., Tang, X., Christian, W. V., Yoon, Y. & Tieu, K. Perturbations in mitochondrial dynamics induced by human mutant PINK1 can be rescued by the mitochondrial division inhibitor mdivi-1. *J. Biol. Chem.* **285,** 11740–11752 (2010).

161. Kim, J. M., Rasmussen, J. P. & Rudensky, A. Y. Regulatory T cells prevent catastrophic autoimmunity throughout the lifespan of mice. *Nat. Immunol.* **8,** 191–197 (2007).

162. Brian N. Finck & J, D. P. K. PGC-1 coactivators: inducible regulators of energy metabolism in health and disease. *J Clin Invest* **116,** 615–622 (2006).

163. Spiegelman, B. M. Transcriptional control of energy homeostasis through the PGC1 coactivators. *Novartis Found. Symp.* **286,** 3–12 (2007).

164. Fernandez-Marcos, P. & Auwerx, J. Regulation of PGC-1a , a nodal regulator of mitochondrial biogenesis. *Am. J. Clin. …* **93,** 884–890 (2011).

165. Borniquel, S. *et al.* Inactivation of Foxo3a and Subsequent Downregulation of PGC-1 Mediate Nitric Oxide-Induced Endothelial Cell Migration. *Mol. Cell. Biol.* **30,** 4035–4044 (2010).

166. Olmos, Y. *et al.* Mutual dependence of Foxo3a and PGC-1α in the induction of Oxidative stress genes. *J. Biol. Chem.* **284,** 14476–14484 (2009).

167. Sukumar, M. *et al.* Mitochondrial Membrane Potential Identifies Cells with Enhanced Stemness for Cellular Therapy. *Cell Metab.* **23,** 63–76 (2016).

168. Xiao, B., Deng, X., Zhou, W. & Tan, E.-K. Flow Cytometry-Based Assessment of Mitophagy Using MitoTracker. *Front. Cell. Neurosci.* **10,** 1–4 (2016).

169. Macintyre, A. N. *et al.* Protein Kinase B Controls Transcriptional Programs that Direct Cytotoxic T Cell Fate but Is Dispensable for T Cell Metabolism. *Immunity* **34,** 224–236 (2011).

170. Álvarez-Guardia, D. *et al.* The p65 subunit of NF-B binds to PGC-1, linking inflammation and metabolic disturbances in cardiac cells. *Cardiovasc. Res.* **87,** 449–458 (2010).

171. Haghikia, A. *et al.* Interferon-beta affects mitochondrial activity in CD4+lymphocytes: Implications for mechanism of action in multiple sclerosis. *Mult. Scler. J.* **21,** 1262–1270 (2015).

172. Kauppinen, A., Suuronen, T., Ojala, J., Kaarniranta, K. & Salminen, A. Antagonistic crosstalk between NF-κB and SIRT1 in the regulation of inflammation and metabolic disorders. *Cell. Signal.* **25,** 1939–1948 (2013).

173. Kim, M. S. *et al.* Tumor necrosis factor and interleukin 1 decrease RXRα, PPARα, PPARγ, LXRα, and the coactivators SRC-1, PGC-1α, and PGC-1β in liver cells. *Metabolism.* **56,** 267–279 (2007).

174. Palomer, X. *et al.* TNF-α reduces PGC-1α expression through NF-κB and p38 MAPK leading to increased glucose oxidation in a human cardiac cell model. *Cardiovasc. Res.* **81,** 703–712 (2009).

175. Scarpulla, R. C. Metabolic control of mitochondrial biogenesis through the PGC-1 family regulatory network. *Biochim. Biophys. Acta - Mol. Cell Res.* **1813,** 1269–1278 (2011).

176. Wherry, E. J. T cell exhaustion. *Nat. Publ. Gr.* **131,** 492–499 (2011).

177. Pauken, K. E. *et al.* Epigenetic stability of exhausted T cells limits durability of reinvigoration by PD-1 blockade. *Science* **354,** 1160–1165 (2016).

178. Blackburn, S. D., Shin, H., Freeman, G. J. & Wherry, E. J. Selective expansion of a subset of exhausted CD8 T cells by PD-L1 blockade. *Proc. Natl. Acad. Sci.* **105,** 15016–15021 (2008).

179. Paley, M. A. *et al.* Progenitor and Terminal Subsets of CD8+ T Cells Cooperate to Contain Chronic Viral Infection Michael. *Science (80-.).* **1220,** 1220–1226 (2012).

180. Grilli, A. *et al.* High-dimensional single cell analysis identifies stem-like cytotoxic CD8 + T cells infiltrating human tumors . *J. Exp. Med.* **215,** 2520–2535 (2018).

181. Im, S. J. *et al.* Defining CD8+ T cells that provide the proliferative burst after PD-1 therapy. *Nature* **537,** 417–421 (2016).

182. Philip, M. *et al.* Chromatin states define tumour-specific T cell dysfunction and reprogramming. *Nature* **545,** 452–456 (2017).

183. Scott, A. C. *et al.* The role of thymocyte selection-associated HMG box protein (TOX) in CD8 T cell differentiation and dysfunction. *J. Immunol.* **200,** 57.36 LP – 57.36 (2018).

184. Pradervand, S. *et al.* Intratumoral Tcf1+PD-1+CD8+ T Cells with Stem-like Properties Promote Tumor Control in Response to Vaccination and Checkpoint Blockade Immunotherapy. *Immunity* **50,** 195–211.e10 (2019).

185. Anderson, A. C. *et al.* Checkpoint Blockade Immunotherapy Induces Dynamic Changes in PD-1−CD8+ Tumor-Infiltrating T Cells. *Immunity* **50,** 181–194.e6 (2019).

186. Gabriel, S. S. *et al.* Transcription Factor IRF4 Promotes CD8+ T Cell Exhaustion and Limits the Development of Memory-like T Cells during Chronic Infection. *Immunity* **47,** 1129–1141.e5 (2017).

187. Miller, B. C. *et al.* Subsets of exhausted CD8+ T cells differentially mediate tumor control and respond to checkpoint blockade. *Nat. Immunol.* **20,** 326–336 (2019).

188. Birnbaum, M. J. *et al.* Memory CD8+ T Cells Use Cell-Intrinsic Lipolysis to Support the Metabolic Programming Necessary for Development. *Immunity* **41,** 75–88 (2014).

189. Mehta, M. M., Weinberg, S. E. & Chandel, N. S. Mitochondrial control of immunity: beyond ATP. *Nat. Rev. Immunol.* **17,** 608 (2017).

190. O'Neill, L. A. J., Kishton, R. J. & Rathmell, J. A guide to immunometabolism for immunologists. *Nat. Rev. Immunol.* **16,** 553 (2016).

191. Miko, M. *et al.* Manganese superoxide dismutase : A regulator of T cell activation-induced oxidative signaling and cell death. **1823,** 1041–1052 (2012).

192. Oliver Stehling and Roland Lill. The Role of Mitochondria in Cellular Iron–Sulfur Protein Biogenesis: Mechanisms, Connected Processes, and Diseases. *Cold Spring Harb Perspect Biol* 1–17 (2013). doi:10.1101/cshperspect.a011312

193. Handschin, C., Rhee, J., Lin, J., Tarr, P. T. & Spiegelman, B. M. An autoregulatory loop controls peroxisome proliferator-activated receptor gamma coactivator 1 alpha expression in muscle. *Proc Natl Acad Sci U S A* **100,** 7111–7116 (2003).

194. Skene, P. J., Henikoff, J. G. & Henikoff, S. Targeted in situ genome-wide profiling with high efficiency for low cell numbers. *Nat. Protoc.* **13,** 1006–1019 (2018).

195. Olzmann, J. A. & Carvalho, P. Dynamics and functions of lipid droplets. *Nat. Rev. Mol. Cell Biol.* **20,** (2018).

196. Muz, B., de la Puente, P., Azab, F. & Azab, A. K. The role of hypoxia in cancer progression, angiogenesis, metastasis, and resistance to therapy. *Hypoxia (Auckland, N.Z.)* **3,** 83–92 (2015).

197. Shin, H. *et al.* Article A Role for the Transcriptional Repressor Blimp-1 in CD8 + T Cell Exhaustion during Chronic Viral Infection. *Immunity* **31,** 309–320 (2009).

198. Martins, G. & Calame, K. Regulation and Functions of Blimp-1 in T and B Lymphocytes. *Annu. Rev. Immunol.* **26,** 133–169 (2008).

199. Matilainen, O., Quirós, P. M. & Auwerx, J. Mitochondria and Epigenetics - Crosstalk in Homeostasis and Stress. *Trends Cell Biol.* **27,** 453–463 (2017).

200. Chisolm, D. A. & Weinmann, A. S. Connections Between Metabolism and Epigenetics in Programming Cellular Differentiation. *Annu. Rev. Immunol.* **36,** 221–246 (2018).

201. Fisicaro, P. *et al.* Targeting mitochondrial dysfunction can restore antiviral activity of exhausted HBV-specific CD8 T cells in chronic hepatitis B. *Nat. Med.* **23,** 327 (2017).

202. Hurst, K. E. *et al.* Endoplasmic Reticulum Stress Contributes to Mitochondrial Exhaustion of CD8⁺ T Cells. *Cancer Immunol. Res.* **7,** 476 LP – 486 (2019).

203. Siska, P. J. *et al.* Mitochondrial dysregulation and glycolytic insufficiency functionally impair CD8 T cells infiltrating human renal cell carcinoma. *JCI Insight* **2,** (2017).

204. Ciccia, A. & Elledge, S. J. The DNA Damage Response: Making It Safe to Play with Knives. *Mol. Cell* **40,** 179–204 (2010).

205. Cooke, M. S., Evans, M. D., Dizdaroglu, M. & Lunec, J. Oxidative DNA damage: mechanisms, mutation, and disease. doi:10.1096/fj.02-0752rev

206. Horton, B. L., Williams, J. B., Cabanov, A., Spranger, S. & Gajewski, T. F. Intratumoral CD8+ T-cell Apoptosis Is a Major Component of T-cell Dysfunction and Impedes Antitumor Immunity. *Cancer Immunol. Res.* **6,** 14 LP – 24 (2018).

207. Man, K. & Kallies, A. Synchronizing transcriptional control of T cell metabolism and function. *Nat. Rev. Immunol.* **15,** 574–584 (2015).

208. Michelet, X. *et al.* Metabolic reprogramming of natural killer cells in obesity limits antitumor responses. *Nat. Immunol.* **19,** 1330–1340 (2018).

209. Zhang, J. *et al.* Long-term antigen exposure irreversibly modifies metabolic requirements for T cell function. *Elife* **7,** 1–24 (2018).

210. Narita, T., Weinert, B. T. & Choudhary, C. Functions and mechanisms of non-histone protein acetylation. *Nat. Rev. Mol. Cell Biol.* **20,** (2018).

211. Lawrence, R. E. & Zoncu, R. The lysosome as a cellular centre for signalling, metabolism and quality control. *Nat. Cell Biol.* **21,** 133–142 (2019).

212. Lamadema, N., Burr, S. & Brewer, A. C. Dynamic regulation of epigenetic demethylation by oxygen availability and cellular redox. *Free Radic. Biol. Med.* **131,** 282–298 (2019).

213. Nagaraj, R. *et al.* Nuclear Localization of Mitochondrial TCA Cycle Enzymes as a Critical Step in Mammalian Zygotic Genome Activation. *Cell* **168,** 210–223.e11 (2017).

214. Östman, A., Frijhoff, J., Sandin, Å. & Böhmer, F. D. Regulation of protein tyrosine phosphatases by reversible oxidation. *J. Biochem.* **150,** 345–356 (2011).

215. Martinez, G. J. *et al.* The Transcription Factor NFAT Promotes Exhaustion of Activated CD8+ T Cells. *Immunity* **42,** 265–278 (2015).

216. Binsfeld, C. *et al.* Glutathione Primes T Cell Metabolism for Inflammation. *Immunity* **46,** 675–689 (2017).

217. Tretter, L. & Adam-Vizi, V. Inhibition of Krebs Cycle Enzymes by Hydrogen Peroxide: A Key Role of α-Ketoglutarate Dehydrogenase in Limiting NADH Production under Oxidative Stress. *J. Neurosci.* **20,** 8972–8979 (2018).

218. Hazen, S. L. Oxidized Phospholipids as Endogenous Pattern Recognition Ligands in Innate Immunity. *J. Biol. Chem.* **283,** 15527–15531 (2008).

219. Blair, I. A. DNA Adducts with Lipid Peroxidation Products. *J. Biol. Chem.* **283,** 15545–15549 (2008).

220. Le Gal, K. *et al.* Antioxidants can increase melanoma metastasis in mice. *Sci. Transl. Med.* **7,** 308re8 LP – 308re8 (2015).

221. Sayin, V. I. *et al.* Antioxidants Accelerate Lung Cancer Progression in Mice. *Sci. Transl. Med.* **6,** 221ra15 LP – 221ra15 (2014).

222. Seo, J. *et al.* Genome-wide profiles of H2AX and γ-H2AX differentiate endogenous and exogenous DNA damage hotspots in human cells. *Nucleic Acids Res.* **40,** 5965–5974 (2012).

223. Tyagi, S., Gupta, P., Saini, A. S., Kaushal, C. & Sharma, S. The peroxisome proliferator-activated receptor: A family of nuclear receptors role in various diseases. *J. Adv. Pharm. Technol. Res.* **2,** 236–240 (2011).

224. Robert-Tissot, C. *et al.* Activation of Peroxisome Proliferator-Activated Receptors α and δ Synergizes with Inflammatory Signals to Enhance Adoptive Cell Therapy. *Cancer Res.* **79,** 445–451 (2018).

225. Chowdhury, P. S., Chamoto, K., Kumar, A. & Honjo, T. PPAR-Induced Fatty Acid Oxidation in T Cells Increases the Number of Tumor-Reactive CD8 + T Cells and Facilitates Anti–PD-1 Therapy . *Cancer Immunol. Res.* **6,** 1375–1387 (2018).

226. Solaini, G., Baracca, A., Lenaz, G. & Sgarbi, G. Hypoxia and mitochondrial oxidative metabolism. *Biochim. Biophys. Acta - Bioenerg.* **1797,** 1171–1177 (2010).

227. Delgoffe, G. M. *et al.* Tumor cell oxidative metabolism as a barrier to PD-1 blockade immunotherapy in melanoma. *JCI Insight* **4,** (2019).

228. Kawalekar, O. U. *et al.* Distinct Signaling of Coreceptors Regulates Specific Metabolism Pathways and Impacts Memory Development in CAR T Cells. *Immunity* **44,** 380–390 (2016).

229. Whiteaker, J. R. *et al.* Phosphoproteomic analysis of chimeric antigen receptor signaling reveals kinetic and quantitative differences that affect cell function. *Sci. Signal.* **11,** eaat6753 (2018).

230. Park, J. H., Geyer, M. B. & Brentjens, R. J. CD19-targeted CAR T-cell therapeutics for hematologic malignancies: Interpreting clinical outcomes to date. *Blood* **127,** 3312–3320 (2016).

231. Menk, A. V. *et al.* 4-1BB costimulation induces T cell mitochondrial function and biogenesis enabling cancer immunotherapeutic responses. *J. Exp. Med.* **215,** (2018).

232. Knochelmann, H. M. *et al.* CAR T Cells in Solid Tumors: Blueprints for Building Effective Therapies. *Front. Immunol.* **9,** 1–20 (2018).